

Docket Number 50-346
License Number NPF-3
Serial Number 2550
Attachment 5

**DESIGN AND LICENSING REPORT
DAVIS-BESSE UNIT 1 CASK PIT RACK INSTALLATION PROJECT
HOLTEC INTERNATIONAL**

NON-PROPRIETARY VERSION

(277 pages follow)

9906070155 990521
PDR ADOCK 05000346
P PDR



Holtec Center, 555 Lincoln Drive West, Marlton, NJ 08053

Telephone (609) 797-0900

Fax (609) 797-0909

**DESIGN AND LICENSING REPORT
DAVIS-BESSE NUCLEAR POWER STATION UNIT 1
CASK PIT RACK INSTALLATION PROJECT**

for the

FIRST ENERGY NUCLEAR OPERATING COMPANY

by

**HOLTEC INTERNATIONAL
555 LINCOLN DRIVE WEST
MARLTON, NJ 08053**

HOLTEC PROJECT NO. 80284

HOLTEC REPORT HI-981933

REPORT CATEGORY: A

REPORT CLASS: SAFETY RELATED

This document version has all proprietary information removed and has replaced those sections, figures, and tables with highlighting and/or notes to designate the removal of such information. This document is to be used only in connection with the performance of work by Holtec International or its designated subcontractors. Reproduction, publication or presentation, in whole or in part, for any other purpose by any party other than the Client is expressly forbidden.

REVIEW AND CERTIFICATION LOG

DOCUMENT NAME :	DESIGN AND LICENSING REPORT DAVIS-BESSE NUCLEAR POWER STATION UNIT 1 CASK PIT RACK INSTALLATION PROJECT
HOLTEC DOCUMENT I.D. NUMBER	981933
HOLTEC PROJECT NUMBER	80284
CUSTOMER/CLIENT:	FIRST ENERGY

REVISION BLOCK

REVISION NUMBER *	AUTHOR & DATE	REVIEWER & DATE	QA & DATE	APPROVED & DATE !	DIST. x
ORIGINAL	Scott H. Pellet SHP 2-23-99	Claudia... AS. 2-28/99	V. Dunlap J. G. P... 3-15-99	Scott H. Pellet SHP 3-15-99	C
REVISION 1	Scott H. Pellet SHP 4-12-99	Carl W. B... C.B. 4/13/99	V. Dunlap J. G. P... 4-12-99	Scott H. Pellet SHP 4-12-99	C
REVISION 2	Scott H. Pellet SHP 5-19-99	Carl W. B... C.B. 5/19/99	V. Dunlap J. G. P... 5-19-99	Scott H. Pellet SHP 5-19-99	C
REVISION 3					
REVISION 4					
REVISION 5					
REVISION 6					

This document conforms to the requirements of the design specification and the applicable sections of the governing codes.

Note : Signatures and printed names required in the review block.

* A revision of this document will be ordered by the Project Manager and carried out if any of its contents is materially affected during evolution of this project. The determination as to the need for revision will be made by the Project Manager with input from others, as deemed necessary by him.

! Must be Project Manager or his designee.

x Distribution : C : Client
M : Designated Manufacturer
F : Florida Office

*** Report category on the cover page indicates the contractual status of this document as ***
A = to be submitted to client for approval I = for client's information N = not submitted externally

THE REVISION CONTROL OF THIS DOCUMENT IS BY A "SUMMARY OF REVISIONS LOG" PLACED BEFORE THE TEXT OF THE REPORT.



Holtec Center, 555 Lincoln Drive West, Marlton, NJ 08053

Telephone (609) 797-0900

Fax (609) 797-0909

QA AND ADMINISTRATIVE INFORMATION LOG

(To Be Filled In By the Principal Author of the Document and Placed After the Title Page)

Document No: HI-981933	CATEGORY: <input type="checkbox"/> Generic <input checked="" type="checkbox"/> Project Specific
Holtec Project No: 80284	
In accordance with the Holtec Quality Assurance Manual, and associated Holtec Quality Procedures (HQPs), this document is categorized as a :	
<input type="checkbox"/> Calculation Package * (Per HQP 3.2)	<input checked="" type="checkbox"/> Technical Report (Per HQP 3.2) (Such as a Licensing report)
<input type="checkbox"/> Design Criterion Document (Per HQP 3.4)	<input type="checkbox"/> Design Specification (Per HQP 3.4)
<input type="checkbox"/> Other (Specify): _____	
The formatting of the contents of this document is in accordance with the instructions of HQP 3.2 or 3.4 except as noted below: _____ _____ _____	
This document is labelled :	
<input type="checkbox"/> Nonproprietary <input checked="" type="checkbox"/> Holtec Proprietary <input type="checkbox"/> Privileged Intellectual Property (PIP)	
Documents labelled Privileged Intellectual Property contains extremely valuable intellectual/commercial property of Holtec International. They can not be released to external organizations or entites without explicit approval of a company corporate officer. The recipient of Holtec's proprietary or Privileged Intellectual Property (PIP) document bears full and undivided responsibility to safeguard it against loss or duplication.	
* Revisions to the calculation Packages may be made by adding supplements to the document and replacing the "Table of Contents", the "Review and Certification" page and the "Revision Log".	

SUMMARY OF REVISIONS

Revision 2 contains the following pages:	
COVER PAGE	1 page
REVIEW AND CERTIFICATION LOG	1 page
QA AND ADMINISTRATIVE INFORMATION LOG	1 page
SUMMARY OF REVISIONS	1 page
TABLE OF CONTENTS	9 pages
1.0 INTRODUCTION	8 pages
2.0 OVERVIEW OF THE PROPOSED CAPACITY EXPANSION	21 pages
3.0 MATERIAL, HEAVY LOAD, AND CONSTRUCTION CONSIDERATIONS	19 pages
4.0 CRITICALITY SAFETY EVALUATION	24 pages
-- APPENDIX 4A BENCHMARK CALCULATIONS	25 pages
5.0 THERMAL-HYDRAULIC CONSIDERATIONS	35 pages
6.0 STRUCTURAL / SEISMIC CONSIDERATIONS	63 pages
7.0 FUEL HANDLING AND MECHANICAL ACCIDENTS	29 pages
8.0 CASK PIT STRUCTURE INTEGRITY CONSIDERATIONS	17 pages
9.0 RADIOLOGICAL EVALUATION	7 pages
10.0 INSTALLATION	9 pages
11.0 ENVIRONMENTAL COST/BENEFIT ASSESSMENT	7 pages
TOTAL	277 pages

Revision 1 primarily incorporates client editorial comments. Revision 1 also incorporates the results of supporting calculation changes based on client comments.

Revision 2 primarily incorporates client editorial comments, transmitted via memo dated May 14, 1999.

TABLE OF CONTENTS

1.0	INTRODUCTION.....	1-1
1.1	<u>References</u>	1-5
2.0	OVERVIEW OF THE PROPOSED CAPACITY EXPANSION.....	2-1
2.1	<u>Introduction</u>	2-1
2.2	<u>Summary of Principal Design Criteria</u>	2-2
2.3	<u>Applicable Codes and Standards</u>	2-4
2.4	<u>Quality Assurance Program</u>	2-9
2.5	<u>Mechanical Design</u>	2-10
2.6	<u>Rack Fabrication Methods</u>	2-10
2.7	<u>Rack Module Description</u>	2-11
3.0	MATERIAL, HEAVY LOAD, AND CONSTRUCTION CONSIDERATIONS.....	3-1
3.1	<u>Introduction</u>	3-1
3.2	<u>Structural Materials</u>	3-1
3.3	<u>Poison Material (Neutron Absorber)</u>	3-1
3.3.1	<u>Boral Material Characteristics</u>	3-3
3.4	<u>Compatibility with Coolant</u>	3-4
3.5	<u>Heavy Load Considerations for the Proposed Rack Installations</u>	3-5
3.6	<u>References</u>	3-10
4.0	CRITICALITY SAFETY EVALUATION.....	4-1
4.1	<u>Design Bases</u>	4-1
4.2	<u>Summary of Criticality Analyses</u>	4-4
4.2.1	<u>Normal Operating Conditions</u>	4-4
4.2.2	<u>Abnormal and Accident Operating Conditions</u>	4-4
4.3	<u>Reference Fuel Storage Cells</u>	4-6
4.3.1	<u>Reference Fuel Assembly</u>	4-6
4.3.2	<u>Fuel Storage Cells</u>	4-6
4.4	<u>Analytical Methodology</u>	4-7
4.4.1	<u>Reference Design Calculations</u>	4-7
4.4.2	<u>Fuel Burnup Calculations and Uncertainties</u>	4-8
4.4.3	<u>Effect of Axial Burnup Distribution</u>	4-9
4.4.4	<u>Long Term Changes in Reactivity</u>	4-10
4.5	<u>Criticality Analyses and Tolerances</u>	4-11
4.5.1	<u>Nominal Design Case</u>	4-11
4.5.2	<u>Determination of Acceptable Burnup and Enrichment Combinations</u>	4-11
4.5.3	<u>Uncertainties Due to Tolerances</u>	4-12
4.5.4	<u>Eccentric Fuel Positioning</u>	4-12
4.5.5	<u>Water-Gap Spacing Between Racks</u>	4-12

TABLE OF CONTENTS

4.6	<u>Abnormal and Accident Conditions</u>	4-13
4.6.1	<u>Temperature and Water Density Effects</u>	4-13
4.6.2	<u>Lateral Rack Movement</u>	4-13
4.6.3	<u>Abnormal Location of a Fuel Assembly</u>	4-14
4.6.4	<u>Dropped Fuel Assembly</u>	4-14
4.7	<u>References</u>	4-16
Appendix 4A	<u>Benchmark Calculations</u>	Total of 25 Pages including 6 figures
4A.1	<u>Introduction and Summary</u>	4A-1
4A.2	<u>Effect of Enrichment</u>	4A-3
4A.3	<u>Effect of ¹⁰B Loading</u>	4A-4
4A.4	<u>Miscellaneous and Minor Parameters</u>	4A-5
4A.4.1	<u>Reflector Material and Spacings</u>	4A-5
4A.4.2	<u>Fuel Pellet Diameter and Lattice Pitch</u>	4A-5
4A.4.3	<u>Soluble Boron Concentration Effects</u>	4A-5
4A.5	<u>MOX Fuel</u>	4A-6
4A.6	<u>References</u>	4A-7
5.0	<u>THERMAL-HYDRAULIC CONSIDERATIONS</u>	5-1
5.1	<u>Introduction</u>	5-1
5.2	<u>Cooling Systems Description</u>	5-3
5.3	<u>Discharge/Cooling Alignment Scenarios</u>	5-5
5.4	<u>Maximum Bulk Pool Temperature Methodology</u>	5-7
5.5	<u>Minimum Time-to-Boil and Maximum Boiloff Rate Methodology</u>	5-10
5.6	<u>Local Water Temperature Methodology</u>	5-12
5.6.1	<u>Local Temperature Evaluation Methodology</u>	5-13
5.7	<u>Fuel Rod Cladding Temperature Methodology</u>	5-17
5.8	<u>Results</u>	5-19
5.8.1	<u>Maximum Bulk Pool Temperatures</u>	5-19
5.8.2	<u>Minimum Time-to-Boil and Maximum Boiloff Rate</u>	5-20
5.8.3	<u>Local Water and Fuel Cladding Temperatures</u>	5-20
5.9	<u>Fuel Handling Area Ventilation (FHAV)</u>	5-22
5.10	<u>References</u>	5-23
6.0	<u>STRUCTURAL/SEISMIC CONSIDERATIONS</u>	6-1
6.1	<u>Introduction</u>	6-1
6.2	<u>Overview of Rack Structural Analysis Methodology</u>	6-1
6.2.1	<u>Background of Analysis Methodology</u>	6-2
6.3	<u>Description of Racks</u>	6-5
6.3.1	<u>Fuel Weights</u>	6-5
6.4	<u>Synthetic Time-Histories</u>	6-6

TABLE OF CONTENTS

6.5	<u>WPMR Methodology</u>	6-7
6.5.1	<u>Model Details for Spent Fuel Racks</u>	6-7
6.5.1.1	<u>Assumptions</u>	6-8
6.5.1.2	<u>Element Details</u>	6-10
6.5.2	<u>Fluid Coupling Effect</u>	6-11
6.5.2.1	<u>Multi-Body Fluid Coupling Phenomena</u>	6-12
6.5.3	<u>Stiffness Element Details</u>	6-13
6.5.4	<u>Coefficients of Friction</u>	6-14
6.5.5	<u>Governing Equations of Motion</u>	6-15
6.6	<u>Structural Evaluation of Spent Fuel Rack Design</u>	6-16
6.6.1	<u>Kinematic and Stress Acceptance Criteria</u>	6-16
6.6.2	<u>Stress Limit Evaluations</u>	6-17
6.6.3	<u>Dimensionless Stress Factors</u>	6-20
6.6.4	<u>Loads and Loading Combinations for Spent Fuel Racks</u>	6-21
6.7	<u>Parametric Simulations</u>	6-22
6.8	<u>Time History Simulation Results</u>	6-25
6.8.1	<u>Rack Displacements</u>	6-25
6.8.2	<u>Pedestal Vertical Forces</u>	6-26
6.8.3	<u>Pedestal Friction Forces</u>	6-26
6.8.4	<u>Rack Impact Loads</u>	6-27
6.8.4.1	<u>Rack to Rack Impacts</u>	6-27
6.8.4.2	<u>Rack to Wall Impacts</u>	6-27
6.8.4.3	<u>Fuel to Cell Wall Impact Loads</u>	6-28
6.9	<u>Rack Structural Evaluation</u>	6-29
6.9.1	<u>Rack Stress Factors</u>	6-29
6.9.2	<u>Pedestal Thread Shear Stress</u>	6-31
6.9.3	<u>Local Stresses Due to Impacts</u>	6-31
6.9.4	<u>Weld Stresses</u>	6-32
6.9.5	<u>Bearing Pad Analysis</u>	6-35
6.10	<u>Level A Evaluation</u>	6-36
6.11	<u>Hydrodynamic Loads on Cask Pit Walls</u>	6-37
6.12	<u>Local Stress Considerations</u>	6-37
6.12.1	<u>Cell Wall Buckling</u>	6-37
6.12.2	<u>Analysis of Welded Joints in Racks</u>	6-38
6.13	<u>References</u>	6-39
7.0	<u>FUEL HANDLING AND MECHANICAL ACCIDENTS</u>	7-1
7.1	<u>Introduction</u>	7-1
7.2	<u>Description of Accidents</u>	7-1
7.2.1	<u>Shallow Drop Events</u>	7-2
7.2.2	<u>Deep Drop Events</u>	7-3
7.2.3	<u>Rack Drop Event</u>	7-4
7.2.4	<u>Uplift Force Evaluation</u>	7-5
7.3	<u>Mathematical Model</u>	7-5

TABLE OF CONTENTS

7.4	<u>Results</u>	7-5
7.4.1	<u>Shallow Drop Event Results</u>	7-5
7.4.2	<u>Deep Drop Event Results</u>	7-6
7.4.3	<u>Rack Drop Event Results</u>	7-7
7.4.4	<u>Uplift Force Evaluation Results</u>	7-8
7.5	<u>Closure</u>	7-8
7.6	<u>References</u>	7-9
8.0	<u>CASK PIT STRUCTURE INTEGRITY CONSIDERATIONS</u>	8-1
8.1	<u>Introduction</u>	8-1
8.2	<u>Description of Cask Pit Structures</u>	8-1
8.3	<u>Definition of Loads</u>	8-2
8.3.1	<u>Static Loading (Dead Loads and Live Loads)</u>	8-2
8.3.2	<u>Seismic Induced Loads</u>	8-3
8.3.3	<u>Thermal Loading</u>	8-3
8.4	<u>Analysis Procedures</u>	8-5
8.4.1	<u>Boundary Conditions</u>	8-6
8.4.2	<u>Material Properties</u>	8-6
8.4.3	<u>Load Combinations</u>	8-6
8.5	<u>Results of Reinforced Concrete Analysis</u>	8-8
8.6	<u>Pool Liner</u>	8-8
8.7	<u>Conclusions</u>	8-8
8.8	<u>References</u>	8-9
9.0	<u>RADIOLOGICAL EVALUATION</u>	9-1
9.1	<u>Solid Radwaste</u>	9-1
9.2	<u>Liquid Releases</u>	9-1
9.3	<u>Gaseous Releases</u>	9-1
9.4	<u>Personnel Doses</u>	9-3
9.5	<u>Anticipated Dose During Rack Installation</u>	9-4
10.0	<u>INSTALLATION</u>	10-1
10.1	<u>Introduction</u>	10-1
10.2	<u>Rack Arrangement</u>	10-4
10.3	<u>Cask Pit Survey and Inspection</u>	10-5
10.4	<u>Cask Pit Cooling and Purification</u>	10-5
10.4.1	<u>Cask Pit Cooling</u>	10-5
10.4.2	<u>Purification</u>	10-6
10.5	<u>Fuel Movement</u>	10-6
10.6	<u>Installation of New Racks</u>	10-6
10.7	<u>Safety, Health Physics, and ALARA Methods</u>	10-7
10.7.1	<u>Safety</u>	10-7
10.7.2	<u>Health Physics</u>	10-8
10.7.3	<u>ALARA</u>	10-8
10.8	<u>Radwaste Material Control</u>	10-9

TABLE OF CONTENTS

11.0	ENVIRONMENTAL COST/BENEFIT ASSESSMENT	11-1
11.1	<u>Introduction</u>	11-1
11.2	<u>Imperative for Rack Installation</u>	11-1
11.3	<u>Appraisal of Alternative Options</u>	11-2
11.3.1	<u>Alternative Option Summary</u>	11-4
11.4	<u>Cost Estimate</u>	11-5
11.5	<u>Resource Commitment</u>	11-6
11.6	<u>Environmental Considerations</u>	11-6
11.7	<u>References</u>	11-7

TABLE OF CONTENTS

Tables

2.1.1	Geometric and Physical Data for High Density Racks.....	2-14
2.5.1	Module Data for Spent Fuel Racks	2-15
3.3.1	Boral Experience List - PWRs	3-11 and 3-12
3.3.2	Boral Experience List - BWRs	3-13 and 3-14
3.3.3	1100 Alloy Aluminum Physical Characteristics	3-15
3.3.4	Chemical Composition - Aluminum (1100 Alloy)	3-16
3.3.5	Chemical Composition and Physical Properties of Boron Carbide	3-17
3.5.1	Heavy Load Handling Compliance Matrix (NUREG-0612).....	3-18
4.1.1	Fuel Assembly Specifications	4-18
4.2.1	Summary of Criticality Safety Analyses	4-19
4.2.2	Reactivity Effects of Abnormal and Accident Conditions	4-20
4.5.1	Reactivity Effects of Manufacturing Tolerances	4-21
4.6.1	Reactivity Effects of Temperature and Void.....	4-22
4A.1	Summary of Criticality Benchmark Calculations.....	4A-9 through 4A-13
4A.2	Comparison of MCNP4a and Keno5a Calculated Reactivities for Various Enrichments	4A-14
4A.3	MCNP4a Calculated Reactivities for Critical Experiments with Neutron Absorbers	4A-15
4A.4	Comparison of MCNP4a and KENO5a Calculated Reactivities for Various ¹⁰ B Loadings.....	4A-16
4A.5	Calculations for Critical Experiments with Thick Lead and Steel Reflectors	4A-17
4A.6	Calculations for Critical Experiments with Various Soluble Boron Concentrations.....	4A-18
4A.7	Calculations for Critical Experiments with MOX Fuel	4A-19
5.3.1	Davis-Besse Historic and Projected Fuel Discharge Schedule	5-24
5.4.1	Data for SFP Bulk Temperature Evaluation.....	5-25
5.5.1	Data for Time-to-Boil Evaluation	5-26
5.6.1	Data for SFP/Cask Pit Local Temperature Evaluation.....	5-27
5.8.1	Results of Bulk Temperature Transient.....	5-28
5.8.2	Results of Minimum Time-to-Boil and Maximum Boiloff Rate Evaluation	5-29
6.2.1	Partial Listing of Fuel Rack Applications Using DYNARACK	6-41 through 6-43
6.3.1	Rack Material Data (200EF) (ASME - Section II, Part D)	6-44
6.4.1	Time-History Statistical Correlation Results	6-45
6.5.1	Degrees-of-Freedom.....	6-46
6.9.1	Comparison of Bounding Calculated Loads/Stresses vs. Code Allowables at Impact Locations and at Welds	6-47

TABLE OF CONTENTS

Tables (continued)

7.2.1	Material Definition.....	7-10
7.3.1	Impactor Weight and Impactor Velocity Calculations	7-11
7.3.2	Structural and Material Definition of Impactor and Target	7-12
8.4.1	Concrete and Rebar Properties.....	8-10
8.4.2	Material Properties.....	8-11
8.4.3	Individual Load Case Description	8-12
8.5.1	North Wall Safety Factors	8-13
8.5.2	South Wall Safety Factors	8-14
8.5.3	West Wall Safety Factors.....	8-15
8.5.4	East Wall Safety Factors.....	8-16
9.3.1	Average Activity of Weekly SFP Samples.....	9-6
9.5.1	Preliminary Estimate of Person-REM Dose During Cask Pit Rack Installation.....	9-7

Figures

- 1.1 Cask Pit Layout - Phase 1
- 1.2 Cask Pit Layout - Phase 2
- 1.3 Cask Pit Layout - Phase 3

- 2.1 Schematic of Typical Davis-Besse Rack Structure
- 2.2 Seam Welded Precision Formed Channels
- 2.3 Composite Box Assembly
- 2.4 Typical Array of Storage Cells
- 2.5 Support Pedestal for Holtec PWR Rack
- 2.6 Three PWR Cells in Elevation View

- 3.5.1 Auxiliary Building Spent Fuel Pool Area Plan View

- 4.2.1 Minimum Required Fuel Assembly Burnup as a Function of Nominal Initial Enrichment to Permit Storage in the Cask Pit
- 4.3.1 A Two Dimensional Representation of the Computational Model Used for the Cask Pit Rack Analyses

- 4A.1 MCNP Calculated k-eff Values for Various Values of the Spectral Index
- 4A.2 KENO5a Calculated k-eff Values for Various Values of the Spectral Index
- 4A.3 MCNP Calculated k-eff Values at Various U-235 Enrichments
- 4A.4 KENO Calculated k-eff Values at Various U-235 Enrichments
- 4A.5 Comparison of MCNP and KENO5a Calculations for Various Fuel Enrichments
- 4A.6 Comparison of MCNP and KENO5a Calculations for Various Boron-10 Areal Densities

- 5.6.1 Two-Dimensional Spent Fuel Pool Geometry Grid
- 5.6.2 Two-Dimensional Cask Pit Geometry Grid
- 5.6.3 Two-Dimensional Spent Fuel Pool Model - Temperature Contours
- 5.6.4 Two-Dimensional Spent Fuel Pool Model - Velocity Vectors
- 5.6.5 Two-Dimensional Cask Pit Model - Temperature Contours
- 5.6.6 Two-Dimensional Cask Pit Model - Velocity Vectors

- 6.4.1 Davis-Besse SFP and Cask Pit Time History Accelerogram (X-Direction, SSE)
- 6.4.2 Davis-Besse SFP and Cask Pit Time History Accelerogram (Y-Direction, SSE)
- 6.4.3 Davis-Besse SFP and Cask Pit Time History Accelerogram (Z-Direction, SSE)
- 6.5.1 Schematic of the Dynamic Model of a Single Rack Module Used in DYNARACK
- 6.5.2 Fuel-to-Rack Gap/Impact Elements at Level of Rattling Mass
- 6.5.3 Two Dimensional View of the Spring-Mass Simulation
- 6.5.4 Rack Degrees-of-Freedom with Shear and Bending Springs

Figures (continued)

- 6.5.5 Rack Periphery Gap/Impact Elements
- 6.5.6 Phase I Rack Layout
- 6.5.7 Phase II Rack Layout
- 6.5.8 Phase III Rack Layout
- 6.9.1 Bearing Pad Finite Element Model
- 6.9.2 Bearing Pad Analysis Concrete Compressive Stress
- 6.9.3 Bearing Pad Analysis Bearing Pad Stress
- 6.11.1 Rack Hydrodynamic Pressures
- 6.12.1 Welded Joint In Rack

- 7.2.1 Plan View of Shallow Drop@
- 7.2.2 Plan View of Deep Drop@ Scenario 1
- 7.2.3 Plan View of Deep Drop@ Scenario 2
- 7.4.1 Isometric of Shallow Drop@ Finite Element Model
- 7.4.2 Isometric of Scenario 1, A Shallow Drop@ Von Mises Stress
- 7.4.3 Isometric of Scenario 2, A Shallow Drop@ Von Mises Stress
- 7.4.4 Isometric of Over-Pedestal "Deep Drop" Finite Element Model
- 7.4.5 Over-Pedestal "Deep Drop" Pedestal Von Mises Stress
- 7.4.6 Over-Pedestal "Deep Drop" Bearing Pad Von Mises Stress
- 7.4.7 Over-Pedestal "Deep Drop" Liner Von Mises Stress
- 7.4.8 Over-Pedestal "Deep Drop" Concrete Von Mises Stress
- 7.4.9 Plan of On-Center Deep Drop@ Finite Element Model
- 7.4.10 On-Center "Deep Drop" Baseplate Von Mises Stress
- 7.4.11 On-Center "Deep Drop" Baseplate Plastic Strain
- 7.4.12 Isometric of On-Center Deep Drop@ Baseplate Deformation
- 7.4.13 "Heaviest Rack" Drop: Maximum Von Mises Stress - Liner
- 7.4.14 "Heaviest Rack" Drop: Maximum Vertical Stress - Concrete

- 8.1.1 Plan View of Cask Pit Area

The Davis-Besse Nuclear Power Station (DBNPS) Spent Fuel Pool (SFP) has not had enough storage capacity to allow full core offload capabilities since the discharge of Cycle 11 fuel in April, 1998. This report was prepared to support a license amendment to add temporary storage capacity to the DBNPS Unit 1 Cask Pit in order to regain full core offload capabilities for the current Fuel Cycle 12 and Fuel Cycle 13. The discussions and results of the design and analyses of the maximum density racks to be supplied by Holtec International are provided herein.

The Davis-Besse Nuclear Power Station is a single unit pressurized water reactor (PWR) facility located 21 miles east of Toledo near Oak Harbor, Ohio. The Babcock & Wilcox (B&W) Company designed the nuclear steam supply system. The facility, capable of an electrical output of 873 net Megawatts-electric, received its operating license from the NRC in April 1977, and commenced commercial operations in January 1978.

The new maximum storage rack array proposed for the DBNPS Unit 1 Cask Pit is shown in the plan views provided by Figures 1.1, 1.2, and 1.3. Figure 1.1 shows the completion of the first phase of the rack installation effort by placing one rack in the Cask Pit to regain full core offload storage capacity for the current Fuel Cycle 12 operation, which is scheduled to be completed in April, 2000. A complete offload of the reactor core in April 2000 is necessary to complete the required 10-year In-Service-Inspection of the reactor vessel. Figure 1.2 shows the completion of the second phase of the rack installation effort by placing an additional rack in the Cask Pit to maintain full core offload storage capacity for Fuel Cycle 13 operation, scheduled to occur between May, 2000 and April, 2002. Installation phases one and two were completed in April 1999 as a plant modification, after evaluation in accordance with 10CFR50.59 demonstrated that installation of two empty racks did not involve an unreviewed safety question. These two racks will remain unused until a license amendment is approved by the United States Nuclear Regulatory Commission (USNRC). The final phase is the installation of two additional racks as shown in Figure 1.3 in order to support the necessary fuel movements that would be required in a full SFP rack replacement effort. It is expected that these two racks will be installed during a

future re-rack effort, which is presently planned for completion during Fuel Cycle 13. These four racks will be emptied and relocated to the SFP during the latter stages of the SFP re-rack. This licensing submittal addresses only the installation and the use of these four racks in the DBNPS Unit 1 Cask Pit.

The new Holtec racks are freestanding and self-supporting. The principal construction materials for the new racks are ASME SA-240-Type 304 stainless steel sheet and plate stock, and ASME SA-564-630 (precipitation hardened stainless steel) for the adjustable support spindles. The only non-stainless material utilized in the rack is the neutron absorber material, which is a boron carbide and aluminum-composite sandwich available under the patented product name Boral™.

The new Holtec racks are designed to the stress limits of, and analyzed in accordance with, Section III, Division 1, Subsection NF of the American Society of Mechanical Engineers (ASME) Boiler and Pressure Vessel (B&PV) Code [1]. The material procurement, analysis, and fabrication of the rack modules conform to 10CFR50 Appendix B requirements.

The rack design and analysis methodologies employed in the storage capacity expansion are a direct evolution of previous re-rack license applications. This Design and Licensing Report documents the design and analyses performed to demonstrate that the new Holtec supplied racks meet all governing requirements of the applicable codes and standards. This report also documents that the racks meet the USNRC "OT Position for Review and Acceptance of Spent Fuel Storage and Handling Applications", and the addendum thereto [2].

Sections 2 and 3 of this report provide an abstract of the design and material information on the new racks.

The criticality safety analysis requires that the neutron multiplication factor for the stored fuel array be bounded by the USNRC k_{eff} limit of 0.95 under assumptions of 95% probability and 95% confidence. The criticality safety analysis provided in Section 4 sets the requirements on

the Boral panel length and the amount of B^{10} per unit area (i.e., loading density) of the Boral panel for the new high density racks.

Thermal-hydraulic considerations require that the fuel cladding will not fail due to excessive temperature, and that the steady state pool bulk temperature will remain within the limits prescribed for the cask pit and spent fuel pool to satisfy the pool structural strength, operational, and regulatory requirements. The thermal-hydraulic analyses carried out in support of this storage expansion effort are described in Section 5.

Rack module structural analysis requires that the primary stresses in the rack module structure will remain below the ASME B&PV Code (Subsection NF) [1] allowables. Demonstrations of seismic and structural adequacy are presented in Section 6.0. The structural qualification also requires that the subcriticality of the stored fuel will be maintained under all postulated accident scenarios. The structural consequences of these postulated accidents are evaluated and presented in Section 7 of this report.

Section 8 contains the structural analysis to demonstrate the adequacy of the Cask Pit reinforced concrete structure. A synopsis of the geometry of the reinforced concrete structure is also presented in Section 8.

The radiological considerations are documented in Section 9.0. Sections 10, and 11, respectively, discuss the salient considerations in the installation of the new racks, and a cost/benefit and environmental assessment to establish the superiority of the wet storage expansion option.

All computer programs utilized to perform the analyses documented in this Design and Licensing Report are benchmarked and verified. These programs have been utilized by Holtec International in numerous re-rack license applications over the past decade.

The analyses presented herein clearly demonstrate that the rack module arrays possess wide margins of safety in respect to all considerations of safety specified in the OT Position Paper [2], namely, nuclear subcriticality, thermal-hydraulic safety, seismic and structural adequacy, radiological compliance, and mechanical integrity.

1.1 References

- [1] American Society of Mechanical Engineers (ASME), Boiler & Pressure Vessel Code, Section III, 1986 Edition, including up to 1988 addenda, Subsection NF, and Appendices.
- [2] USNRC, "OT Position for Review and Acceptance of Spent Fuel Storage and Handling Applications," April 14, 1978, and Addendum dated January 18, 1979.

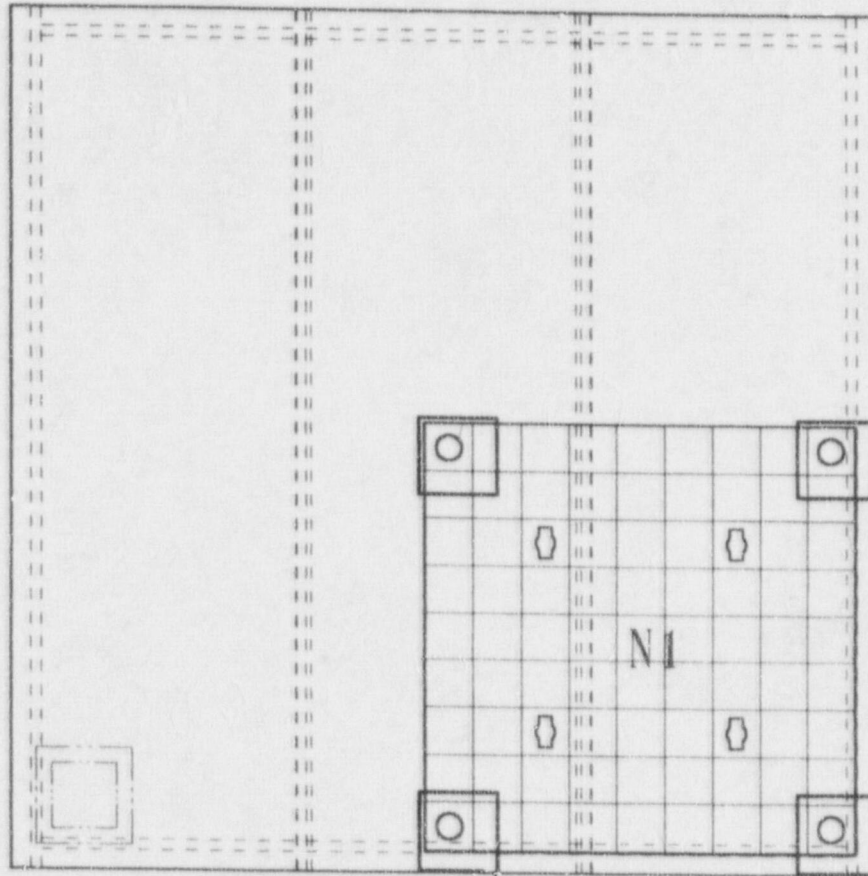


FIGURE 1.1; CASK PIT LAYOUT - PHASE 1

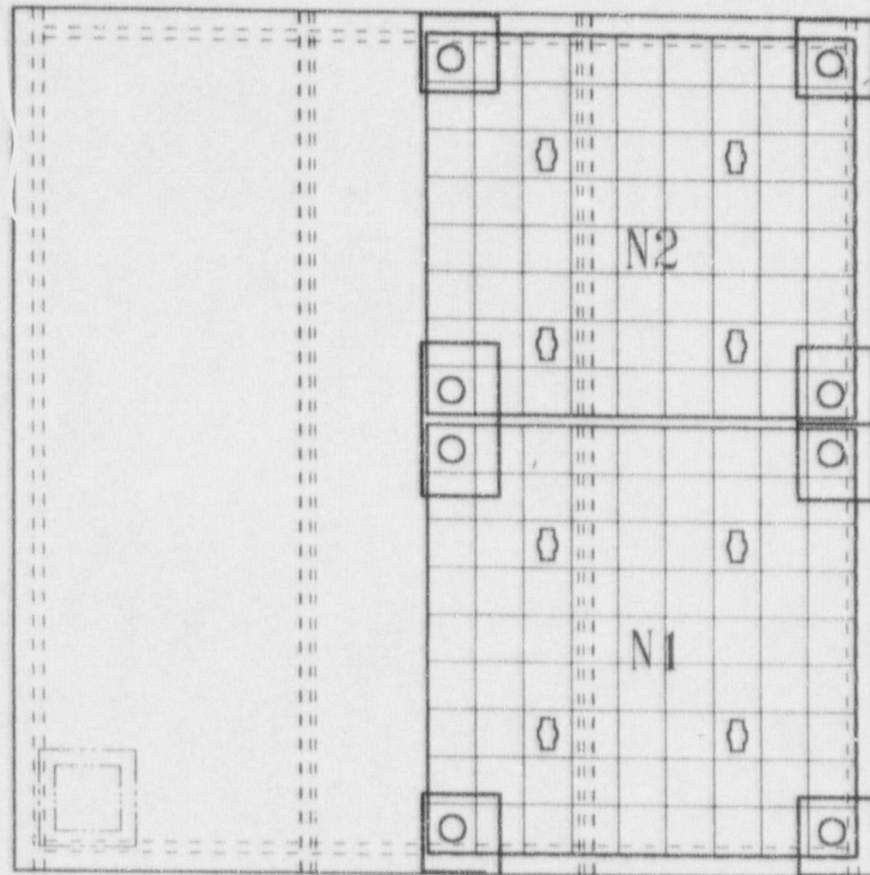


FIGURE 1.2; CASK PIT LAYOUT - PHASE 2

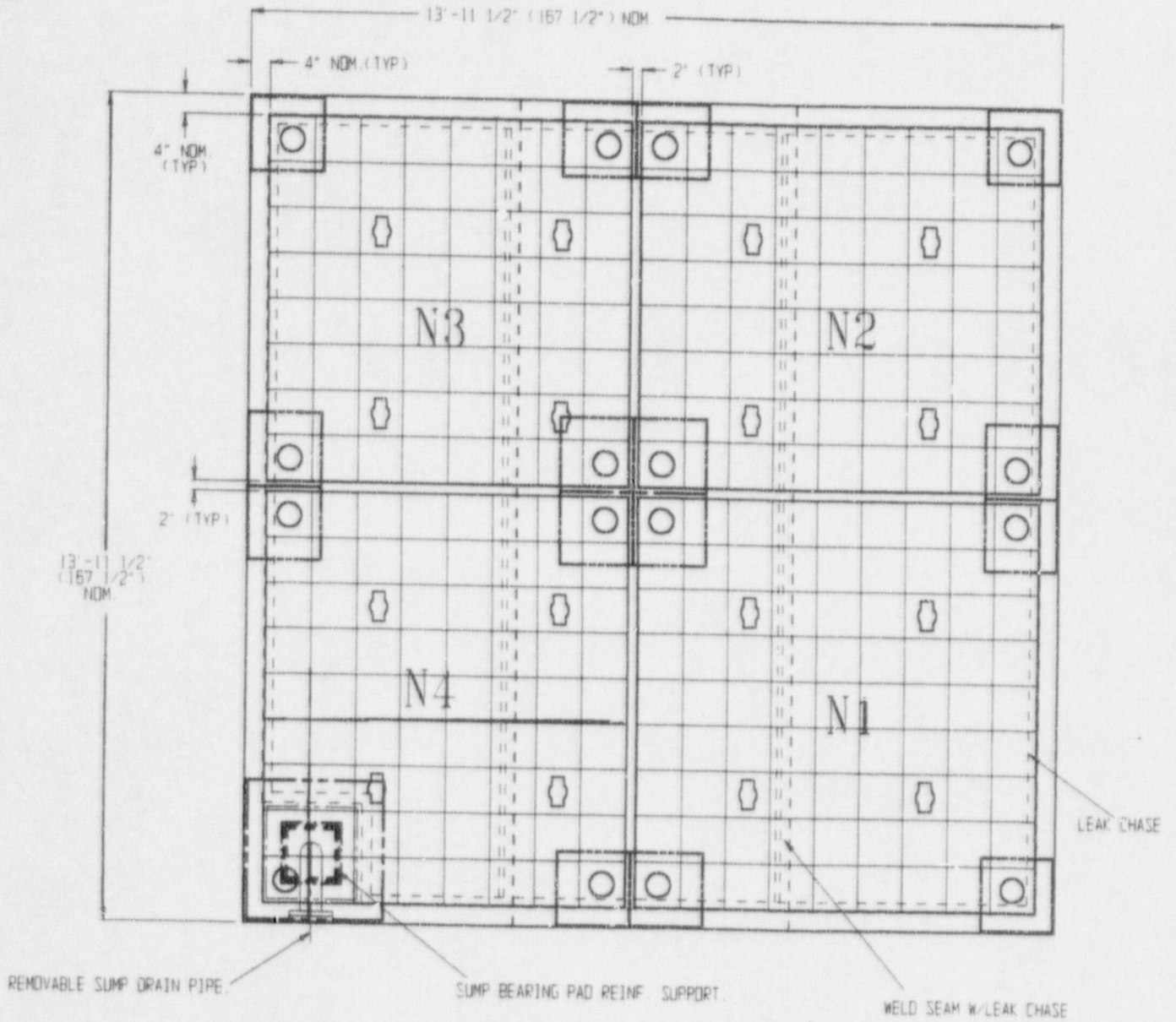


FIGURE 1.3; CASK PIT LAYOUT - PHASE 3

2.0 OVERVIEW OF THE PROPOSED CAPACITY EXPANSION

2.1 Introduction

In its fully implemented configuration, the DBNPS Cask Pit will contain four racks with a total cell count of 289 cells. All storage rack arrays will consist of free-standing modules, made primarily from Type 304 austenitic stainless steel containing honeycomb storage cells interconnected through longitudinal welds. A panel of Boral cermet containing a high areal loading of the Boron-10 (B-10) isotope provides appropriate neutron attenuation between adjacent storage cells. Figure 2.1 provides a schematic of the typical storage rack module. Data on the cross sectional dimensions, weight and cell count for each rack module in the cask pit are presented in Table 2.1.1.

Since the new rack modules will not utilize flux traps between storage cells, in wet storage technology terminology, they are referred to as Region 2 style racks. The baseplates on all rack modules extend out beyond the rack module periphery wall such that the plate protrusions act to set a required minimum separation between the facing cells in adjacent rack modules. This separation between rack modules serves to establish a "flux trap" space between the peripheral cells of adjacent modules. In other words, although there is a single panel of neutron absorber between any two fuel assemblies stored in the same rack, there are two poison panels with a specified water flux trap between them, separating fuel assemblies located in the cells of two facing rack modules.

Each new rack module is supported by a minimum of four pedestals, which are remotely adjustable. Thus, the racks can be made vertical and the top of the racks can easily be made co-planar with each other. The rack module support pedestals are engineered to accommodate minor level variations in the pool floor flatness.

Between the rack module pedestals and the Cask Pit liner is a bearing pad, which serves to diffuse the dead load of the loaded racks into the reinforced concrete structure of the pool slab.

The overall design of the rack modules is similar to those presently in service in the spent fuel pools at many other nuclear plants, among them Donald C. Cook of American Electric Power, and Connecticut Yankee of Northeast Utilities. Altogether, over 50 thousand storage cells of this design have been provided by Holtec International to various nuclear plants around the world.

2.2 Summary of Principal Design Criteria

The key design criteria for the new spent fuel racks are set forth in the USNRC memorandum entitled "OT Position for Review and Acceptance of Spent Fuel Storage and Handling Applications", dated April 14, 1978 as modified by amendment dated January 18, 1979. The individual sections of this report expound on the specific design bases derived from the above-mentioned "OT Position Paper". A brief summary of the design bases for the Cask Pit racks are summarized in the following:

- a. Disposition: All new rack modules are required to be freestanding.
- b. Kinematic Stability: All freestanding modules must be kinematically stable (against tipping or overturning) if a seismic event is imposed on any module.
- c. Structural Compliance: All primary stresses in the rack modules must satisfy the limits postulated in Section III subsection NF of the 1986 ASME B & PV Code.
- d. Thermal-Hydraulic Compliance: The spatial average bulk pool temperature is required to remain under 140°F in the wake of a partial offload, with two SFP Cooling System trains in operation.
- e. Criticality Compliance: Region 2 cells must be able to store the Zircaloy clad fuel of 5.05 weight percent (w/o) nominal enrichment and 53.51 GWD/MTU burnup while maintaining the reactivity less than 0.95.

- f. Radiological Compliance: The re-racking must not lead to a violation of the off-site dose limits, or adversely affect the area dose environment as set forth in the DBNPS Updated Safety Analysis Report (USAR). The radiological implications of the installation of the new racks also need to be ascertained and deemed to be acceptable.
- g. Cask Pit Structure: The ability of the reinforced concrete structure to satisfy the load combinations set forth in the DBNPS USAR must be demonstrated.
- h. Liner Integrity: The integrity of the liner under cyclic in-plane loading during a seismic event must be demonstrated.
- i. Bearing Pads: The bearing pad size and thickness must ensure that the pressure on the liner continues to satisfy the American Concrete Institute (ACI) limits during and after a design basis seismic event.
- j. Accident Events: In the event of postulated drop events (uncontrolled lowering of a fuel assembly, for instance), it is necessary to demonstrate that the subcritical geometry of the rack structure is not compromised.
- k. Construction Events: The field construction services required to be carried out for executing the rack installation must be demonstrated to be within the "state of the proven art".

The foregoing design bases are further articulated in Sections 4 through 9 of this licensing report.

2.3 Applicable Codes and Standards

The following codes, standards and practices are used as applicable for the design, construction, and assembly of the fuel storage racks. Additional specific references related to detailed analyses are given in each section.

a. Design Codes

- (1) American Institute of Steel Construction (AISC) Manual of Steel Construction, 8th Edition, 1980.
- (2) American National Standards Institute (ANSI) N210-1976, "Design Objectives for Light Water Reactor Spent Fuel Storage Facilities at Nuclear Power Stations" (contains guidelines for fuel rack design).
- (3) ASME B & PV Code Section III, 1986 Edition, up to and including 1988 Addenda; ASME Section VIII, 1986 Edition; ASME Section IX, latest version.
- (4) American Society for Nondestructive Testing SNT-TC-1A June, 1980 Recommended Practice for Personnel Qualifications and Certification in Non-destructive Testing.
- (5) American Concrete Institute Building Code Requirements for Reinforced Concrete (ACI 318-63).
- (6) Code Requirements for Nuclear Safety Related Concrete Structures, ACI 349-85/ACI 349R-85, and ACI 349.1R-80.
- (7) ASME Y14.5M, Dimensioning and Tolerancing
- (8) ACI Detailing Manual - 1980.
- (9) ASME B & PV Code, Section II-Parts A and C, 1986 Edition up to and including 1988 Addenda.
- (10) ASME B & PV Code NCA3800 - Metallic Material Organization's Quality System Program.

b. Standards of American Society for Testing and Materials (ASTM)

- (1) ASTM E165 - Standard Test Method for Liquid Penetrant Examination.

- (2) ASTM A240 - Standard Specification for Heat-Resisting Chromium and Chromium-Nickel Stainless Steel Plate, Sheet and Strip for Pressure Vessels.
- (3) ASTM A262 - Standard Practices for Detecting Susceptibility to Intergranular Attack in Austenitic Stainless Steel.
- (4) ASTM A276 - Standard Specification for Stainless Steel Bars and Shapes.
- (5) ASTM A479 - Standard Specification for Stainless Steel Bars and Shapes for use in Boilers and other Pressure Vessels.
- (6) ASTM A564 - Standard Specification for Hot-Rolled and Cold-Finished Age-Hardening Stainless Steel Bars and Shapes.
- (7) ASTM C750 - Standard Specification for Nuclear-Grade Boron Carbide Powder.
- (8) ASTM A380 - Standard Practice for Cleaning, Descaling, and Passivation of Stainless Steel Parts, Equipment and Systems.
- (9) ASTM C992 - Standard Specification for Boron-Based Neutron Absorbing Material Systems for Use in Nuclear Spent Fuel Storage Racks.
- (10) ASTM E3 - Standard Practice for Preparation of Metallographic Specimens.
- (11) ASTM E190 - Standard Test Method for Guided Bend Test for Ductility of Welds.

c. Welding Code:

ASME B & PV Code, Section IX - Welding and Brazing Qualifications, latest version.

d. Quality Assurance, Cleanliness, Packaging, Shipping, Receiving, Storage, and Handling

- (1) ANSI N45.2.1 - Cleaning of Fluid Systems and Associated Components during Construction Phase of Nuclear Power Plants - 1973 (R.G. 1.37).
- (2) ANSI N45.2.2 - Packaging, Shipping, Receiving, Storage and Handling of Items for Nuclear Power Plants - 1972 (R.G. 1.38).
- (3) ANSI N45.2.6 - Qualifications of Inspection, Examination, and Testing Personnel for the Construction Phase of Nuclear Power Plants - 1978 (Regulatory Guide 1.58).

- (4) ANSI N45.2.8 - Supplementary Quality Assurance Requirements for Installation, Inspection and Testing of Mechanical Equipment and Systems for the Construction Phase of Nuclear Plants - 1975 (R.G. 1.116).
- (5) ANSI N45.2.11 - Quality Assurance Requirements for the Design of Nuclear Power Plants - 1974 (R.G. 1.64).
- (6) ANSI N45.2.12 - Requirements for Auditing of Quality Assurance Programs for Nuclear Power Plants - 1977 (R.G. 1.144).
- (7) ANSI N45.2.13 - Quality Assurance Requirements for Control of Procurement of Items and Services for Nuclear Power Plants - 1976 (R. G. 1.123).
- (8) ANSI N45.2.23 - Qualification of Quality Assurance Program Audit Personnel for Nuclear Power Plants - 1978 (R.G. 1.146).
- (9) ASME B & PV Code, Section V, Nondestructive Examination, latest version.
- (10) ANSI N16.9-75 - Validation of Calculation Methods for Nuclear Criticality Safety.

e. USNRC Documents

- (1) "OT Position for Review and Acceptance of Spent Fuel Storage and Handling Applications," dated April 14, 1978, and the modifications to this document of January 18, 1979.
- (2) NUREG 0612, "Control of Heavy Loads at Nuclear Power Plants", USNRC, Washington, D.C., July, 1980.

f. Other ANSI Standards (not listed in the preceding)

- (1) ANSI/ANS 8.1 - Nuclear Criticality Safety in Operations with Fissionable Materials Outside Reactors.
- (2) ANSI/ANS 8.17 - Criticality Safety Criteria for the Handling, Storage, and Transportation of LWR Fuel Outside Reactors.
- (3) ANSI N45.2 - Quality Assurance Program Requirements for Nuclear Power Plants - 1977.
- (4) ANSI N45.2.9 - Requirements for Collection, Storage and Maintenance of Quality Assurance Records for Nuclear Power Plants - 1974.

- (5) ANSI N45.2.10 - Quality Assurance Terms and Definitions - 1973.
- (6) ANSI N14.6 - American National Standard for Special Lifting Devices for Shipping Containers Weighing 10,000 pounds (4500 kg) or more for Nuclear Materials - 1978.
- (7) ANSI/ASME N626-3 - Qualification and Duties of Specialized Professional Engineers.

g. Code-of-Federal Regulations (CFR)

- (1) 10CFR20 - Standards for Protection Against Radiation.
- (2) 10CFR21 - Reporting of Defects and Non-compliance.
- (3) 10CFR50 Appendix A - General Design Criteria for Nuclear Power Plants.
- (4) 10CFR50 Appendix B - Quality Assurance Criteria for Nuclear Power Plants and Fuel Reprocessing Plants.
- (5) 10CFR61 - Licensing Requirements for Land Disposal of Radioactive Waste.
- (6) 10CFR71 - Packaging and Transportation of Radioactive Material.

h. Regulatory Guides (RG)

- (1) RG 1.13 - Spent Fuel Storage Facility Design Basis (Revision 2 Proposed).
- (2) RG 1.25 - Assumptions Used for Evaluating the Potential Radiological Consequences of a Fuel Handling Accident in the Fuel Handling and Storage Facility for Boiling and Pressurized Water Reactors, Rev. 0 - March, 1972.
- (3) RG 1.28 - Quality Assurance Program Requirements - Design and Construction, Rev. 2 - February, 1979 (endorses ANSI N45.2).
- (4) RG 1.29 - Seismic Design Classification, Rev. 2 - February, 1976.
- (5) RG 1.31 - Control of Ferrite Content in Stainless Steel Weld Metal.
- (6) RG 1.38 - Quality Assurance Requirements for Packaging, Shipping, Receiving, Storage and Handling of Items for Water-Cooled Nuclear Power Plants, Rev. 2 - May, 1977 (endorses ANSI N45.2.2).

- (7) RG 1.44 - Control of the Use of Sensitized Stainless Steel.
- (8) RG 1.58 - Qualification of Nuclear Power Plant Inspection, Examination, and Testing Personnel, Rev. 1 - September 1980 (endorses ANSI N45.2.6).
- (9) RG 1.61 - Damping Values for Seismic Design of Nuclear Power Plants, Rev. 0, 1973.
- (10) RG 1.64 - Quality Assurance Requirements for the Design of Nuclear Power Plants, Rev. 2 - June, 1976 (endorses ANSI N45.2.11).
- (11) RG 1.71 - Welder Qualifications for Areas of Limited Accessibility.
- (12) RG 1.74 - Quality Assurance Terms and Definitions, Rev. 2 - February, 1974 (endorses ANSI N45.2.10).
- (13) RG 1.85 - Materials Code Case Acceptability - ASME Section III, Division 1.
- (14) RG 1.88 - Collection, Storage and Maintenance of Nuclear Power Plant Quality Assurance Records, Rev. 2 - October, 1976 (endorses ANSI N45.2.9).
- (15) RG 1.92 - Combining Modal Responses and Spatial Components in Seismic Response Analysis, Rev. 1 - February, 1976.
- (16) RG 1.116 - Quality Assurance Requirements for Installation, Inspection and Testing of Mechanical Equipment and Systems, Rev. 0-R - May, 1977 (endorses ANSI N45.2.8-1975)
- (17) RG 1.123 - Quality Assurance Requirements for Control of Procurement of Items and Services for Nuclear Power Plants, Rev. 1 - July, 1977 (endorses ANSI N45.2.13).
- (18) RG 1.124 - Service Limits and Loading Combinations for Class 1 Linear-Type Component Supports, Revision 1, January, 1978.
- (19) RG 1.144 - Auditing of Quality Assurance Programs for Nuclear Power Plants, Rev. 1 - September, 1980 (endorses ANSI N45.2.12-1977)
- (20) RG 3.4 - Nuclear Criticality Safety in Operations with Fissionable Materials at Fuels and Materials Facilities.
- (21) RG 8.8 - Information Relative to Ensuring that Occupational Radiation Exposures at Nuclear Power Stations will be as Low as Reasonably Achievable (ALARA).

- (22) IE Information Notice 83-29 - Fuel Binding Caused by Fuel Rack Deformation.
- (23) RG 8.38 - Control of Access to High and Very High Radiation Areas in Nuclear Power Plants, June, 1993.

i. Branch Technical Position

- (1) CPB 9.1-1 - Criticality in Fuel Storage Facilities.
- (2) APCS 9-2 - Residual Decay Energy for Light-Water Reactors for Long-Term Cooling - November, 1975.

j. American Welding Society (AWS) Standards

- (1) AWS D1.1 - Structural Welding Code - Steel.
- (2) AWS D1.3 - Structure Welding Code - Sheet Steel.
- (3) AWS D9.1 - Sheet Metal Welding Code.
- (4) AWS A2.4 - Standard Symbols for Welding, Brazing and Nondestructive Examination.
- (5) AWS A3.0 - Standard Welding Terms and Definitions.
- (6) AWS A5.12 - Specification for Tungsten and Tungsten Alloy Electrodes for Arc-welding and Cutting
- (7) AWS QC1 - Standard for AWS Certification of Welding Inspectors.

2.4 Quality Assurance Program

The governing quality assurance requirements for fabrication of the spent fuel racks are stated in 10CFR50 Appendix B. Holtec's Nuclear Quality Assurance program has been reviewed and approved by the DBNPS Nuclear Assurance Department. This program is designed to provide a flexible but highly controlled system for the design, analysis and licensing of customized components in accordance with various codes, specifications, and regulatory requirements.

The manufacturing of the racks will be carried out by Holtec's designated manufacturer, U.S. Tool & Die, Inc. (UST&D). The Quality Assurance system enforced on the manufacturer's shop floor shall

provide for all controls necessary to fulfill all quality assurance requirements. UST&D has manufactured high-density racks for over 60 nuclear plants around the world. UST&D has been audited by the nuclear industry group Nuclear Procurement Issues Committee (NUPIC), and the Quality Assurance branch of the USNRC Office of Nuclear Material Safety and Safeguards (NMSS) with satisfactory results.

The Quality Assurance System that will be used by Holtec to install the racks is also controlled by the Holtec Nuclear Quality Assurance Manual and by the DBNPS site-specific requirements.

2.5 Mechanical Design

The rack modules are designed as cellular structures such that each fuel assembly has a square opening with conforming lateral support and a flat horizontal-bearing surface. All of the storage locations are constructed with multiple cooling flow holes to ensure that redundant flow paths for the coolant are available. The basic characteristics of the spent fuel racks are summarized in Table 2.5.1.

A central objective in the design of the new rack modules is to maximize structural strength while minimizing inertial mass and dynamic response. Accordingly, the rack modules have been designed to simulate multi-flange beam structures resulting in excellent de-tuning characteristics with respect to the applicable seismic events. The next subsection presents an item-by-item description of the rack modules in the context of the fabrication methodology.

2.6 Rack Fabrication Methods

The object of this section is to provide a brief description of the rack module construction activities, which enable an independent appraisal of the adequacy of design. The pertinent methods used in manufacturing the high-density storage racks may be stated as follows:

1. The rack modules are fabricated in such a manner that the storage cell surfaces, which would come in contact with the fuel assembly, will be free of harmful chemicals and projections (e.g., weld splatter).
2. The component connection sequence and welding processes are selected to reduce fabrication distortions.
3. The fabrication process involves operational sequences that permit immediate accessibility for verification by the inspection staff.
4. The racks are fabricated per the UST&D Appendix B Quality Assurance program, which ensures, and documents, that the fabricated rack modules meet all of the requirements of the design and fabrication documents.

2.7 Rack Module Description

The composite box assembly, the baseplate, and the support pedestals constitute the principal components of the fuel rack modules. The following description provides details of all of the major rack components.

- i. Composite box subassembly: The rack module manufacturing begins with fabrication of the "box" from ASME SA-240-304 stainless steel. The boxes are fabricated from two precision formed channels by seam welding in a machine equipped with copper chill bars and pneumatic clamps to minimize distortion due to welding heat input. The minimum weld penetration is 80% of the box metal gage. This process results in a square cross section box, as shown in Figure 2.2. The clear inside nominal dimension of the PWR box cell is 9.0".

Sheathing of ASME SA-240-304 stainless steel is attached to each side of the box with the poison material installed in the sheathing cavity. The sheathing design objective calls

for securing Boral to the box surface. This is accomplished by die forming the internal and external boral sheathings to provide end flares with smooth edges, as shown in Figure 2.3. The flanges of the sheathing are welded to the box using skip welds and spot welds. The sheathings serve to locate and position the poison sheet accurately, and to preclude its movement under seismic conditions. The sheathing also isolates the Boral from the fuel assembly.

The square cross section box with Boral panels affixed to its external surfaces is referred to as the "composite box assembly". Each composite box has at least two one inch diameter lateral holes punched near its bottom edge to provide auxiliary flow holes. For those cells located over support legs, four flow holes are required to compensate for the loss of the baseplate flow holes described below.

The composite boxes are arranged in a checkerboard array and welded edge-to-edge to form an assemblage of storage cell locations, as shown in Figure 2.4. Austenitic stainless steel corner welds connect the storage cells to each other. The extent of welding is selected to "detune" the racks from the stipulated seismic input motion. Filler panels and corner angles are welded to the edges of boxes at the outside boundary of the rack to complete the formation of the peripheral cells. The inter-box welding and pitch adjustment is accomplished by small longitudinal connectors. The connectors are sized and placed to ensure that the 9.0" inside cell clear dimension on developed boxes is maintained after inclusion of any reductions from the sheathing. This assemblage of box assemblies results in a honeycomb structure with axial, flexural and torsional rigidity depending on the extent of intercell welding provided. It can be seen from Figure 2.4 that all four corners of each interior box are connected to the contiguous boxes resulting in a well-defined path for "shear flow".

- ii. Baseplate: A 3/4 inch thick baseplate of ASME SA-240-304 provides a continuous horizontal surface for supporting the fuel assemblies. The baseplate has a 5 inch diameter hole in each cell location, except at lift locations. For the four lift locations, the flow

holes are a 3.12 inch diameter hole with a coincidental 2.625 inch by 5.125 inch slot to allow insertion and engagement of the lifting rig. The location of all baseplate holes coincide with the cell centerlines. The baseplate is attached to the base of the cell assemblage by fillet welds and extends horizontally approximately 1" beyond the periphery of the rack cell assemblage at locations where racks interface. The baseplate extensions beyond rack edges, located around the periphery of the Cask Pit, vary between ¼" and 1"

- iii. The neutron absorber material: As mentioned in the preceding section, Boral is used as the neutron absorber material. Each storage cell side is equipped with one integral Boral sheet (poison material).
- iv. Sheathing: As described earlier, the sheathing serves as the locator and retainer of the poison material and isolates the Boral from the fuel assembly.
- v. Support Pedestals: All support pedestals are the adjustable type as shown in Figure 2.5. The 10 inch square top (female threaded) portion is made of austenitic steel material. The bottom (male threaded) part is made of ASME SA-564-630 (17:4 Ph series) stainless steel to avoid galling problems. Each support pedestal is equipped with a readily accessible socket to enable remote leveling of the rack after its placement in the pool. The support pedestals are located at the centerlines of cells to ensure accessibility of the leveling tool through the 5 inch diameter flow hole in the baseplate.

The assembly of the rack modules is carried out by welding the composite boxes in a vertical fixture with the baseplate serving as the bottom positioner.

An elevation view of the PWR storage cell is shown in Figure 2.6.

TABLE 2.1.1: GEOMETRIC AND PHYSICAL DATA FOR HIGH DENSITY RACKS

MODULE I.D.	NO. OF CELLS		MODULE ENVELOPE SIZE		WEIGHT (lbs)	NO. OF CELLS PER RACK
	N-S Direction	E-W Direction	N-S	E-W		
	N1	9	9	83.355"		
N2	9	8	83.355"	74.135"	10,800	72
N3	8	8	74.135"	74.135"	9,500	64
N4	8	9	74.135"	83.355"	10,800	72

Table 2.5.1

MODULE DATA FOR SPENT FUEL RACKS *

Storage cell inside nominal dimension	9.0 in.
Cell pitch	9.22 in.
Storage cell height (above the plate)	161.625 in.
Baseplate hole size (away from pedestal)	5.0 in. **
Baseplate thickness	0.75 in.
Support pedestal height	4.25 in.
Support pedestal type	Remotely adjustable pedestals
Number of support pedestals	4
Number of cell walls containing 3/4" diameter supplemental flow holes at base for cells located away from pedestals	2
Number of cell walls containing 3/4" diameter flow holes at base for cells located above pedestals	4
Remote lifting and handling provisions	Yes
Poison material	Boral
Poison length	148 in.
Poison width	7.5 in.

* All dimensions provide nominal values

** Except at lifting locations

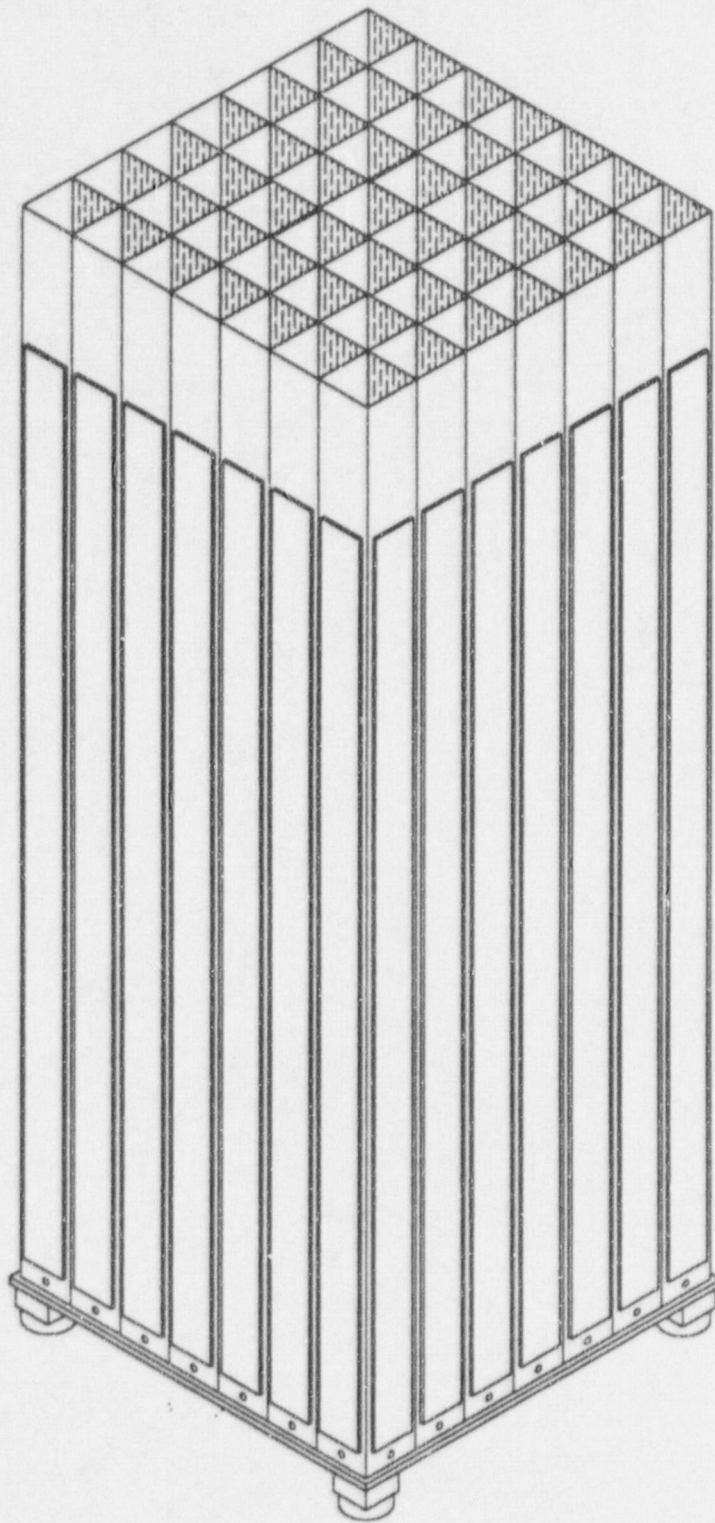


FIGURE 2.1; SCHEMATIC OF TYPICAL DAVIS-BESSE RACK STRUCTURE

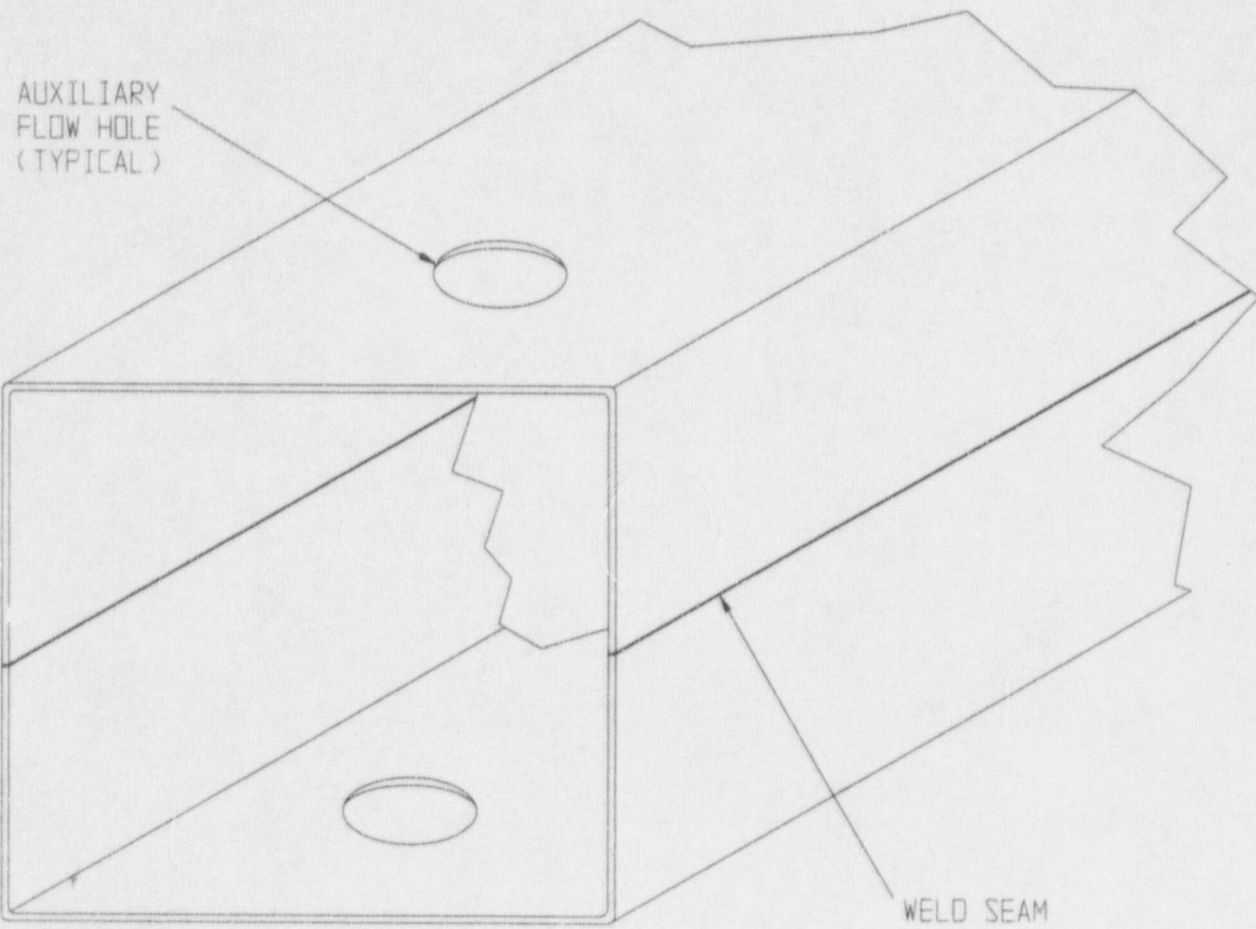


FIGURE 2.2; SEAM WELDED PRECISION FORMED CHANNELS

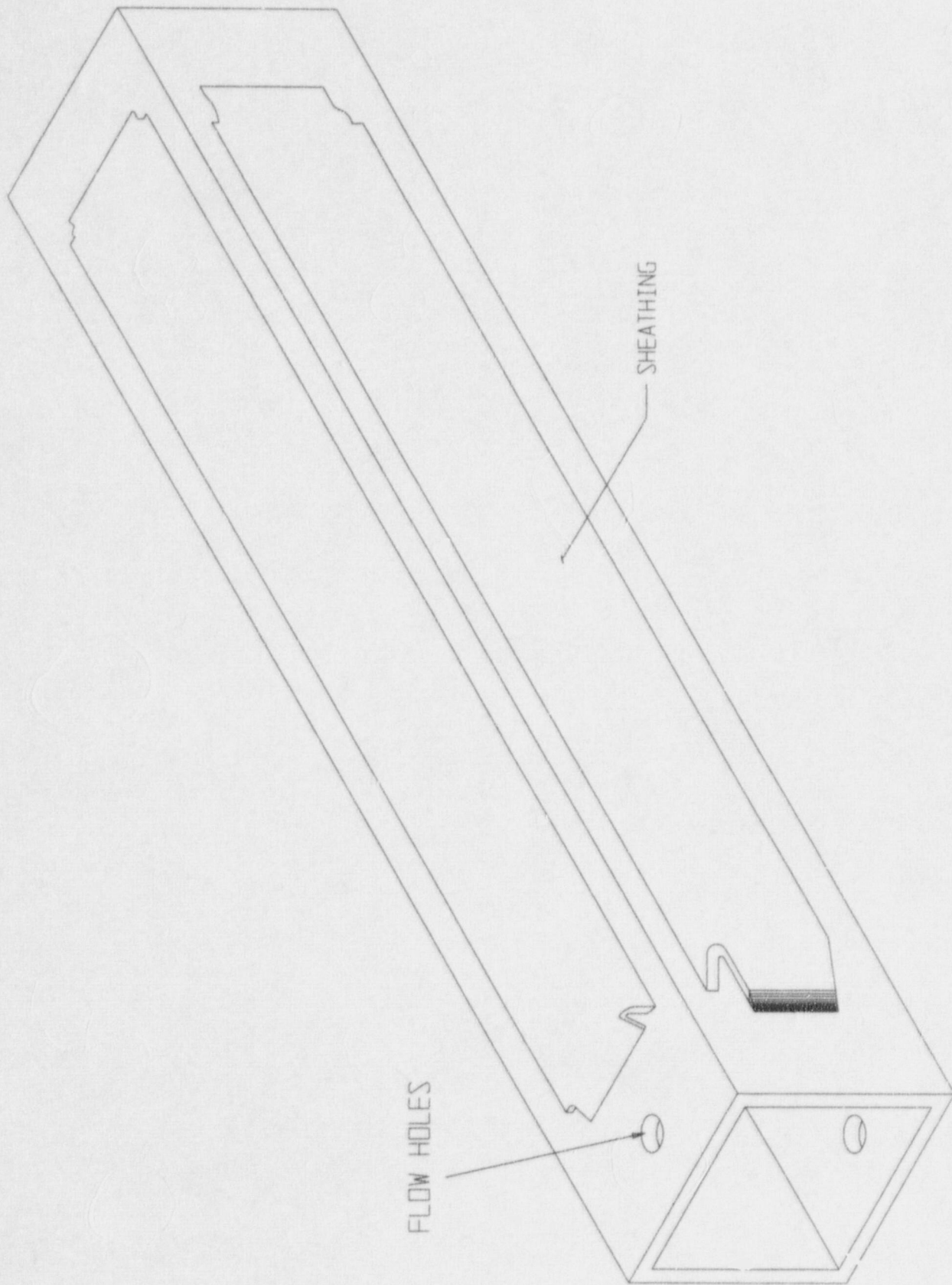


FIGURE 2.3; COMPOSITE BOX ASSEMBLY

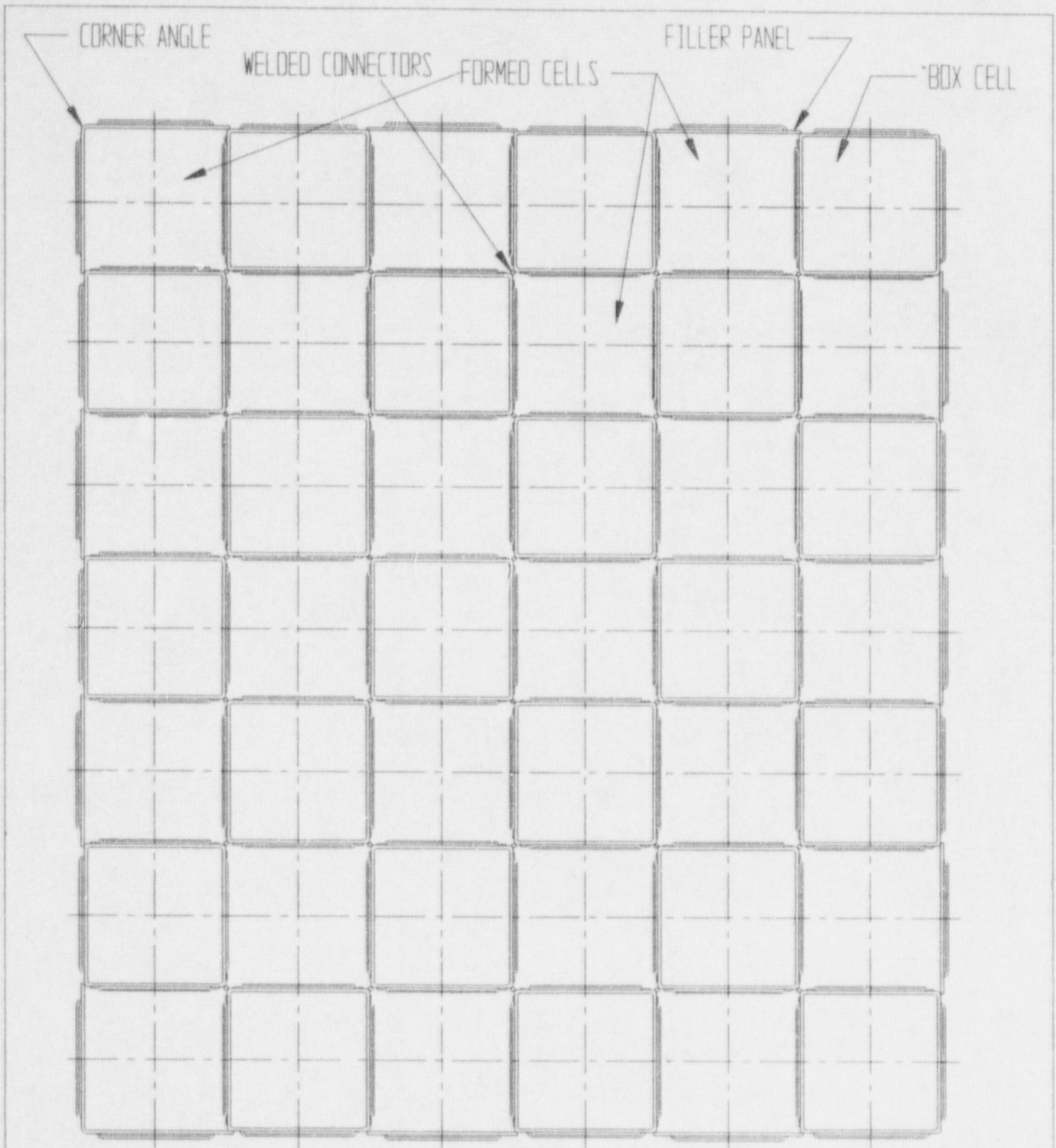


FIGURE 2.4; TYPICAL ARRAY OF STORAGE CELLS
(NON-FLUX TRAP CONSTRUCTION)

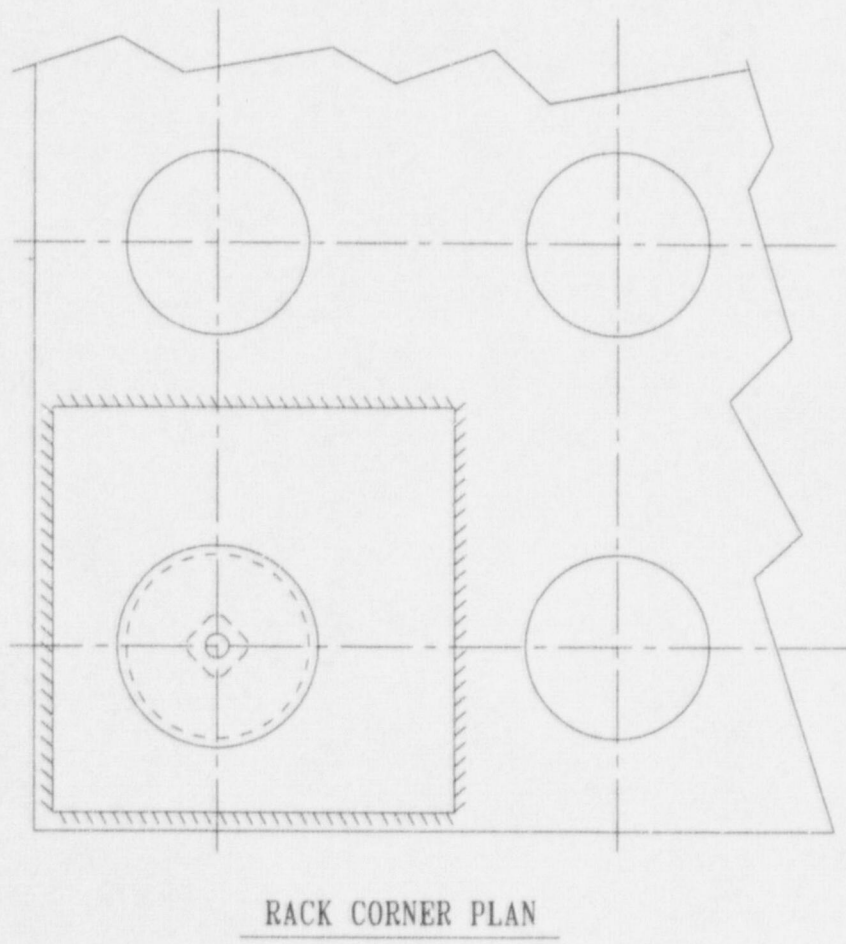
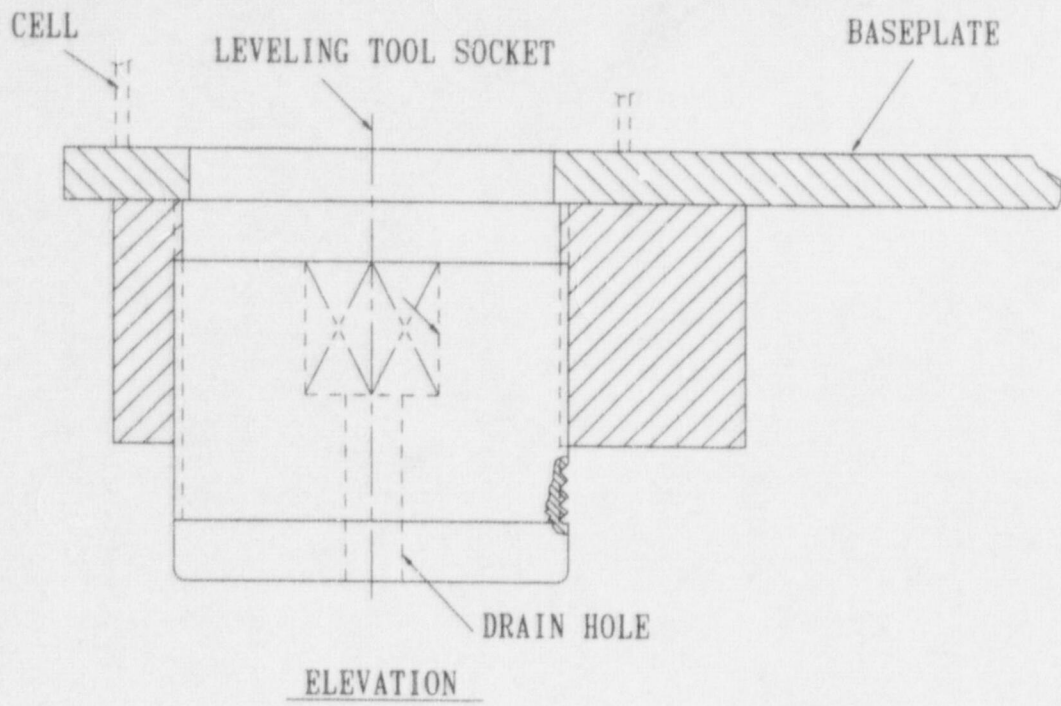


FIGURE 2.5; SUPPORT PEDESTAL FOR HOLTEC PWR RACK

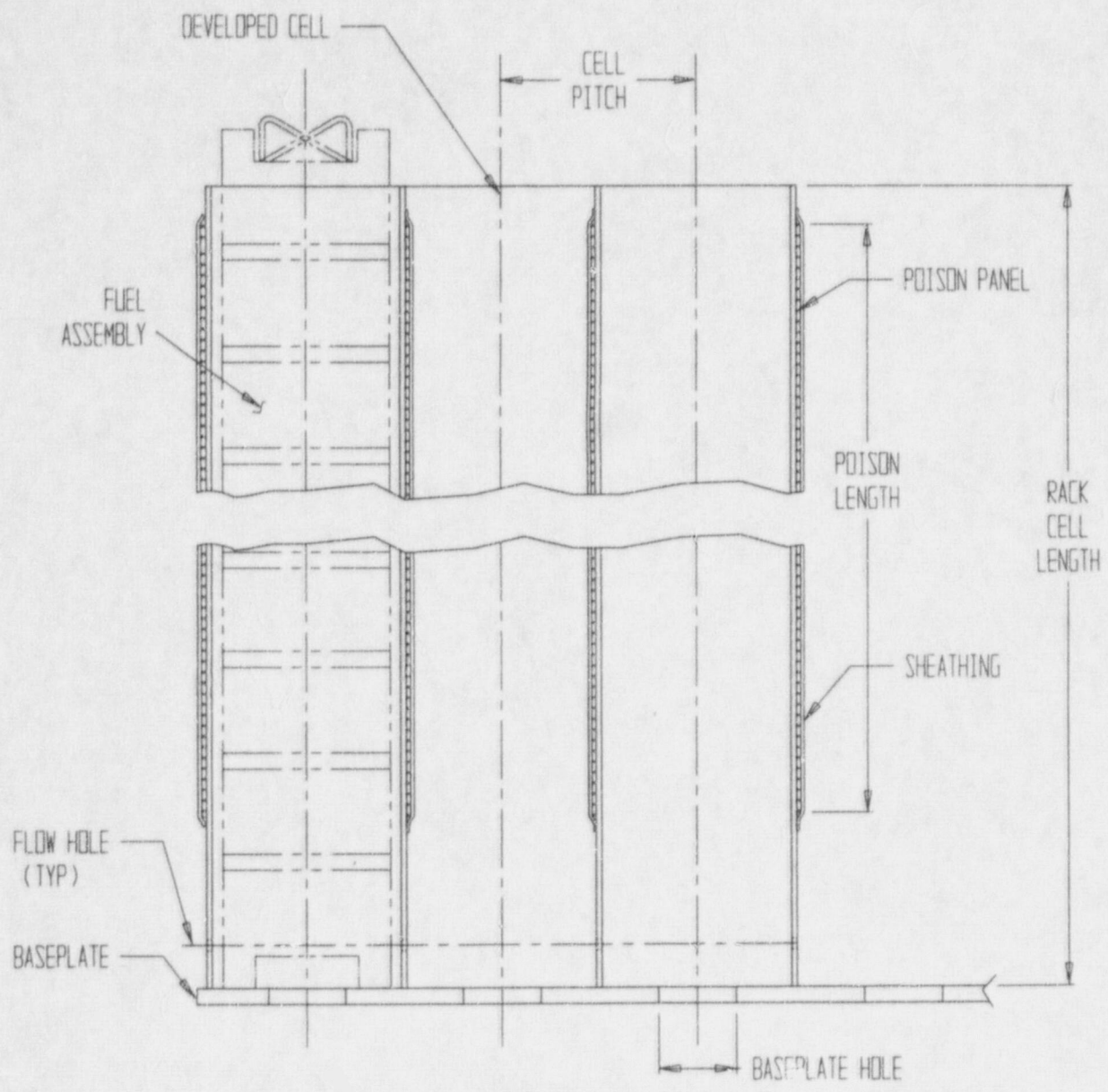


FIGURE 2.6: THREE PWR CELLS IN ELEVATION VIEW

HI981933

3.0 MATERIAL, HEAVY LOAD, AND CONSTRUCTION CONSIDERATIONS

3.1 Introduction

Safe storage of nuclear fuel in the Cask pit requires that the materials utilized in the rack fabrication be of proven durability and compatible with the pool water environment. Likewise, all activities in the rack installations must comply with the provisions of NUREG-0612 [3.1.1] to eliminate the potential for damage to fuel presently stored in the SFP or any safety related equipment. This section provides a synopsis of the considerations with regard to long-term service life and short-term construction safety.

3.2 Structural Materials

The following structural materials are utilized in the fabrication of the new spent fuel racks:

- a. ASME SA-240-304 for all composite box subassembly sheet metal, baseplate and cell connecting bar stock
- b. Internally threaded support pedestals: ASME SA-240-304
- c. Externally threaded spindle for the support pedestal: ASME SA-564-630 precipitation hardened stainless steel (heat treated to 1100°F)
- d. Weld material: ASME Type 308 and Type 308L

3.3 Poison Material (Neutron Absorber)

In addition to the structural and non-structural stainless steel material, the racks employ Boral™, a patented product of AAR Manufacturing, as the neutron absorber material. Boral is a hot-rolled cermet of aluminum and boron carbide, clad in aluminum. A brief description of Boral and its pool experience list follows.

Boral is a thermal neutron poison material composed of boron carbide and 1100 alloy aluminum. Boron carbide is a compound having a high boron content in a physically stable and chemically inert form. The 1100 alloy aluminum is a lightweight metal with high tensile strength, which is protected from corrosion by a highly resistant oxide film. The oxide film is formed by a strongly adhering film of impervious hydrated aluminum oxide, which passivates the surface of the aluminum in the SFP environment. The corrosion layer penetrates the aluminum surface of the boral only a few microns. There is no net loss of aluminum cladding through the passivation process. The central matrix of the cermet is not affected by corrosion. The two materials, boron carbide and aluminum, are chemically compatible and ideally suited for long-term use in the radiation, thermal and chemical environment of the SFP. Boral has been shown [3.3.1] to be superior to alternative materials previously used as neutron absorbers in storage racks.

Boral has been extensively used in fuel rack applications in recent years. Its use in the spent fuel pools as the neutron absorbing material can be attributed to its proven performance (over 150 pool years of experience) and the following unique characteristics:

- i. The content and placement of boron carbide provides a very high removal cross-section for thermal neutrons.
- ii. Boron carbide, in the form of fine particles, is homogeneously dispersed throughout the central layer of the Boral panels.
- iii. The boron carbide and aluminum materials in Boral do not degrade as a result of long-term exposure to radiation.
- iv. The neutron absorbing central layer of Boral is clad with permanently bonded surfaces of aluminum.
- v. Boral is stable, strong, durable, and corrosion resistant.

Boral is manufactured by AAR Manufacturing under the control and surveillance of Holtec International's Quality Assurance/Quality Control Program that conforms to the requirements of 10CFR50 Appendix B, "Quality Assurance Criteria for Nuclear Power Plants". Holtec International has been evaluated by the DBNPS Nuclear Assurance Department and is an approved supplier for the design, fabrication and installation of the Cask Pit racks.

As indicated in Tables 3.3.1 and 3.3.2, Boral has been licensed by the USNRC for use in numerous BWR and PWR spent fuel storage racks and has been extensively used in international nuclear installations.

3.3.1 Boral Material Characteristics

Aluminum: Aluminum is a silvery-white, ductile metallic element. The 1100 alloy aluminum is used extensively in heat exchangers, pressure and storage tanks, chemical equipment, reflectors and sheet metal work.

It has high resistance to corrosion in industrial and marine atmospheres. Aluminum has an atomic number of 13, atomic weight of 26.98, specific gravity of 2.69 and valence of 3. The physical, mechanical and chemical properties of the 1100 alloy aluminum are listed in Tables 3.3.3 and 3.3.4.

The excellent corrosion resistance of the 1100 alloy aluminum is provided by the protective oxide film that quickly develops on its surface from exposure to the atmosphere or water. This film prevents the loss of metal from general corrosion or pitting corrosion.

Boron Carbide: The boron carbide contained in Boral is a fine granulated powder that conforms to ASTM C-750-80 nuclear grade Type III. The material conforms to the chemical composition and properties listed in Table 3.3.5.

References [3.3.2], [3.3.3], and [3.3.4] provide further discussion as to the suitability of these materials for use in spent fuel storage module applications.

3.4 Compatibility with Coolant

All materials used in the construction of the Holtec racks have been determined to be compatible with the DBNPS Spent Fuel Pool/Cask Pit, and have an established history of in-plant usage. As evidenced in Tables 3.3.1 and 3.3.2, Boral has been successfully used in fuel pools. Austenitic stainless steel (304) is perhaps the most widely used stainless alloy in nuclear power plants.

3.5 Heavy Load Considerations for the Proposed Rack Installations

The Spent Fuel Cask Crane (SFCC) will be used for the installation of the new storage racks in the Cask Pit and is subject to the requirements of NUREG-0612, "Control of Heavy Loads at Nuclear Power Plants". Safe handling of heavy loads by the SFCC will be ensured by following the defense in depth approach guidelines of NUREG 0612:

- Defined safe load paths in accordance with approved procedures
- Supervision of heavy load lifts by designated individuals
- Crane operator training and qualification that satisfies the requirements of ANSI/ASME B30.2-1976 [3.5.1]
- Use of lifting devices (slings) that are selected, inspected and maintained in accordance with ANSI B30.9-1971 [3.5.2]
- Inspection, testing and maintenance of cranes in accordance with ANSI/ASME B30.2-1976
- Ensuring the design of the SFCC is equivalent to the requirements of CMAA-70 [3.5.3] and ANSI/ASME B30.2-1976
- Reliability of special lifting devices by application of design safety margins, and periodic inspection and examinations using approved procedures

The salient features of the lifting devices and associated procedures are described as follows:

a. Safe Load Paths and Procedures

Safe load paths will be defined for moving the new racks in the Fuel Building. As shown in Figure 3.5.1, the Cask Pit is located west of the SFP, between the Auxiliary Building Train Bay / Loading Area and the SFP. This location precludes any heavy load from being lifted over the SFP or any safety-related equipment. The SFCC is interlocked to prohibit travel over the Spent Fuel Pool. Therefore, during installation of the new racks in the Cask Pit, the new racks will not be carried directly over any portion of the SFP.

The SFCC interlocks will be modified to further prohibit lifting of a heavy load over the Cask Pit when there is fuel stored in the Cask Pit. The rack upending or laying down will be carried out in an area which is not overlapping to any safety-related system or component.

All phases of rack installation activities will be conducted in accordance with written procedures, which will be reviewed and approved by the owner.

b. Supervision of Lifts

Procedures used during the installation of the Cask Pit Racks require supervision of heavy load lifts by a designated individual who is responsible for ensuring procedure compliance and safe lifting practices.

c. Crane Operator Training

All crew members involved in the use of the lifting and upending equipment will be given training by Holtec International using a videotape-aided instruction course which has been utilized in previous rerack operations.

d. Lifting Devices Design and Reliability

The SFCC is comprised of a main hook rated for 140 tons as well as an auxiliary hook rated for 20 tons. A temporary hoist with an appropriate capacity will be attached to the SFCC hook to prevent submergence of the hook.

The following table determines the maximum lift weight during rack installation.

Item	Weight (lbs)
Rack	12,150 (maximum)
Lift Rig	1,000
Rigging	500
Temporary hoist	2,000
Total Lift	15,650

It is clear, based on the heaviest rack weight to be lifted, that the heaviest load being lifted is well below the rating of the SFCC hooks. The temporary hoist to be used in conjunction with the SFCC hook will be selected to provide an adequate load capacity and comply with NUREG-0612.

Remotely engaging lift rigs, meeting all requirements of NUREG-0612, will be used to lift the new rack modules. The new rack lift rig consists of four independently loaded traction rods in a lift configuration, which ensures that failure of one traction rod will not result in uncontrolled lowering of the load. Therefore, the lift rig complies with the duality feature called for in Section 5.1.6 (3a) of NUREG 0612.

The rig has the following attributes:

- The traction rod is designed to prevent loss of its engagement with the rig in the locked position. Moreover, the locked configuration can be directly verified from above the pool water without the aid of an underwater camera.

- The stress analysis of the rig is carried out and the primary stress limits postulated in ANSI N14.6 [3.5.4] are met.
- The rig is load tested with 300% of the maximum weight to be lifted. The test weight is maintained in the air for 10 minutes. All critical weld joints are liquid penetrant examined to establish the soundness of all critical joints.

e. Crane Maintenance

The SFCC is maintained functional per the DBNPS preventative maintenance procedures.

The proposed heavy loads compliance will be in accordance with the guidelines of NUREG-0612, which calls for measures to "provide an adequate defense-in-depth for handling of heavy loads near spent fuel...". The NUREG-0612 guidelines cite four major causes of load handling accidents, namely

- i. operator errors
- ii. rigging failure
- iii. lack of adequate inspection
- iv. inadequate procedures

The racking program ensures maximum emphasis on mitigating the potential load drop accidents by implementing measures to eliminate shortcomings in all aspects of the operation including the four aforementioned areas. A summary of the measures specifically planned to deal with the major causes is provided below.

Operator errors: As mentioned above, comprehensive training will be provided to the installation crew. All training shall be in compliance with ANSI B30.2.

Rigging failure: The lifting device designed for handling and installation of the new racks has redundancies in the lift legs and lift eyes such that there are four independent load members in the new rack lift rig, and three independent load members in the existing rack lifting rig. Failure of any one load bearing member would not lead to uncontrolled lowering of the load. The rig

complies with all provisions of ANSI 14.6-1978, including compliance with the primary stress criteria, load testing at 300% of maximum lift load, and dye examination of critical welds.

The rig designs are similar to the rigs used in the initial racking or the rerack of numerous other plants, such as Hope Creek, Millstone Unit 1, Indian Point Unit Two, Ulchin II, Laguna Verde, J.A. FitzPatrick, and Three Mile Island Unit 1.

Lack of adequate inspection: The designer of the racks has developed a set of inspection points that have been proven to eliminate any incidence of rework or erroneous installation in numerous prior rerack projects. Surveys and measurements are performed on the storage racks prior to and subsequent to placement into the pools to ensure that the as-built dimensions and installed locations are acceptable. Measurements of the pool and floor elevations are also performed to determine actual pool configuration and to allow height adjustments of the pedestals prior to rack installation. These inspections minimize rack manipulation during placement into the pool.

Inadequate procedures: Procedures will be developed to address operations pertaining to the rack installation effort, including, but not limited to, mobilization, rack handling, upending, lifting, installation, verticality, alignment, dummy gage testing, site safety, and ALARA compliance. The procedures will be the successors of the procedures successfully implemented in previous projects.

Table 3.5.1 provides a synopsis of the requirements delineated in NUREG-0612, and its intended compliance.

- [3.1.1] NUREG-0612, "Control of Heavy Loads at Nuclear Power Plants," July 1980.
- [3.3.1] "Nuclear Engineering International," July 1997 issue, pp 20-23.
- [3.3.2] "Spent Fuel Storage Module Corrosion Report," Brooks & Perkins Report 554, June 1, 1977.
- [3.3.3] "Suitability of Brooks & Perkins Spent Fuel Storage Module for Use in PWR Storage Pools," Brooks & Perkins Report 578, July 7, 1978.
- [3.3.4] "Boral Neutron Absorbing/Shielding Material - Product Performance Report," Brooks & Perkins Report 624, July 20, 1982.
- [3.5.1] ANSI/ASME B30.2, "Overhead and Gantry Cranes, (Top Running Bridge, Single or Multiple Girder, Top Running Trolley Hoist)," American Society of Mechanical Engineers, 1976.
- [3.5.2] ANSI B30.9, "Safety Standards for Slings," 1971.
- [3.5.3] CMAA Specification 70, "Electrical Overhead Traveling Cranes," Crane Manufacturers Association of America, Inc., 1983.
- [3.5.4] ANSIN14.6-1978, Standard for Special Lifting Devices for Shipping Containers Weighing 10000 Pounds or more for Nuclear Materials," American National Standard Institute, Inc., 1978.
- [3.5.5] ANSI/ASME B30.20, "Below-the-Hook Lifting Devices," American Society of Mechanical Engineers, 1993.

Table 3.3.1

BORAL EXPERIENCE LIST - PWRs

Plant	Utility	Docket No.	Mfg. Year
Maine Yankee	Maine Yankee Atomic Power	50-309	1977
Donald C. Cook	Indiana & Michigan Electric	50-315/316	1979
Sequoyah 1,2	Tennessee Valley Authority	50-327/328	1979
Salem 1,2	Public Service Electric & Gas	50-272/311	1980
Zion 1,2	Commonwealth Edison	50-295/304	1980
Bellefonte 1, 2	Tennessee Valley Authority	50-438/439	1981
Yankee Rowe	Yankee Atomic Power	50-29	1964/1983
Gosgen	Kernkraftwerk Gosgen-Daniken AG (Switzerland)		1984
Koeberg 1,2	ESCOM (South Africa)		1985
Beznau 1,2	Nordostschweizerische Kraftwerke AG (Switzerland)		1985
12 various Plants	Electricite de France (France)	--	1986
Indian Point 3	NY Power Authority	50-286	1987
Byron 1,2	Commonwealth Edison	50-454/455	1988
Braidwood 1,2	Commonwealth Edison	50-456/457	1988
Yankee Rowe	Yankee Atomic Power	50-29	1988
Three Mile Island I	GPU Nuclear	50-289	1990
Sequoyah (rerack)	Tennessee Valley Authority	50-327	1992
Donald C. Cook (rerack)	American Electric Power	50-315/316	1992
Beaver Valley Unit 1	Duquesne Light Company	50-334	1993
Fort Calhoun	Omaha Public Power District	50-285	1993

Table 3.3.1

BORAL EXPERIENCE LIST - PWRs

Plant	Utility	Docket No.	Mfg. Year
Zion 1 & 2 (rerack)	Commonwealth Edison	50-295/304	1993
Salem Units 1 & 2 (rerack)	Public Gas and Electric Company	50-272/311	1995
Ulchin Unit 1	Korea Electric Power Company (Korea)	--	1995
Haddam Neck	Connecticut Yankee Atomic Power Company	50-213	1996
Ulchin Unit 2	Korea Electric Power Company (Korea)	--	1996
Kori-4	Korea Electric Power Company (Korea)	--	1996
Yonggwang 1,2	Korea Electric Power Company (Korea)	--	1996
Sizewell B	Nuclear Electric, plc (United Kingdom)	--	1997
Angra 1	Furnas Centrais-Elétricas SA (Brazil)	--	1997
Waterford 3	Entergy Operations	50-382	1997
Callaway	Union Electric	50-483	1998

Table 3.3.2

BORAL EXPERIENCE LIST - BWRs

Plant	Utility	Docket No.	Mfg. Year
Cooper	Nebraska Public Power	50-298	1979
J.A. FitzPatrick	NY Power Authority	50-333	1978
Duane Arnold	Iowa Electric Light & Power	50-331	1979
Browns Ferry 1,2,3	Tennessee Valley Authority	50-259/260/296	1980
Brunswick 1,2	Carolina Power & Light	50-324/325	1981
Clinton	Illinois Power	50-461/462	1981
Dresden 2,3	Commonwealth Edison	50-237/249	1981
E.I. Hatch 1,2	Georgia Power	50-321/366	1981
Hope Creek	Public Service Electric & Gas	50-354/355	1985
Humboldt Bay	Pacific Gas & Electric Company	50-133	1985
LaCrosse	Dairyland Power	50-409	1976
Limerick 1,2	Philadelphia Electric Company	50-352/353	1980
Monticello	Northern States Power	50-263	1978
Peachbottom 2,3	Philadelphia Electric	50-277/278	1980
Perry 1,2	Cleveland Electric Illuminating	50-440/441	1979
Pilgrim	Boston Edison Company	50-293	1978
Susquehanna 1,2	Pennsylvania Power & Light	50-387,388	1979
Vermont Yankee	Vermont Yankee Atomic Power	50-271	1978/1986
Hope Creek	Public Service Electric & Gas	50-354/355	1989
Harris Pool 'B' †	Carolina Power & Light	50-401	1991
Duane Arnold	Iowa Electric Light & Power	50-331	1993
Pilgrim	Boston Edison Company	50-293	1993

Table 3.3.2

BORAL EXPERIENCE LIST - BWRs

Plant	Utility	Docket No.	Mfg. Year
LaSalle 1	Commonwealth Edison	50-373	1992
Millstone Unit 1	Northeast Utilities	50-245	1989
James A. FitzPatrick	NY Power Authority	50-333	1990
Hope Creek	Public Service Electric & Gas Company	50-354	1991
Duane Arnold Energy Center	Iowa Electric Power Company	50-331	1994
Limerick Units 1,2	PECO Energy	50-352/50-353	1994
Harris Pool 'B' †	Carolina Power & Light Company	50-401	1996
Chinshan 1,2	Taiwan Power Company (Taiwan)	--	1986
Kuosheng 1,2	Taiwan Power Company (Taiwan)	--	1991
Laguna Verde 1,2	Comision Federal de Electricidad (Mexico)	--	1991
Harris Pool 'B' †	Carolina Power & Light Company	50-401	1996
James A. FitzPatrick	NY Power Authority	50-333	1998

† Fabricated racks for storage of spent fuel transhipped from Brunswick.

Table 3.3.3

1100 ALLOY ALUMINUM PHYSICAL CHARACTERISTICS

Density	0.098 lb/in ³ 2.713 g/cm ³
Melting Range	1190°F - 1215°F 643° - 657°C
Thermal Conductivity (77°F)	128 BTU/hr/ft ² /F/ft 0.53 cal/sec/cm ² /°C/cm
Coefficient of Thermal Expansion (68°F - 212°F)	13.1 x 10 ⁻⁶ in/in-°F 23.6 x 10 ⁻⁶ cm/cm-°C
Specific Heat (221°F)	0.22 BTU/lb/°F 0.23 cal/g/°C
Modulus of Elasticity	10 x 10 ⁶ psi
Tensile Strength (75°F)	13,000 psi (annealed) 18,000 psi (as rolled)
Yield Strength (75°F)	5,000 psi (annealed) 17,000 psi (as rolled)
Elongation (75°F)	35-45% (annealed) 9-20% (as rolled)
Hardness (Brinell)	23 (annealed) 32 (as rolled)
Annealing Temperature	650°F 343°C

Table 3.3.4

CHEMICAL COMPOSITION - ALUMINUM
(1100 ALLOY)

99.00% min.	Aluminum
1.00% max.	Silicone and Iron
0.05-0.20% max.	Copper
0.05% max.	Manganese
0.10% max.	Zinc
0.15% max.	Other

Table 3.3.5

CHEMICAL COMPOSITION AND PHYSICAL PROPERTIES
OF BORON CARBIDE

CHEMICAL COMPOSITION (WEIGHT PERCENT)	
Total boron	70.0 min.
B ¹⁰ isotopic content in natural boron	18.0
Boric oxide	3.0 max.
Iron	2.0 max.
Total boron plus total carbon	94.0 min.
PHYSICAL PROPERTIES	
Chemical formula	B ₄ C
Boron content (weight percent)	78.28%
Carbon content (weight percent)	21.72%
Crystal structure	rhombohedral
Density	0.0907 lb/in ³ 2.51 g/cm ³
Melting Point	4442°F 2450°C
Boiling Point	6332°F 3500°C
Boral Loading (minimum grams B ¹⁰ per cm ²)	0.030

Table 3.5.1

HEAVY LOAD HANDLING COMPLIANCE MATRIX (NUREG-0612)

Criterion	Compliance
1. Are safe load paths defined for the movement of heavy loads to minimize the potential of impact, if dropped, on irradiated fuel?	Yes
2. Will procedures be developed to cover: identification of required equipment, inspection and acceptance criteria required before movement of load, steps and proper sequence for handling the load, defining the safe load paths, and special precautions?	Yes
3. Will crane operators be trained and qualified?	Yes
4. Will special lifting devices meet the guidelines of ANSI 14.6-1978?	Yes
5. Will non-custom lifting devices be installed and used in accordance with ANSI B30.20 [3.5.5], latest edition?	Yes
6. Will the cranes be inspected and tested prior to use in rack installation?	Yes
7. Does the crane meet the intent of ANSI B30.2-1976 and CMMA-70?	Yes

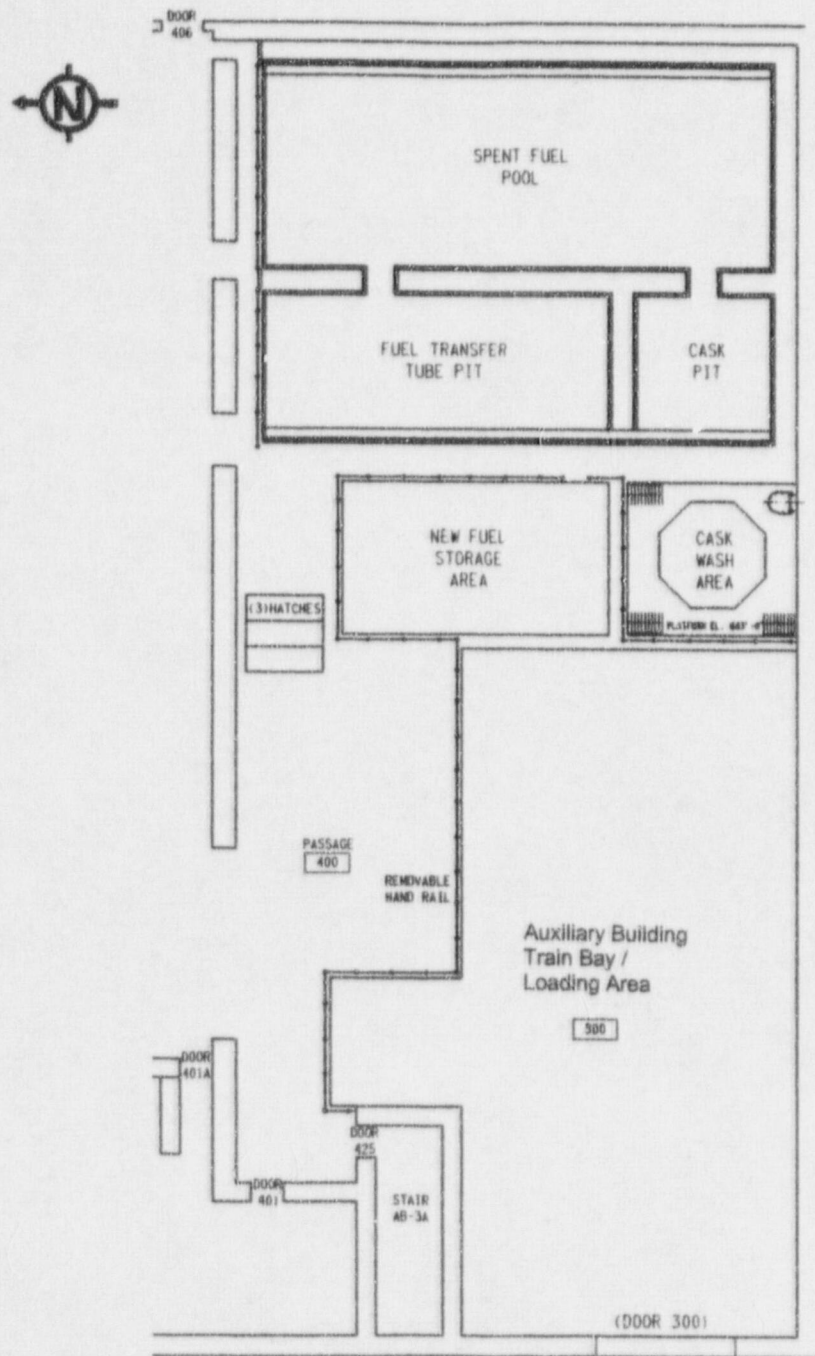


FIGURE 3.5.1; AUXILIARY BUILDING
 SPENT FUEL POOL AREA PLAN VIEW

4.0 CRITICALITY SAFETY EVALUATION

4.1 Design Bases

The high density spent fuel storage racks in the Cask Pit at the Davis-Besse Nuclear Power Station are designed to assure that the effective neutron multiplication factor, k_{eff} , is equal to or less than 0.95 with the racks fully loaded with fuel of the highest anticipated reactivity, and flooded with un-borated water at a temperature within the Cask Pit temperature operating range corresponding to the highest reactivity. Including all applicable uncertainties, the maximum k_{eff} is shown to be less than 0.95 with a 95% probability at a 95% confidence level [4.1.1].

Reactivity effects of abnormal and accident conditions have also been evaluated to assure that under credible abnormal and accident conditions, the reactivity will not exceed 0.95.

Applicable codes, standards, and regulations or pertinent sections thereof, include the following:

- *Code of Federal Regulations*, Title 10, Part 50, Appendix A, General Design Criterion 62, Prevention of Criticality in Fuel Storage and Handling.
- USNRC Standard Review Plan, NUREG-0800, Section 9.1.2, Spent Fuel Storage, Rev. 3 - July 1981.
- USNRC letter of April 14, 1978, to all Power Reactor Licensees - OT Position for Review and Acceptance of Spent Fuel Storage and Handling Applications, including modification letter dated January 18, 1979.
- L.I. Kopp, "Guidance on the Regulatory Requirements for Criticality Analysis of Fuel Storage at Light-Water Reactor Power Plants," June 1998.
- USNRC Regulatory Guide 1.13, Spent Fuel Storage Facility Design Basis, Rev. 2 (proposed), December 1981.
- ANSI ANS-8.17-1984, Criticality Safety Criteria for the Handling, Storage and Transportation of LWR Fuel Outside Reactors.

USNRC guidelines [4.1.2] and the applicable ANSI standards specify that the maximum effective multiplication factor, k_{eff} , including bias, uncertainties, and calculational statistics, shall be less than or equal to 0.95, with 95% probability at the 95% confidence level. In the present criticality safety evaluation of the storage racks, the design basis target maximum k_{eff} was selected to be 0.945, which is more conservative than the limit specified in the regulatory guidelines.

To ensure that the true reactivity will always be less than the calculated reactivity, the following conservative assumptions were made:

- Moderator is un-borated water at a temperature within the Cask Pit temperature operating range that results in the highest reactivity (4°C, corresponding to the maximum possible moderator density).
- The racks are assumed to be fully loaded with the most reactive fuel authorized to be stored in the facility without any control rods or burnable poison.
- No soluble poison (boron) is assumed to be present in the Cask Pit water under normal operating conditions.
- Neutron absorption in minor structural members is neglected, i.e., spacer grids are replaced by water.
- The effective multiplication factor of an infinite radial array of storage cells containing fuel assemblies is used, except for the assessment of peripheral effects and certain abnormal/accident conditions where neutron leakage is inherent.
- No credit is assumed for the water gap between the racks (2.0 inches, as limited by the base plate extensions) or the additional Boral panel between adjacent racks.

- In-core depletion calculations assumed conservative operating conditions: highest fuel and moderator temperature (1300 °F and 610 °F, respectively), a conservative allowance for the soluble boron concentrations (1000 ppm), and burnable poison (4.0 wt% B₄C) rods present in each guide tube (removed at 35 GWD/MTU). These conditions produce Plutonium in excess of normal operating conditions.

The spent fuel storage racks are designed to accommodate B&W 15x15 Mark B fuel assemblies characterized by the dimensions listed in Table 4.1.1. The fuel specifications in Table 4.1.1 allow for variations in the cladding thickness, and thus, calculations were performed to demonstrate that the most reactive assembly design corresponds to the minimum cladding thickness (minimum clad O.D.). The design basis fuel assembly is the most reactive (minimum cladding thickness) B&W 15x15 Mark B assembly containing UO₂ at a maximum initial enrichment of 5.05 ± 0.05 wt% ²³⁵U.

The water in the Cask Pit normally contains soluble boron, which would result in a large sub-criticality margin under actual operating conditions. However, the NRC guidelines, based upon the accident condition in which all soluble poison is assumed to have been lost, specify that the limiting k_{eff} of 0.95 for normal storage be evaluated for the accident condition that assumes the loss of soluble boron. The double contingency principle of ANSI N16.1-1975 and of the April 1978 NRC letter allows credit for soluble boron under other abnormal or accident conditions, since only a single independent accident need be considered at one time. Consequences of abnormal and accident conditions have also been evaluated, where "abnormal" refers to conditions which may reasonably be expected to occur during the lifetime of the plant, and "accident" refers to conditions which are not expected to occur but nevertheless must be protected against.

4.2 Summary of Criticality Analyses

4.2.1 Normal Operating Conditions

Calculations have been performed to qualify the racks for storage of fuel assemblies with a maximum nominal initial enrichment of 5.05 wt% ^{235}U which have accumulated a minimum burnup of 53.51 GWD/MTU, or fuel of initial nominal enrichment and burnup combinations within the acceptable domain depicted in Figure 4.2.1. For burnup-enrichment combinations within the acceptable domain depicted in Figure 4.2.1, the maximum k_{eff} value is shown to be less than 0.95 (95% probability at the 95% confidence level). The criticality analyses for the Cask Pit are summarized in Table 4.2.1. The calculated maximum reactivity includes the reactivity effect of the axial distribution in burnup and provides an additional margin of uncertainty for the depletion calculations.

The burnup criteria identified in Figure 4.2.1 for acceptable storage will be implemented by appropriate administrative procedures.

4.2.2 Abnormal and Accident Conditions

Although credit for the soluble poison normally present in the Cask Pit water is permitted under abnormal or accident conditions, most abnormal or accident conditions will not result in exceeding the limiting reactivity even in the absence of soluble poison. The effects on reactivity of credible abnormal and accident conditions are discussed in Section 4.6 and summarized in Table 4.2.2. Administrative procedures, to assure the presence of soluble poison during fuel handling operations, preclude the possibility of the simultaneous occurrence of two independent accident conditions.

Assuring the presence of soluble poison during fuel handling operations will preclude the possibility of the simultaneous occurrence of the two independent accident conditions. The largest

reactivity increase would occur if a fresh fuel assembly of 5.05 wt% ^{235}U enrichment were to be inadvertently loaded into a cell with the remainder of the rack fully loaded with fuel of the highest permissible reactivity (i.e., minimum burnup of the initial enrichment). Under these accident conditions, credit for the presence of soluble poison is permitted by the NRC guidelines[†]. Calculations were performed to demonstrate that 650 ppm soluble boron is adequate to assure that the maximum k_{eff} remains below 0.945.

[†] Double contingency principle of ANSI N16.1-1975, as specified in the April 14, 1978 NRC letter (Section 1.2) and implied in the proposed revision to Reg. Guide 1.13 (Section 1.4, Appendix A).

4.3 Reference Fuel Storage Cells

4.3.1 Reference Fuel Assembly

The design basis fuel assembly, illustrated in Figure 4.3.1, is the B&W 15x15 Mark B assembly. Table 4.1.1 summarizes the fuel assembly design specifications.

4.3.2 Fuel Storage Cells

Figure 4.3.1 shows the calculational model of the nominal spent fuel storage cell containing a B&W 15x15 Mark B assembly. The storage cells are composed of stainless steel walls with a single fixed neutron absorber panel, Boral, (held in place by a 0.035 inch stainless steel sheathing) centered on each side in a 0.11 inch channel. Stainless steel boxes are arranged in an alternating pattern such that the connection of the box corners form storage cells between those of the stainless steel boxes. These cells are located on a lattice spacing of $9.22 \pm$ [REDACTED] inches. The $0.075 \pm$ [REDACTED] inch thick steel walls define a storage cell which has a 9.0 inches nominal inside dimension. The Boral absorber has a thickness of $0.101 \pm$ [REDACTED] inches and a nominal B-10 areal density of 0.0324 g/cm^2 (minimum of [REDACTED] g/cm^2). The Boral absorber panels are $7.5 \pm$ [REDACTED] inches in width and $148 +$ [REDACTED]/- [REDACTED] inches in length. Boral panels are installed on all exterior walls facing other racks, as well as, non-fueled regions, i.e., the Cask Pit walls. The minimum gap between neighboring racks is 2.0 inches, as assured by the base plate extensions.

4.4 Analytical Methodology

4.4.1 Reference Design Calculations

The principal method for criticality analysis of the high density storage racks is the three-dimensional Monte Carlo code MCNP4a [4.4.1]. MCNP4a is a continuous energy three-dimensional Monte Carlo code developed at the Los Alamos National Laboratory. MCNP4a calculations used continuous energy cross-section data based on ENDF/B-V, as distributed with the code. Independent verification calculations were performed with KENO5a [4.4.2], which is a three-dimensional multigroup Monte Carlo code developed at the Oak Ridge National Laboratory. The KENO5a calculations used the 238-group cross-section library, which is based on ENDF/B-V data and is distributed as part of the SCALE-4.3 package [4.4.3], coupled with the NITAWL-II program [4.4.4], which adjusts the uranium-238 cross sections to compensate for resonance self-shielding effects. Benchmark calculations, presented in Appendix A, indicate a bias of 0.0009 with an uncertainty of ± 0.0011 for MCNP4a and 0.0030 ± 0.0012 for KENO5a, both evaluated at the 95% probability, 95% confidence level [4.1.1].

Fuel depletion analyses during core operation were performed with CASMO-4, a two-dimensional multigroup transport theory code based on capture probabilities [4.4.5 - 4.4.7]. Restarting the CASMO-4 calculations in the storage rack geometry at 4 °C yields the two-dimensional infinite multiplication factor (k_{∞}) for the storage rack. Parallel calculations with CASMO-4 for the storage rack at various enrichments enable a reactivity equivalent enrichment (fresh fuel) to be determined that provides the same reactivity in the rack as the depleted fuel. CASMO-4 was also used to determine the small reactivity uncertainties (differential calculations) of manufacturing tolerances.

In the geometric models used for the calculations, each fuel rod and its cladding were described explicitly and reflecting boundary conditions were used in the radial direction, which has the effect of creating an infinite radial array of storage cells. Monte Carlo calculations inherently include a statistical uncertainty due to the random nature of neutron tracking. To minimize the statistical

uncertainty of the MCNP4a and KENO5a calculated reactivities and to assure convergence, a minimum of 1 million neutron histories were accumulated in each calculation.

4.4.2 Fuel Burnup Calculations and Uncertainties

CASMO-4 was used for burnup calculations in the hot operating condition. CASMO-4 has been extensively benchmarked [4.4.6, 4.4.7] against cold, clean, critical experiments (including plutonium-bearing fuel), Monte Carlo calculations, reactor operations, and heavy element concentrations in irradiated fuel.

In the CASMO-4 geometric models, each fuel rod and its cladding were described explicitly and reflective boundary conditions were used between storage cells. These boundary conditions have the effect of creating an infinite array of storage cells.

Conservative assumptions of moderator and fuel temperatures and the average operating soluble boron concentration, along with the presence of burnable poison rods, were used to assure the highest plutonium production and hence conservatively high values of reactivity during burnup. Since critical experiment data with spent fuel is not available for determining the uncertainty in depletion calculations, an allowance for uncertainty in reactivity[†] was assigned based upon other considerations [4.1.2]. Assuming the uncertainty in depletion calculations is less than 5% of the total reactivity decrement, a burnup dependent uncertainty in reactivity for burnup calculations was assigned. Thus, the burnup uncertainty varies (increases) with burnup. This allowance for burnup uncertainty was included in determination of the acceptable burnup versus enrichment combinations.

[†] The majority of the uncertainty in depletion calculations derives from uncertainties in fuel and moderator temperatures and the effect of reactivity control methods (e.g., soluble boron). For depletion calculations, bounding values of these operating parameters were assumed to assure conservative results in the analyses.

4.4.3 Effect of Axial Burnup Distribution

Initially, fuel loaded into a reactor will burn with a slightly skewed cosine power distribution. As burnup progresses, the burnup distribution tends to flatten, becoming more highly burned in the central region than in the upper and lower regions. At high burnup, the more reactive fuel near the ends of the fuel assembly (less than average burnup) occurs in regions of high neutron leakage. Consequently, it is expected that over most of the burnup history, fuel assemblies with distributed burnups will exhibit a slightly lower reactivity than that calculated for the uniform average burnup. As burnup progresses, the distribution, to some extent, tends to be self-regulating as controlled by the axial power distribution, precluding the existence of large regions of significantly reduced burnup.

Among others, Turner [4.4.8] has provided generic analytic results of the axial burnup effect based upon calculated and measured axial burnup distributions. These analyses confirm the minor and generally negative reactivity effect of the axially distributed burnups at values less than about 27 GWD/MTU with small positive reactivity effects at higher burnup values. However, for the present criticality analyses, a very conservative bounding axial burnup distribution, as supplied by Toledo Edison, was used, which resulted in a larger than typical positive reactivity effect. This distribution was developed by incorporating the most reactive top and bottom regions from all assemblies (including assemblies with only one cycle burnup), and thus is not based on any single assembly. Moreover, this distribution includes the effect of partially inserted control rods, and therefore, is not typical and is very conservative. Burnup-equivalent enrichments were determined with CASMO-4 for each of 18 equally spaced axial zones (a very conservative representation) and used in three-dimensional Monte Carlo calculations. Results of these calculations, therefore, inherently include the effect of the axial distribution in burnup. Comparison of these results to results of calculations with uniform axial burnup allows the reactivity effect of the axial burnup distribution to be quantified. This reactivity effect is included in the calculation of the maximum k_{eff} values.

4.4.4 Long-Term Changes in Reactivity

At reactor shutdown, the reactivity of the fuel initially decreases due to the growth of Xe-135. Subsequently, the Xenon decays and the reactivity increases to a maximum at several hundred hours when the Xenon is gone. Therefore, for conservatism, the Xe is set to zero in the calculations to assure maximum reactivity. During the next 50 years, the reactivity continuously decreases due primarily to Pu-241 decay and Am-241 growth. No credit is taken for this long-term decrease in reactivity other than to indicate additional and increasing conservatism in the design criticality analysis.

4.5 Criticality Analyses and Tolerances

4.5.1 Nominal Design Case

For the nominal storage cell design in the Cask Pit, the criticality safety analyses are summarized in Table 4.2.1. These data confirm that the maximum reactivity remains conservatively less than the regulatory limit (k_{eff} of 0.95). An independent calculation with the KENO5a code provides confirmation of the validity of the reference MCNP4a calculations.

4.5.2 Determination of Acceptable Burnup and Enrichment Combinations

CASMO-4 was used for the depletion analysis, and the restart option was used to analytically transfer the spent fuel into the storage rack configuration at a reference temperature of 4 °C. Calculations were also made for fuel of several different initial enrichments and interpolated to define the burnup-dependent equivalent enrichments[†], at each burnup. An MCNP4a calculation was then made for the equivalent enrichment to establish the limiting k_{eff} value, which includes all applicable uncertainties and the effect of the axial burnup distribution. This calculation was used to define the boundary of the acceptable domain shown in Figure 4.2.1. Assuming the uncertainty in depletion calculations is 5% of the total reactivity decrement, a burnup dependent uncertainty in reactivity for burnup calculations was assigned. Thus, the burnup uncertainty varies (increases) with burnup. This allowance for burnup uncertainty was included in determination of the acceptable burnup versus enrichment combinations.

[†] The (reactivity) equivalent enrichment is the fresh un-burned fuel enrichment that yields the same reactivity as the depleted fuel, both evaluated in the storage rack configuration. The equivalent enrichment may then be used in three-dimensional MCNP4a or KENO5a calculations.

4.5.3 Uncertainties Due to Tolerances

The reactivity effects of manufacturing tolerances are tabulated, along with the actual tolerances, in Table 4.5.1. To determine the Δk associated with a specific manufacturing tolerance, the reference k_{inf} was compared to the k_{inf} from a calculation with the tolerance included. All of the positive Δk values from the various tolerances are statistically combined (square root of the sum of the squares) to determine the final reactivity uncertainty allowance for manufacturing tolerances. All of the individual reactivity allowances were calculated for the reference fresh unburned fuel assembly and for burnups enveloping the required burnup. The largest final statistically combined reactivity uncertainty allowance was conservatively used in the determination of the maximum k_{eff} . The individual reactivity allowances are shown in Table 4.5.1.

4.5.4 Eccentric Fuel Positioning

The fuel assembly is assumed to be normally located in the center of the storage rack cell. However, calculations were also made with the fuel assemblies assumed to be in the corner of the storage rack cell (four-assembly cluster at closest approach). These calculations indicated that the reactivity effect is small and negative. Therefore, the reference case in which the fuel assemblies are centered is controlling and no uncertainty for eccentricity is necessary.

4.5.5 Water-Gap Spacing Between Racks

The minimum water-gap between racks, which is 2.0 inches between neighboring racks, constitutes a neutron flux-trap for the storage cells of facing racks. The racks are constructed with the base plates extending beyond the edge of the cells which assures that the minimum spacing between storage racks is maintained under all credible conditions. However, no credit is taken for the water-gaps between racks.

4.6 Abnormal and Accident Conditions

4.6.1 Temperature and Water Density Effects

The temperature and void coefficients of reactivity in the Cask Pit are negative. Therefore, a water temperature of 4°C (39°F) was assumed for the reference calculations, which assures that the true reactivity will always be lower over the expected range of the Cask Pit water temperatures. Temperature effects on reactivity have been calculated (CASMO-4) and the results are shown in Table 4.6.1. In addition, the introduction of voids in the water internal to the storage cell (to simulate boiling) decreased reactivity, as shown in Table 4.6.1.

With soluble boron present, the temperature coefficients of reactivity would differ from those listed in Table 4.6.1. However, the reactivities would also be substantially lower at all temperatures with soluble boron present. The data in Table 4.6.1 is pertinent to the higher-reactivity unborated case.

Since the Monte Carlo codes, MCNP4a and KENO5a, cannot handle temperature dependence, all MCNP4a and KENO5a calculations were performed at 20°C and a positive temperature correction factor (the value of Δk between CASMO-4 calculations at 20°C and 4°C) was applied to the results.

4.6.2 Lateral Rack Movement

Lateral motion of the storage racks under seismic conditions could potentially alter the spacing between racks. However, no credit for the flux-trap is assumed in the analysis, and thus, the calculated maximum reactivity does not rely on the spacing between racks. The minimum water gap between the racks (2.0 inches, as limited by the base plate extensions) and the Boral panels, which are installed on all exterior walls of the racks, assure that the reactivity is always less than the design limitation. Therefore, there is no positive reactivity effect of lateral rack movement.

4.6.3 Abnormal Location of a Fuel Assembly

The misplacement of a fresh un-irradiated fuel assembly could, in the absence of soluble poison, result in exceeding the regulatory limit (k_{eff} of 0.95). This analysis is based on a fresh fuel assembly of the highest permissible enrichment (5.05 wt%) being inadvertently misloaded into one of the storage cells, which are intended for burned fuel. Soluble boron in the Cask Pit water, for which credit is permitted under these accident conditions, would assure that the reactivity is maintained substantially less than the design limitation. Calculations were performed to demonstrate that a soluble boron concentration of 650 ppm is more than adequate to assure that the maximum k_{eff} remains below 0.945.

In addition, the mislocation of a fresh unirradiated fuel assembly could, in the absence of soluble poison, result in exceeding the regulatory limit (k_{eff} of 0.95). This analysis is based on a fresh fuel assembly of the highest permissible enrichment (5.05 wt%) being accidentally mislocated outside of a storage rack adjacent to other fuel assemblies. The worst case would be an assembly mislocated in a corner formed by three storage racks. Calculations were performed for this condition to demonstrate that a soluble boron concentration of 550 ppm is more than adequate to assure that the maximum k_{eff} remains below 0.945.

4.6.4 Dropped Fuel Assembly

For the case in which a fuel assembly is assumed to be dropped on top of a rack, the fuel assembly will come to rest horizontally on top of the rack with a minimum separation distance from the active fuel in the rack of more than 12 inches. At this separation distance, the effect on reactivity is insignificant. Furthermore, the soluble boron in the Cask Pit water assures that the true reactivity is always less than the limiting value for this dropped fuel accident.

It is also possible to vertically drop an assembly into a location occupied by another assembly. Such a vertical impact would at most cause a small compression of the stored assembly, reducing the water-to-fuel ratio and thereby reducing reactivity. In addition, the distance between the active fuel regions of both assemblies will be more than sufficient to ensure no neutron interaction between the two assemblies.

Structural analysis has shown that dropping an assembly into an unoccupied cell could result in a localized deformation of the baseplate of the rack. The resultant effect would be the lowering of a single fuel assembly by the amount of the deformation. This could potentially result in the active fuel height of that assembly no longer being completely covered by the Boral. The immediate eight surrounding fuel cells could also be affected. However, the amount of deformation for these cells would be considerably less. Structural analysis has shown that the amount of localized deformation may be as great as 3.36 inches. The reactivity consequence of this situation was calculated and found to be statistically insignificant. For simplicity in modeling, the calculation conservatively assumed an infinite array of assemblies in this damaged condition, and demonstrated the reactivity effect to be negligible. Since this is a localized event (nine storage cells at most) the actual reactivity effect will be even less than the calculated value. Furthermore, the soluble boron in the spent fuel pool water assures that the true reactivity is always less than the limiting value for this dropped fuel accident. Consequently, a dropped fuel bundle will have a negligible impact on reactivity.

4.7 References

- [4.1.1] M. G. Natrella, Experimental Statistics, National Bureau of Standards Handbook 91, August 1963.
- [4.1.2] L.I. Kopp, "Guidance on the Regulatory Requirements for Criticality Analysis of Fuel Storage at Light-Water Reactor Power Plants," June 1998.
- [4.4.1] J.F. Briesmeister, Editor, "MCNP - A General Monte Carlo N-Particle Transport Code, Version 4A," LA-12625, Los Alamos National Laboratory (1993).
- [4.4.2] L.M. Petrie and N.F. Landers, "KENO Va - An Improved Monte Carlo Criticality Program with Supergrouping," Volume 2, Section F11 from "SCALE: A Modular System for Performing Standardized Computer Analysis for Licensing Evaluation" NUREG/CR-0200, Rev. 4, January 1990.
- [4.4.3] "SCALE 4.3: A Modular System for Performing Standardized Computer Analysis for Licensing Evaluation For Workstations and Personal Computers, Volume 0," CCC-545, ORNL-RSICC, Oak Ridge National Laboratory (1995).
- [4.4.4] N.M. Greene, L.M. Petrie and R.M. Westfall, "NITAWL-II: Scale System Module for Performing Shielding and Working Library Production," Volume 1, Section F1 from "SCALE: A Modular System for Performing Standardized Computer Analysis for Licensing Evaluation" NUREG/CR-0200, Rev. 4, January 1990.
- [4.4.5] M. Edenius, K. Ekberg, B.H. Forssen, and D. Knott, "CASMO-4 A Fuel Assembly Burnup Program User's Manual," Studsvik/SOA-95/1, Studsvik of America (1995).

- [4.4.6] D. Knott, "CASMO-4 Benchmark Against Critical Experiments," Studsvik/SOA-94/13 (proprietary), Studsvik of America (1995).
- [4.4.7] D. Knott, "CASMO-4 Benchmark Against MCNP," Studsvik/SOA-94/12 (proprietary), Studsvik of America (1995).
- [4.4.8] S.E. Turner, "Uncertainty Analysis - Burnup Distributions", presented at the DOE/SANDIA Technical Meeting on Fuel Burnup Credit, Special Session, ANS/ENS Conference, Washington, D.C., November 2, 1988.

Table 4.1.1
Fuel Assembly Specifications

Fuel Rod Data	
Fuel pellet outside diameter, in.	0.370
Cladding thickness, in.	0.0195 - 0.0265
Cladding outside diameter, in.	0.416 - 0.430
Cladding inside diameter, in.	0.377
Cladding material	Zr-4
Pellet density, g/cc	10.522
Maximum enrichment, wt% ²³⁵ U	5.05 ± 0.05
Fuel Assembly Data	
Fuel rod array	15x15
Number of fuel rods	208
Fuel rod pitch, in.	0.568
Number of guide tubes	16
Guide tube outside diameter, in.	0.530
Guide tube inside diameter, in.	0.498
Instrument tube outside diameter, in.	0.493
Instrument tube inside diameter, in.	0.441
Active fuel length, in.	145

Table 4.2.1
Summary of the Criticality Safety Analyses

Design Basis Burnup at 5.05 wt% ²³⁵ U	53.51 GWD/MTU
Uncertainties	
Bias Uncertainty (95%/95%)	± 0.0011
Calculational Statistics [†] (95%/95%)	± 0.0010
Depletion Uncertainty	± 0.0176
Fuel Eccentricity	negative
Manufacturing Tolerances	± 0.0055
Statistical Combination of Uncertainties ^{††}	± 0.0185
Reference k_{eff} (MCNP4a)	0.8521
Total Uncertainty (above)	0.0185
Axial Burnup Distribution	0.0714
Calculational Bias (see Appendix A)	0.0009
Temperature Correction to 4°C (39°F)	0.0023
Maximum k_{eff}	0.9452 ^{†††}
Regulatory Limiting k_{eff}	0.9500

[†] The value used for the MCNP4a (or KENO5a) statistical uncertainty is 1.84 times the estimated standard deviation. Each final k value calculated by MCNP4a (or KENO5a) is the result of averaging a minimum of 200 cycle k values, and thus, is based on a minimum sample size of 200. The K multiplier, for a one-sided statistical tolerance with 95% probability at the 95% confidence level, corresponding to a sample size of 200, is 1.84 [6].

^{††} Square root of the sum of the squares.

^{†††} KENO5a verification calculation resulted in a maximum k_{eff} of 0.9456.

Table 4.2.2
Reactivity Effects of Abnormal and Accident Conditions

Abnormal/Accident Conditions	Reactivity Effect
Temperature Increase (above 4°C)	Negative (Table 4.6.1)
Void (boiling)	Negative (Table 4.6.1)
Assembly Drops	Negligible or Negative
Lateral Rack Movement	Negative
Misplacement or Mislocation of a Fresh Fuel Assembly	Positive - controlled by less than 650 ppm soluble boron

Table 4.5.1
Reactivity Effects of Manufacturing Tolerances

Tolerance	Reactivity Effect, Δk
Minimum Boral loading (█████ g/cm ² , 0.0324 g/cm ² nominal)	±0.0026
Minimum Boral width (█████", 7.5" nominal)	±0.0008
Minimum Cell Pitch (█████", 9.22" nominal)	±0.0011
Box wall thickness (█████" max., █████" min.; 0.075" nominal)	Negative [†]
Enrichment (5.10 wt% ²³⁵ U, 5.05 wt% ²³⁵ U nominal)	±0.0030
Density tolerance (10.722 g/cm ³ , 10.522 g/cm ³ nominal)	±0.0036
Total (statistical sum) ^{††}	±0.0055

[†] The nominal box wall dimension results in the highest reactivity.

^{††} Square root of the sum of the squares.

Table 4.6.1
Reactivity Effects of Temperature and Void

Temperature	Reactivity Effect, Δk
4°C (39°F)	reference
20°C (68°F)	-0.0023
60°C (140°F)	-0.0092
120°C (248°F)	-0.0218
120°C w/ 10% void	-0.0448

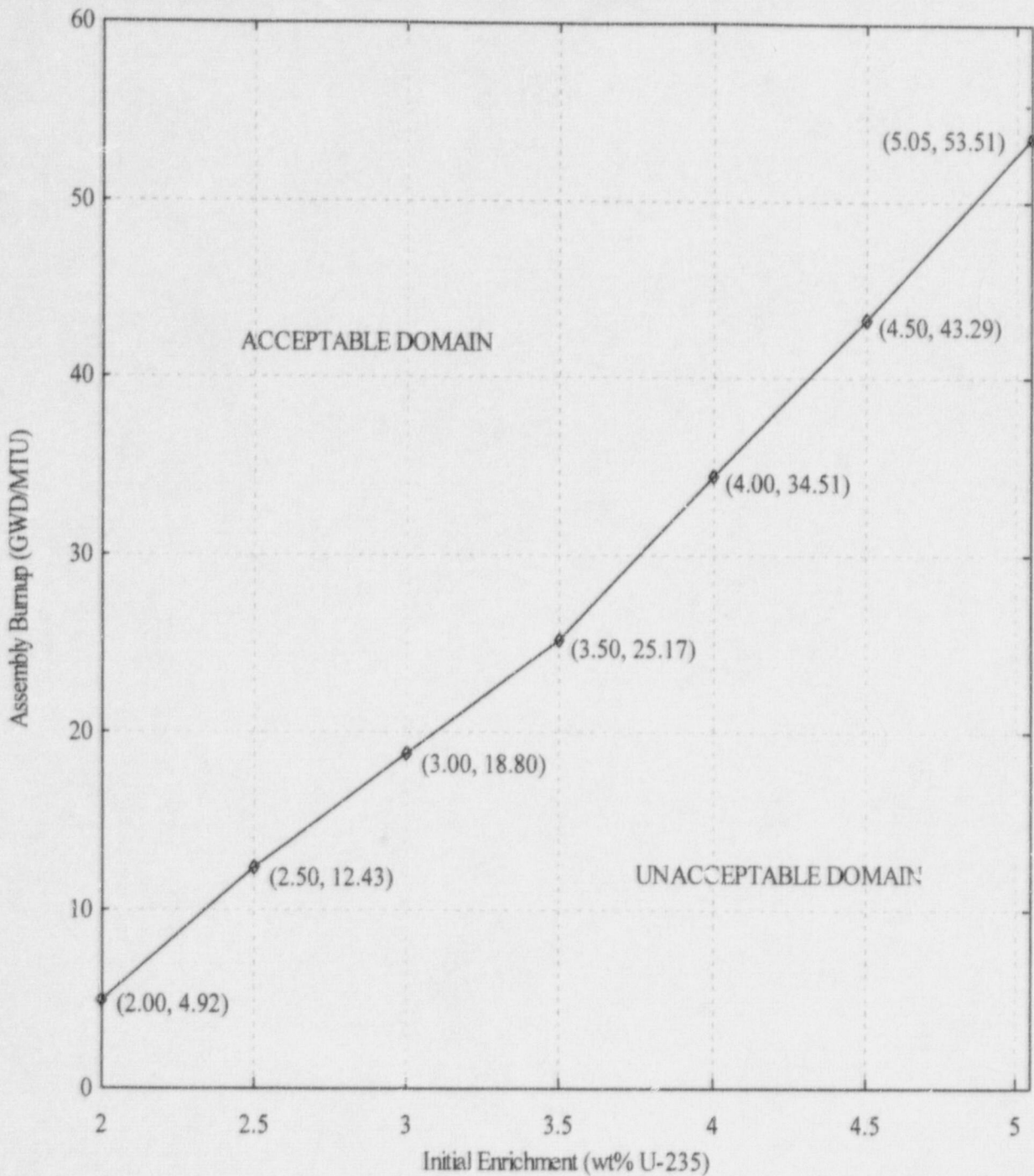
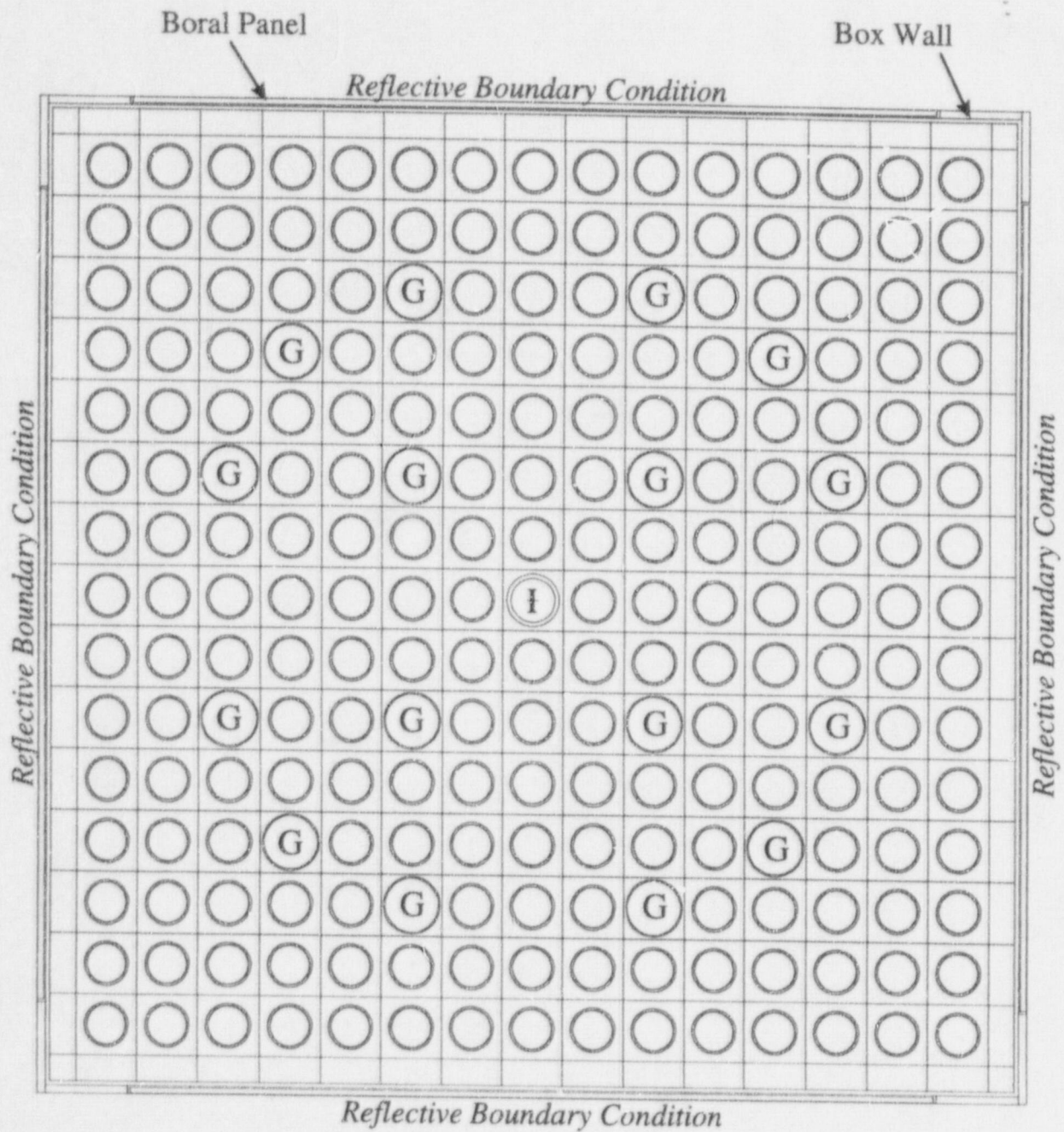


Figure 4.2.1 Minimum Required Fuel Assembly Burnup as a Function of Nominal Initial Enrichment to Permit Storage in the Cask Pit.

Note: Fuel assemblies with initial enrichments less than 2.0 wt% ²³⁵U will conservatively be required to meet the burnup requirements of 2.0 wt% ²³⁵U assemblies.



G = Guide Tube

I = Instrument Tube

Figure 4.3.1 A Two-Dimensional Representation of the Calculational Model Used for the Cask Pit Rack Analyses.

APPENDIX 4A: BENCHMARK CALCULATIONS

4A.1 INTRODUCTION AND SUMMARY

Benchmark calculations have been made on selected critical experiments, chosen, in so far as possible, to bound the range of variables in the rack designs. Two independent methods of analysis were used, differing in cross section libraries and in the treatment of the cross sections. MCNP4a [4A.1] is a continuous energy Monte Carlo code and KENO5a [4A.2] uses group-dependent cross sections. For the KENO5a analyses reported here, the 238-group library was chosen, processed through the NITAWL-II [4A.2] program to create a working library and to account for resonance self-shielding in uranium-238 (Nordheim integral treatment). The 238 group library was chosen to avoid or minimize the errors[†] (trends) that have been reported (e.g., [4A.3 through 4A.5]) for calculations with collapsed cross section sets.

In rack designs, the three most significant parameters affecting criticality are (1) the fuel enrichment, (2) the ¹⁰B loading in the neutron absorber, and (3) the lattice spacing (or water-gap thickness if a flux-trap design is used). Other parameters, within the normal range of rack and fuel designs, have a smaller effect, but are also included in the analyses.

Table 4A.1 summarizes results of the benchmark calculations for all cases selected and analyzed, as referenced in the table. The effect of the major variables are discussed in subsequent sections below. It is important to note that there is obviously considerable overlap in parameters since it is not possible to vary a single parameter and maintain criticality; some other parameter or parameters must be concurrently varied to maintain criticality.

One possible way of representing the data is through a spectrum index that incorporates all of the variations in parameters. KENO5a computes and prints the "energy of the average lethargy causing fission" (EALF). In MCNP4a, by utilizing the tally option with the identical 238-group energy structure as in KENO5a, the number of fissions in each group may be collected and the EALF determined (post-processing).

[†] Small but observable trends (errors) have been reported for calculations with the 27-group and 44-group collapsed libraries. These errors are probably due to the use of a single collapsing spectrum when the spectrum should be different for the various cases analyzed, as evidenced by the spectrum indices.

Figures 4A.1 and 4A.2 show the calculated k_{eff} for the benchmark critical experiments as a function of the EALF for MCNP4a and KENO5a, respectively (UO₂ fuel only). The scatter in the data (even for comparatively minor variation in critical parameters) represents experimental error[†] in performing the critical experiments within each laboratory, as well as between the various testing laboratories. The B&W critical experiments show a larger experimental error than the PNL criticals. This would be expected since the B&W criticals encompass a greater range of critical parameters than the PNL criticals.

Linear regression analysis of the data in Figures 4A.1 and 4A.2 show that there are no trends, as evidenced by very low values of the correlation coefficient (0.13 for MCNP4a and 0.21 for KENO5a). The total bias (systematic error, or mean of the deviation from a k_{eff} of exactly 1.000) for the two methods of analysis are shown in the table below.

Calculational Bias of MCNP4a and KENO5a	
MCNP4a	0.0009 ± 0.0011
KENO5a	0.0030 ± 0.0012

The bias and standard error of the bias were derived directly from the calculated k_{eff} values in Table 4A.1 using the following equations^{††}, with the standard error multiplied by the one-sided K-factor for 95% probability at the 95% confidence level from NBS Handbook 91 [4A.18] (for the number of cases analyzed, the K-factor is ~2.05 or slightly more than 2).

$$\bar{k} = \frac{1}{n} \sum_i^n k_i \quad (4A.1)$$

[†] A classical example of experimental error is the corrected enrichment in the PNL experiments, first as an addendum to the initial report and, secondly, by revised values in subsequent reports for the same fuel rods.

^{††} These equations may be found in any standard text on statistics, for example, reference [4A.6] (or the MCNP4a manual) and is the same methodology used in MCNP4a and in KENO5a.

$$\sigma_{\bar{k}}^2 = \frac{\sum_{i=1}^n k_i^2 - (\sum_{i=1}^n k_i)^2 / n}{n(n-1)} \quad (4A.2)$$

$$Bias = (1 - \bar{k}) \pm K \sigma_{\bar{k}} \quad (4A.3)$$

where k_i are the calculated reactivities of n critical experiments; $\sigma_{\bar{k}}$ is the unbiased estimator of the standard deviation of the mean (also called the standard error of the bias (mean)); K is the one-sided multiplier for 95% probability at the 95% confidence level (NBS Handbook 91 [4A.18]).

Formula 4.A.3 is based on the methodology of the National Bureau of Standards (now NIST) and is used to calculate the values presented on page 4.A-2. The first portion of the equation, $(1 - \bar{k})$, is the actual bias which is added to the MCNP4a and KENO5a results. The second term, $K\sigma_{\bar{k}}$, is the uncertainty or standard error associated with the bias. The K values used were obtained from the National Bureau of Standards Handbook 91 and are for one-sided statistical tolerance limits for 95% probability at the 95% confidence level. The actual K values for the 56 critical experiments evaluated with MCNP4a and the 53 critical experiments evaluated with KENO5a are 2.04 and 2.05, respectively.

The bias values are used to evaluate the maximum k_{eff} values for the rack designs. KENO5a has a slightly larger systematic error than MCNP4a, but both result in greater precision than published data [4A.3 through 4A.5] would indicate for collapsed cross section sets in KENO5a (SCALE) calculations.

4A.2 Effect of Enrichment

The benchmark critical experiments include those with enrichments ranging from 2.46 w/o to 5.74 w/o and therefore span the enrichment range for rack designs. Figures 4A.3 and 4A.4 show the calculated k_{eff} values (Table 4A.1) as a function of the fuel enrichment reported for the critical experiments. Linear regression analyses for these data confirms that there are no trends, as indicated by low values of the correlation coefficients (0.03 for MCNP4a and 0.38 for KENO5a). Thus, there are no corrections to the bias for the various

enrichments.

As further confirmation of the absence of any trends with enrichment, a typical configuration was calculated with both MCNP4a and KENO5a for various enrichments. The cross-comparison of calculations with codes of comparable sophistication is suggested in Reg. Guide 3.41. Results of this comparison, shown in Table 4A.2 and Figure 4A.5, confirm no significant difference in the calculated values of k_{eff} for the two independent codes as evidenced by the 45° slope of the curve. Since it is very unlikely that two independent methods of analysis would be subject to the same error, this comparison is considered confirmation of the absence of an enrichment effect (trend) in the bias.

4A.3 Effect of ^{10}B Loading

Several laboratories have performed critical experiments with a variety of thin absorber panels similar to the Boral panels in the rack designs. Of these critical experiments, those performed by B&W are the most representative of the rack designs. PNL has also made some measurements with absorber plates, but, with one exception (a flux-trap experiment), the reactivity worth of the absorbers in the PNL tests is very low and any significant errors that might exist in the treatment of strong thin absorbers could not be revealed.

Table 4A.3 lists the subset of experiments using thin neutron absorbers (from Table 4A.1) and shows the reactivity worth (Δk) of the absorber.[†]

No trends with reactivity worth of the absorber are evident, although based on the calculations shown in Table 4A.3, some of the B&W critical experiments seem to have unusually large experimental errors. B&W made an effort to report some of their experimental errors. Other laboratories did not evaluate their experimental errors.

To further confirm the absence of a significant trend with ^{10}B concentration in the absorber, a cross-comparison was made with MCNP4a and KENO5a (as suggested in Reg. Guide 3.41). Results are shown in Figure 4A.6 and Table 4A.4 for a typical geometry. These data substantiate the absence of any error (trend) in either of the two codes for the conditions analyzed (data points fall on a 45° line, within an expected 95% probability limit).

[†] The reactivity worth of the absorber panels was determined by repeating the calculation with the absorber analytically removed and calculating the incremental (Δk) change in reactivity due to the absorber.

4A.4 Miscellaneous and Minor Parameters

4A.4.1 Reflector Material and Spacings

PNL has performed a number of critical experiments with thick steel and lead reflectors.[†] Analysis of these critical experiments are listed in Table 4A.5 (subset of data in Table 4A.1). There appears to be a small tendency toward overprediction of k_{eff} at the lower spacing, although there are an insufficient number of data points in each series to allow a quantitative determination of any trends. The tendency toward overprediction at close spacing means that the rack calculations may be slightly more conservative than otherwise.

4A.4.2 Fuel Pellet Diameter and Lattice Pitch

The critical experiments selected for analysis cover a range of fuel pellet diameters from 0.311 to 0.444 inches, and lattice spacings from 0.476 to 1.00 inches. In the rack designs, the fuel pellet diameters range from 0.303 to 0.3805 inches O.D. (0.496 to 0.580 inch lattice spacing) for PWR fuel and from 0.3224 to 0.494 inches O.D. (0.488 to 0.740 inch lattice spacing) for BWR fuel. Thus, the critical experiments analyzed provide a reasonable representation of power reactor fuel. Based on the data in Table 4A.1, there does not appear to be any observable trend with either fuel pellet diameter or lattice pitch, at least over the range of the critical experiments applicable to rack designs.

4A.4.3 Soluble Boron Concentration Effects

Various soluble boron concentrations were used in the B&W series of critical experiments and in one PNL experiment, with boron concentrations ranging up to 2550 ppm. Results of MCNP4a (and one KENO5a) calculations are shown in Table 4A.6. Analyses of the very high boron concentration experiments (> 1300 ppm) show a tendency to slightly overpredict reactivity for the three experiments exceeding 1300 ppm. In turn, this would suggest that the evaluation of the racks with higher soluble boron concentrations could be slightly conservative.

[†] Parallel experiments with a depleted uranium reflector were also performed but not included in the present analysis since they are not pertinent to the Holtec rack design.

The number of critical experiments with PuO_2 bearing fuel (MOX) is more limited than for UO_2 fuel. However, a number of MOX critical experiments have been analyzed and the results are shown in Table 4A.7. Results of these analyses are generally above a k_{eff} of 1.00, indicating that when Pu is present, both MCNP4a and KENO5a overpredict the reactivity. This may indicate that calculation for MOX fuel will be expected to be conservative, especially with MCNP4a. It may be noted that for the larger lattice spacings, the KENO5a calculated reactivities are below 1.00, suggesting that a small trend may exist with KENO5a. It is also possible that the overprediction in k_{eff} for both codes may be due to a small inadequacy in the determination of the Pu-241 decay and Am-241 growth. This possibility is supported by the consistency in calculated k_{eff} over a wide range of the spectral index (energy of the average lethargy causing fission).

- [4A.1] J.F. Briesmeister, Ed., "MCNP4a - A General Monte Carlo N-Particle Transport Code, Version 4A; Los Alamos National Laboratory, LA-12625-M (1993).
- [4A.2] SCALE 4.3, "A Modular Code System for Performing Standardized Computer Analyses for Licensing Evaluation", NUREG-0200 (ORNL-NUREG-CSD-2/U2/R5, Revision 5, Oak Ridge National Laboratory, September 1995.
- [4A.3] M.D. DeHart and S.M. Bowman, "Validation of the SCALE Broad Structure 44-G Group ENDF/B-Y Cross-Section Library for Use in Criticality Safety Analyses", NUREG/CR-6102 (ORNL/TM-12460) Oak Ridge National Laboratory, September 1994.
- [4A.4] W.C. Jordan et al., "Validation of KENO.V.a", CSD/TM-238, Martin Marietta Energy Systems, Inc., Oak Ridge National Laboratory, December 1986.
- [4A.5] O.W. Hermann et al., "Validation of the Scale System for PWR Spent Fuel Isotopic Composition Analysis", ORNL-TM-12667, Oak Ridge National Laboratory, undated.
- [4A.6] R.J. Larsen and M.L. Marx, An Introduction to Mathematical Statistics and its Applications, Prentice-Hall, 1986.
- [4A.7] M.N. Baldwin et al., Critical Experiments Supporting Close Proximity Water Storage of Power Reactor Fuel, BAW-1484-7, Babcock and Wilcox Company, July 1979.
- [4A.8] G.S. Hoovier et al., Critical Experiments Supporting Underwater Storage of Tightly Packed Configurations of Spent Fuel Pins, BAW-1645-4, Babcock & Wilcox Company, November 1991.
- [4A.9] L.W. Newman et al., Urania Gadolinia: Nuclear Model Development and Critical Experiment Benchmark, BAW-1810, Babcock and Wilcox Company, April 1984.

- [4A.10] J.C. Manaranche et al., "Dissolution and Storage Experimental Program with 4.75 w/o Enriched Uranium-Oxide Rods," Trans. Am. Nucl. Soc. 33: 362-364 (1979).
- [4A.11] S.R. Bierman and E.D. Clayton, Criticality Experiments with Subcritical Clusters of 2.35 w/o and 4.31 w/o ^{235}U Enriched UO_2 Rods in Water with Steel Reflecting Walls, PNL-3602, Battelle Pacific Northwest Laboratory, April 1981.
- [4A.12] S.R. Bierman et al., Criticality Experiments with Subcritical Clusters of 2.35 w/o and 4.31 w/o ^{235}U Enriched UO_2 Rods in Water with Uranium or Lead Reflecting Walls, PNL-3926, Battelle Pacific Northwest Laboratory, December, 1981.
- [4A.13] S.R. Bierman et al., Critical Separation Between Subcritical Clusters of 4.31 w/o ^{235}U Enriched UO_2 Rods in Water with Fixed Neutron Poisons, PNL-2615, Battelle Pacific Northwest Laboratory, October 1977.
- [4A.14] S.R. Bierman, Criticality Experiments with Neutron Flux Traps Containing Voids, PNL-7167, Battelle Pacific Northwest Laboratory, April 1990.
- [4A.15] B.M. Durst et al., Critical Experiments with 4.31 wt % ^{235}U Enriched UO_2 Rods in Highly Borated Water Lattices, PNL-4267, Battelle Pacific Northwest Laboratory, August 1982.
- [4A.16] S.R. Bierman, Criticality Experiments with Fast Test Reactor Fuel Pins in Organic Moderator, PNL-5803, Battelle Pacific Northwest Laboratory, December 1981.
- [4A.17] E.G. Taylor et al., Saxton Plutonium Program Critical Experiments for the Saxton Partial Plutonium Core, WCAP-3385-54, Westinghouse Electric Corp., Atomic Power Division, December 1965.
- [4A.18] M.G. Natrella, Experimental Statistics, National Bureau of Standards, Handbook 91, August 1963.

Table 4A.1

Summary of Criticality Benchmark Calculations

	Reference	Identification	Enrich.	Calculated k_{eff}			EALF ¹ (eV)
				MCNP4a	KENO5a	MCNP4a	
1	B&W-1484 (4A.7)	Core I	2.46	0.9964 ± 0.0010	0.9898 ± 0.0006	0.1759	0.1753
2	B&W-1484 (4A.7)	Core II	2.46	1.0008 ± 0.0011	1.0015 ± 0.0005	0.2553	0.2446
3	B&W-1484 (4A.7)	Core III	2.46	1.0010 ± 0.0012	1.0005 ± 0.0005	0.1999	0.1939
4	B&W-1484 (4A.7)	Core IX	2.46	0.9956 ± 0.0012	0.9901 ± 0.0006	0.1422	0.1426
5	B&W-1484 (4A.7)	Core X	2.46	0.9980 ± 0.0014	0.9922 ± 0.0006	0.1513	0.1499
6	B&W-1484 (4A.7)	Core XI	2.46	0.9978 ± 0.0012	1.0005 ± 0.0005	0.2031	0.1947
7	B&W-1484 (4A.7)	Core XII	2.46	0.9988 ± 0.0011	0.9978 ± 0.0006	0.1718	0.1662
8	B&W-1484 (4A.7)	Core XIII	2.46	1.0020 ± 0.0010	0.9952 ± 0.0006	0.1988	0.1965
9	B&W-1484 (4A.7)	Core XIV	2.46	0.9953 ± 0.0011	0.9928 ± 0.0006	0.2022	0.1986
10	B&W-1484 (4A.7)	Core XV ^{††}	2.46	0.9910 ± 0.0011	0.9909 ± 0.0006	0.2092	0.2014
11	B&W-1484 (4A.7)	Core XVI ^{††}	2.46	0.9935 ± 0.0010	0.9889 ± 0.0006	0.1757	0.1713
12	B&W-1484 (4A.7)	Core XVII	2.46	0.9962 ± 0.0012	0.9942 ± 0.0005	0.2083	0.2021
13	B&W-1484 (4A.7)	Core XVIII	2.46	1.0036 ± 0.0012	0.9931 ± 0.0006	0.1705	0.1708

Table 4A.1
Summary of Criticality Benchmark Calculations

Reference	Identification	Enrich.	Calculated k_{eff}				
			MCNP4a	KENO5a	MCNP4a	KENO5a	
						EALF [†] (eV)	
14	B&W-1484 (4A.7)	Core XIX	2.46	0.9961 ± 0.0012	0.9971 ± 0.0005	0.2103	0.2011
15	B&W-1484 (4A.7)	Core XX	2.46	1.0008 ± 0.0011	0.9932 ± 0.0006	0.1724	0.1701
16	B&W-1484 (4A.7)	Core XXI	2.46	0.9994 ± 0.0010	0.9918 ± 0.0006	0.1544	0.1536
17	B&W-1645 (4A.8)	S-type Fuel, w/886 ppm B	2.46	0.9970 ± 0.0010	0.9924 ± 0.0006	1.4475	1.4680
18	B&W-1645 (4A.8)	S-type Fuel, w/746 ppm B	2.46	0.9990 ± 0.0010	0.9913 ± 0.0006	1.5463	1.5660
19	B&W-1645 (4A.8)	SO-type Fuel, w/1156 ppm B	2.46	0.9972 ± 0.0009	0.9949 ± 0.0005	0.4241	0.4331
20	B&W-1810 (4A.9)	Case 1 1337 ppm B	2.46	1.0023 ± 0.0010	NC	0.1531	NC
21	B&W-1810 (4A.9)	Case 12 1899 ppm B	2.46/4.02	1.0060 ± 0.0009	NC	0.4493	NC
22	French (4A.10)	Water Moderator 0 gap	4.75	0.9966 ± 0.0013	NC	0.2172	NC
23	French (4A.10)	Water Moderator 2.5 cm gap	4.75	0.9952 ± 0.0012	NC	0.1778	NC
24	French (4A.10)	Water Moderator 5 cm gap	4.75	0.9943 ± 0.0010	NC	0.1677	NC
25	French (4A.10)	Water Moderator 10 cm gap	4.75	0.9979 ± 0.0010	NC	0.1736	NC
26	PNL-3602 (4A.11)	Steel Reflector, 0 separation	2.35	NC	1.0004 ± 0.0006	NC	0.1018

Table 4A.1

Summary of Criticality Benchmark Calculations

Reference	Identification	Enrich.	Calculated k_{eff}			$E\Delta LF^+$ (eV)	
			MCNP4a	KENO5a	MCNP4a		KENO5a
27	PNL-3602 (4A.11)	Steel Reflector, 1.321 cm sepn.	2.35	0.9980 ± 0.0009	0.9992 ± 0.0006	0.1000	0.0909
28	PNL-3602 (4A.11)	Steel Reflector, 2.616 cm sepn	2.35	0.9968 ± 0.0009	0.9964 ± 0.0006	0.0981	0.0975
29	PNL-3602 (4A.11)	Steel Reflector, 3.912 cm sepn.	2.35	0.9974 ± 0.0010	0.9980 ± 0.0006	0.0976	0.0970
30	PNL-3602 (4A.11)	Steel Reflector, infinite sepn.	2.35	0.9962 ± 0.0008	0.9939 ± 0.0006	0.0973	0.0968
31	PNL-3602 (4A.11)	Steel Reflector, 0 cm sepn.	4.306	NC	1.0003 ± 0.0007	NC	0.3282
32	PNL-3602 (4A.11)	Steel Reflector, 1.321 cm sepn.	4.306	0.9997 ± 0.0010	1.0012 ± 0.0007	0.3016	0.3039
33	PNL-3602 (4A.11)	Steel Reflector, 2.616 cm sepn.	4.306	0.9994 ± 0.0012	0.9974 ± 0.0007	0.2911	0.2927
34	PNL-3602 (4A.11)	Steel Reflector, 5.405 cm sepn.	4.306	0.9969 ± 0.0011	0.9951 ± 0.0007	0.2828	0.2860
35	PNL-3602 (4A.11)	Steel Reflector, Infinite sepn. ^{††}	4.306	0.9910 ± 0.0020	0.9947 ± 0.0007	0.2851	0.2864
36	PNL-3602 (4A.11)	Steel Reflector, with Boral Sheets	4.306	0.9941 ± 0.0011	0.9970 ± 0.0007	0.3135	0.3150
37	PNL-3926 (4A.12)	Lead Reflector, 0 cm sepn.	4.306	NC	1.0003 ± 0.0007	NC	0.3159
38	PNL-3926 (4A.12)	Lead Reflector, 0.55 cm sepn.	4.306	1.0025 ± 0.0011	0.9997 ± 0.0007	0.3030	0.3044
39	PNL-3926 (4A.12)	Lead Reflector, 1.956 cm sepn.	4.306	1.0000 ± 0.0012	0.9985 ± 0.0007	0.2883	0.2930

Table 4A.1

Summary of Criticality Benchmark Calculations

	Reference	Identification	Enrich.	Calculated k_{eff}			EALF ⁺ (eV)
				MCNP4a	KENO5a	MKNP4a	
40	PNL-3926 (4A.12)	Lead Reflector, 5.405 cm sepn.	4.306	0.9971 ± 0.0012	0.9946 ± 0.0007	0.2831	0.2854
41	PNL-2615 (4A.13)	Experiment 004/032 - no absorber	4.306	0.9925 ± 0.0012	0.9950 ± 0.0007	0.1155	0.1159
42	PNL-2615 (4A.13)	Experiment 030 - Zr plates	4.306	NC	0.9971 ± 0.0007	NC	0.1154
43	PNL-2615 (4A.13)	Experiment 013 - Steel plates	4.306	NC	0.9965 ± 0.0007	NC	0.1164
44	PNL-2615 (4A.13)	Experiment 014 - Steel plates	4.306	NC	0.9972 ± 0.0007	NC	0.1164
45	PNL-2615 (4A.13)	Exp. 009 1.05% Boron-Steel plates	4.306	0.9982 ± 0.0010	0.9981 ± 0.0007	0.1172	0.1162
46	PNL-2615 (4A.13)	Exp. 012 1.62% Boron-Steel plates	4.306	0.9996 ± 0.0012	0.9982 ± 0.0007	0.1161	0.1173
47	PNL-2615 (4A.13)	Exp. 031 - Boral plates	4.306	0.9994 ± 0.0012	0.9969 ± 0.0007	0.1165	0.1171
48	PNL-7167 (4A.14)	Experiment 214R - with flux trap	4.306	0.9991 ± 0.0011	0.9956 ± 0.0007	0.3722	0.3812
49	PNL-7167 (4A.14)	Experiment 214V3 - with flux trap	4.306	0.9969 ± 0.0011	0.9963 ± 0.0007	0.3742	0.3826
50	PNL-4267 (4A.15)	Case 173 - 0 ppm B	4.306	0.9974 ± 0.0012	NC	6.2893	NC
51	PNL-4267 (4A.15)	Case 177 - 2550 ppm B	4.306	1.0057 ± 0.0010	NC	0.5509	NC
52	PNL-5803 (4A.16)	MOX Fuel - Type 3.2 Exp. 21	20% Pu	1.0041 ± 0.0011	1.0046 ± 0.0006	0.9171	0.8868

Table 4A.1

Summary of Criticality Benchmark Calculations

Reference	Identification	Enrich.	Calculated k_{eff}				EALF [†] (eV)
			MCNP4a	KENO5a	MCNP4a	KENO5a	
53	PNL-5803 (4A.16)	20% Pu	1.0058 ± 0.0012	1.0036 ± 0.0006	0.2968	0.2944	
54	PNL-5803 (4A.16)	20% Pu	1.0083 ± 0.0011	0.9989 ± 0.0006	0.1665	0.1706	
55	PNL-5803 (4A.16)	20% Pu	1.0079 ± 0.0011	0.9966 ± 0.0006	0.1139	0.1165	
56	WCAP-3385 (4A.17)	6.6% Pu	0.9996 ± 0.0011	1.0005 ± 0.0006	0.8665	0.8417	
57	WCAP-3385 (4A.17)	5.74	1.0000 ± 0.0010	0.9956 ± 0.0007	0.4476	0.4580	
58	WCAP-3385 (4A.17)	6.6% Pu	1.0036 ± 0.0011	1.0047 ± 0.0006	0.5289	0.5197	
59	WCAP-3385 (4A.17)	6.6% Pu	1.0008 ± 0.0010	NC	0.6389	NC	
60	WCAP-3385 (4A.17)	5.74	0.9994 ± 0.0011	0.9967 ± 0.0007	0.2923	0.2954	
61	WCAP-3385 (4A.17)	6.6% Pu	1.0063 ± 0.0011	1.0133 ± 0.0006	0.1520	0.1555	
62	WCAP-3385 (4A.17)	5.74	1.0039 ± 0.0011	1.0008 ± 0.0006	0.1036	0.1047	

Notes: NC stands for not calculated.

[†] EALF is the energy of the average lethargy causing fission.

^{††} These experimental results appear to be statistical outliers ($> 3\sigma$) suggesting the possibility of unusually large experimental error. Although they could justifiably be excluded, for conservatism, they were retained in determining the calculational basis.

Table 4A.2

COMPARISON OF MCNP4a AND KENO5a CALCULATED REACTIVITIES[†]
FOR VARIOUS ENRICHMENTS

Enrichment	Calculated $k_{\text{eff}} \pm 1\sigma$	
	MCNP4a	KENO5a
3.0	0.8465 ± 0.0011	0.8478 ± 0.0004
3.5	0.8820 ± 0.0011	0.8841 ± 0.0004
3.75	0.9019 ± 0.0011	0.8987 ± 0.0004
4.0	0.9132 ± 0.0010	0.9140 ± 0.0004
4.2	0.9276 ± 0.0011	0.9237 ± 0.0004
4.5	0.9400 ± 0.0011	0.9388 ± 0.0004

[†] Based on the GE 8x8R fuel assembly.

Table 4A.3

MCNP4a CALCULATED REACTIVITIES FOR
CRITICAL EXPERIMENTS WITH NEUTRON ABSORBERS

Ref.	Experiment		Δk Worth of Absorber	MCNP4a Calculated k_{eff}	EALF [†] (eV)
4A.13	PNL-2615	Boral Sheet	0.0139	0.9994 ± 0.0012	0.1165
4A.7	B&W-1484	Core XX	0.0165	1.0008 ± 0.0011	0.1724
4A.13	PNL-2615	1.62% Boron-steel	0.0165	0.9996 ± 0.0012	0.1161
4A.7	B&W-1484	Core XIX	0.0202	0.9961 ± 0.0012	0.2103
4A.7	B&W-1484	Core XXI	0.0243	0.9994 ± 0.0010	0.1544
4A.7	B&W-1484	Core XVII	0.0519	0.9962 ± 0.0012	0.2083
4A.11	PNL-3602	Boral Sheet	0.0708	0.9941 ± 0.0011	0.3135
4A.7	B&W-1484	Core XV	0.0786	0.9910 ± 0.0011	0.2092
4A.7	B&W-1484	Core XVI	0.0845	0.9935 ± 0.0010	0.1757
4A.7	B&W-1484	Core XIV	0.1575	0.9953 ± 0.0011	0.2022
4A.7	B&W-1484	Core XIII	0.1738	1.0020 ± 0.0011	0.1988
4A.14	PNL-7167	Expt 214R flux trap	0.1931	0.9991 ± 0.0011	0.3722

[†]EALF is the energy of the average lethargy causing fission.

Table 4A.4

COMPARISON OF MCNP4a AND KENO5a
CALCULATED REACTIVITIES[†] FOR VARIOUS ¹⁰B LOADINGS

¹⁰ B, g/cm ²	Calculated $k_{\text{eff}} \pm 1\sigma$	
	MCNP4a	KENO5a
0.005	1.0381 \pm 0.0012	1.0340 \pm 0.0004
0.010	0.9960 \pm 0.0010	0.9941 \pm 0.0004
0.015	0.9727 \pm 0.0009	0.9713 \pm 0.0004
0.020	0.9541 \pm 0.0012	0.9560 \pm 0.0004
0.025	0.9433 \pm 0.0011	0.9428 \pm 0.0004
0.03	0.9325 \pm 0.0011	0.9338 \pm 0.0004
0.035	0.9234 \pm 0.0011	0.9251 \pm 0.0004
0.04	0.9173 \pm 0.0011	0.9179 \pm 0.0004

[†] Based on a 4.5% enriched GE 8x8R fuel assembly.

Table 4A.5

CALCULATIONS FOR CRITICAL EXPERIMENTS WITH
THICK LEAD AND STEEL REFLECTORS[†]

Ref.	Case	E, wt%	Separation, cm	MCNP4a k_{eff}	KENO5a k_{eff}
4A.11	Steel Reflector	2.35	1.321	0.9980 ± 0.0009	0.9992 ± 0.0006
		2.35	2.616	0.9968 ± 0.0009	0.9964 ± 0.0006
		2.35	3.912	0.9974 ± 0.0010	0.9980 ± 0.0006
		2.35	∞	0.9962 ± 0.0008	0.9939 ± 0.0006
4A.11	Steel Reflector	4.306	1.321	0.9997 ± 0.0010	1.0012 ± 0.0007
		4.306	2.616	0.9994 ± 0.0012	0.9974 ± 0.0007
		4.306	3.405	0.9969 ± 0.0011	0.9951 ± 0.0007
		4.306	∞	0.9910 ± 0.0020	0.9947 ± 0.0007
4A.12	Lead Reflector	4.306	0.55	1.0025 ± 0.0011	0.9997 ± 0.0007
		4.306	1.956	1.0000 ± 0.0012	0.9985 ± 0.0007
		4.306	5.405	0.9971 ± 0.0012	0.9946 ± 0.0007

[†] Arranged in order of increasing reflector-fuel spacing.

Table 4A.6

CALCULATIONS FOR CRITICAL EXPERIMENTS WITH VARIOUS SOLUBLE
BORON CONCENTRATIONS

Reference	Experiment	Boron Concentration, ppm	Calculated k_{eff}	
			MCNP4a	KENO5a
4A.15	PNL-4267	0	0.9974 ± 0.0012	-
4A.8	B&W-1645	886	0.9970 ± 0.0010	0.9924 ± 0.0006
4A.9	B&W-1810	1337	1.0023 ± 0.0010	-
4A.9	B&W-1810	1899	1.0060 ± 0.0009	-
4A.15	PNL-4267	2550	1.0057 ± 0.0010	-

Table 4A.7

CALCULATIONS FOR CRITICAL EXPERIMENTS WITH MOX FUEL

Reference	Case [†]	MCNP4a		KENO5a	
		k_{eff}	EALF ^{††}	k_{eff}	EALF ^{††}
PNL-5803 [4A.16]	MOX Fuel - Exp. No. 21	1.0041 ± 0.0011	0.9171	1.0046 ± 0.0006	0.8868
	MOX Fuel - Exp. No. 43	1.0058 ± 0.0012	0.2968	1.0076 ± 0.0006	0.2944
	MOX Fuel - Exp. No. 13	1.0083 ± 0.0011	0.1665	0.9989 ± 0.0006	0.1706
	MOX Fuel - Exp. No. 32	1.0079 ± 0.0011	0.1139	0.9966 ± 0.0006	0.1165
WCAP-3385-54 [4A.17]	Saxton @ 0.52" pitch	0.9996 ± 0.0011	0.8665	1.0005 ± 0.0006	0.8417
	Saxton @ 0.56" pitch	1.0036 ± 0.0011	0.5289	1.0047 ± 0.0006	0.5197
	Saxton @ 0.56" pitch borated	1.0008 ± 0.0010	0.6389	NC	NC
	Saxton @ 0.79" pitch	1.0063 ± 0.0011	0.1520	1.0133 ± 0.0006	0.1555

Note: NC stands for not calculated

[†] Arranged in order of increasing lattice spacing.

^{††} EALF is the energy of the average lethargy causing fission.

--- Linear Regression with Correlation Coefficient of 0.13

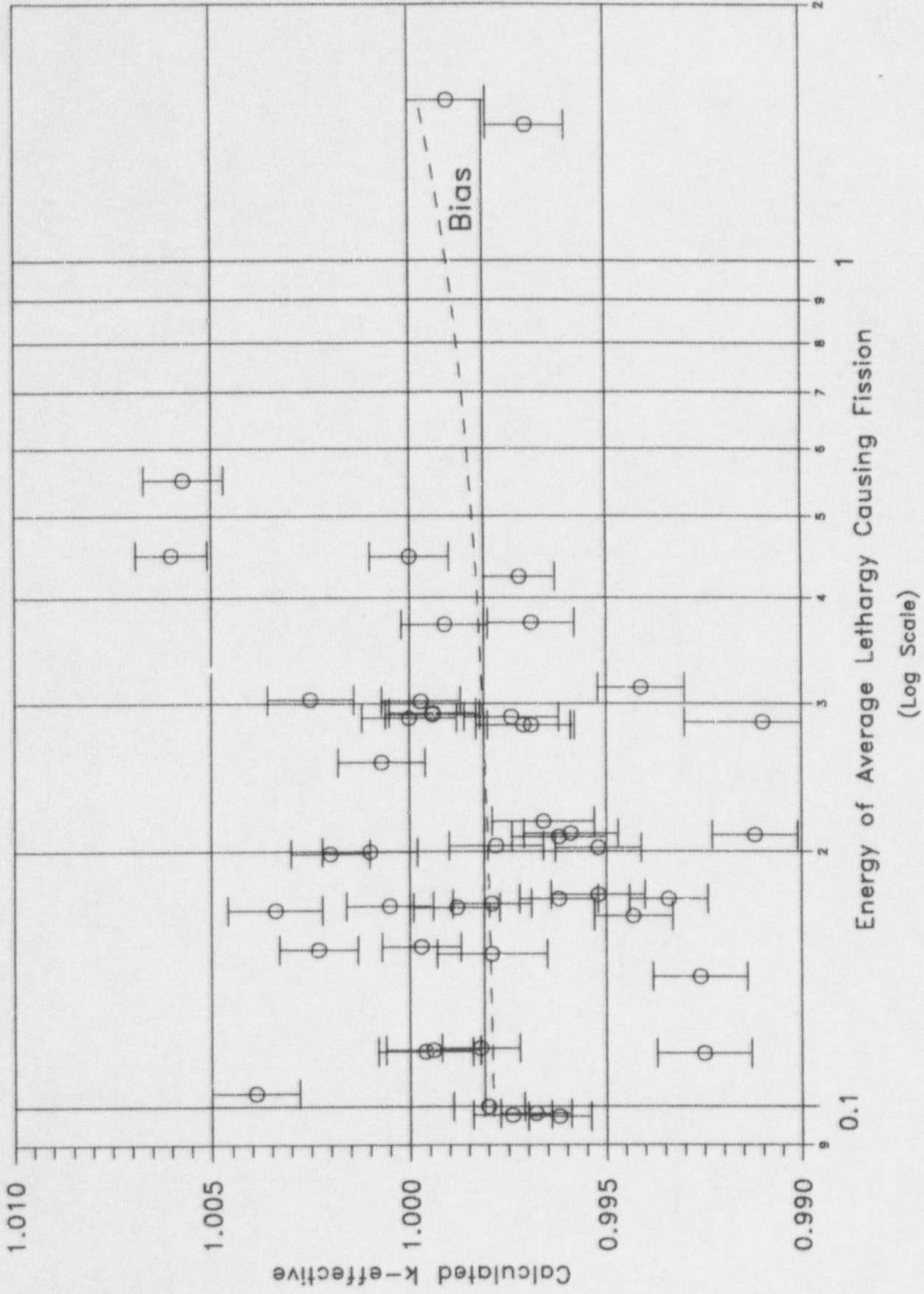


FIGURE 4A.1 MCNP CALCULATED k_{eff} VALUES for VARIOUS VALUES OF THE SPECTRAL INDEX

--- Linear Regression with Correlation Coefficient of 0.21

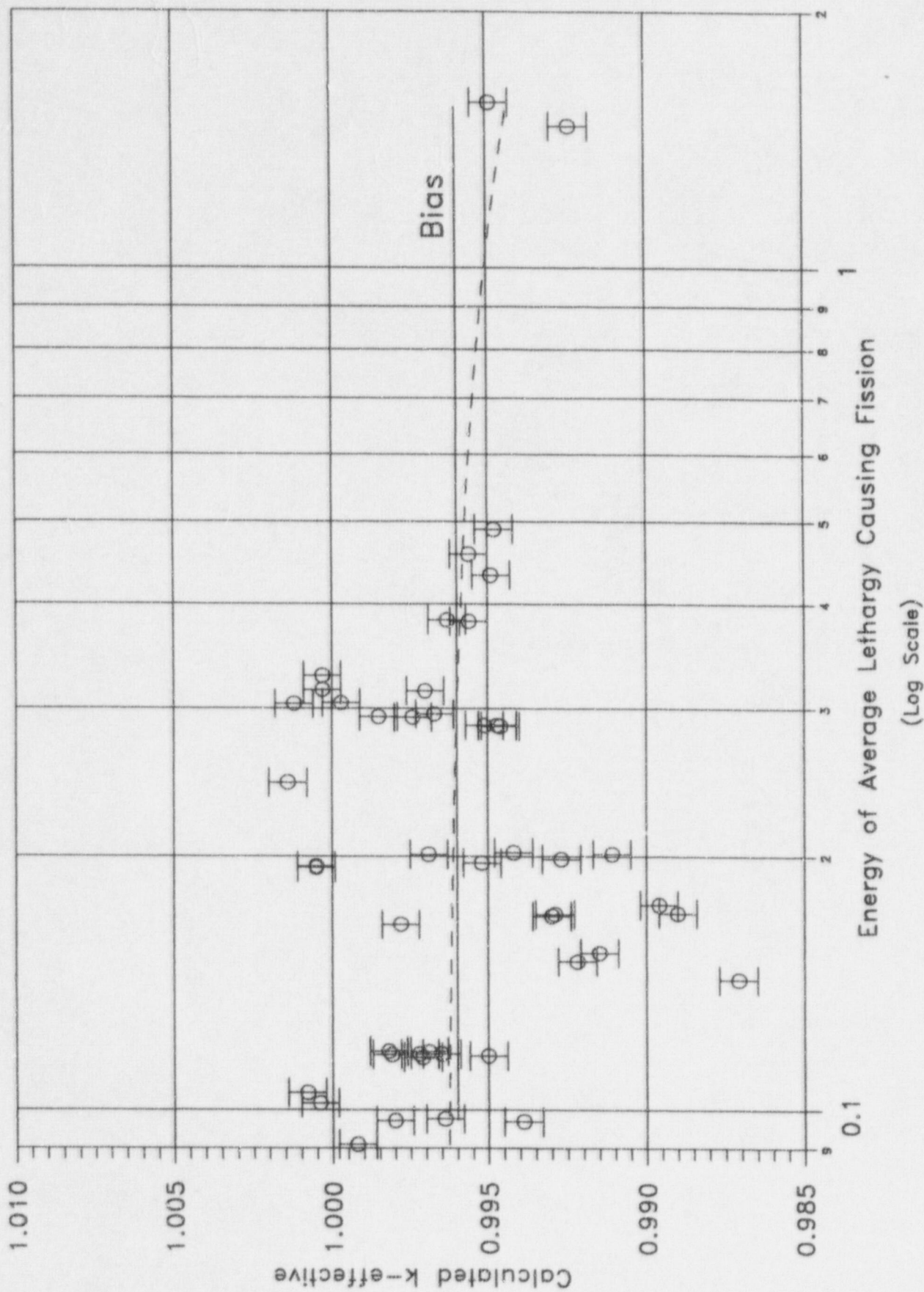


FIGURE 4A.2 KEN05a CALCULATED k-eff VALUES FOR VARIOUS VALUES OF THE SPECTRAL INDEX

--- Linear Regression with Correlation Coefficient of 0.03

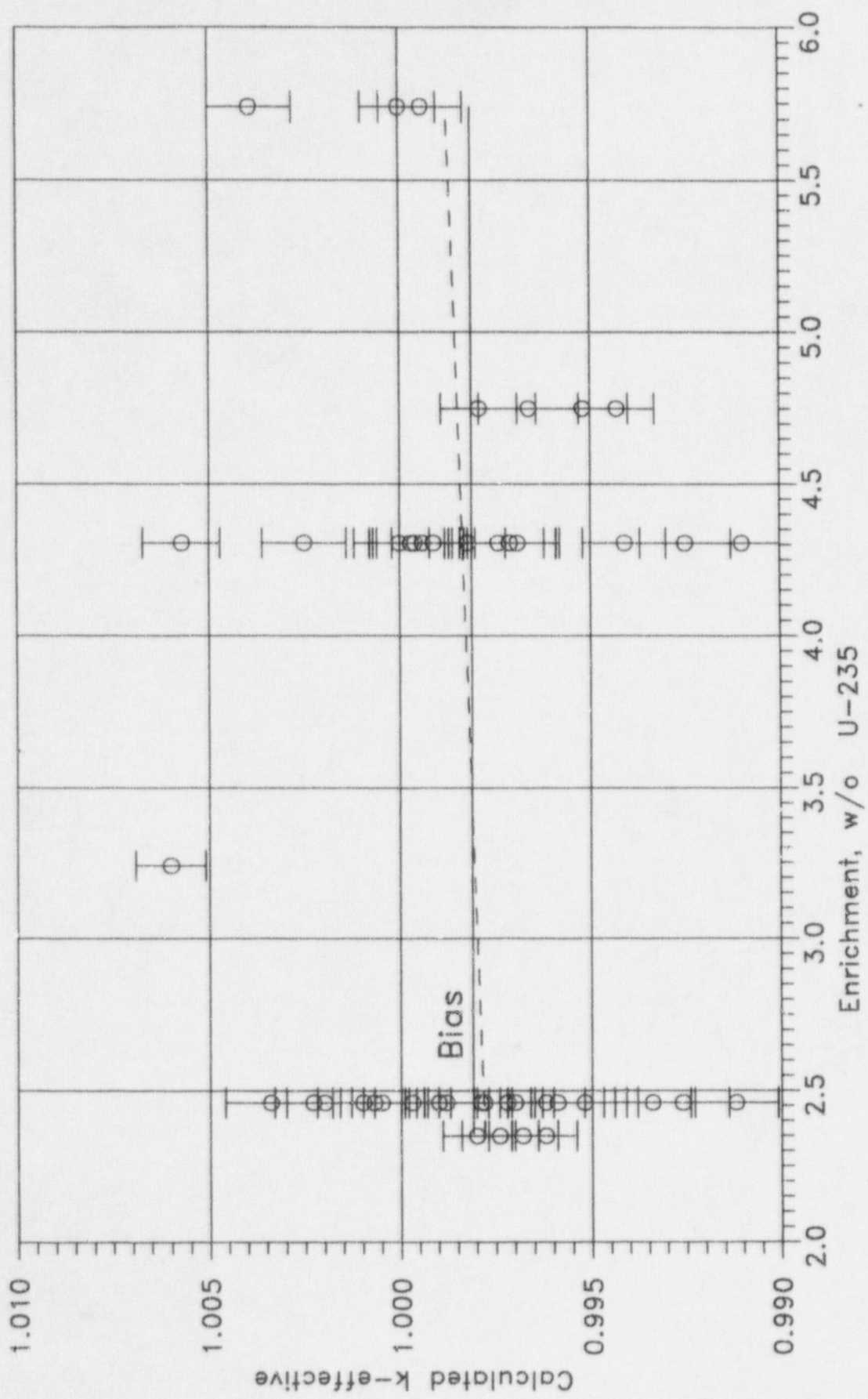


FIGURE 4A.3 MCNP CALCULATED k-eff VALUES AT VARIOUS U-235 ENRICHMENTS

-- Linear Regression with Correlation Coefficient of 0.38

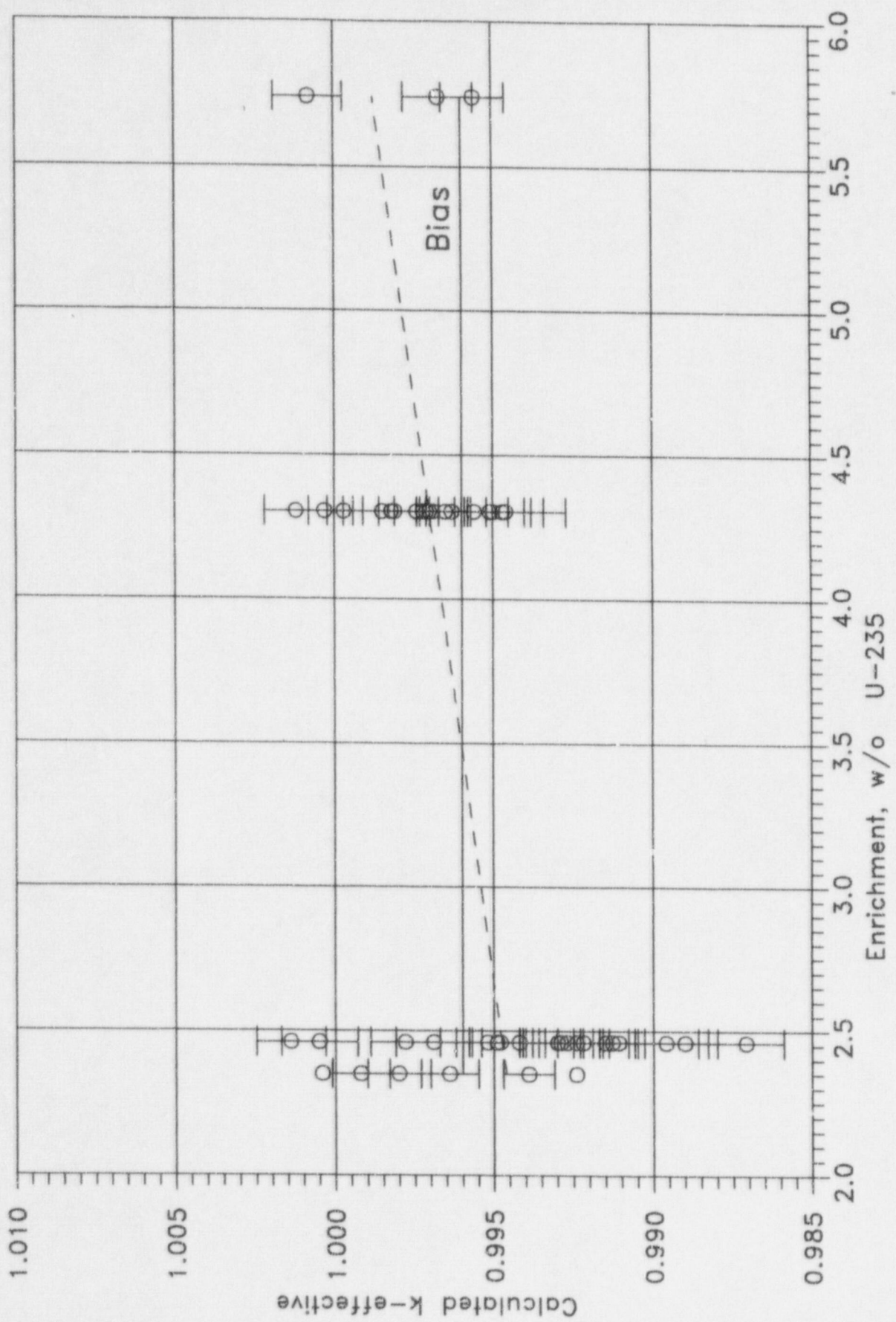


FIGURE 4A.4 KENO CALCULATED k-eff VALUES AT VARIOUS U-235 ENRICHMENTS

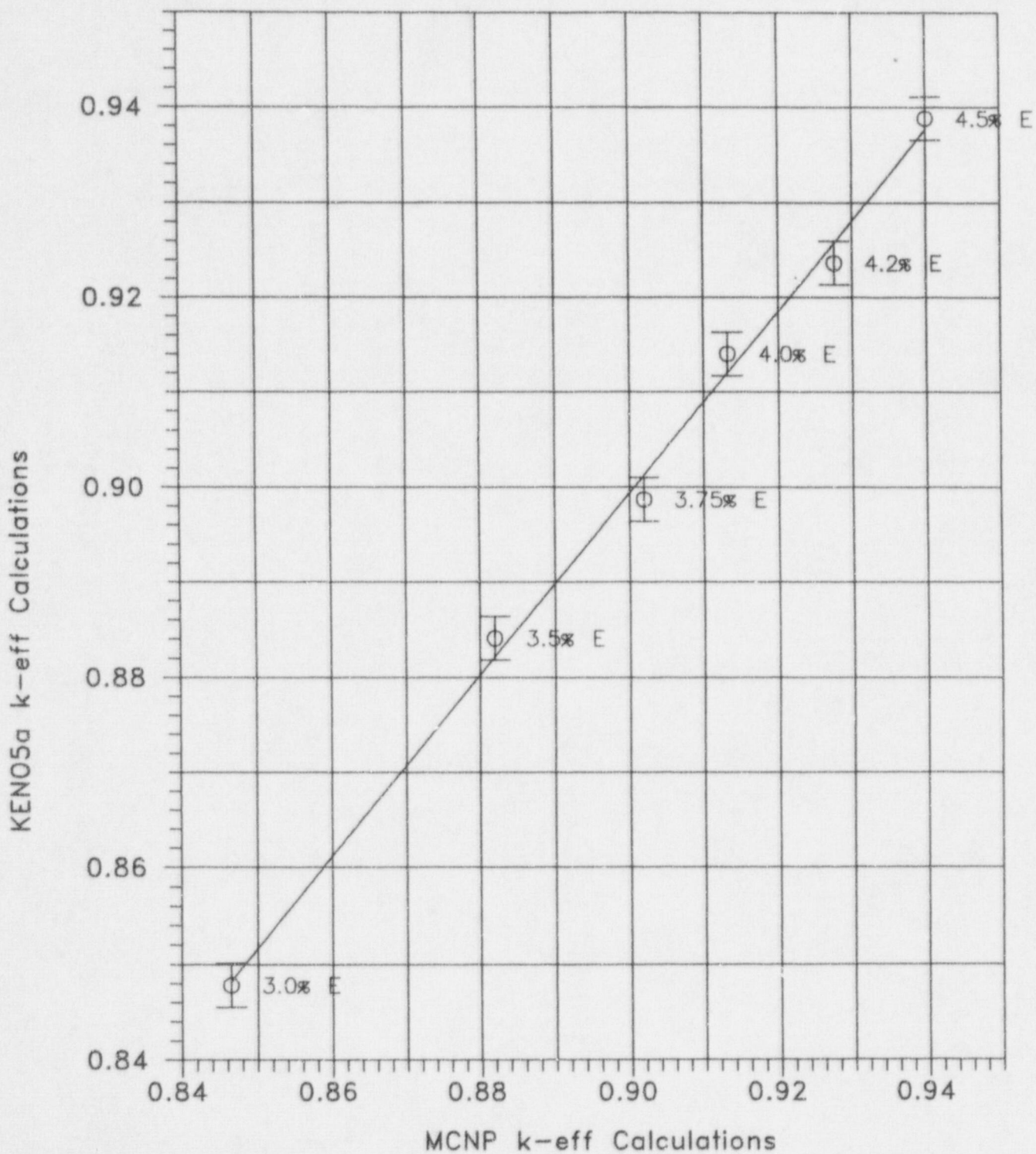


FIGURE 4A.5 COMPARISON OF MCNP AND KENO5A CALCULATIONS FOR VARIOUS FUEL ENRICHMENTS

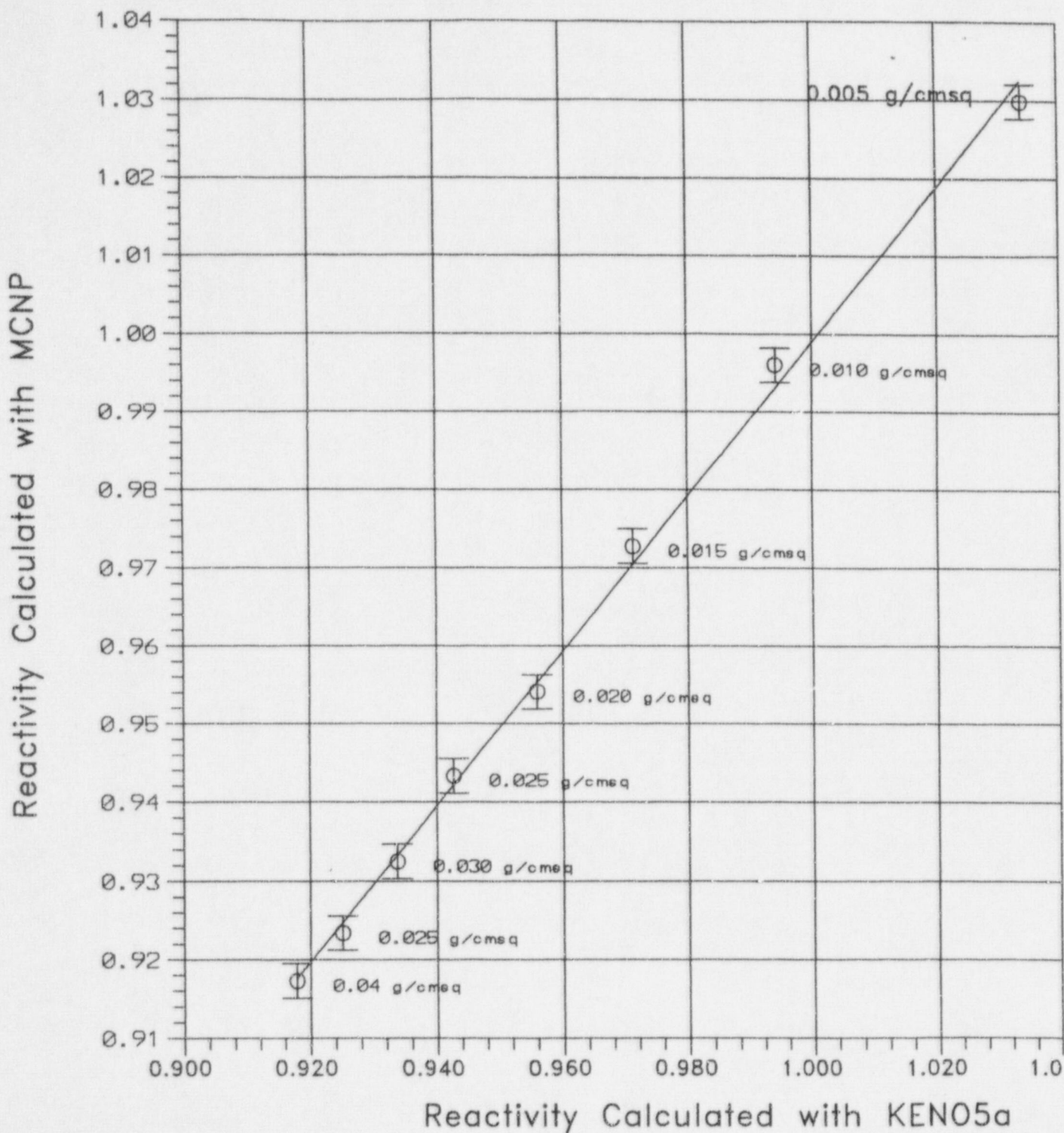


FIGURE 4A.6 COMPARISON OF MCNP AND KENO5a CALCULATIONS FOR VARIOUS BORON-10 AREAL DENSITIES

5.0 THERMAL-HYDRAULIC CONSIDERATIONS

5.1 Introduction

This chapter provides a summary of the methods, models, analyses, and numerical results of the thermal hydraulic evaluations performed for installation of fuel storage racks in the Cask Pit. These evaluations demonstrate compliance to the provisions of Section III of the USNRC "OT Position Paper for Review and Acceptance of Spent Fuel Storage and Handling Applications," dated April 14, 1978. Evaluations were performed for the Spent Fuel Pool Cooling System (SFPCS), Decay Heat Removal System (DHRS), Cask Pit and SFP.

The DBNPS is requesting approval to place four high density fuel racks in the DBNPS Cask Pit. These four racks will add a total of 289 fuel storage spaces. The racks can be installed in three phases as described in Chapter 1 of this report. The installation of additional racks will re-establish full core offload capability, allow defueling of the reactor in April of the year 2000 for the required 10 year in-service inspection of the reactor vessel, and facilitate the planned complete re-racking of the SFP. The re-racking will increase the total fuel storage capacity of the SFP to approximately 1650 fuel assemblies.

There is no direct, forced cooling of the Cask Pit. The heat produced by the fuel stored in the Cask Pit will be transferred to the SFP by an exchange of water through the open gate, which connects the two bodies. Therefore, the Cask Pit gate must be open at all times that fuel assemblies are stored in the Cask Pit. The SFP heat removal systems are shown to have adequate capacity to remove the additional heat load of the fuel placed in the Cask Pit.

The thermal hydraulic qualification analyses for the Cask Pit racks were performed to show that fuel stored in the Cask Pit will be adequately cooled and the pit structure temperature will be appropriately limited. The analyses can be further described as follows:

- i. An evaluation of the maximum bulk SFP temperature for the predicted DBNPS fuel discharge schedule was performed. This analysis was performed to establish that maximum bulk coolant temperature limits and Cask Pit structural temperature limits would not be exceeded. To account for the future re-racking of the SFP, the bulk temperature analysis was performed using a conservative storage capacity of approximately 1,650 fuel assemblies in the SFP. Since the current capacity of the SFP is 735 spaces, the selection of 1,650 spaces will bound the addition of 289 spaces to the Cask Pit. The selection of 1,650 spaces will also bound the final SFP storage capacity because the 4 Cask Pit racks will be relocated to the SFP near the end of the future SFP re-racking.
- ii. An evaluation of loss-of-forced cooling scenarios in the Spent Fuel Pool was completed to establish the minimum time to perform corrective actions to prevent boiling and maximum makeup water requirements. This analysis was also performed based on the assumption that approximately 1650 fuel assemblies were stored in the SFP. The time-to-boil and water makeup requirement analyses are conservative for the addition of 289 storage spaces to the current SFP capacity.
- iii. An evaluation of the temperature gradient between the Cask Pit and the SFP was completed for an assumed Cask Pit heat load. This analysis verified that the Cask Pit will be sufficiently cooled by the natural circulation driven exchange of water between the two bodies, such that the resulting water temperature will not exceed the maximum temperature limit for the Cask Pit structure. As a limiting case, the maximum bulk temperature of the SFP was used as the starting temperature for this evaluation.

- iv. The maximum fuel rod cladding temperature for fuel stored in the Cask Pit was determined to establish that departure from nucleate boiling at any location around the fuel is not possible. This evaluation was based conservatively on the maximum water temperature in the Cask Pit and the water-to-clad temperature difference for the hottest fuel assembly in the SFP.

The following sections present plant system descriptions, analysis assumptions, a synopsis of the analysis methods employed, and the final results.

5.2 Cooling Systems Description

A complete description of the SFPCS is found in the DBNPS USAR, Section 9.1.3. The SFPCS is designed to remove decay heat from the fuel stored in the SFP. The SFPCS at the DBNPS consists of two half-capacity recirculating pumps, two half-capacity heat exchangers, the associated valves and piping. The SFPCS pumps are horizontal, centrifugal units with a rated capacity of 1,100 gpm. The SFPCS heat exchangers are shell and tube units. The cold cooling water shell side flow is supplied from the plant Component Cooling Water (CCW) system. SFP water is pumped through the heat exchange tube side. The SFPCS heat exchanger design performance is listed below.

Heat Transferred:	5.25×10 ⁶ Btu/hr
Shell Side Flow Rate:	650 gpm
Shell Side Inlet Temperature:	95°F
Shell Side Outlet Temperature:	111.2°F
Tube Side Flow Rate:	1000 gpm
Tube Side Inlet Temperature:	120°F
Tube Side Outlet Temperature:	109.5°F

The DHRS, described in the DBNPS USAR Section 9.3.5, serves as the Seismic Class I backup cooling system to the SFPCS. The DHRS consists of two recirculating pumps and two heat exchangers. The DHRS is permanently connected to the SFPCS via a 10 inch line. Two normally closed gate valves provide isolation between the DHRS and the SFPCS. The DHRS pumps are single-stage, centrifugal units with a rated capacity of 3,000 gpm. The DHRS heat exchangers, which are also cooled by the CCW system, are shell and tube units with the following design performance:

Heat Transferred: 26.9×10^6 Btu/hr
SFP Water Flow Rate: 3000 gpm
SFP Water Inlet Temperature: 140°F
CCW Flow Rate: 6000 gpm
CCW Inlet Temperature: 95°F

Loss of water from the SFP is unlikely since the SFP and piping within the SFP are Seismic Class I. Makeup water is readily available. The DHRS is permanently connected to the Class I boundary of the SFP. This system can provide borated make up water to the SFP from the Borated Water Storage Tank. SFP makeup water is also available from the Seismic Class II Demineralized Water Storage Tank or Clean Waste Receiver Tank.

5.3 Discharge/Cooling Alignment Scenarios

A total of six reactor core discharge/cooling scenarios were postulated. These scenarios are:

Scenario	Discharge Type	Cooling System Alignment
1	Partial Core	2 SFPCS Pumps and Heat Exchangers
2	Partial Core	1 SFPCS Pump and Heat Exchanger
3A	Type A Full Core (65 days at power)	2 SFPCS Pumps and Heat Exchangers
3B	Type B Full Core (2 years at power)	2 SFPCS Pumps and Heat Exchangers
4A	Type A Full Core (65 days at power)	1 DHRS Train
4B	Type B Full Core (2 years at power)	1 DHRS Train

The DBNPS does not routinely perform a full core discharge at each refueling outage. Scenarios 2, 3A and 3B correspond to discharge type and cooling alignment combinations which are not typically used during fuel discharge operations. These scenarios are included to demonstrate that the bulk temperature will remain below boiling even under extreme circumstances. Time-to-boil, boiloff rate, and local temperature analyses are performed for the most limiting (i.e., highest bulk temperature and decay heat flux) of the full core discharge Scenarios 4A and 4B.

Thermal hydraulic analyses were performed to conservatively account for the future re-racking of the SFP. The re-racked SFP will have a total capacity of approximately 1,650 spaces. Since the current SFP capacity is 735 spaces, the analyses performed will bound the addition of 289 spaces to the Cask Pit.

A partial core discharge is comprised of 72 assemblies discharged into the SFP, which already contains 1609 previously discharged assemblies. This analyzed stored fuel inventory (1681) conservatively exceeds the maximum possible inventory. The minimum decay time of the previously discharged fuel assemblies for these scenarios is 2 years.

A "Type A" full core discharge is comprised of 177 assemblies discharged into the SFP, which already contains 1537 previously discharged assemblies. This analyzed fuel inventory (1714) conservatively exceeds the maximum possible inventory. This full core discharge takes place after 65 days of full power operation since the last partial core discharge. The minimum decay time of the previously discharged fuel assemblies for these scenarios is 65 days.

A "Type B" full core discharge is comprised of 177 assemblies discharged into an SFP that already contains 1537 previously discharged assemblies. This analyzed fuel inventory (1714) conservatively exceeds the maximum possible inventory. This full core discharge takes place after 2 years of full power operation since the last partial core discharge. The minimum decay time of the previously discharged fuel assemblies for these scenarios is 2 years.

Table 5.3.1 presents the historic and projected discharge schedule used for these analyses.

In all scenarios, the cooling water which removes heat from the SFPCS and DHRS heat exchangers is assumed to be at its design maximum temperature and design basis flow rate.

5.4 Maximum Bulk Pool Temperature Methodology

This section presents the methodology for calculating the maximum SFP bulk temperatures for the scenarios presented in the preceding section. The maximum SFP bulk temperature will be used as the inlet temperature to the Cask Pit. The following conservatisms are applied in the maximum pool bulk temperature calculations:

- The decay heat load is based on a discharge schedule with bounding projected fuel parameters.
- The minimum initial enrichment for projected discharged batches is used for previously discharged fuel decay heat calculations.
- The thermal capacity of the SFP is based on the net SFP water volume only. The considerable energy storage capability of the fuel racks, fuel assemblies, and pool structure is neglected.
- The cooling effects of evaporation heat losses and all other passive heat removal mechanisms (i.e., conduction through walls and slab) are neglected.
- The SFP and Cask Pit are treated as a "lumped" system with a single bulk temperature, however no credit is taken for the thermal capacity of the Cask Pit. This maximizes the applied decay heat load and minimizes the thermal energy storage.

The transient thermal response of the SFP and the attendant cooling systems is governed by a first-order, ordinary differential equation. The governing differential equation can be written by utilizing conservation of energy as:

$$C \frac{dT}{d\tau} = Q(\tau) - Q_{HX}(T) - Q_{EV}(T)$$

where:

C = Pool thermal capacity, Btu/°F

T = Pool bulk temperature, °F

τ = Time after reactor shutdown, hr

$Q(\tau)$ = Time varying decay heat generation rate, Btu/hr

$Q_{HX}(T)$ = Temperature dependent SFPCS or DHRS heat rejection rate, Btu/hr

$Q_{EV}(T)$ = Temperature dependent passive heat losses to the surrounding environment, Btu/hr

$Q_{HX}(T)$ is a function of the SFP temperature and the cooling water flow rate and temperature can be written in terms of the temperature effectiveness (p) as follows:

$$Q_{HX}(T) = W_1 C_1 p (T - t_1)$$

where:

W_1 = CCW water flow rate, lb/hr

C_1 = CCW water specific heat capacity, Btu/(lb×°F)

p = SFPCS or DHRS heat exchanger temperature effectiveness

T = Bulk pool water temperature, °F

t_1 = CCW water inlet temperature, °F

The temperature effectiveness, a measure of the heat transfer efficiency of the SFPCS or DHRS heat exchangers, is defined as:

$$P = \frac{t_o - t_i}{T - t_i}$$

where t_o is the CCW outlet temperature ($^{\circ}\text{F}$) and all other terms are as defined above.

$Q_{EV}(T)$ is a nonlinear function of the pool temperature and ambient temperature. This term is conservatively neglected in the maximum pool bulk temperature calculations. However, a discussion of this term is provided for understanding of the conservatism applied to this calculation. Q_{EV} contains the passive heat losses from the pool surface which includes evaporation, natural convection and thermal radiation from the pool surface, and heat conduction through the pool walls and slab. Experiments show that heat conduction through the pool walls and slab takes only about 4% of the total heat loss and is conservatively neglected [5.4.1]. The temperature dependent passive heat loss can be expressed as [5.4.2]:

$$Q_{EV}(T) = h A (T - t_a) + \epsilon \sigma A (T^4 - t_a^4) + \alpha A (P_w - P_a)$$

where:

h = Natural convection heat transfer coefficient, $\text{Btu}/(\text{hr} \times \text{ft}^2 \times ^{\circ}\text{F})$

A = Pool surface area, ft^2

t_a = Ambient SFP building temperature, $^{\circ}\text{F}$

ϵ = Emissivity of pool water

σ = Stephan-Boltzmann constant

α = Evaporation rate constant, $\text{Btu}/(\text{hr} \times \text{ft}^2 \times \text{psi})$

P_w = Vapor pressure of water at pool temperature, psi

P_a = Vapor pressure of water at ambient temperature, psi

The differential equation that defines the transient thermal response of the pool is solved numerically. The decay heat load from previously discharged fuel assemblies is calculated using Holtec's QA validated LONGOR program [5.4.3]. This program incorporates the ORIGEN2 isotope generation and depletion code [5.4.4] to perform the decay heat calculations. The transient decay heat loads and pool bulk temperatures are calculated using Holtec's QA validated BULKTEM program [5.4.5], which also incorporates the ORIGEN2 code. The maximum SFP bulk temperature is extracted from the results of the transient evaluations. The major input values for this analysis are summarized in Table 5.4.1.

5.5 Minimum Time-to-Boil and Maximum Boiloff Rate Methodology

This section presents the methodology for calculating the minimum time-to-boil and corresponding maximum boiloff rate for the scenarios presented in Section 5.3. This analysis is conducted for the number of fuel assemblies in a re-racked SFP and therefore will bound the addition of 289 spaces in the Cask Pit.

The following conservatisms are applied in the SFP time-to-boil and boiloff rate calculations:

- The SFP bulk temperature and decay heat generation rates are assumed to be the calculated maximum bulk temperature and the coincident decay heat generation rates. Maximizing the initial temperature and utilizing the coincident decay heat generation rates will conservatively minimize the time-to-boil.
- The thermal capacity of the SFP is based on the net water volume only. The considerable energy storage capability of the fuel racks, fuel assemblies, and pool structure is neglected.

- Heat losses through the pool walls and slab are neglected.
- In calculating the spent fuel pool evaporation heat losses, the building housing the spent fuel pool is assumed to have a conservative ambient air temperature of 110°F and 100% relative humidity. These conditions yield a conservative time-reducing pool thermal capacity while minimizing the credit for evaporative and other passive heat losses.
- The SFP and Cask Pit are treated as a “lumped” system with a single bulk temperature, however no credit is taken for the thermal capacity of the Cask Pit. This maximizes the applied decay heat load and minimizes the thermal energy storage.

The governing enthalpy balance equation for this condition, subject to these conservative assumptions, can be written as:

$$C(\tau) \frac{dT}{d\tau} = Q(\tau + \tau_0) - Q_{EV}(T)$$

where $C(\tau)$ is the time-reducing thermal capacity, τ is the time after cooling is lost (hr) and τ_0 is the loss of cooling time after shutdown (hr). The other terms of this equation are defined in Section 5.4, including a discussion of $Q_{EV}(T)$. Temperature dependent passive heat losses from the pool surface are accounted for in this analysis.

This differential equation is solved using a numerical solution technique to obtain the bulk SFP temperature as a function of time. This analysis is performed using Holtec’s QA validated TBOIL program [5.5.1]. This program utilizes the highly conservative correlations of ASB 9-2 [5.5.2] to perform the decay heat calculations, thereby imparting even more conservatism to the results. The major input values for this analysis are summarized in Table 5.5.1.

5.6 Local Water Temperature Methodology

This section summarizes the methodology for evaluating the maximum local water temperature for the SFP and Cask Pit. A conservative evaluation for a bounding amalgam of conditions is performed. The result of this evaluation is a bounding temperature difference between the maximum local water temperature and the bulk pool temperature. The maximum temperature difference is added to the maximum bulk SFP temperature to determine the maximum local temperature in the SFP. The maximum SFP local temperature is determined to ensure the SFPCS and DHRS heat removal capacity is acceptable to remove the additional heat of the fuel stored in the Cask Pit. The maximum Cask Pit local temperature is compared to the maximum SFP bulk temperature to ensure the Cask Pit temperature is not excessive and will demonstrate the exchange of water with the SFP.

In order to determine the maximum local water temperature, a series of conservative assumptions are made. The most important of these assumptions are:

- With a full core discharged into the SFP racks, approximately equidistant from the coolant water inlet and outlet, the remaining cells in the spent fuel pool are postulated to be occupied with previously discharged fuel.
- The hottest assemblies, located together in the pool, are assumed to be located in pedestal cells of the racks. These cells have a reduced water entrance area, caused by the pedestal blocking the baseplate hole, and a correspondingly increased hydraulic resistance.
- No downcomer flow is assumed to exist between the rack modules.
- All rack cells are conservatively assumed to be 50% blocked at the cell outlet to account for drop accidents resulting in damage to the upper end of the cells.

- The hydraulic resistance parameters for the rack cells, permeability and inertial resistance, are worsened by 15% and 25%, respectively.
- For evaluating maximum local water and fuel cladding temperatures, the SFP is modeled as separate from the Cask Pit. The fuel decay heat that would normally be in the Cask Pit is assumed to be in the SFP.
- For evaluating the exchange of water between the Cask Pit and the SFP, a separate model of the Cask Pit and a large, pseudo-constant temperature fluid reservoir is used. While the depth of the reservoir is taken as the SFP depth, the other details of the reservoir are selected to minimize reservoir temperature gradients.
- For evaluating the exchange of water between the Cask Pit and the SFP, the decay heat generation rate in the Cask Pit racks is calculated based on the maximum heat generation rate from the fuel discharge schedule of Table 5.3.1 (1,609 fuel assemblies). The resultant heat generation rate is 1,404,009 watts. This yields a total Cask Pit heat generation rate of 252,200 watts or 860,759 Btu/hr for 289 fuel assemblies.

5.6.1 Local Temperature Evaluation Methodology

The inlet piping that returns cooled water from the SFPCS terminates above the level of the fuel racks. It is not apparent from heuristic reasoning alone that the cooled water delivered to the SFP would not bypass the hot fuel racks and exit through the outlet piping. To demonstrate adequate cooling of hot fuel in the SFP, it is therefore necessary to rigorously quantify the velocity field in the pool created by the interaction of buoyancy driven flows and water injection/egress. A Computational Fluid Dynamics (CFD) analysis for this demonstration is required. The objective of this study is to demonstrate that the principal thermal-hydraulic criterion of ensuring local subcooled conditions in the SFP is met for all postulated fuel discharge/cooling alignment

scenarios. The local thermal-hydraulic analysis is performed such that partial cell blockage and slight fuel assembly variations are bounded. An outline of the CFD approach is described in the following.

There are several significant geometric and thermal-hydraulic features of the DBNPS SFP which need to be considered for a rigorous CFD analysis. From a fluid flow modeling standpoint, there are two regions to be considered. One region is the bulk SFP/Cask Pit region where the classical Navier-Stokes equations are solved with turbulence effects included. The other region is the heat generating fuel assemblies located in the spent fuel racks located near the bottom of the SFP. In this region, water flow is directed vertically upwards due to buoyancy forces through relatively small flow channels formed by the Babcock and Wilcox (B&W) 15×15 fuel assembly rod arrays in each rack cell. This situation shall be modeled as a porous solid region in which the classical Darcy's Law, given below, governs fluid flow:

$$\frac{\partial P}{\partial X_i} = - \frac{\mu}{K(i)} V_i - C \rho |V| \frac{V_i}{2}$$

where $\partial P/\partial X_i$ is the pressure gradient, $K(i)$, V_i and C are the corresponding permeability, velocity and inertial resistance parameters and μ is the fluid viscosity. The permeability and inertial resistance parameters for the rack cells loaded with B&W 15×15 fuel were determined based on friction factor correlations for the laminar flow conditions typically encountered due to the low buoyancy induced velocities and the small size of the flow channels.

The DBNPS SFP geometry required an adequate portrayal of large scale and small scale features, spatially distributed heat sources in the spent fuel racks, and water inlet/outlet configuration. Relatively cooler bulk pool water normally flows down between the fuel rack outline and pool wall liner clearance known as the downcomer. Near the bottom of the racks, the flow turns from a vertical to horizontal direction into the bottom plenum supplying cooling water to the rack cells. Heated water issuing out of the top of the racks mixes with the bulk pool water. An

adequate modeling of these features on the CFD program involves meshing the large scale bulk pool region and small scale downcomer and bottom plenum regions with sufficient number of computational cells to capture the bulk and local features of the flow field.

Two distinct CFD models have been developed for the DBNPS SFP. The first model addresses the local thermal hydraulic acceptability of storing hot, recently discharged fuel assemblies in the SFP, which is supplied with forced cooling. The second model addresses the adequacy of the cooling of the low heat generation rate previously discharged fuel assemblies to be stored in the Cask Pit. A synopsis of both models is provided in the following.

The distributed heat sources in the SFP racks are modeled by identifying distinct heat generation zones considering full-core discharge, bounding peak effects, and presence of background decay heat from previous discharges. Three heat generating zones were modeled. The first zone contains the heat generated by fuel from previous discharges and the second and third zones contain the decay heat generated by fuel from a bounding full-core-discharge scenario. The two full core discharge zones are differentiated by one zone with higher than average decay heat generation and the other with less than average decay heat generation. This is a conservative model, since all of the fuel with higher than average decay heat is placed in a contiguous area. A uniformly distributed heat generation rate was applied throughout each distinct zone.

In the Cask Pit water exchange model, the entire fuel storage rack region in the Cask Pit is modeled as containing decay heat from previous discharges. A uniform volumetric decay heat generation rate is applied to the fuel racks region. A pseudo-constant temperature reservoir representing the SFP bulk temperature is included in the model.

The CFD analysis was performed on the FLUENT [5.6.4] fluid flow and heat transfer modeling program. The FLUENT code enables buoyancy flow and turbulence effects to be included in the CFD analysis. Turbulence effects are modeled by relating time-varying Reynolds' Stresses to the mean bulk flow quantities with the k - ϵ turbulence model. The k - ϵ model is appropriate for the

DBNPS CFD analysis. The k-ε turbulence model is a time-tested, general-purpose turbulence model. This model has been demonstrated to give good results for the majority of turbulent fluid flow phenomena.

Rigorous modeling of fluid flow problems requires a solution to the classical Navier-Stokes equations of fluid motion [5.6.1]. The governing equations (in modified form for turbulent flows with buoyancy effects included) are written as:

$$\frac{\partial \rho_o u_i}{\partial t} + \frac{\partial \rho_o \langle u'_i u'_j \rangle}{\partial x_i} = \frac{\partial}{\partial x_j} \left[\mu \left(\frac{\partial u_i}{\partial x_j} + \frac{\partial u_j}{\partial x_i} \right) \right] - \frac{\partial p}{\partial x_i} - (\rho - \rho_o) g_i + \frac{\partial \rho_o \langle u'_i u'_j \rangle}{\partial x_j}$$

where u_i are the three time-averaged velocity components. $\rho \langle u'_i u'_j \rangle$ are time-averaged Reynolds stresses derived from the turbulence induced fluctuating velocity components u'_i . ρ_o is the fluid density at temperature T_o , μ is the fluid viscosity, g_i are the components of gravitational acceleration and x_j are the Cartesian coordinate directions. The Reynolds stress tensor is expressed in terms of the mean flow quantities by defining a turbulent viscosity F_t and a turbulent velocity scale $k^{1/2}$ as shown below [5.6.2]:

$$\rho \langle u'_i u'_j \rangle = 2/3 \rho k \delta_{ij} - \mu_t \left[\frac{\partial u_i}{\partial x_j} + \frac{\partial u_j}{\partial x_i} \right]$$

The procedure to obtain the turbulent viscosity and velocity length scales involves a solution of two additional transport equations for kinetic energy (k) and rate of energy dissipation (ϵ). This methodology, known as the k-ε model for turbulent flows, is described by Launder and Spalding [5.6.3].

Some of the major input values for this analysis are summarized in Table 5.6.1. Views of the assembled CFD models for the SFP and the Cask Pit are presented in Figures 5.6.1 and 5.6.2. Figures 5.6.3 and 5.6.4 present temperature contours and velocity vectors, respectively, in the SFP model. Figures 5.6.5 and 5.6.6 present temperature contours and velocity vectors, respectively, in the Cask Pit model.

5.7 Fuel Rod Cladding Temperature Methodology

This section summarizes the method to calculate the temperature of the fuel rod cladding. Similar to the local water temperature calculation methodology presented in the preceding section, this evaluation is performed for a single, bounding scenario. The maximum temperature difference between the fuel cladding and the local water temperature is calculated for the hottest fuel assembly in the SFP. This temperature difference is used to conservatively show that the cooling systems can acceptably remove from the SFP the heat generated by 289 additional fuel assemblies in the Cask Pit.

The maximum specific power of a fuel assembly (q_A) can be given by:

$$q_A = q F_{xy}$$

where:

F_{xy} = Radial peaking factor

q = Average fuel assembly specific power, Btu/hr

The peaking factors are given in Table 5.6.1. The maximum temperature rise of pool water is computed for the most disadvantageously located fuel assembly, described in the assumptions to Section 5.6 as the one which is subject to the highest local pool water temperature. Having determined the maximum local water temperature in the pool, it is possible to determine the maximum fuel cladding temperature. A fuel rod can produce F_z times the average heat emission rate over a small length, where F_z is the axial rod peaking factor. The axial heat distribution in a

rod is generally a maximum in the central region, and tapers off at its two extremities. Thus, peak cladding heat flux over an infinitesimal area is given by the equation:

$$q_c = \frac{q F_{xy} F_z}{A_c}$$

where A_c is the total cladding external heat transfer area in the active fuel length region.

Within each fuel assembly sub-channel, water is continuously heated by the cladding as it moves axially upwards from bottom to top under laminar flow conditions. Rohsenow and Hartnett [5.7.1] report a Nusselt-number based heat transfer correlation for laminar flow in a heated channel. The film temperature driving force (ΔT_f) at the peak cladding flux location is calculated as follows:

$$h_f \frac{D_h}{K_w} = Nu$$

$$\Delta T_f = \frac{q_c}{h_f}$$

where, h_f is the water side film heat transfer coefficient, D_h is sub-channel hydraulic diameter, K_w is water thermal conductivity and Nu is the Nusselt number for laminar flow heat transfer.

In order to introduce some additional conservatism in the analysis, we assume that the fuel cladding has a crud deposit resistance R_c (equal to $0.0005 \text{ ft}^2\text{-hr-}^\circ\text{F/Btu}$) that covers the entire surface. Thus, including the temperature drop across the crud resistance, the cladding to water local temperature difference (ΔT_c) is given by:

$$\Delta T_c = \Delta T_f + R_c q_c$$

5.8 Results

This section contains results from the analyses performed for the postulated discharge scenarios.

5.8.1 Maximum Bulk Pool Temperatures

For the discharge/cooling scenarios postulated in Section 5.3, the maximum calculated pool bulk temperatures are summarized in Table 5.8.1. The worst case decay heat load in the SFP for the full core discharge scenario 4A was determined to be 30.15×10^6 btu/hr. For Scenarios 1, 4A, and 4B, SFP bulk temperatures must remain within the limits of the American Concrete Institute (ACI) Code Requirements for Nuclear Safety Related Concrete Structures ACI-349, to protect the integrity of the SFP structure. The ACI Code permits long-term temperatures of up to 150°F and short-term temperature excursions in localized areas (e.g., skin effects) up to 350°F. As discussed in Section 5.3, Scenarios 2, 3A and 3B are considered accident conditions and are only compared to the bulk boiling temperature of 212°F.

The results presented in Table 5.8.1 demonstrate that calculated bulk temperatures for the first four scenarios listed remain below their respective allowable limits. The calculated peak bulk temperatures for Scenarios 4A and 4B exceed the 150°F concrete temperature limit for long term normal operating conditions by less than 1.5°F. In both scenarios, the bulk pool temperature will remain above 150°F for less than 28 hours. The effect of this bulk SFP temperature condition is evaluated and determined to be acceptable in the structural evaluations in Section 8. Given the conservatisms incorporated into the calculations, actual SFP bulk temperatures will be lower than the calculated values reported in Table 5.8.1.

5.8.2 Minimum Time-to-Boil and Maximum Boiloff Rate

For discharge/cooling Scenarios 1 and 4A, the calculated time-to-boil and maximum boiloff rates are summarized in Table 5.8.2. These results show that, in the extremely unlikely event of a complete failure of both the SFPCS and DHRS, there would be at least 3.78 hours available for corrective actions. The maximum water boiloff rate is less than 70 gpm.

5.8.3 Local Water and Fuel Cladding Temperatures

The CFD study has analyzed a bounding local thermal-hydraulic scenario. In this scenario, a bounding full-core discharge is considered in which the 177 assemblies are located in the pool, approximately equidistant from the water inlet and outlet, while the balance of the rack cells are postulated to be occupied by fuel from previous discharges. In this analysis, the difference between the peak local temperature and the coincident bulk pool temperature was conservatively calculated to be 42.75°F.

The peak fuel cladding superheat is determined for the hottest cell location in the pool as obtained from the CFD model for the DBNPS pool. The maximum temperature difference between the fuel cladding and the local water (ΔT_c) is calculated to be 36.1°F. This calculated cladding ΔT_c is applied, along with the maximum temperature difference between the local water temperature and the bulk SFP temperature, to the calculated maximum SFP bulk temperature (Scenarios 4A and 4B) of approximately 151.5°F. This yields a conservatively bounding 194.25°F maximum local water temperature and a conservatively bounding 230.35°F peak cladding temperature. These conservative bounding maximum local temperatures are less than the 239°F local boiling temperature on top of the racks. Thus, boiling does not occur anywhere within the DBNPS SFP. Based on these results, the SFPCS and DHRS will acceptably remove the heat generated from fuel placed in the Cask Pit.

The evaluation of the buoyancy driven, natural convection water exchange between the Cask Pit and the SFP, which was modeled as a pseudo-constant temperature reservoir, yields a maximum temperature difference of 4°F. Note that this is the difference between the Cask Pit maximum local temperature and the SFP bulk temperature. The maximum temperature of the water in the Cask Pit, based on the calculated maximum SFP bulk temperature of approximately 151.5°F, would therefore be 155.5°F. This is well below the local saturation temperature at the top of the Cask Pit racks which, due to the greater depth of the Cask Pit, is even greater than the 239°F saturation temperature at the top of the SFP racks.

The maximum Cask Pit water temperature of 155.5°F stated above is based on the maximum local temperature at the top of the Cask Pit racks. The Cask Pit bulk water temperature would be approximately 154.5°F. As stated above, the ACI code permits long-term temperatures of up to 150°F and short-term temperature excursions in localized areas up to 350°F. Based on the SFP bulk temperature analyses for scenarios 4A and 4B, the long-term limit would be exceeded by less than 4.5°F for approximately 100 hours. The effect of this bulk Cask Pit temperature condition is evaluated as acceptable to the Cask Pit structure in Chapter 8. Given the conservatism assumed in the thermal hydraulic calculations, the actual Cask Pit bulk temperatures will be less than the calculated value of 154.5°F.

Due to the low heat generation rate of the background fuel stored in the Cask Pit, fuel cladding temperatures will be only slightly greater than the local water temperature. As the bounding fuel cladding temperature in the SFP is based on maximum decay heat fluxes from freshly discharged fuel, the fuel cladding temperatures in the Cask Pit are bounded by the previously calculated value. This demonstrates the adequacy of cooling the Cask Pit via the buoyancy driven exchange of water between the pit and the SFP.

5.9 Fuel Handling Area Ventilation (FHAV)

An evaluation of the FHAV system was performed. This evaluation was performed for the full core discharge scenario 4A, which provides the greatest heat load burden to the FHAV system. Using the design inlet air parameters from the DBNPS USAR, the maximum calculated building temperature is 103°F. The relative humidity was calculated to increase by less than 25 percent relative humidity. Therefore, it is concluded that the additional burden on the FHAV system, as a result of the peak heat loads from the SFP, is within the design capability of the FHAV system.

5.10 References

- [5.4.1] "Heat Loss to the Ambient from Spent Fuel Pools: Correlation of Theory with Experiment", Holtec Report HI-90477, Rev. 0, April 3, 1990.
- [5.4.2] "An Improved Correlation for Evaporation from Spent Fuel Pools", Holtec Report HI-971664, Rev. 0.
- [5.4.3] "QA Documentation for LONGOR v1.0," Holtec Report HI-951390, Revision 0.
- [5.4.4] Croff, A.G., "ORIGEN2 - A Revised and Updated Version of the Oak Ridge Isotope Generation and Depletion Code," ORNL-5621, Oak Ridge National Laboratory, 1980.
- [5.4.5] "QA Documentation for BULKTEM v3.0," Holtec Report HI-951391, Revision 1.
- [5.5.1] "QA Validation for TBOIL v1.6," Holtec Report HI-92832, Revision 2.
- [5.5.2] USNRC Branch Technical Position ASB 9-2, "Residual Decay Energy for Light Water Reactors for Long Term Cooling," Revision 2, July 1981.
- [5.6.1] Batchelor, G.K., "An Introduction to Fluid Dynamics", Cambridge University Press, 1967.
- [5.6.2] Hinze, J.O., "Turbulence", McGraw Hill Publishing Co., New York, NY, 1975.
- [5.6.3] Launder, B.E., and Spalding, D.B., "Lectures in Mathematical Models of Turbulence", Academic Press, London, 1972.
- [5.6.4] "QA Documentation and Validation of the FLUENT Version 4.32 CFD Analysis Program", Holtec Report HI-961444, Revision 0.
- [5.7.1] Rohsenow, N.M., and Hartnett, J.P., "Handbook of Heat Transfer", McGraw Hill Book Company, New York, 1973.

Table 5.3.1

Davis-Besse Historic and Projected Fuel Discharge Schedule

Number of Assemblies	Discharge Date (Month & Year)	Average Burnup (MWd/MTU)	²³⁵ U Enrichment (wt%)	Uranium Weight (kgU)
53	March 1982	23888	2.48	472.16
85	July 1983	26996	2.67	472.21
65	September 1984	28153	2.64	471.06
65	March 1988	34190	3.00	468.75
60	January 1990	31142	3.02	468.21
59	August 1991	36254	3.18	468.25
61	March 1993	38046	3.15	467.85
65	October 1994	41039	3.45	468.37
74	April 1996	42948	3.71	467.88
77	April 1998	46492	3.90	467.89
77	March 2000	49491	4.32	467.93
73	March 2002	51134	4.43	467.83
73	March 2004	52972	4.20	479.86
73	March 2006	55782	3.99	489.51
73	March 2008	55783	3.99	489.51
72	March 2010	55881	4.00	489.80
72	March 2012	55881	4.00	489.80
72	March 2014	55881	4.00	489.80
72	March 2016	55881	4.00	489.80
72	March 2018	55881	4.00	489.80
72	March 2020	55881	4.00	489.80
72	March 2022	55881	4.00	489.80
72	March 2024	55881	4.00	489.80

Note: In performing calculations, the listed burnup values are increased by 2% to include uncertainties in the reactor thermal power.

TABLE 5.4.1	
DATA FOR SFP BULK TEMPERATURE EVALUATION	
Reactor Thermal Power	2827.5 MWt
Reactor Core Size	177 assemblies
SFPCS HX Coolant Flow Rate	650 gpm
SFPCS HX Coolant Temperature	95°F
DHRS HX Coolant Flow Rate	6000 gpm
DHRS HX Coolant Temperature	95°F
Minimum In-Core Hold Time	150 hours
Fuel Assembly Discharge Rate	4 per hour
Spent Fuel Pool Length (N-S)	635.5 inches
Spent Fuel Pool Length (E-W)	239.5 inches
Spent Fuel Pool Depth	36.86 feet
SFPCS HX Design Conditions	
Coolant Inlet Temperature	95°F
Coolant Outlet Temperature	111.2°F
SFP Water Inlet Temperature	120°F
DHRS HX Design Conditions	
Coolant Inlet Temperature	95°F
SFP Water Inlet Temperature	140°F
Coolant Flow Rate	6000 gpm
Heat Removal Rate	26.9×10^6 Btu/hr
Branding Fuel Assembly Weight	1682 pounds

TABLE 5.5.1**DATA FOR TIME-TO-BOIL EVALUATION**

Spent Fuel Pool Length (N-S)	635.5 inches
Spent Fuel Pool Length (E-W)	239.5 inches
Spent Fuel Pool Depth	36.9 feet
Total Rack Weight	268,000 lb
Bounding Fuel Assembly Weight	1682 pounds
Pool Building Ambient Temperature	110°F
Emissivity of Water	0.96
Pool Net Water Volume	31,580 ft ³

TABLE 5.6.1	
DATA FOR SFP/CASK PIT LOCAL TEMPERATURE EVALUATION	
Bounding Assembly Weight	1682 pounds
Radial Peaking Factor	1.64
Axial Peaking Factor	1.52
Maximum Number of Fuel Assemblies Assumed for Analysis (SFP/Cask Pit)	1714/289
Cooled Water Flow Rate	3000 gpm
Type of fuel assembly	Babcock and Wilcox 15x15
Fuel Rod Outer Diameter	0.430 inches max. 0.416 inches min.
Rack Cell Inner Dimension	9.0 inches
Active Fuel Length	145 inches
Number of Rods per Assembly*	225 rods
Rack Cell Length	161 5/8 inches
Bottom Plenum Height	6 inches

* Note: Fuel assembly is modeled as a square array with all locations containing fuel rods for permeability determinations. 208 fuel rods are used for heat transfer calculations.

TABLE 5.8.1

RESULTS OF BULK TEMPERATURE TRANSIENT

Scenario	Maximum Bulk Temperature (°F)	Coincident Decay Heat Load (Btu/hr)	Time After Reactor Shutdown (hrs)
1	132.98	15.89×10^6	183
2	169.32	15.55×10^6	197
3A	165.87	29.66×10^6	205*
3B	164.90	29.28×10^6	205
4A	151.42	29.75×10^6	203*
4B	150.67	29.38×10^6	203

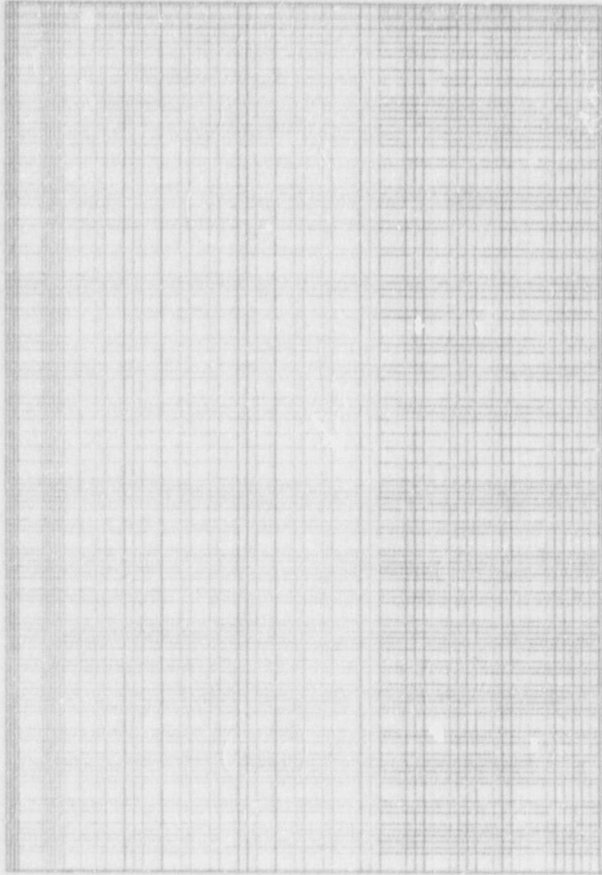
* Note: Time for these scenarios is measured from the second reactor shutdown.

TABLE 5.8.2

**RESULTS OF MINIMUM TIME-TO-BOIL AND
MAXIMUM BOILOFF RATE EVALUATION**

Scenario*	Minimum Time-to-Boil (hrs)	Maximum Boiloff Rate (gpm)
1	10.42	34.45
4A	3.78	69.57

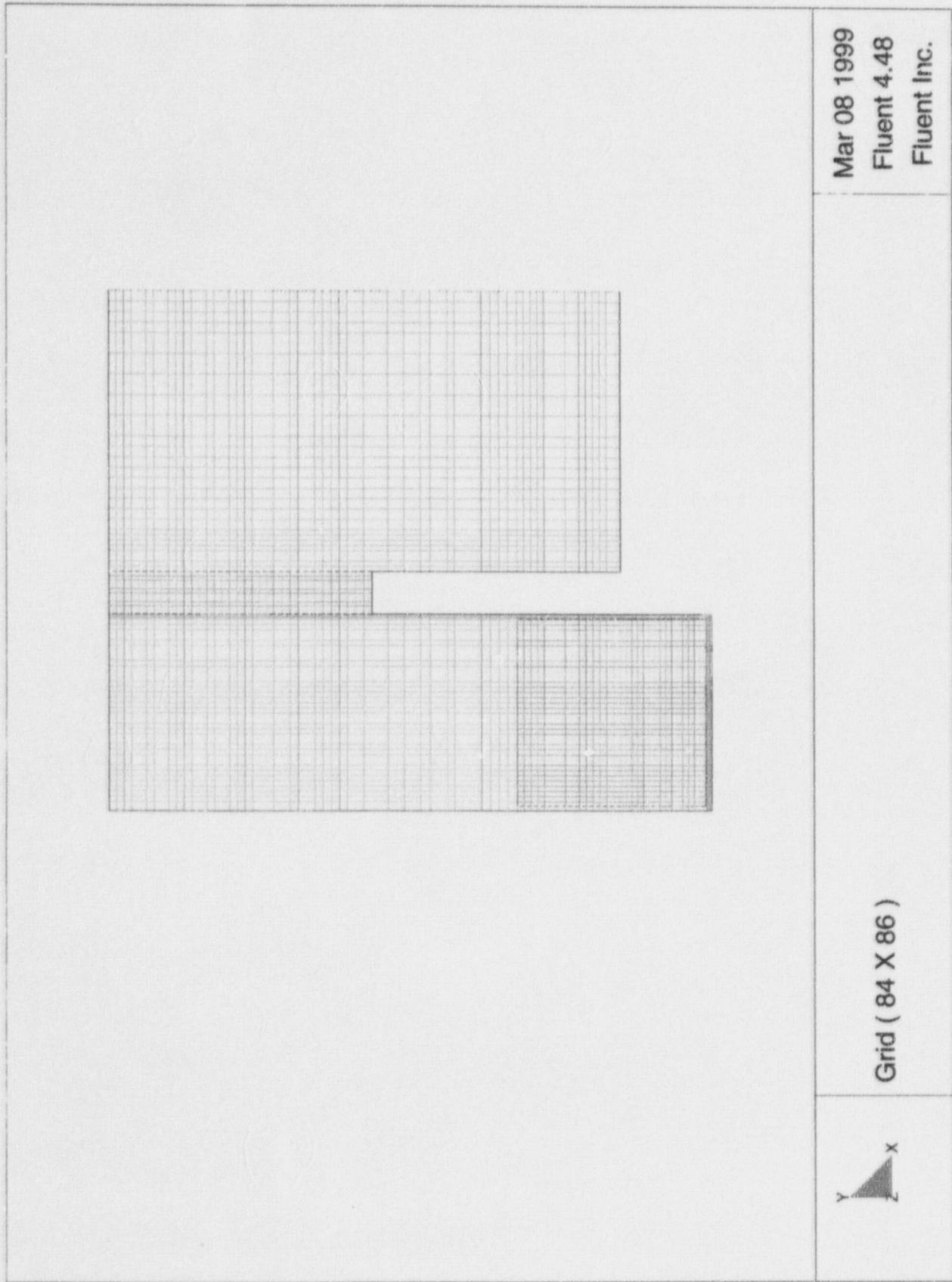
*Note: As discussed in Section 5.3, boiling evaluations are not performed for Scenarios 2, 3A and 3B, and only performed for the most limiting of Scenarios 4A and 4B.



Grid (148 X 79)

Mar 08 1999
Fluent 4.48
Fluent Inc.

FIGURE 5.6.1: Two-Dimensional Spent Fuel Pool Geometry Grid



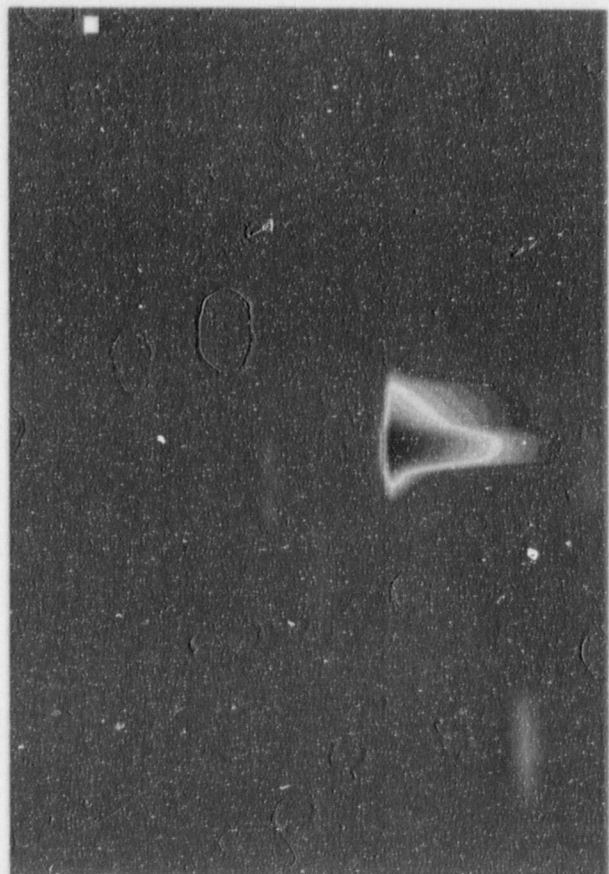
Mar 08 1999
 Fluent 4.48
 Fluent Inc.

Grid (84 X 86)



FIGURE 5.6.2: Two-Dimensional Cask Pit Geometry Grid

3.64E+02
 3.63E+02
 3.62E+02
 3.60E+02
 3.59E+02
 3.58E+02
 3.57E+02
 3.55E+02
 3.54E+02
 3.53E+02
 3.52E+02
 3.51E+02
 3.49E+02
 3.48E+02
 3.47E+02
 3.46E+02
 3.45E+02
 3.43E+02
 3.42E+02
 3.41E+02
 3.40E+02
 3.39E+02
 3.37E+02
 3.36E+02
 3.35E+02
 3.34E+02
 3.32E+02
 3.31E+02
 3.30E+02
 3.29E+02
 3.28E+02



Mar 08 1999
 Fluent 4.48
 Fluent Inc.

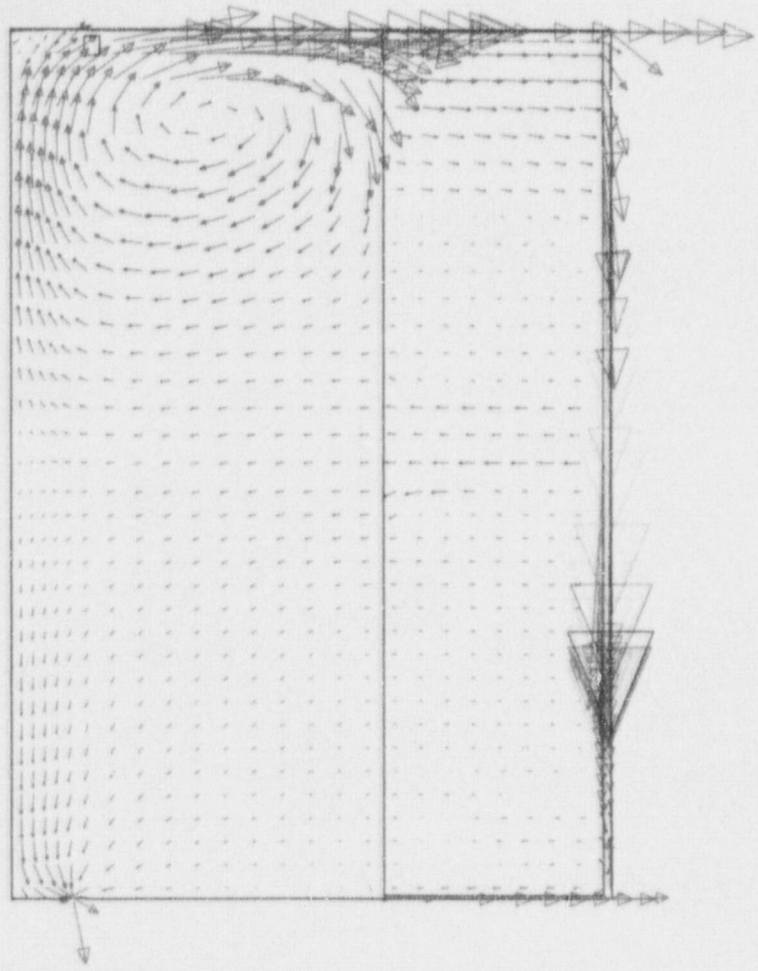
DAVIS-BESSE SPENT FUEL POOL TWO-DIMENSIONAL CFD MODEL

Temperature (K)

Max = 3.639E+02 Min = 3.276E+02

FIGURE 5.6.3: Two-Dimensional Spent Fuel Pool Model - Temperature Contours

3.77E-01
 3.64E-01
 3.51E-01
 3.38E-01
 3.25E-01
 3.12E-01
 2.99E-01
 2.86E-01
 2.73E-01
 2.60E-01
 2.47E-01
 2.34E-01
 2.21E-01
 2.08E-01
 1.95E-01
 1.82E-01
 1.69E-01
 1.56E-01
 1.43E-01
 1.30E-01
 1.17E-01
 1.04E-01
 9.10E-02
 7.81E-02
 6.51E-02
 5.21E-02
 3.91E-02
 2.61E-02
 1.32E-02
 1.72E-04

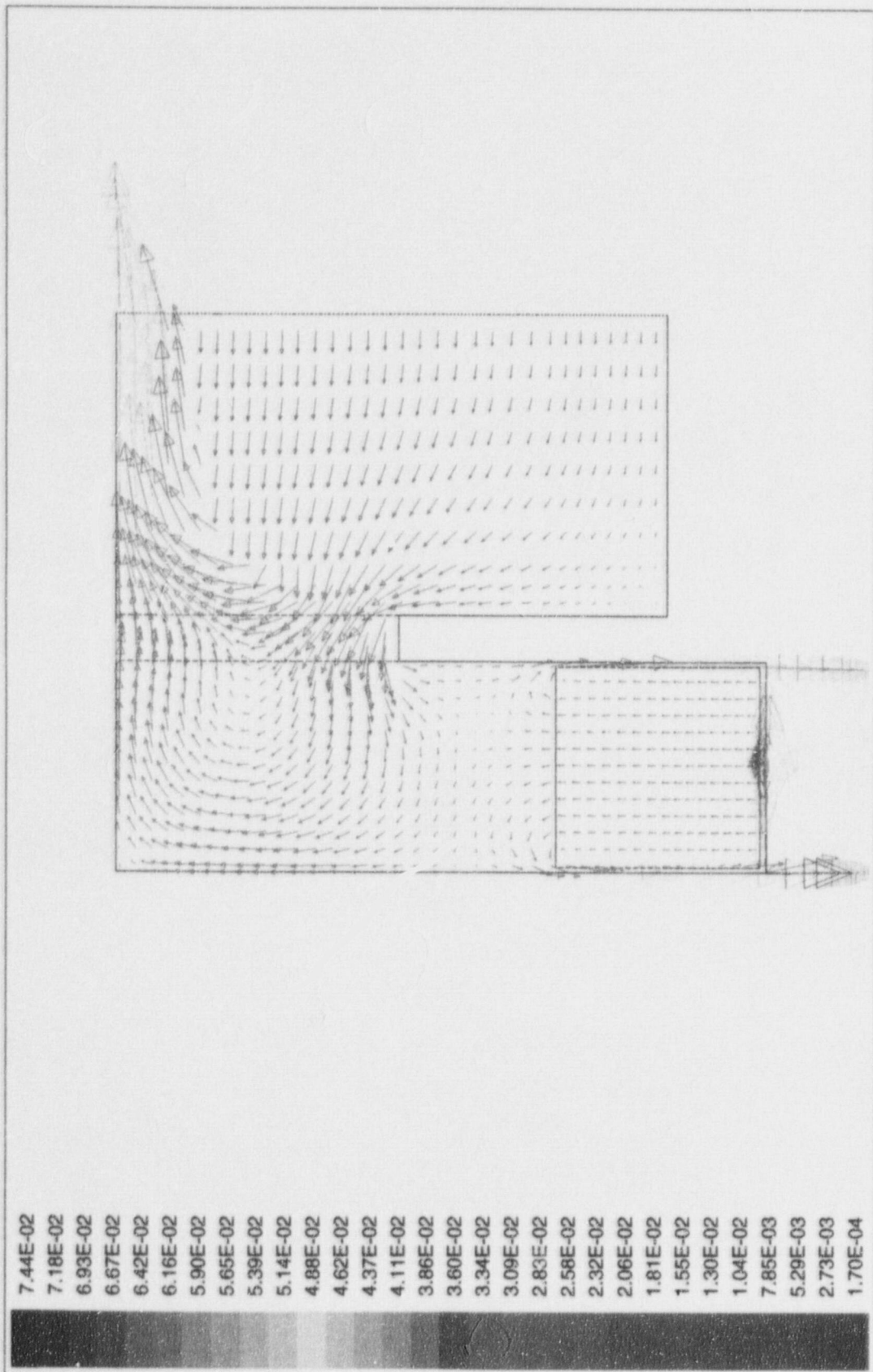


Mar 08 1999
 Fluent 4.48
 Fluent Inc.

DAVIS-BESSE SPENT FUEL POOL TWO-DIMENSIONAL CFD MODEL
 Velocity Vectors (M/S)
 Max = 3.766E-01 Min = 1.720E-04

FIGURE 5.6.4: Two-Dimensional Spent Fuel Pool Model - Velocity Vectors

7.44E-02
 7.18E-02
 6.93E-02
 6.67E-02
 6.42E-02
 6.16E-02
 5.90E-02
 5.65E-02
 5.39E-02
 5.14E-02
 4.88E-02
 4.62E-02
 4.37E-02
 4.11E-02
 3.86E-02
 3.60E-02
 3.34E-02
 3.09E-02
 2.83E-02
 2.58E-02
 2.32E-02
 2.06E-02
 1.81E-02
 1.55E-02
 1.30E-02
 1.04E-02
 7.85E-03
 5.29E-03
 2.73E-03
 1.70E-04



Velocity Vectors (M/S)
 Max = 7.440E-02 Min = 1.704E-04

Mar 08 1999
 Fluent 4.48
 Fluent Inc.

FIGURE 5.6.6: Two-Dimensional Cask Pit Model - Velocity Vectors

6.0 STRUCTURAL / SEISMIC CONSIDERATIONS

6.1 Introduction

This section considers the structural adequacy of the new Cask Pit maximum density spent fuel racks under all loadings postulated for normal, seismic, and accident conditions at the DBNPS. The analyzed storage rack configurations with the new racks in place subsequent to each campaign are depicted in Figures 1.1 through 1.3. The three campaign phases are analyzed separately.

The analyses, undertaken to confirm the structural integrity of the racks, are performed in compliance with the USNRC Standard Review Plan [6.1.1] and the OT Position Paper [6.1.2]. For each of the analyses, an abstract of the methodology, modeling assumptions, key results, and summary of parametric evaluations are presented. Delineation of the relevant criteria is discussed in the text associated with each analysis.

6.2 Overview of Rack Structural Analysis Methodology

The response of a free-standing rack module to seismic inputs is highly nonlinear and involves a complex combination of motions (sliding, rocking, twisting, and turning), resulting in impacts and friction effects. Some of the unique attributes of the rack dynamic behavior include a large fraction of the total structural mass in a confined rattling motion, friction support of rack pedestals against lateral motion, and large fluid coupling effects due to deep submergence and independent motion of closely spaced adjacent structures.

Linear methods, such as modal analysis and response spectrum techniques, cannot accurately simulate the structural response of such a highly nonlinear structure to seismic excitation. An accurate simulation is obtained only by direct integration of the nonlinear equations of motion with the three pool slab acceleration time-histories applied as the forcing functions acting simultaneously.

Whole Pool Multi-Rack (WPMR) analysis is the vehicle utilized in this project to simulate the dynamic behavior of the complex storage rack structures. The following sections provide the basis for this selection and discussion on the development of the methodology.

6.2.1 Background of Analysis Methodology

Reliable assessment of the stress field and kinematic behavior of the rack modules calls for a conservative dynamic model incorporating all *key attributes* of the actual structure. This means that the model must feature the ability to execute the concurrent motion forms compatible with the free-standing installation of the modules.

The model must possess the capability to effect momentum transfers which occur due to rattling of fuel assemblies inside storage cells and the capability to simulate lift-off and subsequent impact of support pedestals with the pool liner (or bearing pad). The contribution of the water mass in the interstitial spaces around the rack modules and within the storage cells must be modeled in an accurate manner, since erring in quantification of fluid coupling on either side of the actual value is no guarantee of conservatism.

The Coulomb friction coefficient at the pedestal-to-pool liner (or bearing pad) interface may lie in a rather wide range and a conservative value of friction cannot be prescribed *a priori*. In fact, a perusal of results of rack dynamic analyses in numerous docket (Table 6.2.1) indicates that an upper bound value of the coefficient of friction often maximizes the computed rack displacements as well as the equivalent elastostatic stresses.

In short, there are a large number of parameters with potential influence on the rack kinematics. The comprehensive structural evaluation must deal with all of these without sacrificing conservatism.

The three-dimensional single rack dynamic model introduced by Holtec International in the Enrico Fermi Unit 2 rack project (ca. 1980) and used in some 50 re-rack projects since that time (Table 6.2.1) addresses most of the above mentioned array of parameters. The details of this methodology are also published in the permanent literature [6.2.1]. Despite the versatility of the 3-D seismic model, the accuracy of the single rack simulations has been suspect due to one key element; namely, hydrodynamic participation of water around the racks. During dynamic rack motion, hydraulic energy is either drawn from or added to the moving rack, modifying its submerged motion in a significant manner. Therefore, the dynamics of one rack affects the motion of all others in the pool.

A dynamic simulation, which treats only one rack, or a small grouping of racks, is intrinsically inadequate to predict the motion of rack modules with any quantifiable level of accuracy. Three-dimensional Whole Pool Multi-Rack analyses carried out on several previous plants demonstrate that single rack simulations under predict rack displacement during seismic responses [6.2.2].

Briefly, the 3-D rack model dynamic simulation, involving one or more spent fuel racks, handles the array of variables as follows:

Interface Coefficient of Friction Parametric runs are made with upper bound and lower bound values of the coefficient of friction. The limiting values are based on experimental data which have been found to be bounded by the values 0.2 and 0.5. Simulations are also performed with the array of pedestals having randomly chosen coefficients of friction in a Gaussian distribution with a mean of 0.5 and lower and upper limits of 0.2 and 0.8, respectively. In the fuel rack simulations, the Coulomb friction interface between rack support pedestal and liner is simulated by piecewise linear (friction) elements. These elements function only when the pedestal is physically in contact with the pool liner.

Rack Beam Behavior Rack elasticity, relative to the rack base, is included in the model by introducing linear springs to represent the elastic bending action, twisting, and extensions.

Impact Phenomena Compression-only gap elements are used to provide for opening and closing of interfaces such as the pedestal-to-bearing pad interface, and the fuel assembly-to-cell wall interface. These interface gaps are modeled using nonlinear spring elements. The term "nonlinear spring" is a generic term used to denote the mathematical representation of the condition where a restoring force is not linearly proportional to displacement.

Fuel Loading Scenarios The fuel assemblies are conservatively assumed to rattle in unison which obviously exaggerates the contribution of impact against the cell wall.

Fluid Coupling Holtec International extended Fritz's classical two-body fluid coupling model to multiple bodies and utilized it to perform the first two-dimensional multi-rack analysis (Diablo Canyon, ca. 1987). Subsequently, laboratory experiments were conducted to validate the multi-rack fluid coupling theory. This technology was incorporated in the computer code DYNARACK [6.2.4] which handles simultaneous simulation of all racks in the pool as a Whole Pool Multi-Rack 3-D analysis. This development was first utilized in Chinshan, Oyster Creek, and Shearon Harris plants [6.2.1, 6.2.3] and, subsequently, in numerous other re-rack projects. The WPMR analyses have corroborated the accuracy of the single rack 3-D solutions in predicting the maximum structural stresses, and also serve to improve predictions of rack kinematics.

For closely spaced racks, demonstration of kinematic compliance is verified by including all modules in one comprehensive simulation using a WPMR model. In WPMR analysis, all rack modules are modeled simultaneously and the coupling effect due to this multi-body motion is included in the analysis. Due to the superiority of this technique in predicting the dynamic behavior of closely spaced submerged storage racks, the Whole Pool Multi-Rack analysis methodology is used for this project.

6.3 Description of Racks

The new high density storage racks are analyzed for installation in three separate campaigns as follows:

<u>Campaign</u>	<u>Rack</u>	<u>Storage Locations</u>
I	N1	81
II	N2	72
III	N3	64
III	N4	72

Rack material is defined in Table 6.3.1.

Figures 1.1 through 1.3 provide pool plan layouts for the Cask Pit storage configuration at the end of each possible campaign. The walls separating the Spent Fuel Pool and the Cask Pit allow the proposed rack configurations to be dynamically analyzed separately from the racks located in the Spent Fuel Pool.

The cartesian coordinate system utilized within the rack dynamic model has the following nomenclature:

- x = Horizontal axis along plant North
- y = Horizontal axis along plant West
- z = Vertical axis upward from the rack base

6.3.1 Fuel Weights

For the dynamic rack simulations, the dry fuel weight is conservatively taken to be 1682 lbs. The actual fuel assembly weight is 1550 lbs. The higher fuel weight value of 1682 lbs is used to account for control components being stored along with fuel assemblies. Therefore, the analyses conservatively consider control components to be stored along with an assembly at every location.

6.4 Synthetic Time-Histories

The synthetic time-histories in three orthogonal directions (N-S, E-W, and vertical) are generated in accordance with the provisions of SRP 3.7.1 [6.4.1]. In order to prepare an acceptable set of acceleration time-histories, Holtec International's proprietary code GENEQ [6.4.2] is utilized.

A preferred criterion for the synthetic time-histories in SRP 3.7.1 calls for both the response spectrum and the power spectral density corresponding to the generated acceleration time-history to envelope their target (design basis) counterparts with only finite enveloping inflections. The time-histories for the pools have been generated to satisfy this preferred criterion. The seismic files also satisfy the requirements of statistical independence mandated by SRP 3.7.1.

Figures 6.4.1 through 6.4.3 provide plots of the time-history accelerograms which were generated over a 20 second duration for the SSE event. These artificial time-histories are used in all non-linear dynamic simulations of the racks.

Results of the correlation function of the three time-histories are given in Table 6.4.1. Absolute values of the correlation coefficients are shown to be less than 0.15, indicating that the desired statistical independence of the three data sets has been met.

6.5 WPMR Methodology

Recognizing that the analysis work effort must deal with both stress and displacement criteria, the sequence of model development and analysis steps that are undertaken are summarized in the following:

- a. Prepare 3-D dynamic models suitable for a time-history analysis of the new maximum density racks. These models include the assemblage of the rack modules in the Cask Pit. Include all fluid coupling interactions and mechanical coupling appropriate to performing an accurate non-linear simulation. This 3-D simulation is referred to as a Whole Pool Multi-Rack model.
- b. Perform 3-D dynamic analyses on various physical conditions (such as coefficient of friction and extent of cells containing fuel assemblies). Archive appropriate displacement and load outputs from the dynamic model for post-processing.
- c. Perform stress analysis of high stress areas for the limiting case of all the rack dynamic analyses. Demonstrate compliance with ASME Code Section III, Subsection NF limits on stress and displacement.

6.5.1 Model Details for Spent Fuel Racks

The dynamic modeling of the rack structure is prepared with special consideration of all nonlinearities and parametric variations. Particulars of modeling details and assumptions for the Whole Pool Multi-Rack analysis of racks are given in the following:

6.5.1.1 Assumptions

- a. The fuel rack structure motion is captured by modeling the rack as a 12 degree-of-freedom structure. Movement of the rack cross-section at any height is described by six degrees-of-freedom of the rack base and six degrees-of-freedom at the rack top. In this manner, the response of the module, relative to the base-plate, is captured in the dynamic analyses once suitable springs are introduced to couple the rack degrees-of-freedom and simulate rack stiffness.
- b. Rattling fuel assemblies within the rack are modeled by five lumped masses located at H , $.75H$, $.5H$, $.25H$, and at the rack base (H is the rack height measured above the base-plate). Each lumped fuel mass has two horizontal displacement degrees-of-freedom. Vertical motion of the fuel assembly mass is assumed equal to rack vertical motion at the base-plate level. The centroid of each fuel assembly mass can be located off-center, relative to the rack structure centroid at that level, to simulate a partially loaded rack.
- c. Seismic motion of a fuel rack is characterized by random rattling of fuel assemblies in their individual storage locations. All fuel assemblies are assumed to move in-phase within a rack. This exaggerates computed dynamic loading on the rack structure and, therefore, yields conservative results.
- d. Fluid coupling between the rack and fuel assemblies, and between the rack and wall, is simulated by appropriate inertial coupling in the system kinetic energy. Inclusion of these effects uses the methods of [6.5.2, 6.5.3] for rack / assembly coupling and for rack-to-rack coupling.
- e. Fluid damping and form drag are conservatively neglected.

- f. Sloshing is found to be negligible at the top of the rack and is, therefore, neglected in the analysis of the rack.
- g. Potential impacts between the cell walls of the new racks and the contained fuel assemblies are accounted for by appropriate compression-only gap elements between masses involved. The possible incidence of rack-to-wall or rack-to-rack impact is simulated by gap elements at the top and bottom of the rack in two horizontal directions. Bottom gap elements are located at the base-plate elevation. The initial gaps reflect the presence of baseplate extensions, and the rack stiffnesses are chosen to simulate local structural detail.
- h. Pedestals are modeled by gap elements in the vertical direction and as "rigid links" for transferring horizontal stress. Each pedestal support is linked to the pool liner (or bearing pad) by two friction springs. The spring rate for the friction springs includes any lateral elasticity of the stub pedestals. Local pedestal vertical spring stiffness accounts for floor elasticity and for local rack elasticity just above the pedestal.
- i. Rattling of fuel assemblies inside the storage locations causes the gap between fuel assemblies and cell wall to change from a maximum of twice the nominal gap to a theoretical zero gap. Fluid coupling coefficients are based on the nominal gap in order to provide a conservative measure of fluid resistance to gap closure.
- j. The model for the rack is considered supported, at the base level, on four pedestals modeled as non-linear compression only gap spring elements and eight piecewise linear friction spring elements. These elements are properly located with respect to the centerline of the rack beam, and allow for arbitrary rocking and sliding motions.

6.5.1.2 Element Details

Figure 6.5.1 shows a schematic of the dynamic model of a single rack. The schematic depicts many of the characteristics of the model including all of the degrees-of-freedom and some of the spring restraint elements.

Table 6.5.1 provides a complete listing of each of the 22 degrees-of-freedom for a rack model. Six translational and six rotational degrees-of-freedom (three of each type on each end) describe the motion of the rack structure. Rattling fuel mass motions (shown at nodes 1*, 2*, 3*, 4*, and 5* in Figure 6.5.1) are described by ten horizontal translational degrees-of-freedom (two at each of the five fuel masses). The vertical fuel mass motion is assumed (and modeled) to be the same as that of the rack baseplate.

Figure 6.5.2 depicts the fuel to rack impact springs (used to develop potential impact loads between the fuel assembly mass and rack cell inner walls) in a schematic isometric. Only one of the five fuel masses is shown in this figure. Four compression only springs, acting in the horizontal direction, are provided at each fuel mass.

Figure 6.5.3 provides a 2-D schematic elevation of the storage rack model, discussed in more detail in Section 6.5.3. This view shows the vertical location of the five storage masses and some of the support pedestal spring members.

Figure 6.5.4 shows the modeling technique and degrees-of-freedom associated with rack elasticity. In each bending plane a shear and bending spring simulate elastic effects [6.5.4]. Linear elastic springs coupling rack vertical and torsional degrees-of-freedom are also included in the model.

Figure 6.5.5 depicts the inter-rack impact springs (used to develop potential impact loads between racks or between rack and wall).

Figures 6.5.6 through 6.5.8 show the rack numbering schemes used for the WPMR analyses of the three Cask Pit campaigns.

6.5.2 Fluid Coupling Effect

In its simplest form, the so-called "fluid coupling effect" [6.5.2, 6.5.3] can be explained by considering the proximate motion of two bodies under water. If one body (mass m_1) vibrates adjacent to a second body (mass m_2), and both bodies are submerged in frictionless fluid, then Newton's equations of motion for the two bodies are:

$$(m_1 + M_{11}) \ddot{X}_1 + M_{12} \ddot{X}_2 = \text{applied forces on mass } m_1 + O(X_1^2)$$

$$M_{21} \ddot{X}_1 + (m_2 + M_{22}) \ddot{X}_2 = \text{applied forces on mass } m_2 + O(X_2^2)$$

\ddot{X}_1 , and \ddot{X}_2 denote absolute accelerations of masses m_1 and m_2 , respectively, and the notation $O(X^2)$ denotes nonlinear terms.

M_{11} , M_{12} , M_{21} , and M_{22} are fluid coupling coefficients which depend on body shape, relative disposition, etc. Fritz [6.5.3] gives data for M_{ij} for various body shapes and arrangements. The fluid adds mass to the body (M_{11} to mass m_1), and an inertial force proportional to acceleration of the adjacent body (mass m_2). Thus, acceleration of one body affects the force field on another. This force field is a function of inter-body gap, reaching large values for small gaps. Lateral motion of a fuel assembly inside a storage location encounters this effect. For example, fluid coupling behavior will be experienced between nodes 2 and 2* in Figure 6.5.1. The rack analysis also contains inertial fluid coupling terms, which model the effect of fluid in the gaps between adjacent racks.

Terms modeling the effects of fluid flowing between adjacent racks in a single rack analysis suffer from the inaccuracies described earlier. These terms are usually computed assuming that

all racks adjacent to the rack being analyzed are vibrating in-phase or 180° out of phase. The WPMR analyses do not require any assumptions with regard to phase.

Rack-to-rack gap elements have initial gaps set to 100% of the physical gap between the racks or between outermost racks and the adjacent pool walls.

6.5.2.1 Multi-Body Fluid Coupling Phenomena

During the seismic event, all racks in the pool are subject to the input excitation simultaneously. The motion of each free-standing module would be autonomous and independent of others as long as they did not impact each other and no water were present in the pool. While the scenario of inter-rack impact is not a common occurrence and depends on rack spacing, the effect of water (the so-called fluid coupling effect) is a universal factor. As noted in Ref. [6.5.2, 6.5.4], the fluid forces can reach rather large values in closely spaced rack geometries. It is, therefore, essential that the contribution of the fluid forces be included in a comprehensive manner. This is possible only if all racks in the pool are *allowed* to execute 3-D motion in the mathematical model. For this reason, single rack or even multi-rack models involving only a portion of the racks in the pool, are inherently inaccurate. The Whole Pool Multi-Rack model removes this intrinsic limitation of the rack dynamic models by simulating the 3-D motion of all modules simultaneously. The fluid coupling effect, therefore, encompasses interaction between *every* set of racks in the pool, i.e., the motion of one rack produces fluid forces on all other racks and on the pool walls. Stated more formally, both near-field and far-field fluid coupling effects are included in the analysis.

The derivation of the fluid coupling matrix [6.5.5] relies on the classical inviscid fluid mechanics principles, namely the principle of continuity and Kelvin's recirculation theorem. While the derivation of the fluid coupling matrix is based on no artificial construct, it has been nevertheless verified by an extensive set of shake table experiments [6.5.5].

6.5.3 Stiffness Element Details

Three element types are used in the rack models. Type 1 are linear elastic elements used to represent the beam-like behavior of the integrated rack cell matrix. Type 2 elements are the piece-wise linear friction springs used to develop the appropriate forces between the rack pedestals and the supporting bearing pads. Type 3 elements are non-linear gap elements, which model gap closures and subsequent impact loadings i.e., between fuel assemblies and the storage cell inner walls, and rack outer periphery spaces.

If the simulation model is restricted to two dimensions (one horizontal motion plus one vertical motion, for example), for the purposes of model clarification only, then Figure 6.5.3 describes the configuration. This simpler model is used to elaborate on the various stiffness modeling elements.

Type 3 gap elements modeling impacts between fuel assemblies and racks have local stiffness K_i in Figure 6.5.3. Support pedestal spring rates K_S are modeled by type 3 gap elements. Local compliance of the concrete floor is included in K_S . The type 2 friction elements are shown in Figure 6.5.3 as K_f . The spring elements depicted in Figure 6.5.4 represent type 1 elements.

Friction at support/liner interface is modeled by the piecewise linear friction springs with suitably large stiffness K_f up to the limiting lateral load μN , where N is the current compression load at the interface between support and liner. At every time-step during transient analysis, the current value of N (either zero if the pedestal has lifted off the liner, or a compressive finite value) is computed.

The gap element K_S , modeling the effective compression stiffness of the structure in the vicinity of the support, includes stiffness of the pedestal, local stiffness of the underlying pool slab, and local stiffness of the rack cellular structure above the pedestal.

The previous discussion is limited to a 2-D model solely for simplicity. Actual analyses incorporate 3-D motions.

6.5.4 Coefficients of Friction

To eliminate the last significant element of uncertainty in rack dynamic analyses, multiple simulations are performed to adjust the friction coefficient ascribed to the support pedestal / pool bearing pad interface. These friction coefficients are chosen consistent with the two bounding extremes from Rabinowicz's data [6.5.1]. Simulations are also performed by imposing intermediate value friction coefficients developed by a random number generator with Gaussian normal distribution characteristics. The assigned values are then held constant during the entire simulation in order to obtain reproducible results.[†] Thus, in this manner, the WPMR analysis results are brought closer to the realistic structural conditions.

The coefficient of friction (μ) between the pedestal supports and the pool floor is indeterminate. According to Rabinowicz [6.5.1], results of 199 tests performed on austenitic stainless steel plates submerged in water show a mean value of μ to be 0.503 with standard deviation of 0.125. Upper and lower bounds (based on twice standard deviation) are 0.753 and 0.253, respectively. Analyses are therefore performed for coefficient of friction values of 0.2 (lower limit) and for 0.8 (upper limit), and for random friction values clustered about a mean of 0.5. The bounding values of $\mu = 0.2$ and 0.8 have been found to envelope the upper limit of module response in previous rerack projects.

[†] It is noted that DYNARACK has the capability to change the coefficient of friction at any pedestal at each instant of contact based on a random reading of the computer clock cycle. However, exercising this option would yield results that could not be reproduced. Therefore, the random choice of coefficients is made only once per run.

6.5.5 Governing Equations of Motion

Using the structural model discussed in the foregoing, equations of motion corresponding to each degree-of-freedom are obtained using Lagrange's Formulation [6.5.4]. The system kinetic energy includes contributions from solid structures and from trapped and surrounding fluid. The final system of equations obtained have the matrix form:

$$[M] \left[\frac{d^2 q}{dt^2} \right] = [Q] + [G]$$

where:

- [M] - total mass matrix (including structural and fluid mass contributions). The size of this matrix will be $22n \times 22n$ for a WPMR analysis (n = number of racks in the model).
- q - the nodal displacement vector relative to the pool slab displacement (the term with q indicates the second derivative with respect to time, i.e., acceleration)
- [G] - a vector dependent on the given ground acceleration
- [Q] - a vector dependent on the spring forces (linear and nonlinear) and the coupling between degrees-of-freedom

The above column vectors have length $22n$. The equations can be rewritten as follows:

$$\left[\frac{d^2 q}{dt^2} \right] = [M]^{-1} [Q] + [M]^{-1} [G]$$

This equation set is mass uncoupled, displacement coupled at each instant in time. The numerical solution uses a central difference scheme built into the proprietary computer program DYNARACK [6.2.4].

6.6 Structural Evaluation of Spent Fuel Rack Design

6.6.1 Kinematic and Stress Acceptance Criteria

There are two sets of criteria to be satisfied by the rack modules:

a. Kinematic Criteria

An isolated fuel rack situated in the middle of the storage cavity is most vulnerable to overturning because such a rack would be hydrodynamically uncoupled from any adjacent structures. Therefore, to assess the margin against overturning, a single rack module is evaluated. According to Ref [6.1.1 and 6.1.2], the minimum required safety margins under the OBE and SSE events are 1.5 and 1.1, respectively. The maximum rotations of the rack (about the two principal axes) are obtained from a post processing of the rack time history response output. The ratio of the rotation required to produce incipient tipping in either principal plane to the actual maximum rotation in that plane from the time history solution is the margin of safety. All ratios available for the OBE and SSE events should be greater than 1.5 and 1.1, respectively to satisfy the regulatory acceptance criteria. However, in order to be consistent with the conservative method selected for evaluation of stress factors (as discussed in Section 6.6.3), the worst case displacements from the SSE simulations must ensure a more conservative factor of safety of 1.5.

b. Stress Limit Criteria

Stress limits must not be exceeded under the postulated load combinations provided herein.

6.6.2 Stress Limit Evaluations

The stress limits presented below apply to the rack structure and are derived from the ASME Code, Section III, Subsection NF [6.6.1]. Parameters and terminology are in accordance with the ASME Code. Material properties are obtained from the ASME Code Appendices [6.6.2], and are listed in Table 6.3.1.

(i) Normal and Upset Conditions (Level A or Level B)

- a. Allowable stress in tension on a net section is:

$$F_t = 0.6 S_y$$

Where, S_y = yield stress at temperature, and F_t is equivalent to primary membrane stress.

- b. Allowable stress in shear on a net section is:

$$F_v = .4 S_y$$

- c. Allowable stress in compression on a net section is:

$$F_a = S_y \left(.47 - \frac{k l}{444 r} \right)$$

where kl/r for the main rack body is based on the full height and cross section of the honeycomb region and does not exceed 120 for all sections.

l = unsupported length of component

k = length coefficient which gives influence of boundary conditions. The following values are appropriate for the described end conditions:

1 (simple support both ends)

2 (cantilever beam)

$\frac{1}{2}$ (clamped at both ends)

r = radius of gyration of component

- d. Maximum allowable bending stress at the outermost fiber of a net section, due to flexure about one plane of symmetry is:

$$F_b = 0.60 S_y \quad (\text{equivalent to primary bending})$$

- e. Combined bending and compression on a net section satisfies:

$$\frac{f_a}{F_a} + \frac{C_{mx} f_{bx}}{D_x F_{bx}} + \frac{C_{my} f_{by}}{D_y F_{by}} < 1$$

where:

f_a = Direct compressive stress in the section

f_{bx} = Maximum bending stress along x-axis

f_{by} = Maximum bending stress along y-axis

C_{mx} = 0.85

C_{my} = 0.85

D_x = $1 - (f_a/F'_{ex})$

D_y = $1 - (f_a/F'_{ey})$

$F'_{ex,ey}$ = $(\pi^2 E)/(2.15 (kl/r)_{x,y}^2)$

E = Young's Modulus

and subscripts x,y reflect the particular bending plane.

- f. Combined flexure and compression (or tension) on a net section:

$$\frac{f_a}{0.6 S_y} + \frac{f_{bx}}{F_{bx}} + \frac{f_{by}}{F_{by}} < 1.0$$

The above requirements are to be met for both direct tension or compression.

- g. Welds

Allowable maximum shear stress on the net section of a weld is given by:

$$F_w = 0.3 S_u$$

where S_u is the weld material ultimate strength at temperature. For fillet weld legs in contact with base metal, the shear stress on the gross section is limited to $0.4S_y$, where S_y is the base material yield strength at temperature.

(ii) Level D Service Limits

Section F-1334 (ASME Section III, Appendix F) [6.6.2], states that the limits for the Level D condition are the minimum of $1.2 (S_y/F_t)$ or $(0.7S_u/F_t)$ times the corresponding limits for the Level A condition. S_u is ultimate tensile stress at the specified rack design temperature. Examination of material properties for 304 stainless demonstrates that 1.2 times the yield strength is less than the 0.7 times the ultimate strength.

Exceptions to the above general multiplier are the following:

- a) Stresses in shear shall not exceed the lesser of $0.72S_y$ or $0.42S_u$. In the case of the Austenitic Stainless material used here, $0.72S_y$ governs.
- b) Axial Compression Loads shall be limited to $2/3$ of the calculated buckling load.
- c) Combined Axial Compression and Bending - The equations for Level A conditions shall apply except that:

$$F_a = 0.667 \times \text{Buckling Load} / \text{Gross Section Area},$$

and the terms F'_{ex} and F'_{ey} may be increased by the factor 1.65.

- d) For welds, the Level D allowable maximum weld stress is not specified in Appendix F of the ASME Code. An appropriate limit for weld throat stress is conservatively set here as:

$$F_w = (0.3 S_u) \times \text{factor}$$

where:

$$\text{factor} = (\text{Level D shear stress limit}) / (\text{Level A shear stress limit})$$

6.6.3 Dimensionless Stress Factors

For convenience, the stress results are presented in dimensionless form. Dimensionless stress factors are defined as the ratio of the actual developed stress to the specified limiting value. The limiting value of each stress factor is 1.0. For this project the allowable stress values are taken to be those corresponding to normal conditions. This is conservative, since the increase in stress allowables for OBE and SSE conditions are not considered. The stress factors reported here include adjustments for ASME Code Section III, Subsection NF slenderness ratio requirements. Stress factors reported are:

- R_1 = Ratio of direct tensile or compressive stress on a net section to its allowable value (note pedestals only resist compression)
- R_2 = Ratio of gross shear on a net section in the x-direction to its allowable value
- R_3 = Ratio of maximum x-axis bending stress to its allowable value for the section
- R_4 = Ratio of maximum y-axis bending stress to its allowable value for the section
- R_5 = Combined flexure and compressive factor (as defined in the foregoing)
- R_6 = Combined flexure and tension (or compression) factor (as defined in the foregoing)
- R_7 = Ratio of gross shear on a net section in the y-direction to its allowable value

6.6.4 Loads and Loading Combinations for Spent Fuel Racks

The applicable loads and their combinations, which must be considered in the seismic analysis of rack modules, is excerpted from Refs. [6.1.2] and [6.6.3]. The load combinations considered are identified below:

Loading Combination	Service Level
D + L D + L + T _o D + L + T _o + E	Level A
D + L + T _a + E D + L + T _o + P _f	Level B
D + L + T _a + E' D + L + T _o + F _d	Level D The functional capability of the fuel racks must be demonstrated.

Where:

- D = Dead weight-induced loads (including fuel assembly weight)
- L = Live Load (not applicable for the fuel rack, since there are no moving objects in the rack load path)
- P_f = Upward force on the racks caused by postulated stuck fuel assembly
- F_d = Impact force from accidental drop of the heaviest load from the maximum possible height.
- E = Operating Basis Earthquake (OBE)
- E' = Safe Shutdown Earthquake (SSE)
- T_o = Differential temperature induced loads (normal operating or shutdown condition based on the most critical transient or steady state condition)
- T_a = Differential temperature induced loads (the highest temperature associated with the postulated abnormal design conditions)

T_a and T_o produce local thermal stresses. The worst thermal stress field in a fuel rack is obtained when an isolated storage location has a fuel assembly generating heat at maximum postulated rate and surrounding storage locations contain no fuel. Heated water makes unobstructed contact with the inside of the storage walls, thereby producing maximum possible temperature difference between adjacent cells. Secondary stresses produced are limited to the body of the rack; that is, support pedestals do not experience secondary (thermal) stresses.

6.7 Parametric Simulations

The following table presents a complete listing of the simulations discussed herein. The rack numbering scheme used to identify the racks in each simulation model and the coordinate axes X and Y used to identify displacement orientation are introduced in Figures 6.5.6 through 6.5.8.

Consideration of the parameters described in Section 6.5 resulted in the following runs.

<u>Run</u>	<u>Phase</u>	<u>Load Case</u>	<u>Rack Fuel Loading Pattern</u>	<u>COF</u>	<u>Event</u>
1	I	one rack in pool	fully loaded	0.2	SSE
2	I	one rack in pool	fully loaded	0.8	SSE
3	I	one rack in pool	fully loaded	Random	SSE
4	I	one rack in pool	half loaded (diagonally)	0.2	SSE
5	I	one rack in pool	half loaded (diagonally)	0.8	SSE
6	I	one rack in pool	half loaded (diagonally)	Random	SSE
7	II	two racks in pool	fully loaded	0.2	SSE
8	II	two racks in pool	fully loaded	0.8	SSE
9	II	two racks in pool	fully loaded	Random	SSE
10	II	two racks in pool	half loaded (diagonally)	0.2	SSE
11	II	two racks in pool	half loaded (diagonally)	0.8	SSE
12	II	two racks in pool	half loaded (diagonally)	Random	SSE
13	III	full pool	fully loaded	0.2	SSE
14	III	full pool	fully loaded	0.8	SSE
15	III	full pool	fully loaded	Random	SSE
16	III	full pool	half loaded (diagonally)	0.2	SSE
17	III	full pool	half loaded (diagonally)	0.8	SSE
18	III	full pool	half loaded (diagonally)	Random	SSE
19	III	full pool	nearly empty	0.2	SSE
20	III	full pool	nearly empty	0.8	SSE
21	III	full pool	nearly empty	Random	SSE

OVERTURNING CHECK SIMULATIONS

<u>Run No.</u>	<u>Rack Number</u>	<u>Rack fuel loading pattern</u>	<u>COF</u>	<u>Event</u>
22	N1	fully loaded	0.2	SSE
23	N1	fully loaded	0.8	SSE
24	N1	fully loaded	Random	SSE
25	N1	half loaded in N-S direction	0.2	SSE
26	N1	half loaded in N-S direction	0.8	SSE
27	N1	half loaded in N-S direction	Random	SSE
28	N1	half loaded in E-W direction	0.2	SSE
29	N1	half loaded in E-W direction	0.8	SSE
30	N1	half loaded in E-W direction	Random	SSE

where:

Random = Gaussian distribution with a mean of 0.5 Coefficient of friction (upper and lower limits of 0.8 and 0.2).

All simulations are performed for SSE conditions. Results from the SSE overturning simulations are conservatively compared against allowables for normal conditions, as discussed in Subsection 6.6.1.a.

6.8 Time History Simulation Results

The results from the DYNARACK runs may be seen in the raw data output files. However, due to the huge quantity of output data, a post-processor is used to scan for worst case conditions and develop the stress factors discussed in subsection 6.6.3. Further reduction in this bulk of information is provided in this section by extracting the worst case values from the parameters of interest; namely displacements, support pedestal forces, impact loads, and stress factors. This section also summarizes other analyses performed to develop and evaluate structural member stresses, which are not determined by the post processor.

6.8.1 Rack Displacements

The maximum rack displacements are obtained from the time histories of the motion of the upper and lower four corners of each rack in each of the simulations. The maximum absolute value of displacement in the two horizontal directions, relative to the pool slab, is computed for each rack, at the top and bottom corners. The maximum displacement in either direction, is given below for each of the campaigns:

MAXIMUM RACK DISPLACEMENT

Run	Displacement, in	Campaign	Rack No
1	0.3625	I	1
7	0.4148	II	1
15	0.4450	III	1
24	0.3161	Overturning	1

6.8.2 Pedestal Vertical Forces

The following listing provides the maximum vertical pedestal forces from each campaign.

MAXIMUM PEDESTAL VERTICAL FORCE

Run	Pedestal Force, lbf	Campaign	Rack No
2,3	111000	I	1
8,9	121000	II	1
14	111000	III	4
31	69300	II	2
23	115000	Overturning	1

6.8.3 Pedestal Friction Forces

The maximum interface shear force value in any direction bounding all pedestals in the simulation is reported below for each campaign.

MAXIMUM INTERFACE HORIZONTAL FORCE

Run	Horizontal Force, lbf	Campaign
2	30200	I
8	35900	II
14	40300	III
23	28700	Overturning

6.8.4 Rack Impact Loads

A freestanding rack, by definition, is a structure subject to potential impacts during a seismic event. Impacts arise from rattling of the fuel assemblies in the storage rack locations and, in some instances, from localized impacts between the racks, or between a peripheral rack and the pool wall. The following sections discuss the bounding values of these impact loads.

6.8.4.1 Rack to Rack Impacts

Gap elements track the potential for impacts between any rack and the pool walls. The results for each simulation have been scanned for non-zero values. The simulation results show that no gap element between any rack and any portion of the pool walls and between any two rack tops close. The tabular results do show some contact forces develop between rack-to-rack at the baseplate elevation during the simulations. Baseplate gaps are initially set to zero, so impact loads (contact forces) are expected. Contact loads did occur on simulation nos. 9 and 14 at a localized rack bottom location, and the maximum values from these two simulations are reported as follows:

MAXIMUM LOCAL RACK-RACK CONTACT FORCE (AT BASEPLATE)

Run	Contact Force, lbf	Campaign
9	22490	II
14	26980	III

6.8.4.2 Rack to Wall Impacts

The storage racks do not impact the pool walls under any simulation.

6.8.4.3 Fuel to Cell Wall Impact Loads

A review of all simulations performed allows determination of the maximum instantaneous impact load between fuel assembly and fuel cell wall at any modeled impact site. The maximum fuel/cell wall impact load values are reported in the following table.

FUEL-TO-RACK CELL IMPACT FORCE

Run	Impact Force, lbf	Campaign
1	453	I
9	451	II
13	594	III
29	497	Overturning

The cell wall integrity under these instantaneous impact loads has been evaluated and shown to remain intact with no permanent damage. Based on fuel manufacturer's data, loads of this magnitude will not damage the fuel assembly.

6.9 Rack Structural Evaluation

6.9.1 Rack Stress Factors

The time history results from the DYNARACK solver provide the pedestal normal and lateral interface forces, which may be converted to the limiting bending moment and shear force at the bottom baseplate-pedestal interface. In particular, maximum values for the previously defined stress factors are determined for every pedestal in the array of racks. With this information available, the structural integrity of the pedestal can be assessed and reported. The net section maximum (in time) bending moments and shear forces can also be determined at the bottom baseplate-rack cellular structure interface for each spent fuel rack in the pool. Using these forces and moments, the maximum stress in the limiting rack cell (box) can be evaluated.

The stress factor results for male and female pedestals, and for the entire spent fuel rack cellular cross section just above the bottom casting has been determined. These factors are reported for every rack in each simulation, and for each pedestal in every rack. These locations are the most heavily loaded net sections in the structure so that satisfaction of the stress factor criteria at these locations ensures that the overall structural criteria set forth in Section 6.6 are met.

An evaluation of the stress factors for all of the simulations performed, leads to the conclusion that all stress factors, as defined in Section 6.6.3, are less than the mandated limit of 1.0 for all of the load cases examined.

From all of the simulations reported in the tables, the bounding stress factors for each campaign are summarized as follows:

MAXIMUM PEDESTAL/CELL WALL STRESS FACTORS

Run	Stress factor	Campaign
2,3	0.500 (R6)	I
8	0.600 (R6)	II
14	0.557 (R6)	III
23	0.525 (R6)	Overturning

All of the stress factors reported above are for cell wall stresses, since these control over the pedestal stress factors. The values for all other defined stress factors are archived; it is asserted here that the requirements of Section 6.6 are indeed satisfied for the load levels considered for every limiting location in every rack in the array. Note that stress factors for SSE are calculated based on normal allowable strengths. Therefore, the reported values are conservative by an approximate factor of 2 for the SSE conditions simulated.

6.9.2 Pedestal Thread Shear Stress

The maximum engagement thread stresses under faulted conditions for every pedestal for every rack in the pool are given below for each campaign.

MAXIMUM PEDESTAL THREAD AVERAGE SHEAR STRESS

Run	Shear Stress, psi	Campaign
2,3	4711	I
8,9	5135	II
14	4711	III
22,23,24	4881	Overturning

The maximum stress of 5,135 psi is less than the Level A allowable stress of $0.4 \cdot F_y = 0.4(25,000) = 10,000$ psi.

6.9.3 Local Stresses Due to Impacts

Impact loads at the pedestal base (discussed in subsection 6.8.2) produce stresses in the pedestal for which explicit stress limits are prescribed in the Code. However, impact loads on the cellular region of the racks, as discussed in subsection 6.8.4.3 above, produce stresses which attenuate rapidly away from the loaded region. This behavior is characteristic of secondary stresses.

Even though limits on secondary stresses are not prescribed in the Code for class 3 NF structures, evaluations must be made to ensure that the localized impacts do not lead to plastic deformations in the storage cells which affect the sub-criticality of the stored fuel array.

a. Impact Loading Between Fuel Assembly and Cell Wall

Local cell wall integrity is conservatively estimated from peak impact loads. Plastic analysis is used to obtain the limiting impact load, which would lead to gross permanent deformation. As shown in Table 6.9.1, the limiting impact load (of 3,031 lbf, including a safety factor of 2.0) is much greater than the highest calculated impact load value (of 594 lbf, see subsection 6.8.4.3) obtained from any of the rack analyses. Therefore, fuel impacts do not represent a significant concern with respect to fuel rack cell deformation.

b. Impacts Between Adjacent Racks

As may be seen from subsection 6.8.4.1, the bottom of the storage racks will impact each other at a few locations during seismic events. Since the loading is presented edge-on to the 3/4" baseplate membrane, the distributed stresses after local deformation will be negligible. The impact loading will be distributed over a large area (a significant portion of the entire baseplate length of about 74 inches by its 3/4 inch thickness). The resulting compressive stress from the highest impact load of 26,980 lbs distributed over 55 sq. inches is only 491 psi, which is negligible. This is a conservative computation, since the simulation assumes a local impact site. Therefore, any deformation will not effect the configuration of the stored fuel.

6.9.4 Weld Stresses

Weld locations subjected to significant seismic loading are at the bottom of the rack at the baseplate-to-cell connection, at the top of the pedestal support at the baseplate connection, and at cell-to-cell connections. Bounding values of resultant loads are used to qualify the connections.

a. Baseplate-to-Rack Cell Welds

For Level A or B conditions, Ref. [6.6.1] permits an allowable weld stress of $\tau = .3 S_u = 21300$ psi. As stated in subsection 6.6.2 the allowable may be increased for Level D by some amplification factor. But in order to make a conservative evaluation of the welds, the stress allowable calculated above for Level A or B is used as the stress limit for the stress factors obtained from SSE (Level D) conditions.

Weld dimensionless stress factors are produced through the use of a simple conversion (ratio) factor applied to the corresponding stress factor in the adjacent rack material. The 2.20 is developed from the differences in material thickness and length versus weld throat dimension and length:

$$RATIO = \text{[REDACTED]}$$

The highest predicted weld stress for SSE is calculated from the highest R6 value (see subsection 6.9.1) as follows:

$$R6 * [(0.6) Fy] * RATIO = 0.600 [0.6 * 25000] * 2.2 = 19800 \text{ psi}$$

This value is less than the allowable weld stress value, which is 21,300. Therefore, all weld stresses between the baseplate and cell wall base are acceptable.

b. Baseplate-to-Pedestal Welds

The weld between baseplate and support pedestal is checked using finite element analysis to determine that the maximum stress is 6,421 psi under a Level D event. This calculated stress value is well below the OBE allowable of 21,300 psi, which is conservative.

c. Cell-to-Cell Welds

Cell-to-cell connections are by a series of connecting welds along the cell height. Stresses in storage cell to cell welds develop due to fuel assembly impacts with the cell wall. These weld stresses are conservatively calculated by assuming that fuel assemblies in adjacent cells are moving out of phase with one another so that impact loads in two adjacent cells are in opposite directions; this tends to separate the two cells from each other at the weld.

Table 6.9.1 gives results for the maximum allowable load that can be transferred by these welds based on the available weld area. An upper bound on the load required to be transferred is also given in Table 6.9.1, and is much lower than the allowable load. This upper bound value is very conservatively obtained by applying the bounding rack-to-fuel impact load from any simulation in two orthogonal directions simultaneously, and multiplying the result by 2 to account for the simultaneous impact of two assemblies. An equilibrium analysis at the connection then yields the upper bound load to be transferred. It is seen from the results in Table 6.9.1 that the calculated load is well below the allowable.

The cell-to-cell welds are also subjected to shear resulting from the "shear flow" behavior associated with beam action. Shear flow tends to delaminate the cell boxes and will be maximized near the center of the rack near the baseplate. An evaluation is performed based on the rack dimensionless stress factors R2 and R7 discussed above. It is seen from the results in Table 6.9.1 that the weld stress is determined to be 8,700 psi, which is less than the allowable of 10,000 psi.

6.9.5 Bearing Pad Analysis

To protect the pool slab from highly localized dynamic loadings, bearing pads are placed between the pedestal base and the slab. Fuel rack pedestals impact on these bearing pads during a seismic event and pedestal loading is transferred to the liner. Bearing pad dimensions are set to ensure that the average pressure on the slab surface due to a static load plus a dynamic impact load does not exceed the American Concrete Institute, ACI-349 [6.9.1] limit on bearing pressures. Section 10.17 of [6.9.2] gives the design bearing strength as

$$f_b = \phi (.85 f_c') \epsilon$$

where $\phi = .7$ and f_c' is the specified concrete strength for the spent fuel pool. $\epsilon = 1$ except when the supporting surface is wider on all sides than the loaded area. In that case, $\epsilon = (A_2/A_1)^{.5}$, but not more than 2. A_1 is the actual loaded area, and A_2 is an area greater than A_1 and is defined in [6.9.2]. Using a value of $\epsilon > 1$ includes credit for the confining effect of the surrounding concrete. It is noted that this criterion is in conformance with the ultimate strength primary design methodology of the American Concrete Institute in use since 1971. For the DBNPS, $f_c' = 4,000$ psi and the allowable static bearing pressure is $f_b = 4,760$ psi, assuming full concrete confinement. The allowable bearing pressure computed above is conservatively computed by taking $\epsilon = 1$ to account for lack of total concrete confinement in the leak chase region. Thus, the maximum allowable concrete bearing pressure is 2,380 psi. The acceptance criterion for the bearing pad is to show that this primarily compressive component remains in the elastic range.

The analysis is performed with ANSYS using a finite element model, which places a bearing pad and rack pedestal directly above a leak chase location. This configuration is selected with the intent of bounding all other possible bearing pad / leak chase interfaces by removing a substantial portion of the concrete directly beneath the pedestal. The liner plate is conservatively neglected in order to maximize bearing pad and concrete stresses. The analysis applies the maximum vertical pedestal load from results for all pedestals scanned from the time-history solutions from all simulations. The maximum vertical pedestal load is taken to be 150,000 lbs (which is conservative, since the maximum SSE event pedestal impact load is actually 121,000 lbs).

The bearing pad selected is 1.5" thick, austenitic stainless steel plate stock. Figure 6.9.1 provides an isometric of the ANSYS finite element model. The model permits the bearing pad to deform and lose contact with the liner, if the conditions of elastostatics so dictate. Figure 6.9.1 shows the bearing pad and underlying leak chase located within the supporting concrete. The slab is modeled as an elastic foundation. Figure 6.9.2 shows the pressure profile in the underlying concrete computed by the ANSYS analysis.

The average pressure at the pad to liner interface is computed and compared against the above-mentioned limit. Calculations show that the average pressure at the slab / liner interface is 1,006 psi, which is well below the allowable value of 2,380 psi, providing a factor of safety of 2.36. The stress distribution in the bearing pad is also evaluated, with the results shown in Figure 6.9.3. The peak bending stress in the bearing pad under the maximum vertical load is 16,345 psi. The material yield strength of 25,000 psi at 200°F provides factor of safety against yield of about 1.53.

Section 7.0 also discusses an alternate pedestal / leak chase configuration considering a pedestal adjacent to multiple leak chases under a more extreme load condition resulting from a dropped fuel assembly. The instantaneous peak force from this conservatively analyzed short duration accident is approximately 9 million pounds under which the bearing pad is still shown to be acceptable. Therefore, the bearing pad design devised for the DBNPS Cask Pit is deemed appropriate for the prescribed loadings.

6.10 Level A Evaluation

The Level A condition is not a governing condition for spent fuel racks since the general level of loading is far less than Level D loading. Additionally, the material stresses computed for the Level D loadings were compared against Level A allowables. This practice ensures that both Level B and Level A conditions are bounded.

6.11 Hydrodynamic Loads on Cask Pit Walls

The hydrodynamic pressures that develop between adjacent racks and the Cask Pit walls can be developed from the archived results produced by the WPMR analysis. The time dependent pressures are determined for the rack that resulted in the maximum displacement. The maximum instantaneous hydrodynamic pressure plots for the SSE event are shown in Figure 6.11.1.

6.12 Local Stress Considerations

This section presents the results of evaluations for the possibility of cell wall buckling and the secondary stresses produced by temperature effects.

6.12.1 Cell Wall Buckling

The allowable local buckling stresses in the fuel cell walls are obtained by using classical plate buckling analysis. The evaluation for cell wall buckling is based on the applied stress being uniform along the entire length of the cell wall. In the actual fuel rack, the compressive stress comes from consideration of overall bending of the rack structures during a seismic event, and as such is negligible at the rack top, and maximum at the rack bottom.

The critical buckling stress, with a safety factor of 1.5, is determined to be 6,799 psi. The computed compressive stress in the cell wall, based on the R6 stress factor, is 6,480 psi. Therefore, there is a sufficient margin of safety against local cell wall buckling.

6.12.2 Analysis of Welded Joints in Rack

Cell-to-cell welded joints are examined under the loading conditions arising from thermal effects due to an isolated hot cell in this subsection. This secondary stress condition is evaluated alone and not combined with primary stresses from other load conditions.

A thermal gradient between cells will develop when an isolated storage location contains a fuel assembly emitting maximum postulated heat, while the surrounding locations are empty. We can obtain a conservative estimate of weld stresses along the length of an isolated hot cell by considering a beam strip uniformly heated by the thermal gradient, and restrained from growth along one long edge. This thermal gradient is based on the results of the thermal-hydraulic evaluations, which show that the difference between the local cell maximum temperatures and the bulk temperature in the pool is 4.5°F. The analyzed configuration is shown in Figure 6.12.1.

Using shear beam theory, an estimate of the maximum value of the average shear stress in the strip is given as $\tau_{\max} = 1,240$ psi. Since this is a secondary thermal stress, we use the allowable shear stress criteria for faulted conditions ($0.42 \cdot S_u = 29,820$ psi) as a guide to indicate that the maximum shear is acceptable. The margin of safety against cell wall shear failure due to cell wall growth is greater than 24 for the worst case hot cell conditions.

6.13 References

- [6.1.1] USNRC NUREG-0800, Standard Review Plan, June 1987.
- [6.1.2] (USNRC Office of Technology) "OT Position for Review and Acceptance of Spent Fuel Storage and Handling Applications", dated April 14, 1978, and January 18, 1979 amendment thereto.
- [6.2.1] Soler, A.I. and Singh, K.P., "Seismic Responses of Free Standing Fuel Rack Constructions to 3-D Motions", Nuclear Engineering and Design, Vol. 80, pp. 315-329 (1984).
- [6.2.2] Soler, A.I. and Singh, K.P., "Some Results from Simultaneous Seismic Simulations of All Racks in a Fuel Pool", INNEM Spent Fuel Management Seminar X, January, 1993.
- [6.2.3] Singh, K.P. and Soler, A.I., "Seismic Qualification of Free Standing Nuclear Fuel Storage Racks - the Chin Shan Experience, Nuclear Engineering International, UK (March 1991).
- [6.2.4] Holtec Proprietary Report HI-961465 - WPMR Analysis User Manual for Pre&Post Processors & Solver, August, 1997.
- [6.4.1] USNRC Standard Review Plan, NUREG-0800 (Section 3.7.1, Rev. 2, 1989).
- [6.4.2] Holtec Proprietary Report HI-89364 - Verification and User's Manual for Computer Code GENEQ, January, 1990.
- [6.5.1] Rabinowicz, E., "Friction Coefficients of Water Lubricated Stainless Steels for a Spent Fuel Rack Facility," MIT, a report for Boston Edison Company, 1976.
- [6.5.2] Singh, K.P. and Soler, A.I., "Dynamic Coupling in a Closely Spaced Two-Body System Vibrating in Liquid Medium: The Case of Fuel Racks," 3rd International Conference on Nuclear Power Safety, Keswick, England, May 1982.
- [6.5.3] Fritz, R.J., "The Effects of Liquids on the Dynamic Motions of Immersed Solids," Journal of Engineering for Industry, Trans. of the ASME, February 1972, pp 167-172.

- [6.5.4] Levy, S. and Wilkinson, J.P.D., "The Component Element Method in Dynamics with Application to Earthquake and Vehicle Engineering," McGraw Hill, 1976.
- [6.5.5] Paul, B., "Fluid Coupling in Fuel Racks: Correlation of Theory and Experiment", (Proprietary), NUSCO/Holtec Report HI-88243.
- [6.6.1] ASME Boiler & Pressure Vessel Code, Section III, Subsection NF, 1989 Edition.
- [6.6.2] ASME Boiler & Pressure Vessel Code, Section III, Appendices, 1989 Edition.
- [6.6.3] USNRC Standard Review Plan, NUREG-0800 (Section 3.8.4, Rev. 2, 1989).
- [6.9.1] ACI 349-85, Code Requirements for Nuclear Safety Related Concrete Structures, American Concrete Institute, Detroit, Michigan, 1985.
- [6.9.2] ACI 318-95, Building Code requirements for Structural Concrete," American Concrete Institute, Detroit, Michigan, 1995.

Table 6.2.1

PARTIAL LISTING OF FUEL RACK APPLICATIONS USING DYNARACK

PLANT	DOCKET NUMBER(s)	YEAR
Enrico Fermi Unit 2	USNRC 50-341	1980
Quad Cities 1 & 2	USNRC 50-254, 50-265	1981
Rancho Seco	USNRC 50-312	1982
Grand Gulf Unit 1	USNRC 50-416	1984
Oyster Creek	USNRC 50-219	1984
Pilgrim	USNRC 50-293	1985
V.C. Summer	USNRC 50-395	1984
Diablo Canyon Units 1 & 2	USNRC 50-275, 50-323	1986
Byron Units 1 & 2	USNRC 50-454, 50-455	1987
Braidwood Units 1 & 2	USNRC 50-456, 50-457	1987
Vogtle Unit 2	USNRC 50-425	1988
St. Lucie Unit 1	USNRC 50-335	1987
Millstone Point Unit 1	USNRC 50-245	1989
Chinshan	Taiwan Power	1988
D.C. Cook Units 1 & 2	USNRC 50-315, 50-316	1992
Indian Point Unit 2	USNRC 50-247	1990
Three Mile Island Unit 1	USNRC 50-289	1991
James A. FitzPatrick	USNRC 50-333	1990
Shearon Harris Unit 2	USNRC 50-401	1991
Hope Creek	USNRC 50-354	1990
Kuosheng Units 1 & 2	Taiwan Power Company	1990

Table 6.2.1

PARTIAL LISTING OF FUEL RACK APPLICATIONS USING DYNARACK

PLANT	DOCKET NUMBER(s)	YEAR
Ulchin Unit 2	Korea Electric Power Co.	1990
Laguna Verde Units 1 & 2	Comision Federal de Electricidad	1991
Zion Station Units 1 & 2	USNRC 50-295, 50-304	1992
Sequoyah	USNRC 50-327, 50-328	1992
LaSalle Unit 1	USNRC 50-373	1992
Duane Arnold Energy Center	USNRC 50-331	1992
Fort Calhoun	USNRC 50-285	1992
Nine Mile Point Unit 1	USNRC 50-220	1993
Beaver Valley Unit 1	USNRC 50-334	1992
Salem Units 1 & 2	USNRC 50-272, 50-311	1993
Limerick	USNRC 50-352, 50-353	1994
Ulchin Unit 1	KINS	1995
Yonggwang Units 1 & 2	KINS	1996
Kori-4	KINS	1996
Connecticut Yankee	USNRC 50-213	1996
Angra Unit 1	Brazil	1996
Sizewell B	United Kingdom	1996
Waterford 3	USNRC 50-382	1997
J.A. Fitzpatrick	USNRC 50-333	1998
Callaway	USNRC 50-483	1998
Nine Mile Unit 1	USNRC 50-220	1998

Table 6.2.1

PARTIAL LISTING OF FUEL RACK APPLICATIONS USING DYNARACK

PLANT	DOCKET NUMBER(s)	YEAR
Chin Shan	Taiwan Power Company	1998
Vermont Yankee	USNRC 50-271	1998
Millstone 3	USNRC 50-423	1998
Byron/Braidwood	USNRC 50-454, 50-455, 50-567, 50-457	1999
Wolf Creek	USNRC 50-482	1999
Plant Hatch Units 1 & 2	USNRC 50-321, 50-366	1999
Harris Pools C and D	USNRC 50-401	1999

Table 6.3.1

RACK MATERIAL DATA (200°F)

(ASME - Section II, Part D)

Material	Young's Modulus E (psi)	Yield Strength S _y (psi)	Ultimate Strength S _u (psi)
SA240; 304 S.S.	27.6 x 10 ⁶	25,000	71,000
SUPPORT MATERIAL DATA (200°F)			
SA240, Type 304 (upper part of support feet)	27.6 x 10 ⁶	25,000	71,000
SA-564-630 (lower part of support feet; age hardened at 1100°F)	28.5 x 10 ⁶	106,300	140,000

Table 6.4.1	
TIME-HISTORY STATISTICAL CORRELATION RESULTS	
SSE	
Data1 to Data2	0.064
Data1 to Data3	0.006
Data2 to Data3	-0.004

Data1 corresponds to the time-history acceleration values along the X axis (South)

Data2 corresponds to the time-history acceleration values along the Y axis (East)

Data3 corresponds to the time-history acceleration values along the Z axis (Vertical)

Table 6.5.1

Degrees-of-freedom

LOCATION (Node)	DISPLACEMENT			ROTATION		
	U_x	U_y	U_z	θ_x	θ_y	θ_z
1	p_1	p_2	p_3	q_4	q_5	q_6
2	p_7	p_8	p_9	q_{10}	q_{11}	q_{12}
<p>Node 1 is assumed to be attached to the rack at the bottom most point. Node 2 is assumed to be attached to the rack at the top most point. Refer to Figure 6.5.1 for node identification.</p>						
2*	p_{13}	p_{14}				
3*	p_{15}	p_{16}				
4*	p_{17}	p_{18}				
5*	p_{19}	p_{20}				
1*	p_{21}	p_{22}				
<p>where the relative displacement variables q_i are defined as:</p> <p> $p_i = q_i(t) + U_x(t) \quad i = 1,7,13,15,17,19,21$ $= q_i(t) + U_y(t) \quad i = 2,8,14,16,18,20,22$ $= q_i(t) + U_z(t) \quad i = 3,9$ $= q_i(t) \quad i = 4,5,6,10,11,12$ </p> <p>p_i denotes absolute displacement (or rotation) with respect to inertial space q_i denotes relative displacement (or rotation) with respect to the floor slab</p> <p>* denotes fuel mass nodes $U(t)$ are the three known earthquake displacements</p>						

Table 6.9.1 COMPARISON OF BOUNDING CALCULATED LOADS/STRESSES VS. CODE ALLOWABLES AT IMPACT LOCATIONS AND AT WELDS		
Item/Location	SSE	
	Calculated	Allowable [†]
Fuel assembly/cell wall impact, lbf.	594	3,031 ^{††}
Rack/baseplate weld, psi	19,800	21,300
Female pedestal/baseplate weld, psi	6,421	21,300
Cell/cell welds, psi, based on impact loads	2,640	10,000
Cell/cell welds, psi, based on shear flow	8,700 ^{†††}	10,000

[†] Note that Level A condition allowables were conservatively applied against SSE loads.

^{††} Based on the limit load for a cell wall. The allowable load on the fuel assembly itself may be less than this value, but will be greater than 840 lbs.

^{†††} Based on the base metal stresses adjacent to weld placements resulting from the maximum shear flow developed between two adjacent cells.

Figure 64.1: Davls-Besse SFP and Cask Pit
Time Hlstory Accelerogram
X direction Bounding SSE Spectra (2% Damp (ng)

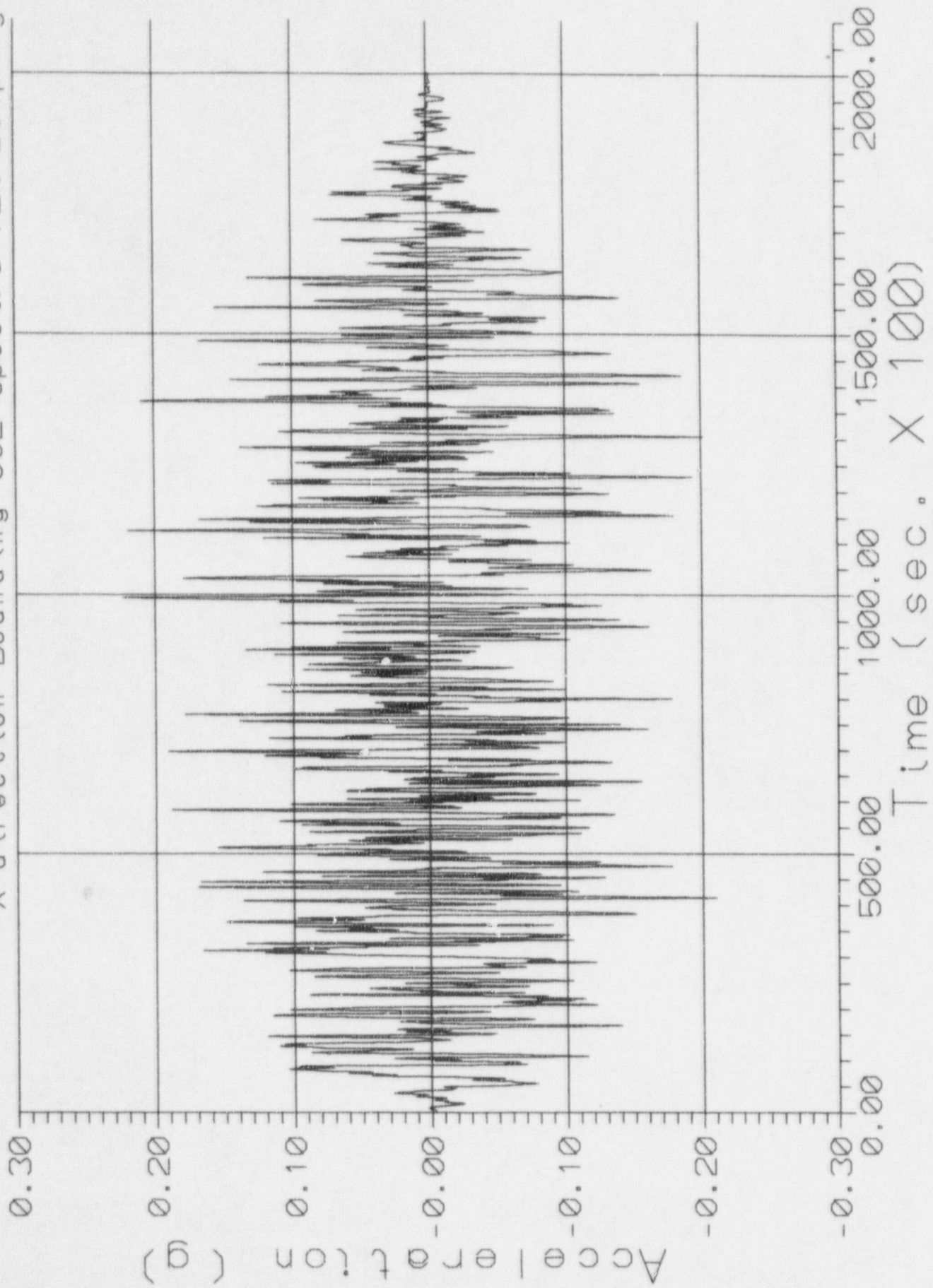


Figure 6.4.2: Davis-Besse SFP and Cask Pit
Time History Accelerogram
Y direction Bounding SSE Spectra (2% Damping)

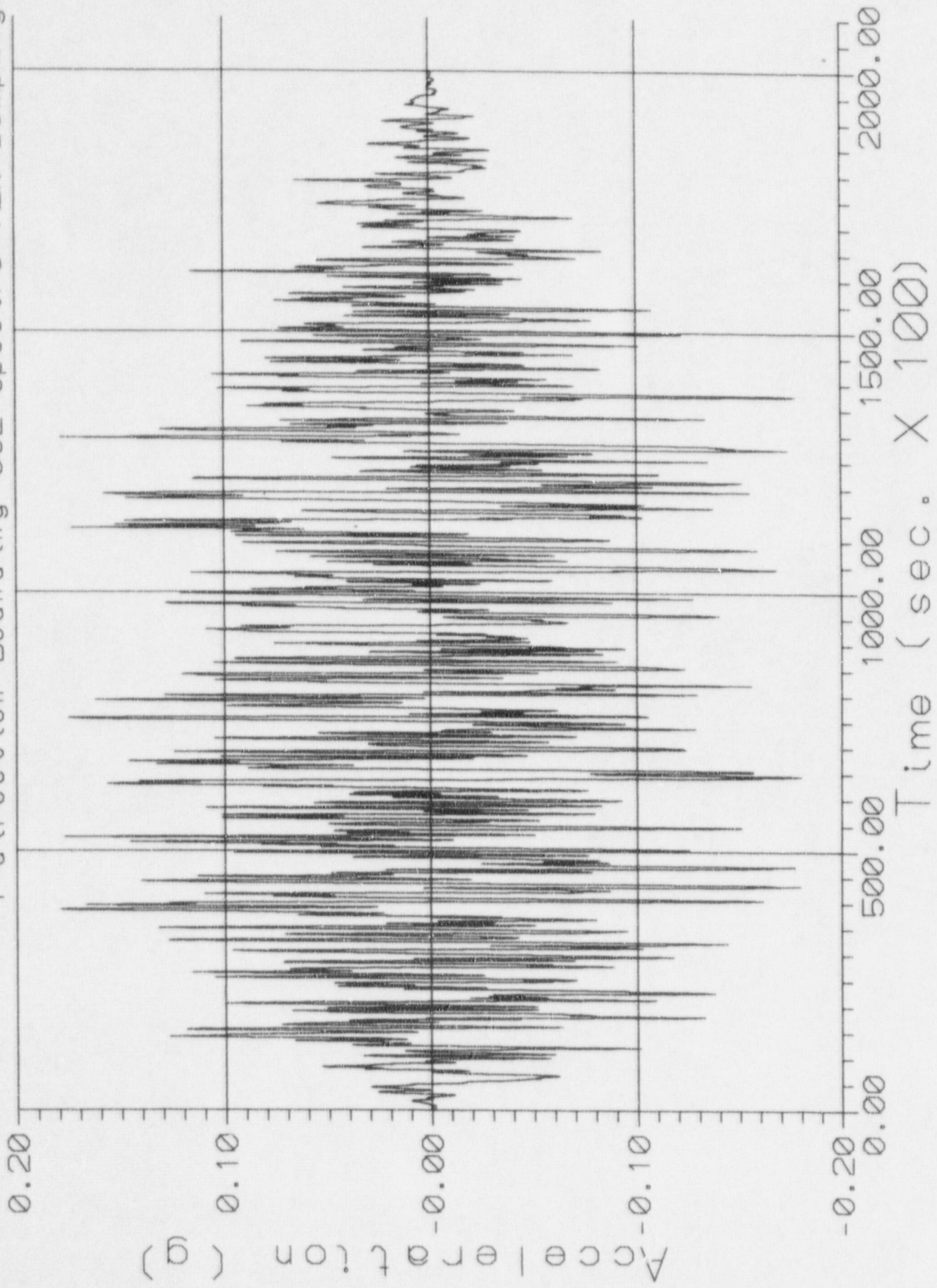
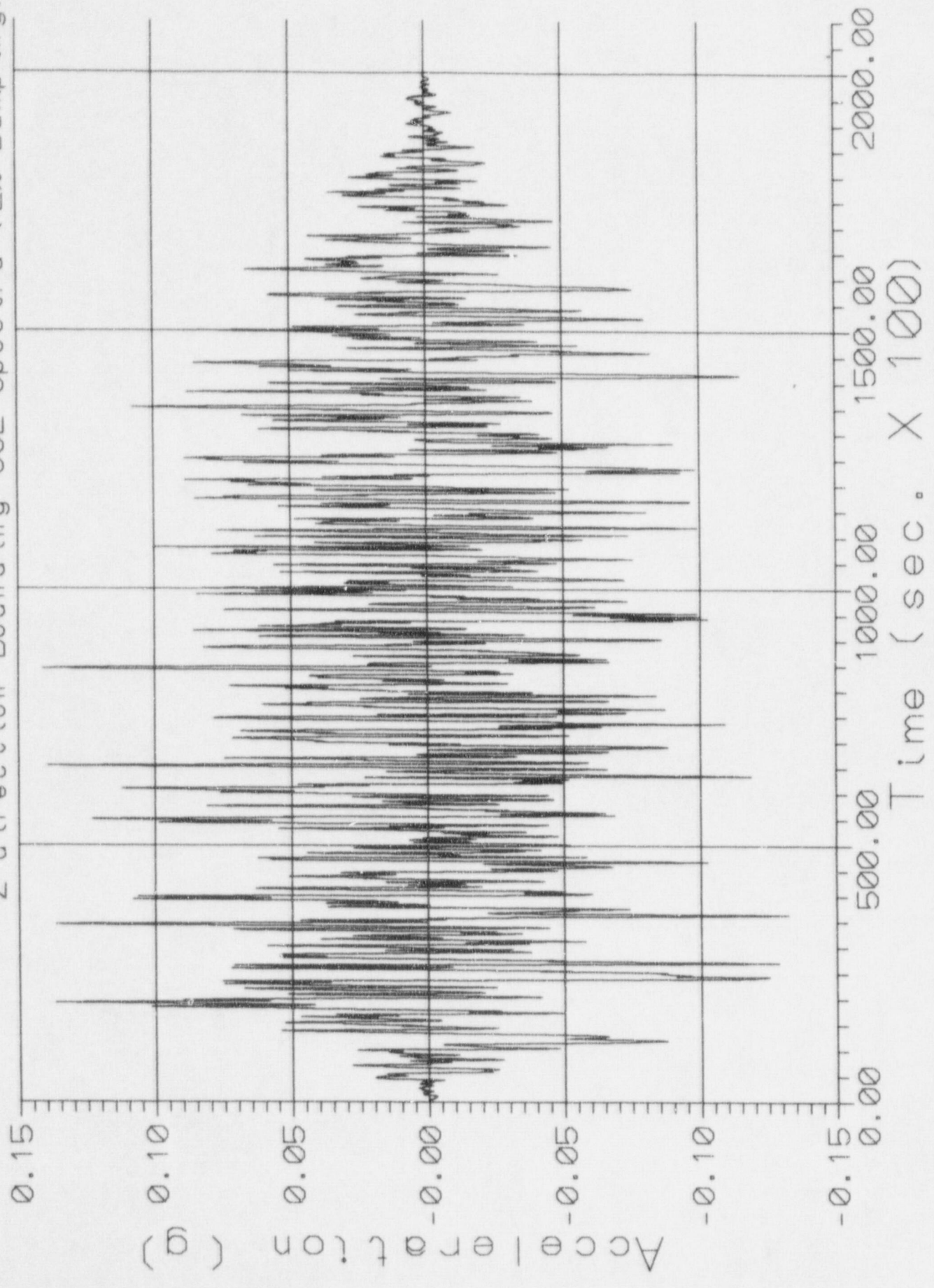


Figure 6.4.3:

Davis-Besse SFP and Cask Pit
Time History Accelerogram
Z direction Bounding SSE Spectra (2% Damping)



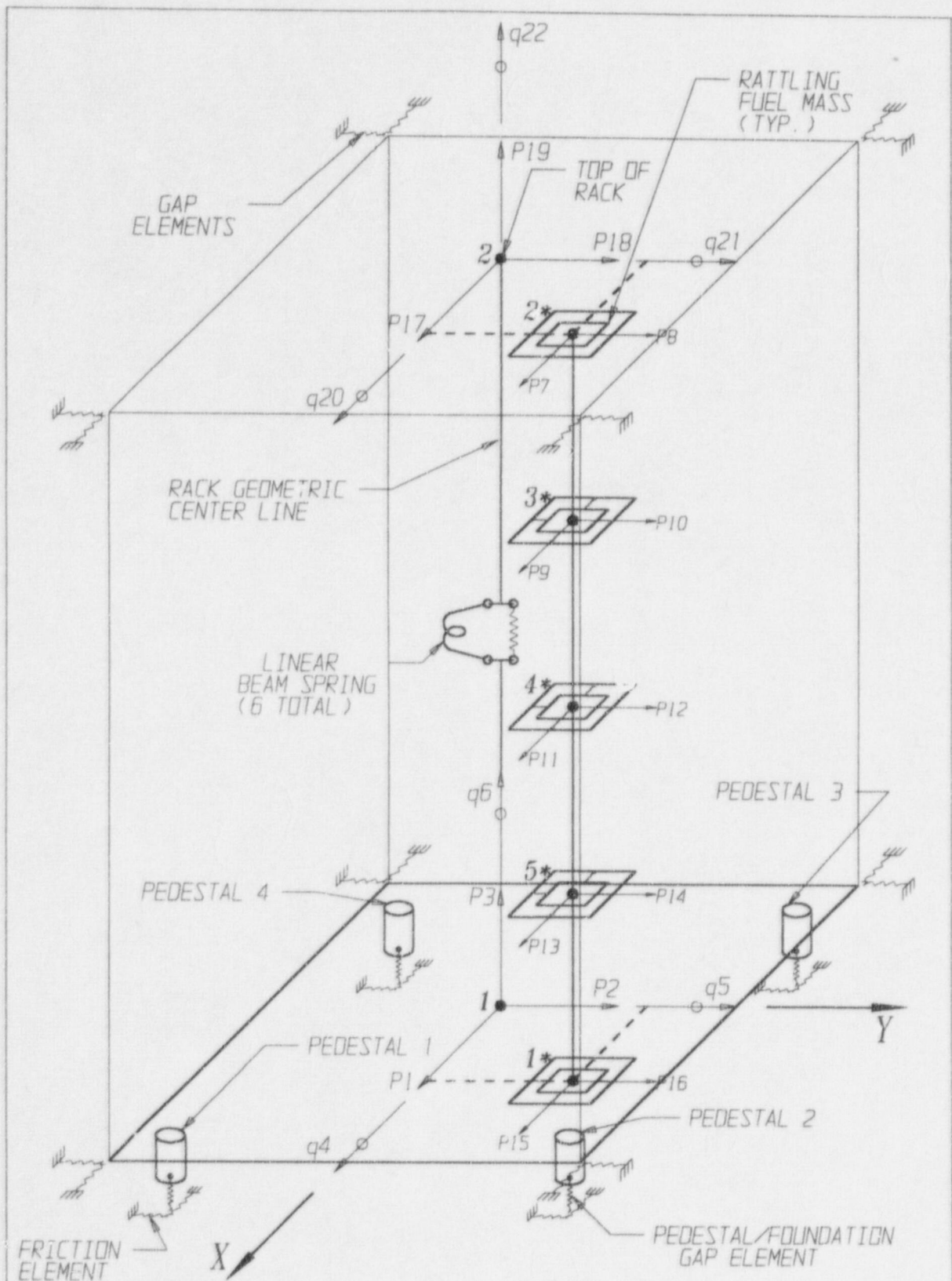


FIGURE 6.5.1; SCHEMATIC OF THE DYNAMIC MODEL OF A SINGLE RACK MODULE USED IN DYNARACK

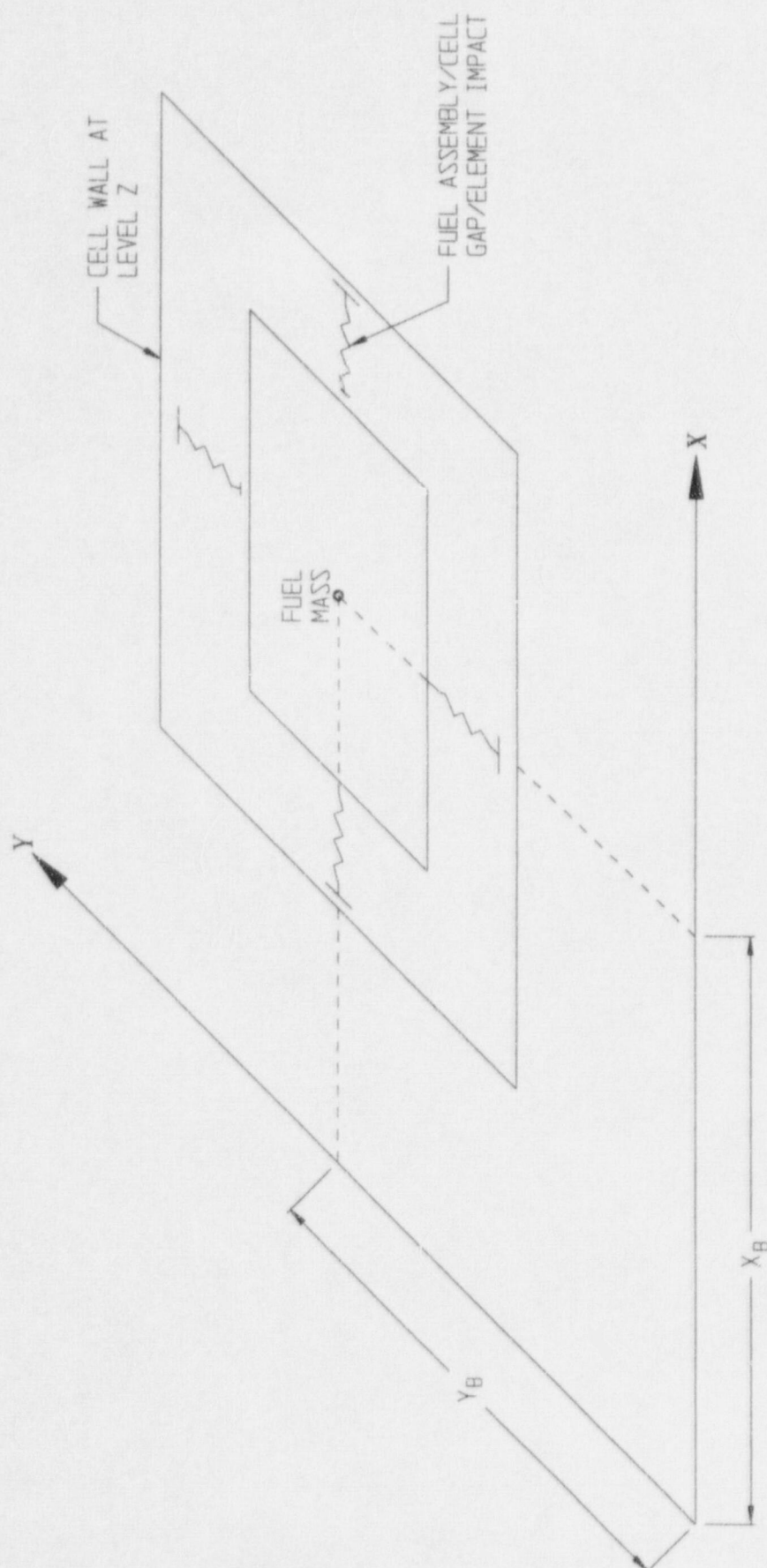
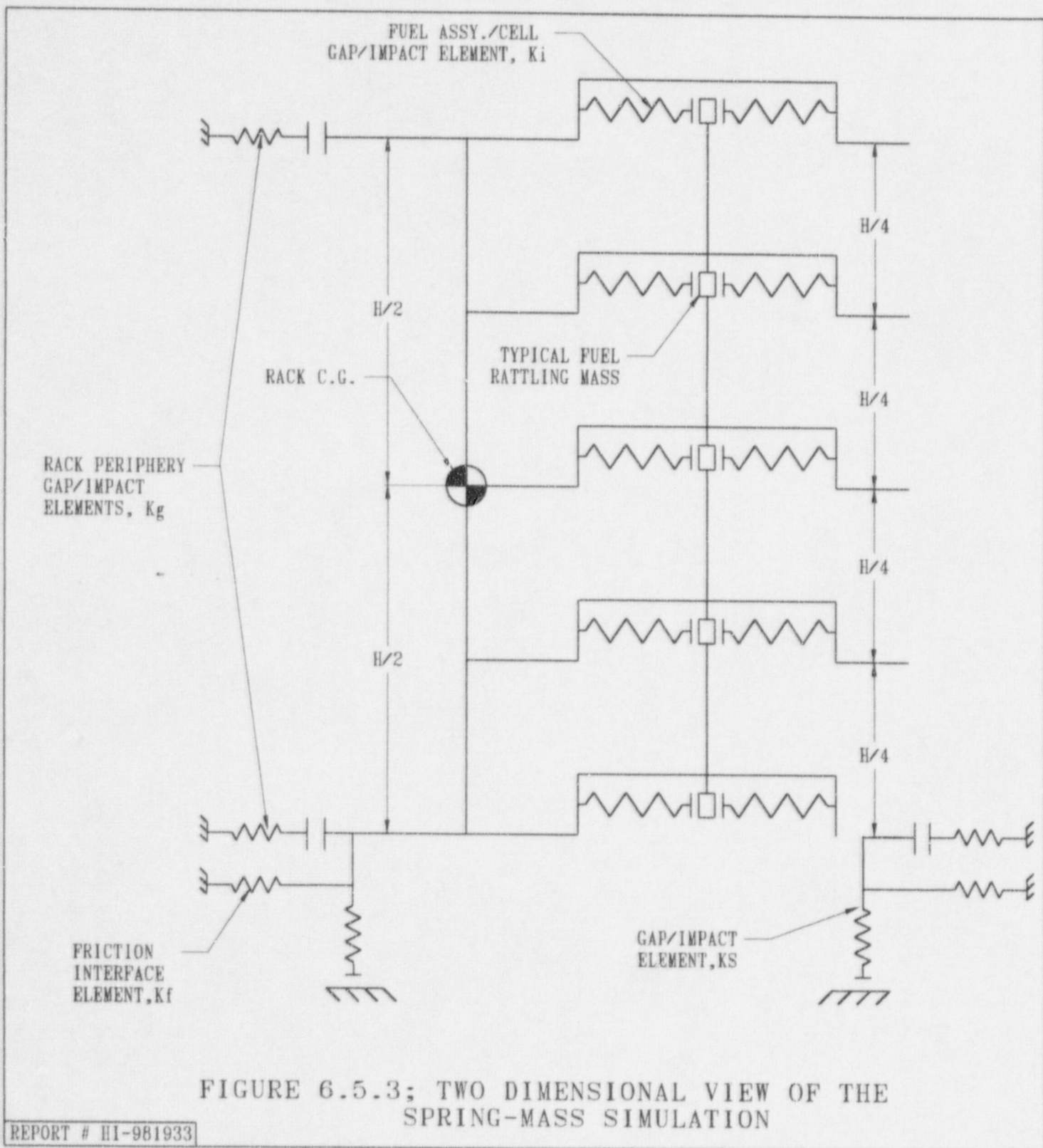
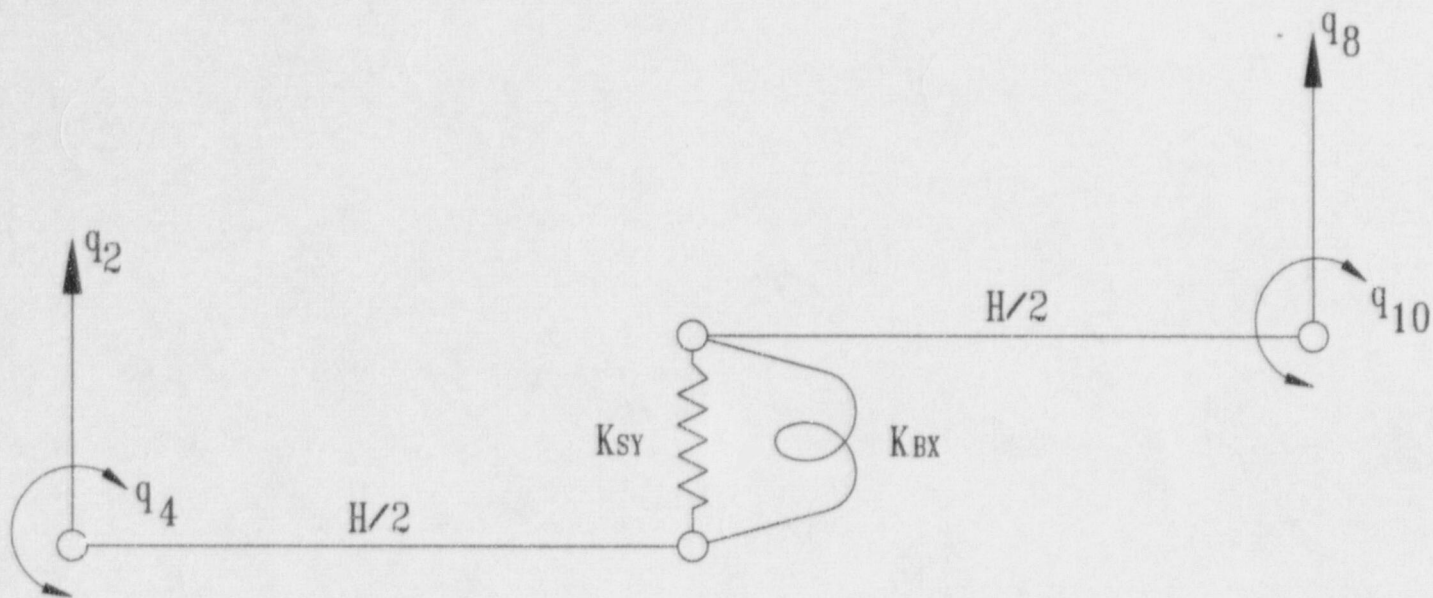
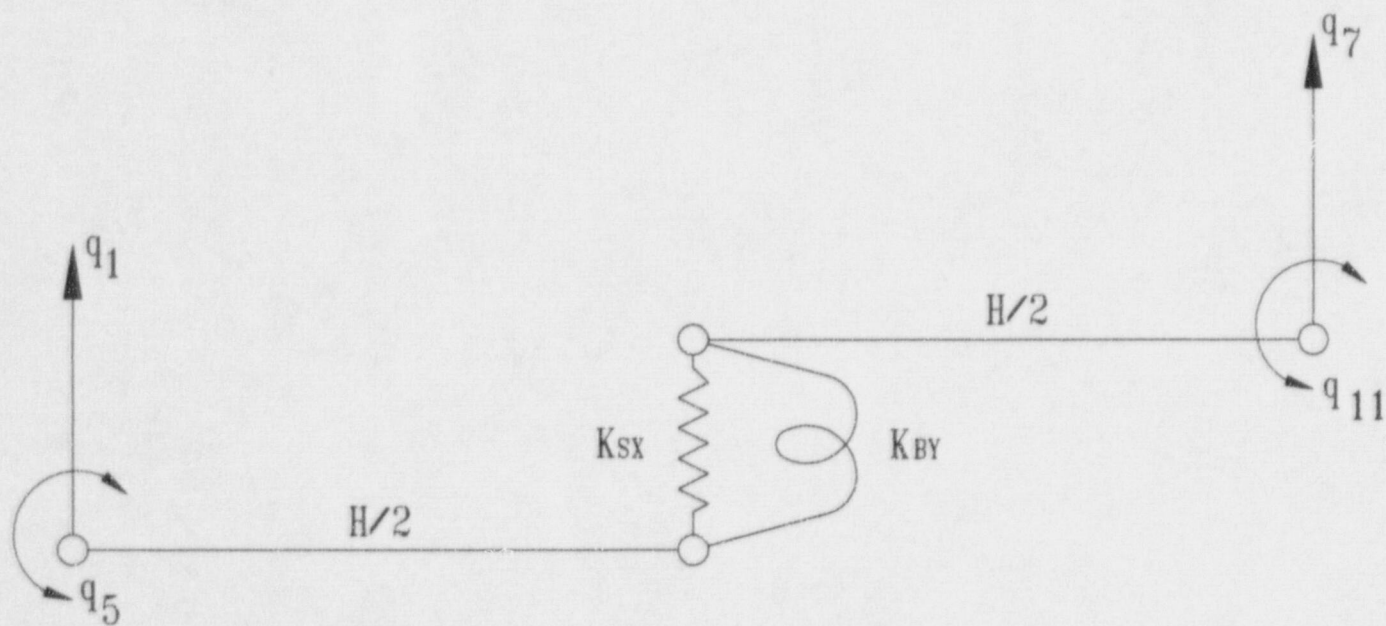


FIGURE 6.5.2 FUEL-TO-RACK GAP/IMPACT ELEMENTS AT LEVEL OF RATTLING MASS





FOR Y-Z PLANE BENDING



FOR X-Z PLANE BENDING

FIGURE 6.5.4; RACK DEGREES-OF-FREEDOM WITH SHEAR AND BENDING SPRINGS

HI-981933

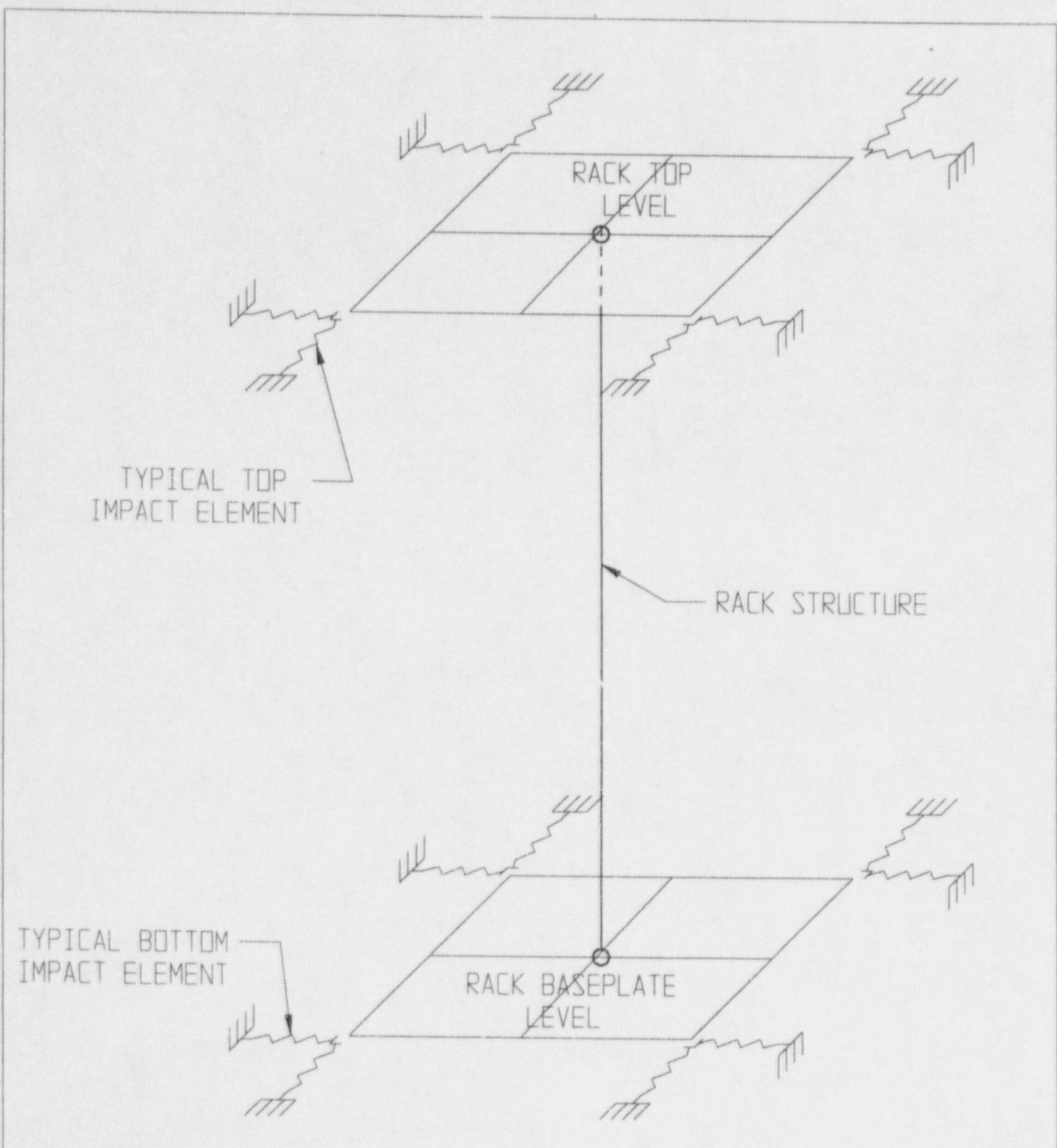


FIGURE 6.5.5; RACK PERIPHERY GAP/IMPACT ELEMENTS

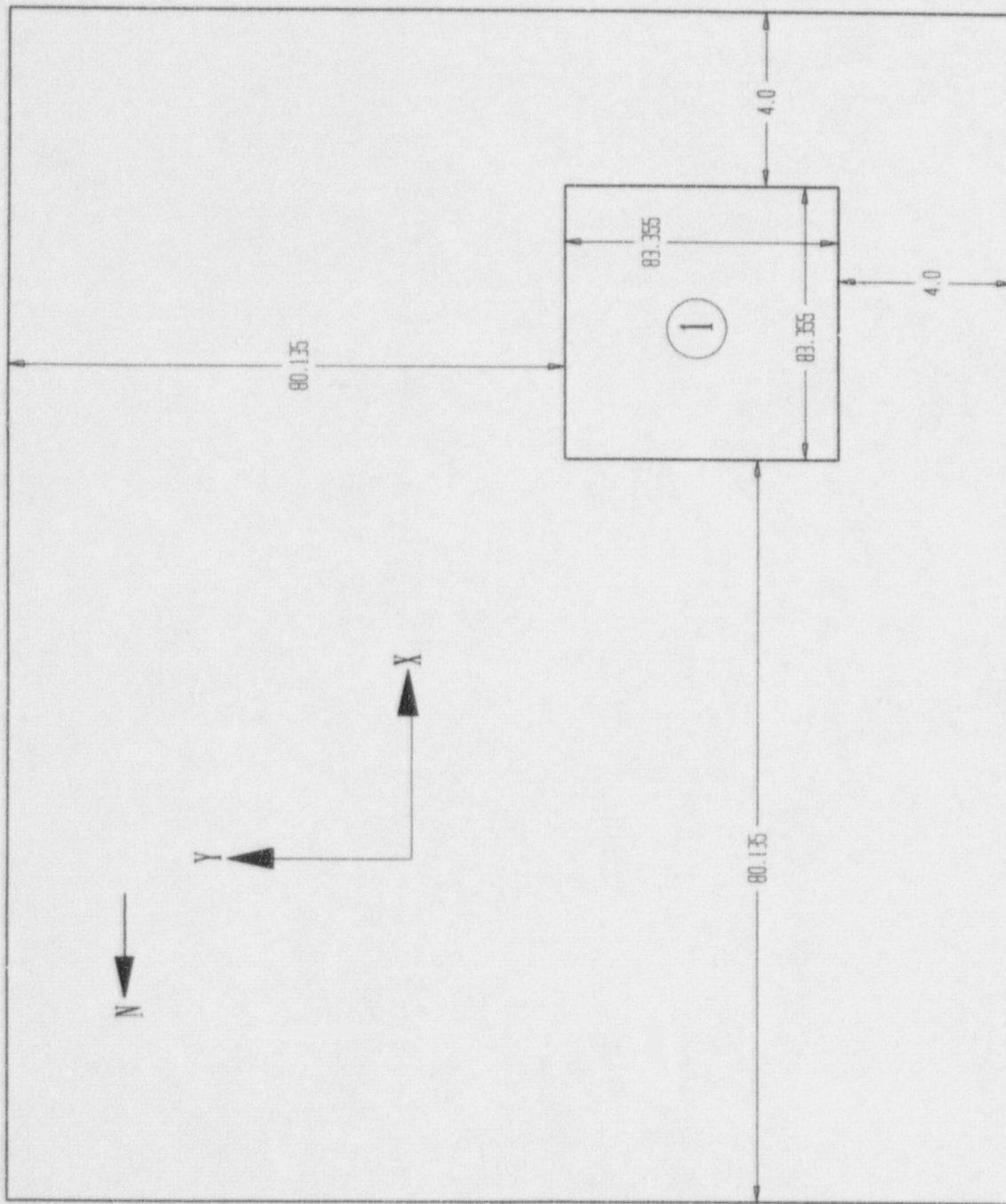


FIGURE 6.5.6; PHASE I RACK LAYOUT

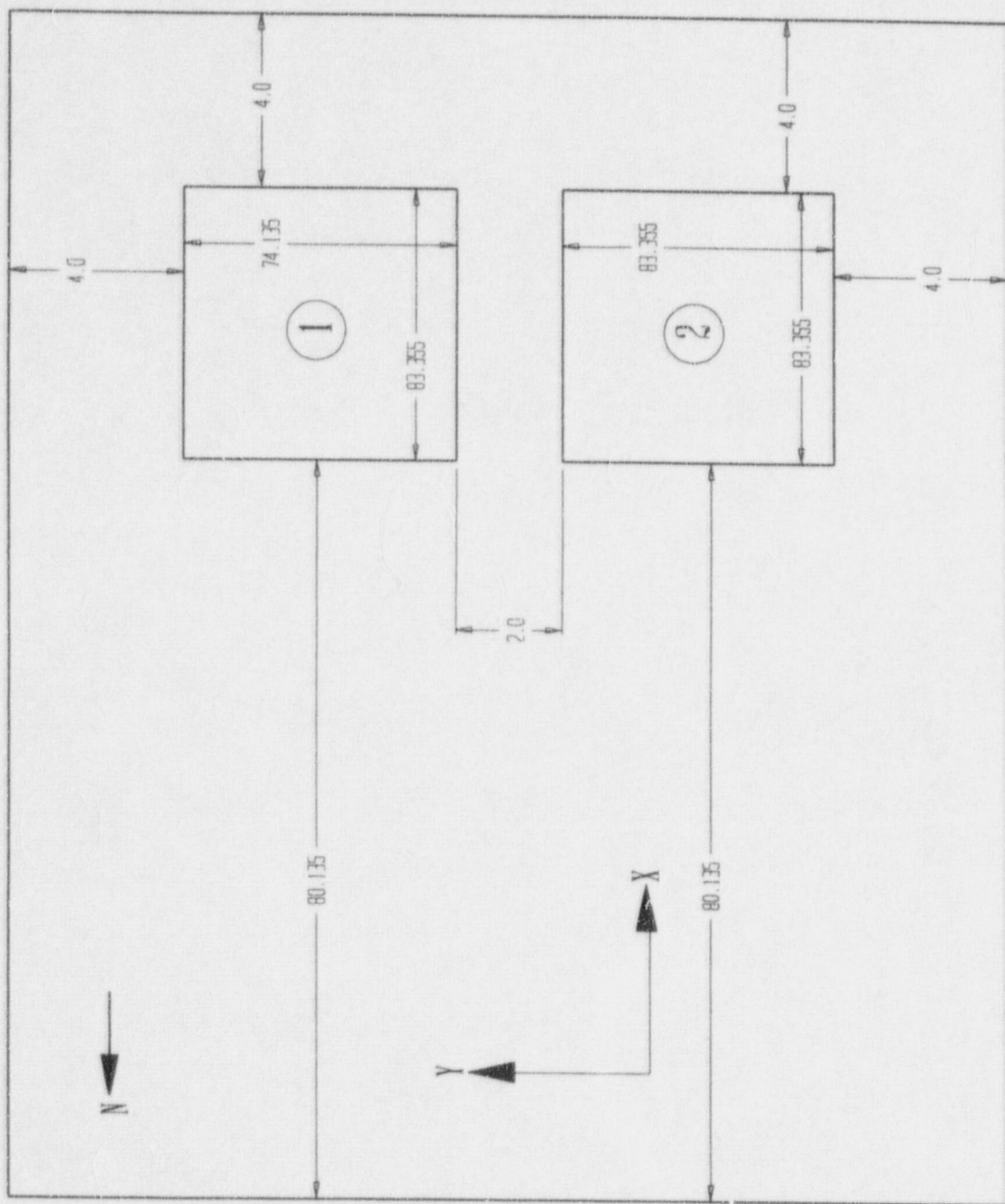


FIGURE 6.5.7; PHASE II RACK LAYOUT

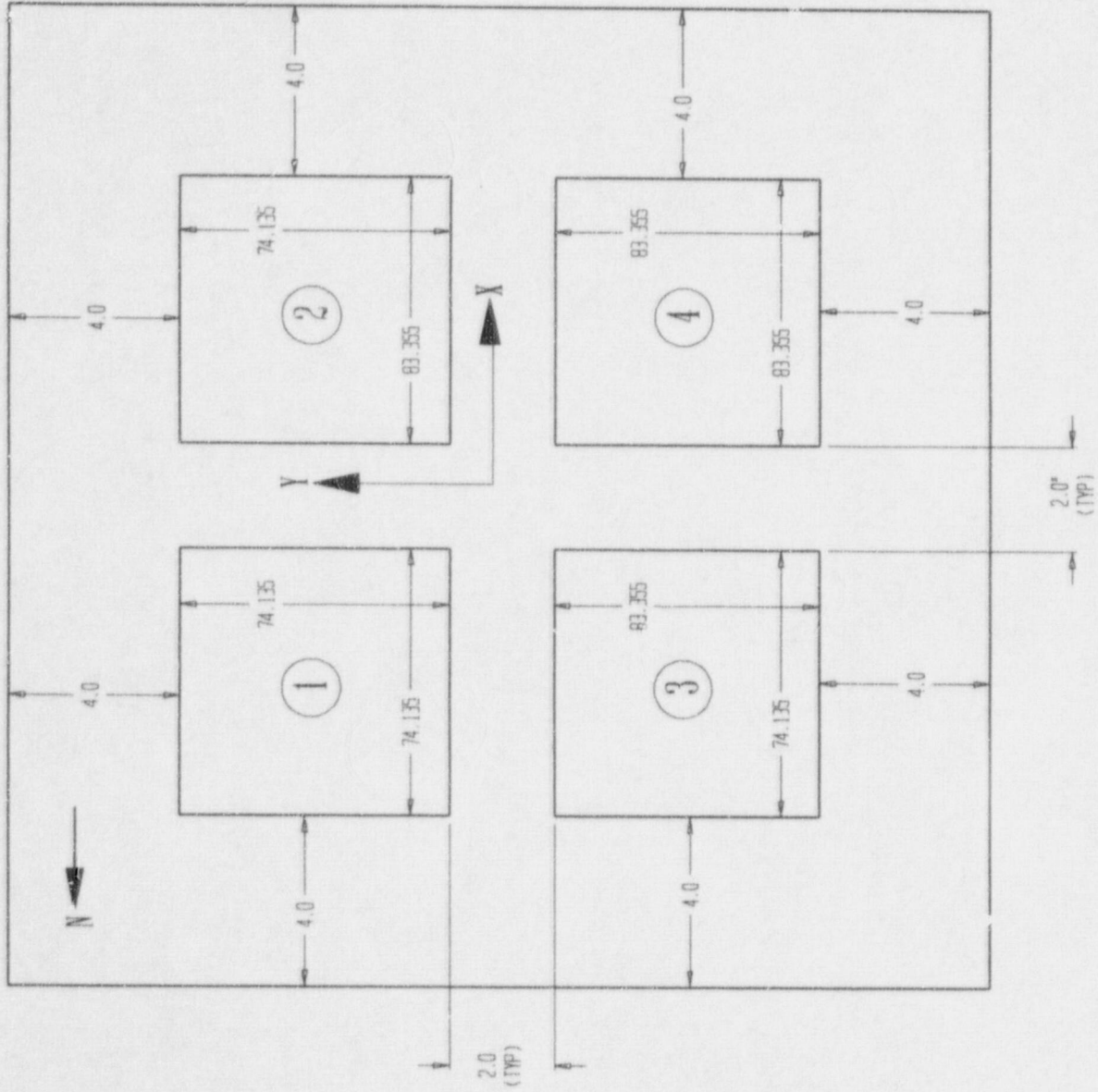
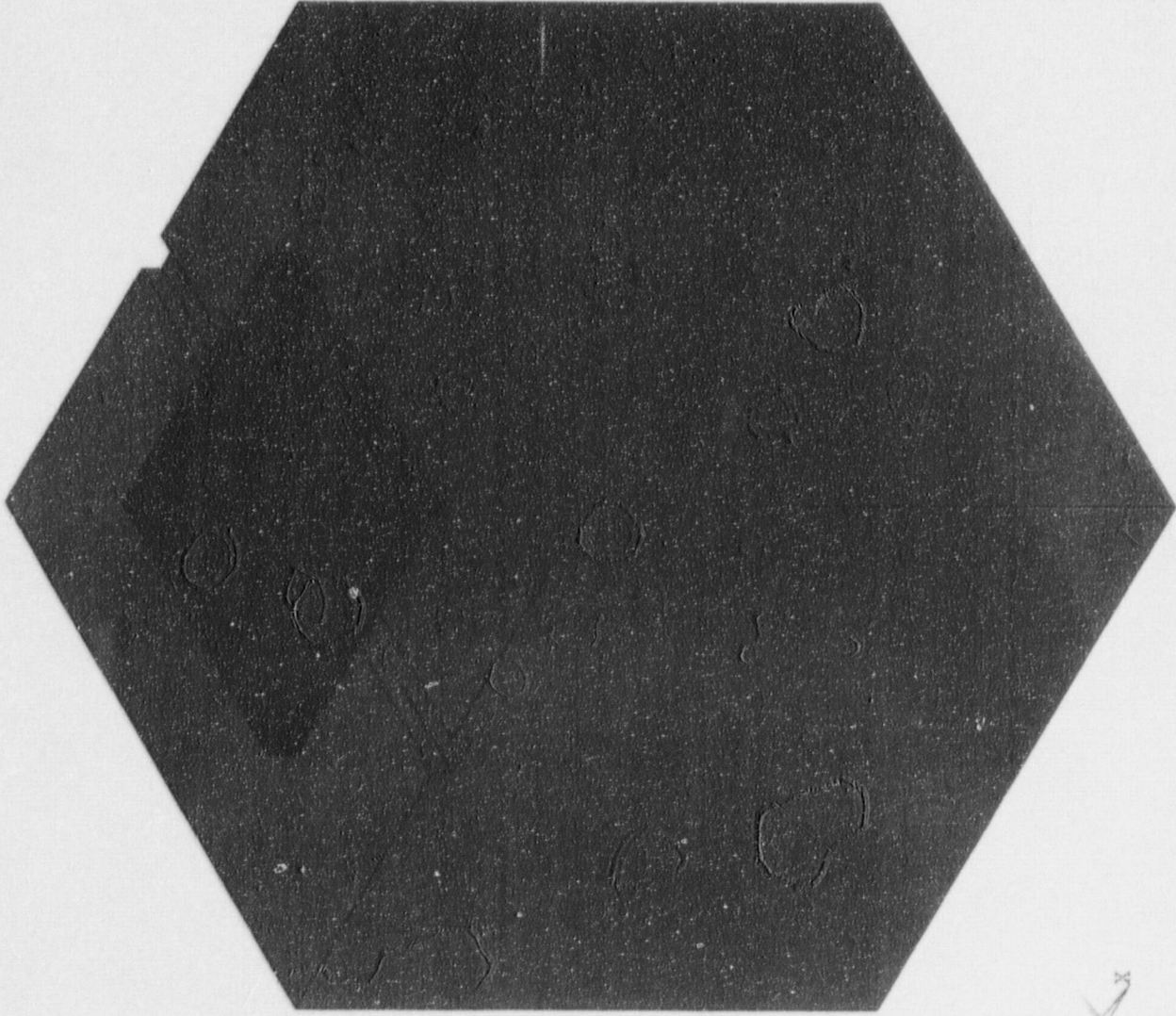


FIGURE 6.5.8; PHASE III RACK LAYOUT

ANSYS 5.3
MAY 22 1998
09:34:01
ELEMENTS
TYPE NUM

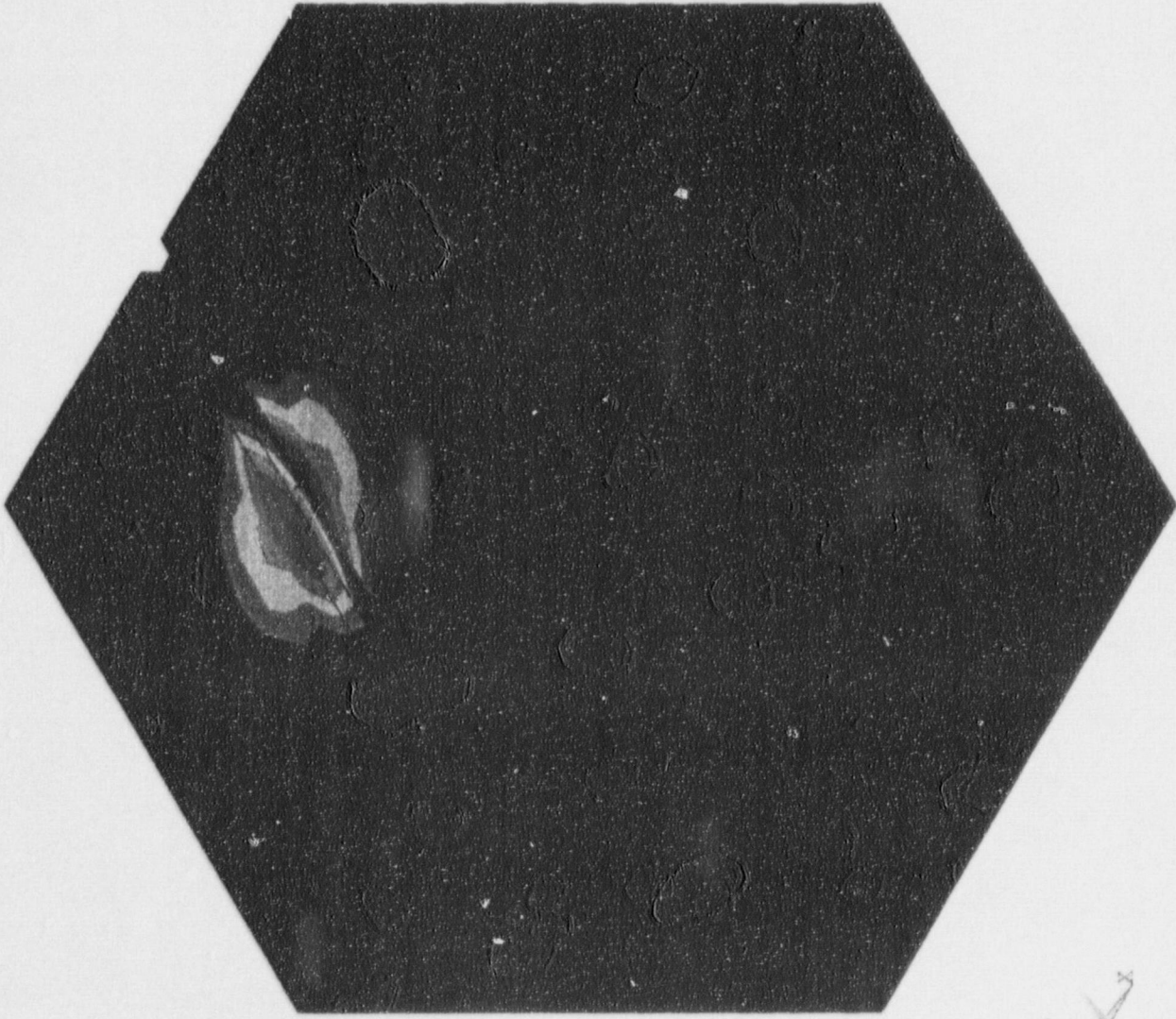
XV =1
YV =-1
ZV =1
DIST=27.618
ZF =-14.25
A-ZS=-60
PRECISE HIDDEN
EDGE



Bearing Pad Analysis

Figure 6.9.1: Bearing Pad Finite Element Model

ANSYS 5.3
 MAY 22 1998
 09:51:02
 NODAL SOLUTION
 STEP=1
 SUB =1
 TIME=1
 SZ (AVG)
 RSYS=0
 DMX =.007096
 SMN =-5354
 SMNB=-7277
 SMX =53.591
 SMXB=784.11
 -5354
 -4753
 -4152
 -3551
 -2951
 -2350
 -1749
 -1148
 -547.236
 53.591



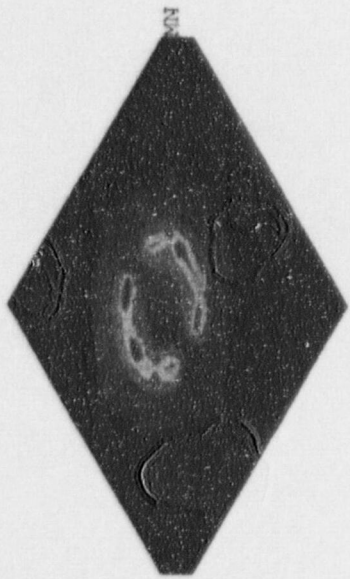
Bearing Pad Analysis

Figure 6.9.2; Bearing Pad Analysis Concrete Compressive Stress

```

ANSYS 5.3
MAY 22 1998
09:51:34
NODAL SOLUTION
STEP=1
SUB =1
TIME=1
SINT (AVG)
DMX =.007096
SMN =52.78
SMX =16345
SMXB=29636
52.78
1863
3673
5484
7294
9104
10915
12725
14535
16345

```



Bearing Pad Analysis

Figure 6.9.3; Bearing Pad Analysis Bearing Pad Stress

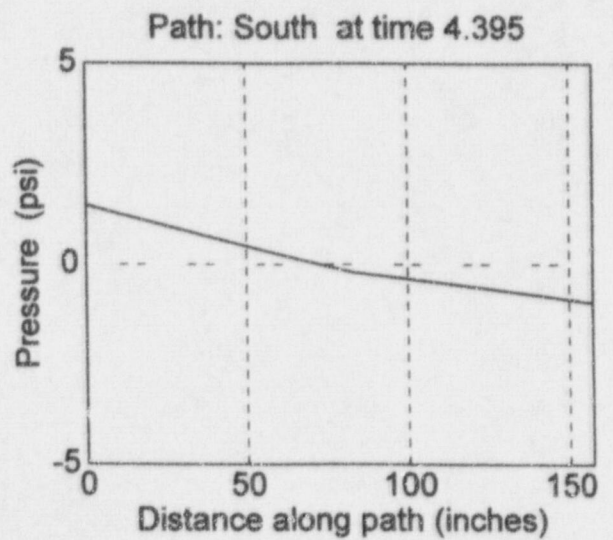
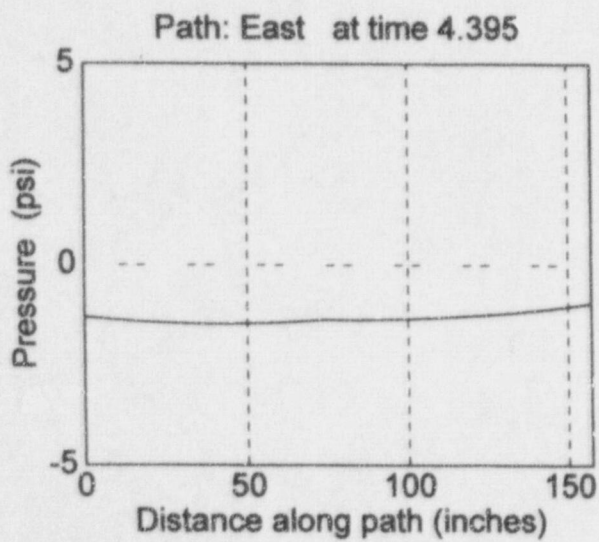
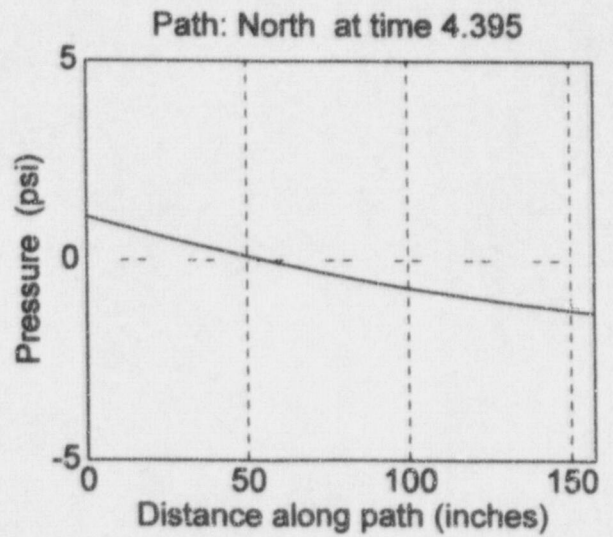
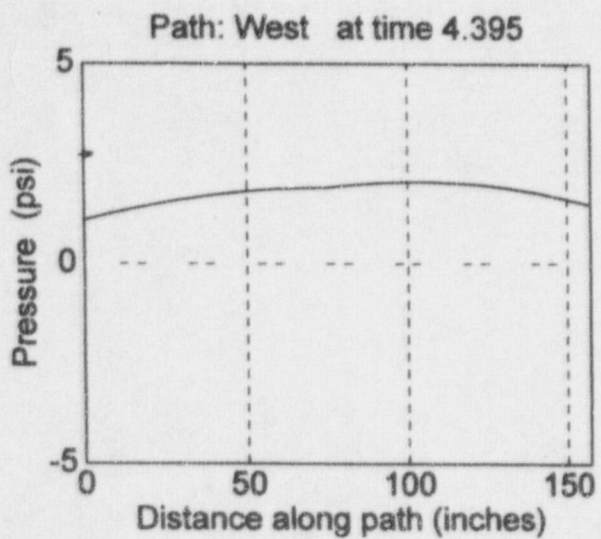


Figure 6.111; Rack Hydrodynamic Pressures

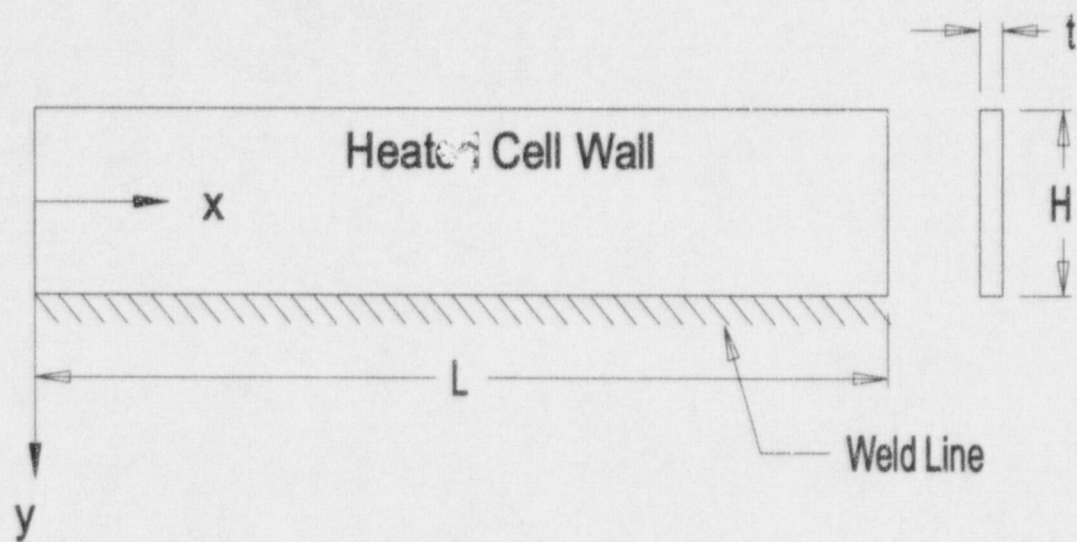


FIGURE 6.12.1; WELDED JOINT IN RACK

7.0 FUEL HANDLING AND MECHANICAL ACCIDENTS

7.1 Introduction

The USNRC OT position paper [7.1] specifies that the design of the rack must ensure the functional integrity of the spent fuel racks under the postulated load drop events in the Cask Pit. This section contains synopses of the analyses carried out to demonstrate the regulatory compliance of the proposed racks under postulated mechanical accidents germane to the DBNPS.

7.2 Description of Accidents

In the evaluation of fuel handling accidents discussed herein, the concern is with the damage to the storage racks, and the Cask Pit structure. The configuration of the rack cell size, spacing, and neutron absorber material must remain consistent with the configurations used in the criticality and thermal-hydraulic evaluations. Maintaining these designed configurations will ensure that the results of the criticality and thermal-hydraulic evaluations remain valid.

Two categories of fuel assembly drop accidents are evaluated: a shallow drop and a deep drop, both of which are discussed in detail below. Each of the fuel handling accidents considers the drop of a fuel assembly, along with the portion of handling tool, which may be severed due to a single element failure. The total dropped weight is 2,482 pounds. The origin of the dropping trajectory is chosen as the highest elevation that the load can be lifted, by the Fuel Storage Handling Bridge, which is 98.13 inches above the upper elevation of the fuel storage rack.

Additional evaluations were also performed to consider the ability of the rack to withstand a 500 pound uplift force and the Cask Pit to withstand a rack drop during installation. Material definitions are provided in Table 7.2.1.

The radiological consequences resulting from fuel damage are not an issue for the proposed changes. The previously evaluated fuel handling design basis accident for the DBNPS continues to bound the radiological consequences of dropping a fuel assembly.

7.2.1 Shallow Drop Events

The first category of fuel handling accidents considers a fuel assembly striking either the top of stored fuel or the top of the storage rack and is referred to herein as a "shallow drop" event. The first shallow drop scenario considers a falling fuel assembly travelling vertically through the stratum of water before striking the top of a stored fuel assembly and subsequently impacting the top of the weakest module, which was determined to be an 8x8 cell rack. A portion of the kinetic energy of the falling assembly is absorbed by damage to the rack.

This first impact scenario determines the depth and extent of plastic deformation of the 0.075 inch thick cell wall. Since the new racks are of honeycomb construction, the deformation produced by the impact will be confined to the region of collision. However, the depth of gross deformation to the cell walls must be demonstrated to remain limited to the portion of the cell above the top of the active fuel region, which is essentially the elevation of the top of the Boral neutron absorber. To meet this criterion, the plastic deformation of the rack cell wall is conservatively specified to not extend more than 4.75 inches downward from the top of the rack. This is the minimum distance down to the top of the Boral, including tolerances. The active fuel area begins at approximately 5.25 inches below the top of the rack cell. Maintaining the Boral and surrounding storage cell will ensure that the configurations considered in the criticality evaluations are not compromised.

The impact zone is chosen to maximize penetration of the falling assembly. From the description of the rack modules in Section 3, the impact resistance of a single vertical cell wall at the rack corner is less than any other potential impact zone represented by multiple cell walls or interior walls. Accordingly, the potential shallow drop scenario is postulated to occur at a rack corner cell in the manner shown in Figure 7.2.1. This impact zone is chosen to minimize the cross

sectional area. In order to maximize the penetration into the top of the rack by the falling assembly, the rack is considered empty, with the exception of the impacted corner cell, where an irradiated fuel assembly is stored.

The second shallow drop accident scenario considers a fuel assembly striking the top of an empty rack cell to maximize cell wall deformation. This drop scenario is performed to maximize cell blockage. As discussed in Section 5.6, the thermal hydraulic evaluations, performed to support the additional Cask Pit storage racks, considered 50 percent cell blockage. Therefore, the rack will be considered acceptable under this drop scenario if 50 percent or more storage cell area remains open for cooling flow subsequent to the event. In this scenario, all other elements of the impacting fuel assembly and the impacted rack assembly are identical to those used in the first shallow drop scenario. Since the rack is considered empty in this scenario, criticality consequences need not be considered.

7.2.2 Deep Drop Events

The second category of fuel assembly drop events postulate that the 2482 lb. impactor falls through an empty storage cell and impacts the rack base-plate. The origin of the dropping trajectory is again chosen as the highest elevation that the load can be lifted by the Fuel Storage Handling Bridge, which is 98.13 inches above the upper elevation of the fuel storage rack. This so-called deep drop scenario evaluates the structural integrity of the rack baseplate. If the baseplate is pierced or deforms sufficiently, then the fuel assembly or base-plate might damage the pool liner and/or create an abnormal condition of the enriched zone of fuel assembly outside the poisoned space of the fuel rack. To preclude damage to the pool liner, and to avoid the potential of an abnormal fuel storage configuration in the aftermath of a deep drop event, it is required that the base-plate remain unpierced. It is also required that the maximum lowering of the fuel assembly support surface is less than the distance from the bottom of the rack base-plate to the liner.

The deep drop event is classified into two scenarios. The first scenario considers dropping an assembly through a cell located above a support pedestal, which is located directly above a leak chase, as shown in Figure 7.2.2. The relative location of the pedestal and leak chase are chosen to account for all possible occurrences of leak chases located beneath pedestals. The second scenario considers dropping the impactor at an interior cell near the center of the rack as shown in Figure 7.2.3.

In the first scenario, the base-plate is buttressed by the support pedestal and presents a hardened impact surface, resulting in a high impact load. The principal design objective is to ensure that the support pedestal does not cause catastrophic damage to the liner and underlying reinforced concrete pool slab such that rapid loss of pool water occurs.

For the second deep drop scenario, the base-plate is not as stiff at cell locations away from the support pedestal. This scenario is evaluated to determine the damage and deformation to the rack baseplate. Baseplate severing or large deflection of the base-plate, such that the liner would be impacted, would constitute an unacceptable result. The deformation must be shown to be less than the distance from the bottom of the baseplate to the pool floor liner, which is 6 inches, including tolerances.

7.2.3 Rack Drop Event

The rack drop event is analyzed to show that dropping a rack into the Cask Pit during installation will not result in catastrophic leakage of the Cask Pit. Damage must not lead to development of cracks through the entire Cask Pit floor section. Although this scenario is evaluated, implementation of the control of heavy loads will preclude its consequences.

7.2.4 Uplift Force Evaluation

The 500 pound uplift force is evaluated to ensure the rack cell wall is able to withstand this load without deforming the rack cell such that it no longer satisfies dimensional requirements. The acceptance criterion for this evaluation is that local cell wall stress shall remain below the yield point.

7.3 Mathematical Model

In the first step of the solution process, the velocity of the dropped object (impactor) is computed for the condition of underwater free fall. Table 7.3.1 summarizes the results for the fuel assembly drop events. In the second step of the solution, an elasto-plastic finite element model of the impacted region on Holtec's computer Code PLASTIPACT (Lawrence Livermore National Laboratory's DYNA3D implemented on Holtec's QA system) is prepared. PLASTIPACT simulates the transient collision event with full consideration of plastic, large deformation, wave propagation, and elastic/plastic buckling modes. The physical properties of material types undergoing deformation in the postulated impact events are summarized in Table 7.3.2.

7.4 Results

7.4.1 Shallow Drop Event Results

Figure 7.4.1 provides an isometric view of the finite element model utilized in the shallow drop impact analysis.

The first shallow drop scenario dynamic analysis shows that the top of the impacted region undergoes localized deformation. The impacting fuel assembly has an initial velocity of 250 in./sec. Figure 7.4.2 shows an isometric view of the post-impact geometry of the rack for this shallow drop scenario, as well as a plot of the Von-Mises stresses. The maximum Von Mises

stress in the cell wall, recorded at maximum displacement time, is 38.39 ksi and the maximum plastic strain is 0.106. Approximately 10% of the cell opening in the impacted cell is blocked. The maximum gross deformation is limited to 3 inches, which is below the acceptance criteria of 4.75 inches. Therefore, the penetration is determined to be acceptable from a criticality perspective and the racks will remain subcritical.

The study of residual plastic strain for the second shallow drop analysis shows that damage remains local to the impacted cell, but is significantly more extensive than the first scenario. Figure 7.4.3 shows an isometric view of the post-impact geometry of the rack for this scenario as well as a plot of the Von-Mises stresses. Deformation of the impacted cell extends 18 inches downward from the top of the undeformed cells. The maximum Von-Mises stress in the cell wall is 40.96 ksi and the maximum plastic strain is 0.264. The effective damaged area measures 12 inches and can obstruct approximately 50 percent of the cross section of the cell. Thus, the acceptance criterion for blockage is met. Since the percentage of obstruction recorded is for an empty cell, it is concluded that this analysis would bound the damage sustained by a loaded cell. Therefore, the partial blockage assumption of 50 percent is shown to be acceptable.

7.4.2 Deep Drop Event Results

The first deep drop scenario considers the impacted area to be over a pedestal that is resting on the ¼ inch thick liner and located near the convergence of two leak chases. Figure 7.4.4 shows an isometric view of the finite element model for the impactor, pedestal, bearing pad, liner and underlying concrete. As shown in Figure 7.4.5, a Von-Mises stress of 106 ksi is observed in the pedestal cylinder at the contact surface with the bearing pad, which is below the failure stress of 140 ksi for the pedestal material. The bearing pad registers a Von-Mises stress of approximately 30 ksi, as shown in Figure 7.4.6.

The numerical analysis of this event shows that the liner is not pierced during the collision, since the maximum Von-Mises liner stress, as shown in Figure 7.4.7, is 27 ksi, which is less than the failure stress of 71 ksi. Therefore, the acceptance criteria is satisfied. The concrete stratum

directly below the pedestal sustains a very localized compressive stress of 21 ksi, as shown in Figure 7.4.8, which results in only localized damage to the concrete.

A plan view of the finite element model for the second deep drop scenario is shown in Figure 7.4.9. This scenario considers the dropped assembly to fall through an interior cell striking the base-plate at a point near the middle of the rack. This drop scenario produces some deformation of the base-plate and localized severing of the base-plate to cell wall welds. The collision between the 2482 lb. impactor and the 0.75 inch thick rack base-plate occurs at 406 in/sec initial velocity and results in an accentuated local deformation of the base-plate extending over a 18 square inch area around the impact zone. Due to the proximity of the fuel assembly lower end fitting, the shock of the initial impact is carried into the walls of the centrally located cell, and fails the connecting welds to the adjoining cells. The base-plate does not break during the impact, but the welds connecting the cells located in the vicinity of the collision area to the plate are severed.

The structural damage resulting from this scenario has no adverse effect on the coolant flow through the storage cells. The maximum calculated Von-Mises stress in the base-plate as shown in Figure 7.4.10 is 46.04 ksi and the maximum calculated plastic strain in the base-plate is 0.109, as shown in Figure 7.4.11. Figure 7.4.12 shows the deformed shape of the base-plate. The maximum displacement of the base-plate is 3.36 inches, which develops 0.0135 seconds after the initial collision. The lower assembly storage position due to the deformed baseplate is shown to be acceptable by the criticality evaluations as discussed in section 4.6.4. This displacement does not result in the baseplate striking the liner. Therefore, the structural consequences are also acceptable.

7.4.3 Rack Drop Event Results

Numerical analysis of the drop of a 12,150 pound rack into the Cask Pit shows that the rack does not pierce the ¼ inch liner. The maximum calculated Von-Mises stress for the liner of about 45 ksi, as shown in Figure 7.4.13, is less than the failure stress of 71 ksi for the liner material. The

concrete stratum directly beneath the pedestal sustains a very localized compressive stress, as shown in Figure 7.4.14, with a maximum value of 23 ksi. This results in only localized damage to the concrete below the liner.

7.4.4 Uplift Force Evaluation Results

This evaluation shows that the rack is able to withstand the uplift force of 500 pounds. For this scenario, the critical location for the load to be applied is at the top of a cell. For a load applied vertically anywhere along a cell wall, the resultant stress is only 1,100 psi, which is well below the yield stress of the material. For a load applied at a 45 degree angle to the top of a cell wall, tear out of the cell wall is evaluated. The damaged region extends no greater than 0.24 inches down the cell wall, which is well above the top edge of the neutron absorber material.

7.5 Closure

The fuel assembly drop accident events postulated for the pools were analyzed and found to produce localized damage well within the design limits for the racks. The configuration of the fuel and poison (Boral) is not compromised from the configurations analyzed in the criticality evaluations discussed in Section 4.0. The base-plate deformation and corresponding fuel displacement is considered in the criticality evaluations. These evaluations concluded there are no criticality concerns for these accidents. The damage to the top of the racks reduces the cross sectional area available for coolant flow. However, the reduction of area is less than that considered in the thermal-hydraulic evaluations. Therefore, the accidents do not represent any thermal-hydraulic concerns. Analyses show that the pool liner will not be pierced by the pedestals, but the underlying concrete will experience local crushing. However, the pool structure will not suffer catastrophic damage. Therefore, there are no significant structural consequences.

7.6 References

[7.1] "OT Position for Review and Acceptance of Spent Fuel Storage and Handling Applications," dated April 14, 1978.

Table 7.2.1

Material Definition

Material Name	Type	Density (pcf)	Elastic Modulus (psi)	Stress		Strain	
				First Yield (psi)	Failure (psi)	Elastic	Failure
Stainless Steel	ASME SA- 240-304	490	2.760e+07	2.500e+04	7.100e+04	7.717e-04	3.800e-01
Stainless Steel	ASME SA- 564-630	490	2.760e+07	1.063e+05	1.400E+05	3.851e-02	3.800e-01
Zircaloy	Irradiated	490	5.649e+06	5.649e+04	5.650e+04	1.000e-02	1.020e-02
Concrete	4000	150	3.605e+06	-	-	-	-

Table No. 7.3.1

Impactor Weight and Impact Velocity Calculations

Drop Event	Impactor: Type	Weight W (lb)	Drop Height H (in)	Drag Surface A _c (in ²)	λ (lb*sec ² /in ²)	K _v (in ² /sec ²)	θ	V _{impact} (in/sec)
"Shallow" Drop	Fuel Assembly	2482	98.13	61.78	0.001443	1.563e+06	4.042e-02	249
"Deep" Drop	Fuel Assembly	2482	264.76	61.78	0.001443	1.563e+06	1.091e-01	403

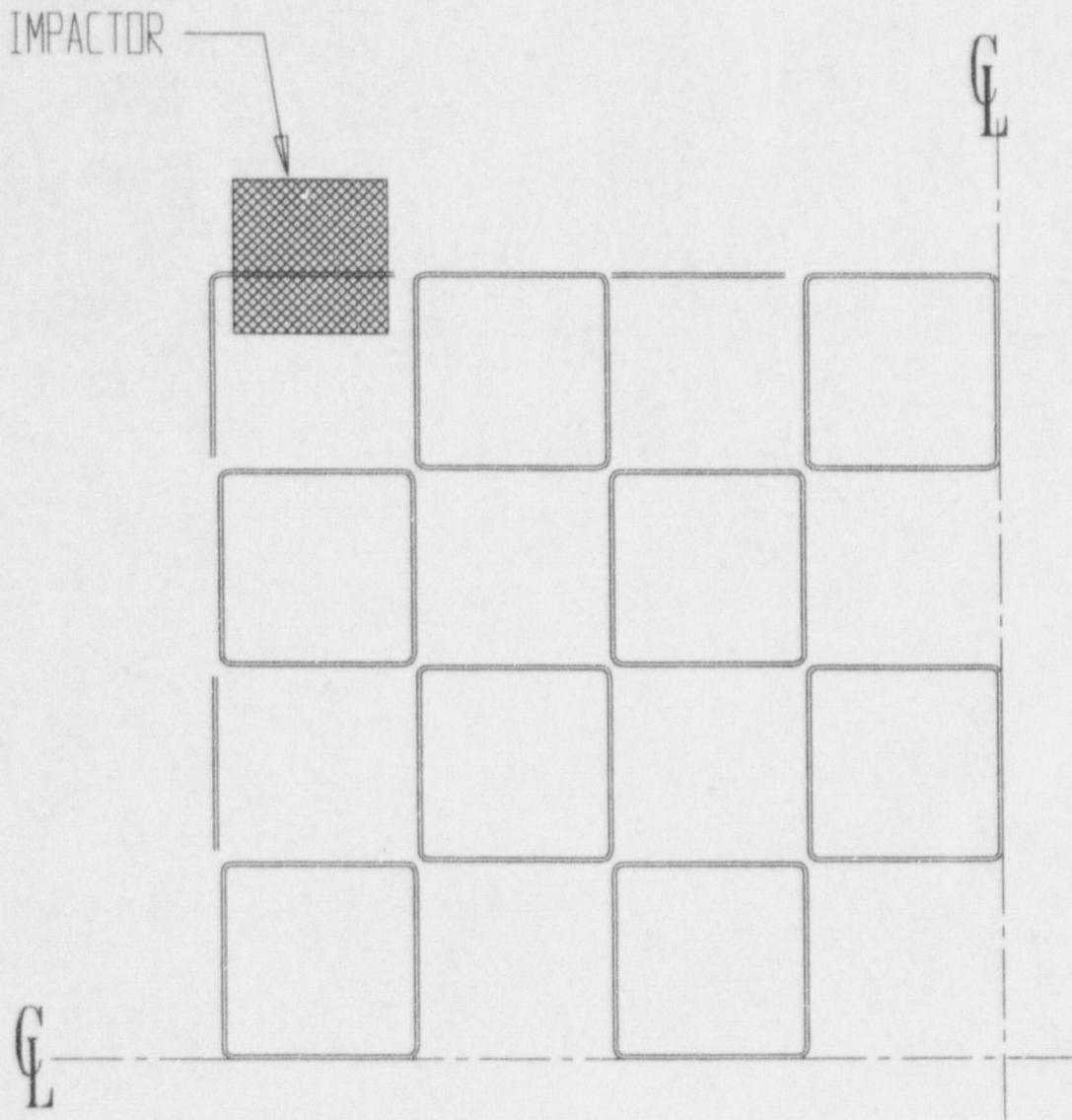
Table No. 7.3.2

Structural and Material Definition of Impactor and Target

Postulated Drop Event	Impactor Description		Target Description			
	Element	Structural Type	Element	Structural Type	Material [†]	
					Behavior	Type
Shallow	Fuel Assembly (2482 lb)	Elasto-Plastic	Corner Cell	Deformable	Elasto-Plastic	ASME SA-240-304
			Adjoining Cells	Deformable	Elasto-Plastic	ASME SA-240-304
Deep drop over rack	Fuel Assembly (2482 lb)	Rigid	Base Plate	Deformable	Elasto-Plastic	ASME SA-240-304
			Adjoining Cells	Deformable	Elasto-Plastic	ASME SA-240-304
Deep drop over rack pedestal	Fuel Assembly (2482 lb)	Rigid	Pedestal Block	Deformable	Elasto-Plastic	ASME SA-240-304
			Pedestal Cylinder	Deformable	Elasto-Plastic	ASME SA-564-630
			Pad	Deformable	Elasto-Plastic	ASME SA-240-304
			Liner	Deformable	Elasto-Plastic	ASME SA-240-304
			Concrete Stratum	Deformable	Elasto-Plastic	$f_c = 4000$

[†] The material properties are shown in Table 7.2.1.

+



+

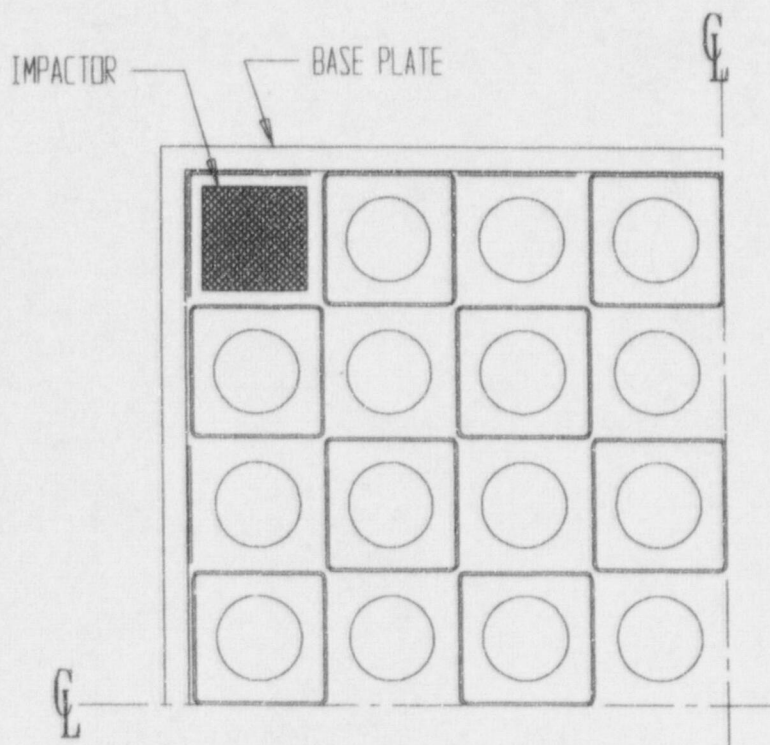


Figure 7.2.2; Plan View of "Deep Drop" Scenario 1

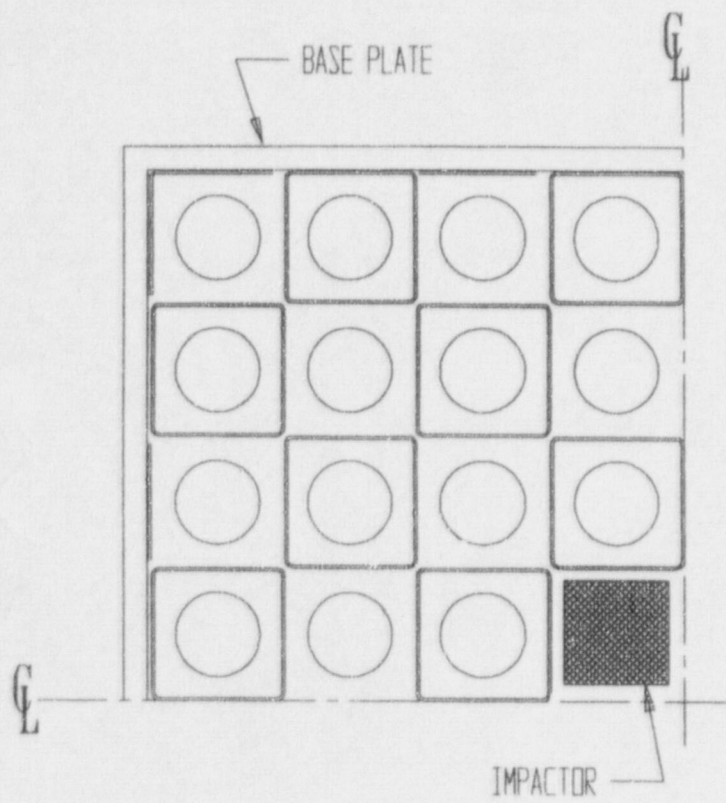
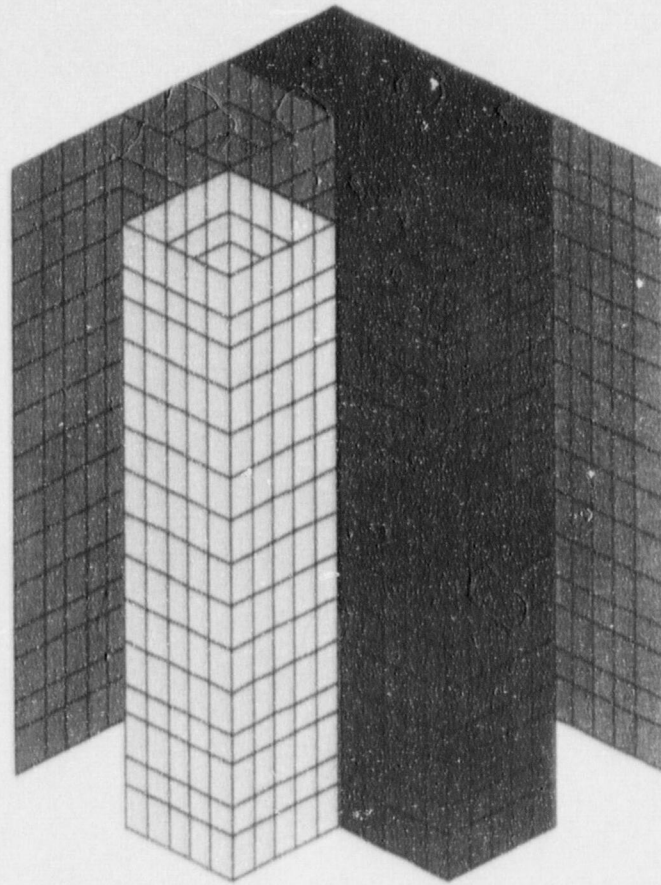
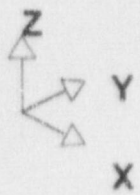
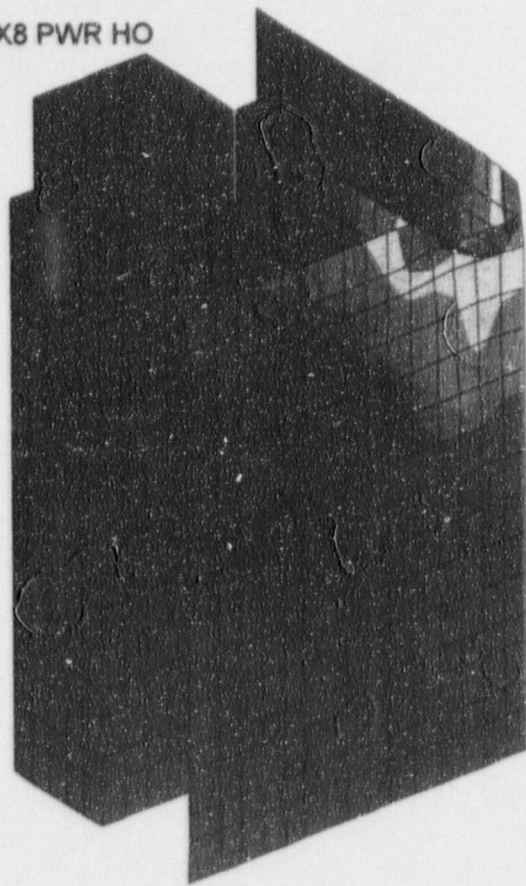


Figure 7.2.3; Plan View of "Deep Drop" Scenario 2



IMPACT ON CELL 8X8 PWR HO
STEP 34 TIME = 8.4998824E-002
MAX_VONMISES



3.8385E+004
3.8385E+004
3.4595E+004
3.0805E+004
2.7016E+004
2.3226E+004
1.9436E+004
1.5647E+004
1.1857E+004
8.0672E+003
4.2775E+003
4.8783E+003
4.8783E+003

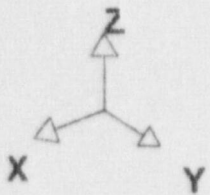
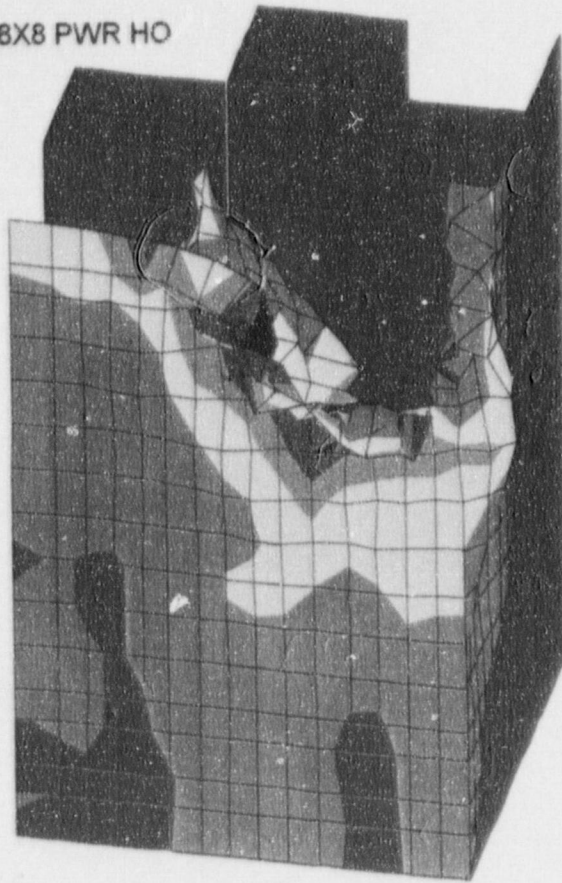
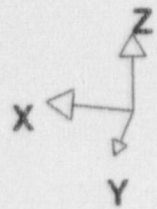


Figure 7.4.2; Isometric of Scenario I

"Shallow Drop" Von Mises Stress

IMPACT ON CELL 8X8 PWR HO
STEP 36 TIME = 8.9999422E-002
MAX_VONMISES



4.0954E+00
4.0954E+00
3.6859E+00
3.2763E+00
2.8668E+00
2.4573E+00
2.0477E+00
1.6382E+00
1.2286E+00
8.1908E+00
4.0954E+00
0.0000E+00
0.0000E+00

Figure 7.4.3; Isometric of Scenario 2

"Shallow Drop" Von Mises Stress

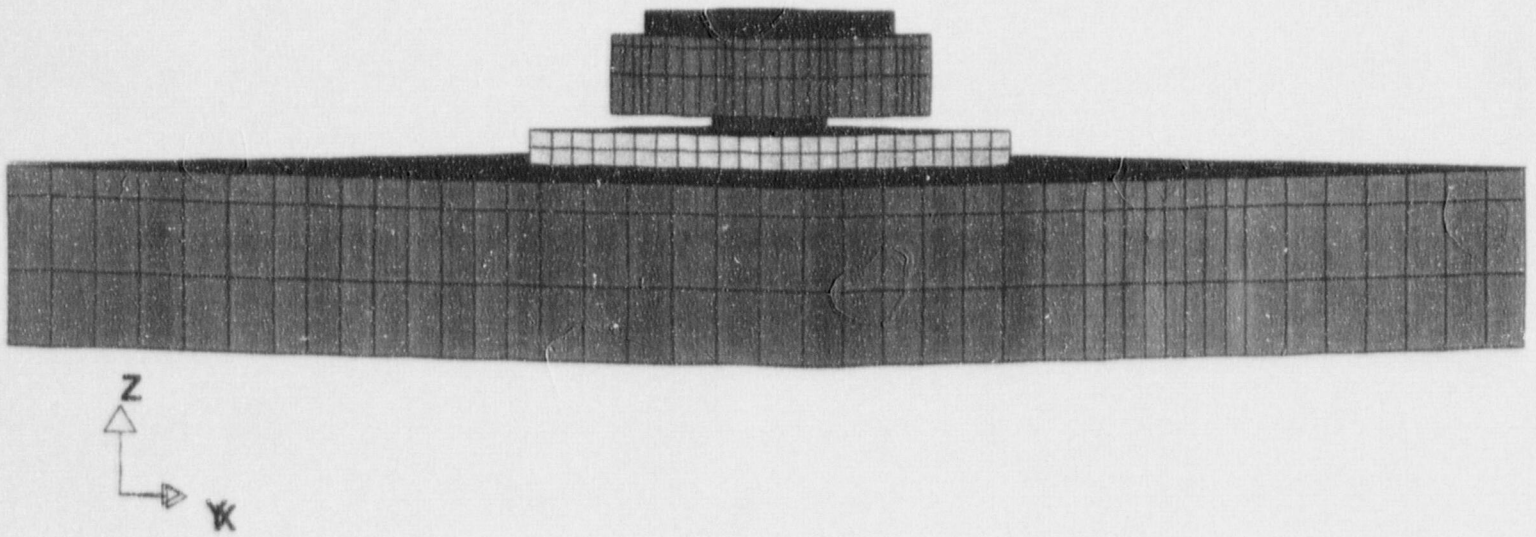


Figure 7.4.4; Isometric of Over-Pedestal "Deep Drop"

Finite Element Model

IMPACT ON RACK PLATE ABOVE
STEP 7 TIME = 1.3997401E-003
MAX_VONMISES

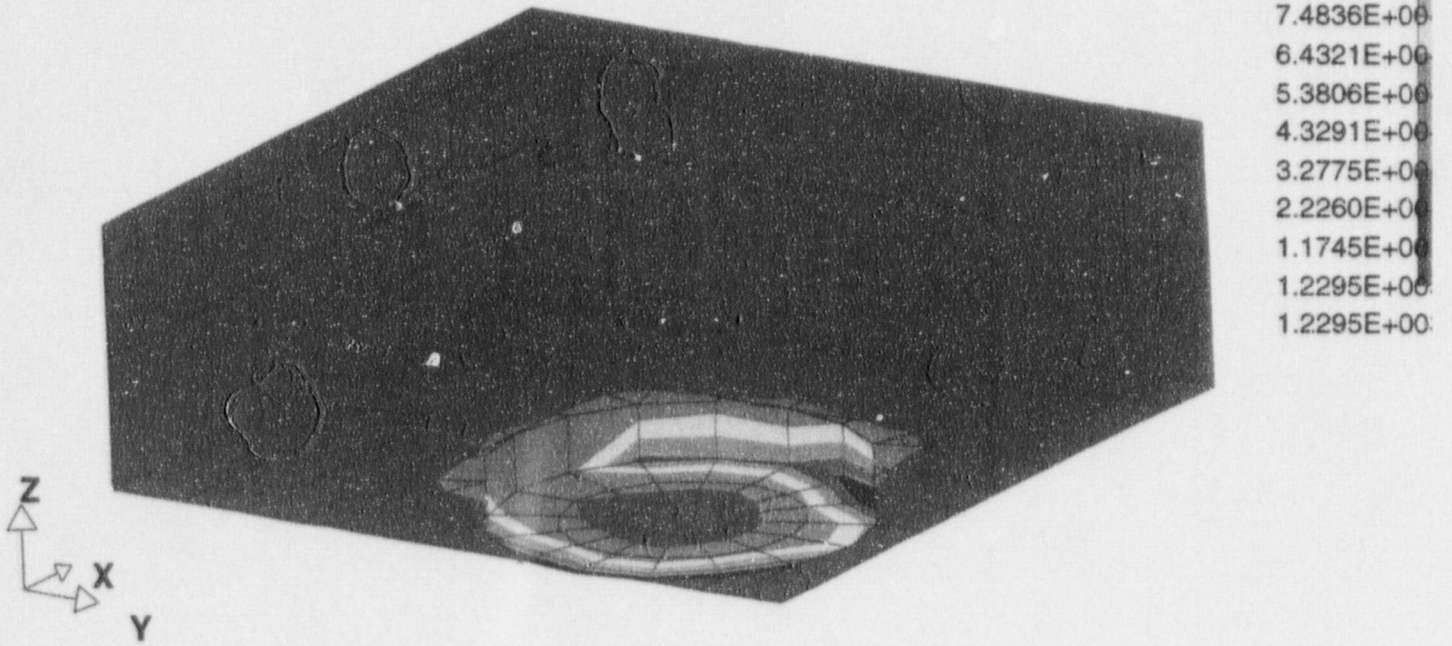
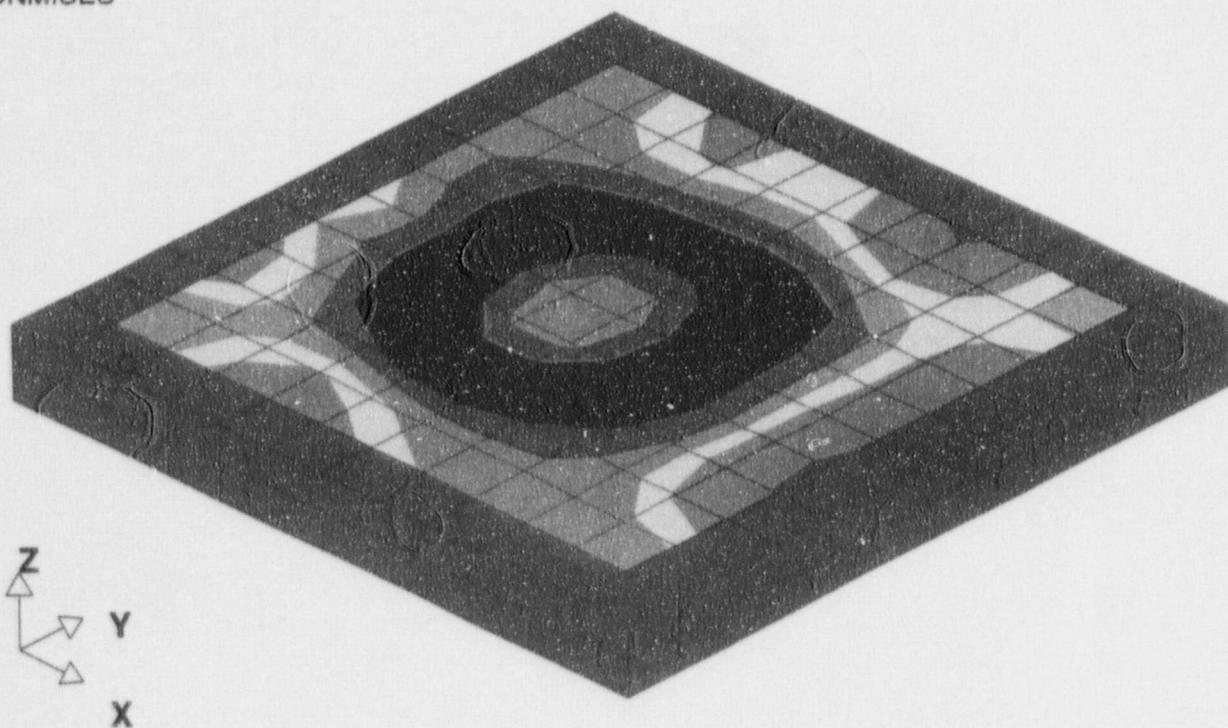


Figure 7.4.5; Over-Pedestal "Deep Drop" Pedestal Von Mises Stress

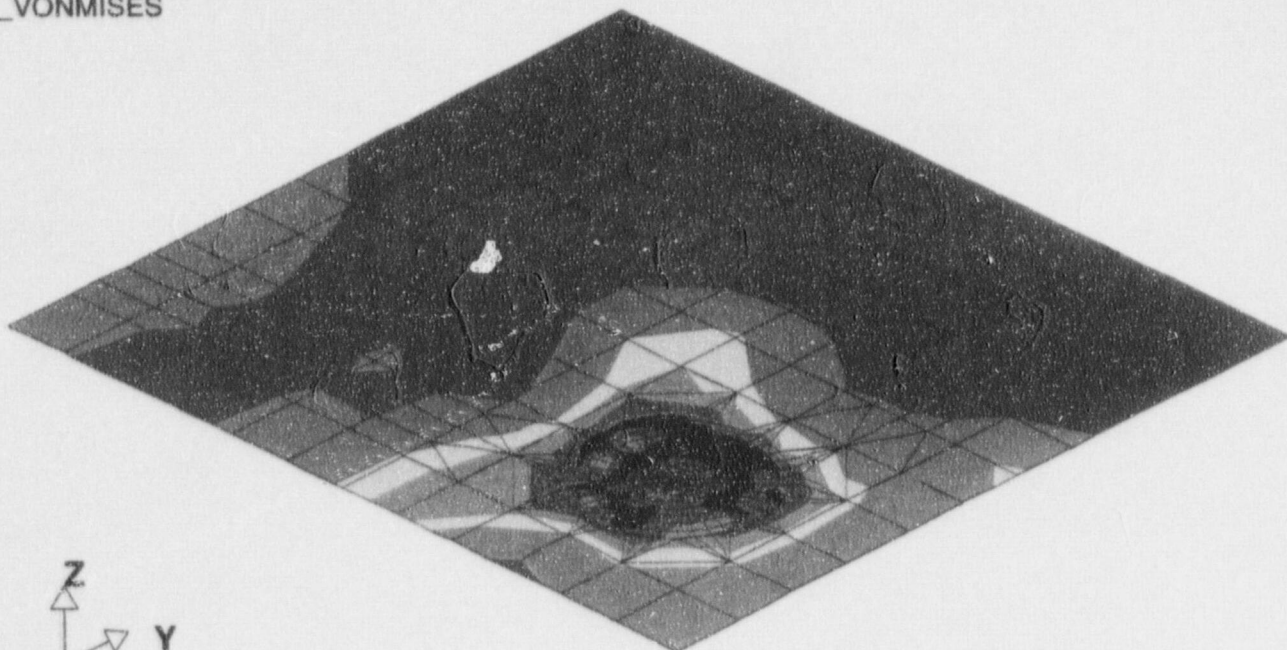
IMPACT ON RACK PLATE ABOVE
STEP 7 TIME = 1.3997401E-003
MAX_VONMISES



3.0144E+004
3.0144E+004
2.7130E+004
2.4117E+004
2.1103E+004
1.8090E+004
1.5076E+004
1.2063E+004
9.0494E+003
6.0359E+003
3.0223E+003
8.8267E+002
8.8267E+002

Figure 7.4.6; Over Pedestal "Deep Drop" Bearing Pad Von Mises Stress

IMPACT ON RACK PLATE ABOVE
STEP 9 TIME = 1.7998922E-003
MAX_VONMISES



2.7378E+004
2.7378E+004
2.4830E+004
2.2281E+004
1.9733E+004
1.7184E+004
1.4636E+004
1.2087E+004
9.5387E+003
6.9901E+003
4.4416E+003
1.8931E+003
1.8931E+003

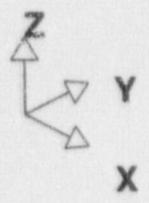
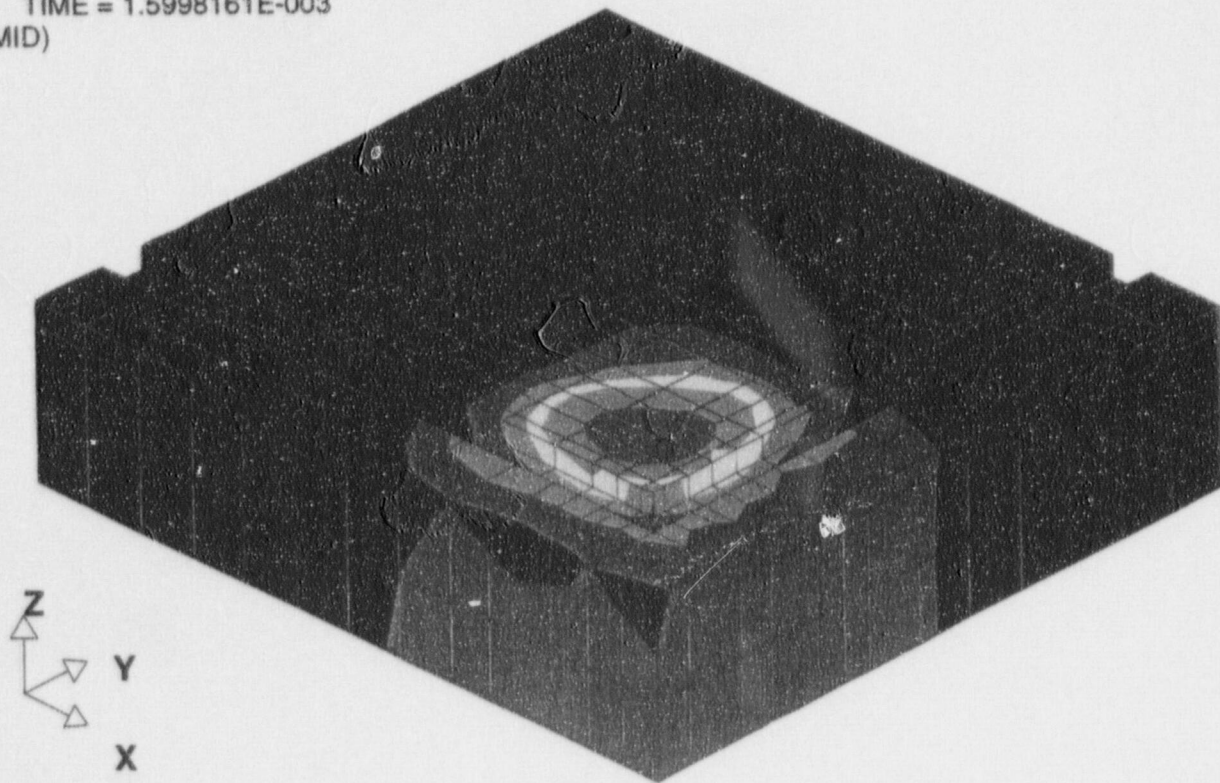


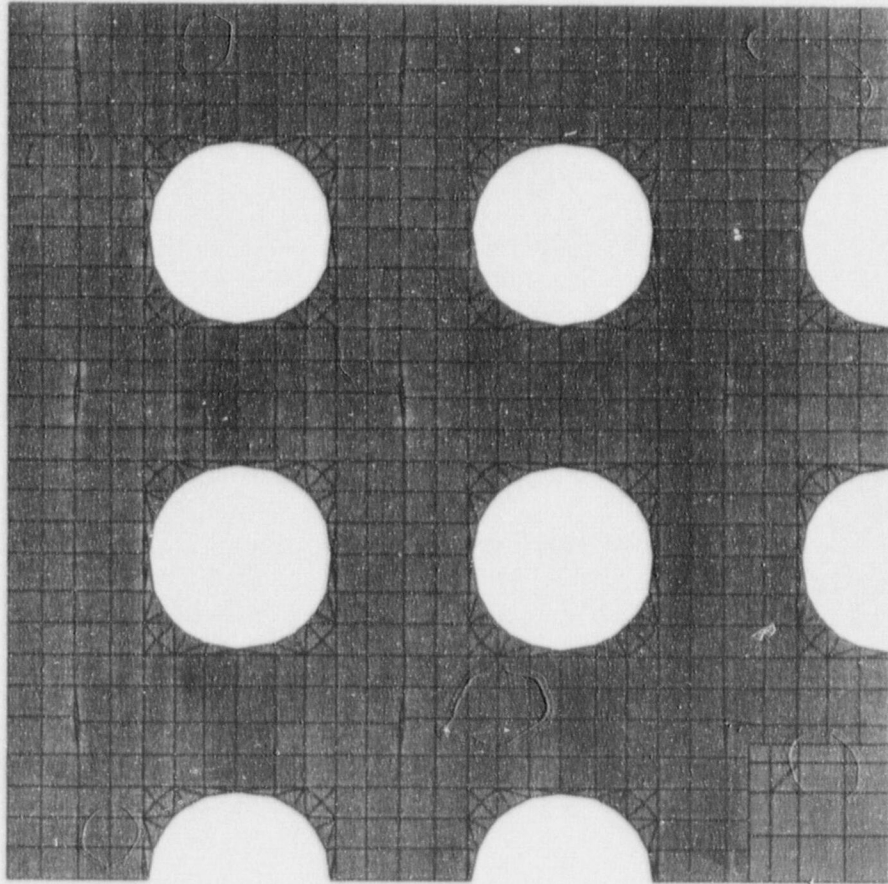
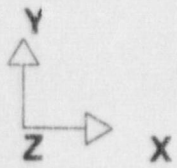
Figure 7.4.7; Over-Pedestal "Deep Drop" Liner Von Mises Stress

IMPACT ON RACK PLATE ABOVE
STEP 8 TIME = 1.5998161E-003
SIGZZ(MID)



1.5233E+00
1.5233E+00
-1.9789E+00
-4.1101E+00
-6.2413E+00
-8.3726E+00
-1.0504E+00
-1.2635E+00
-1.4766E+00
-1.6897E+00
-1.9029E+00
-2.1160E+00
-2.1160E+00

Figure 7.48: Over-Pedestal "Deep Drop" Concrete Von Mises Stress



IMPACT ON PLATE 8X8 PWR H
STEP 27 TIME = 1.3499969E-002
MAX_VONMISES

4.6040E+00
4.6040E+00
4.1756E+00
3.7472E+00
3.3188E+00
2.8904E+00
2.4620E+00
2.0336E+00
1.6052E+00
1.1768E+00
8.484E+00
5.2004E+00
3.2004E+00

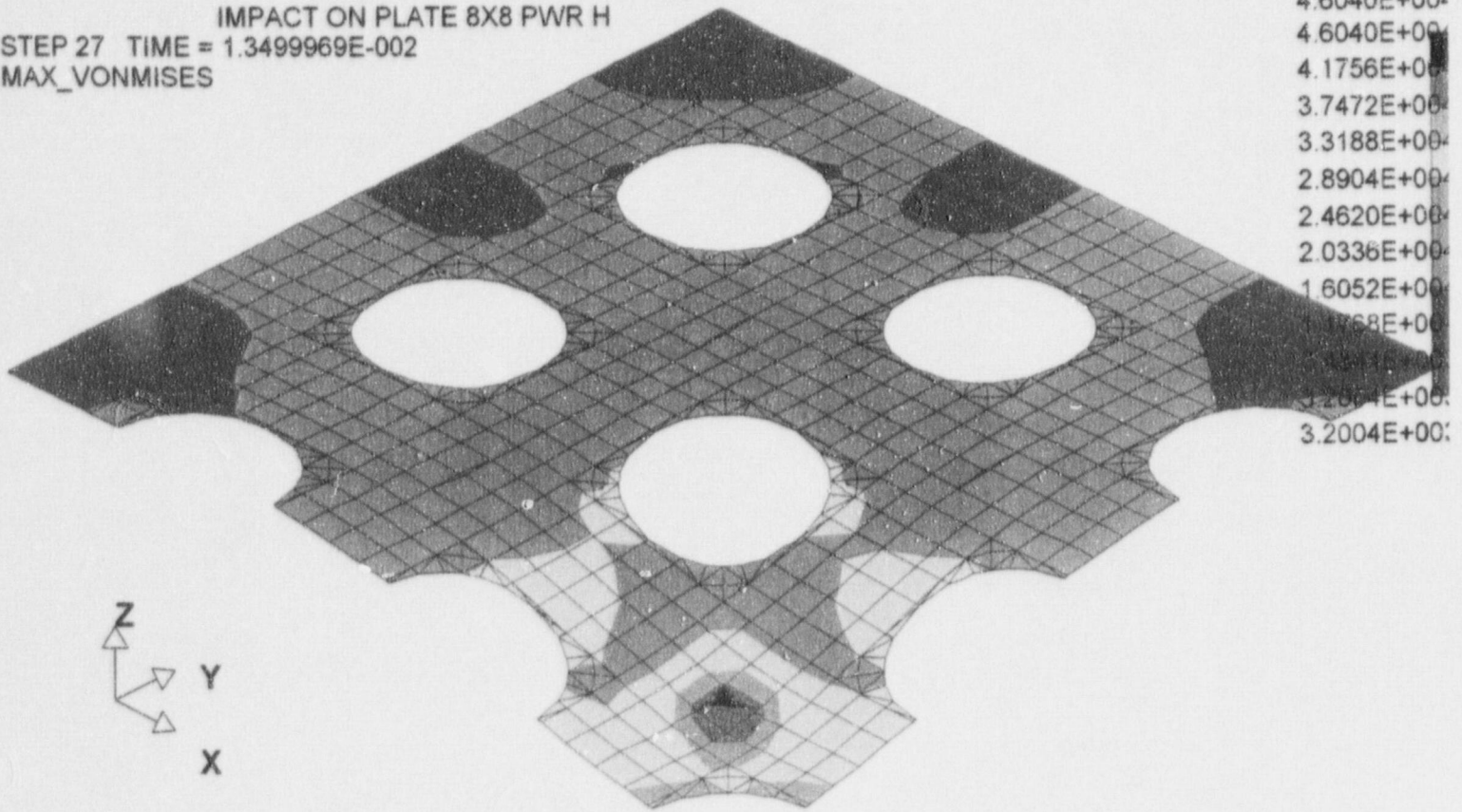


Figure 7.4.10; On-Center "Deep Drop" Baseplate Von Mises Stress

IMPACT ON PLATE 8X8 PWR H
STEP 27 TIME = 1.3499969E-002
PSTN(MID)

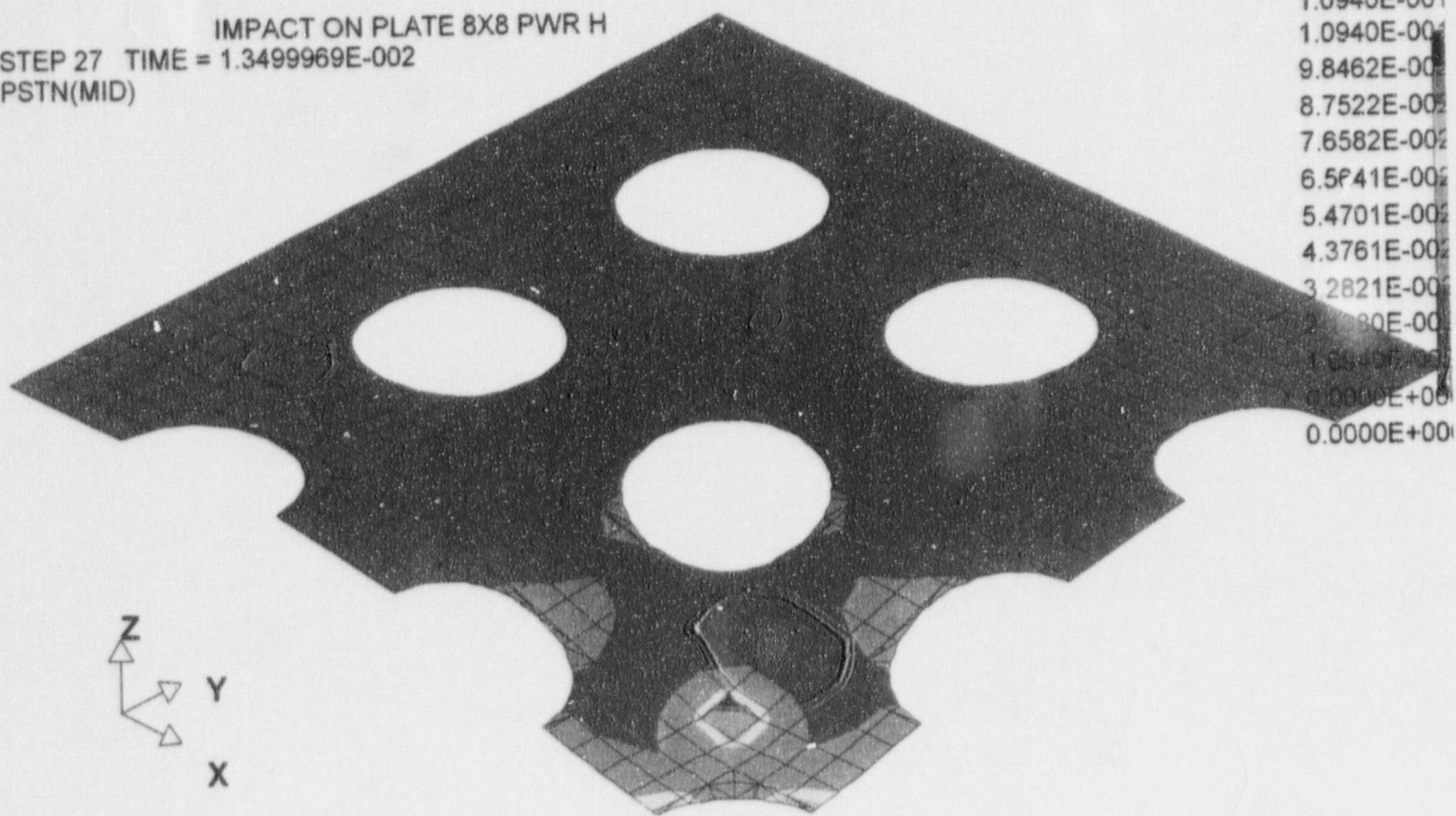


Figure 7.4.11; On-Center "Deep Drop" Baseplate Plastic Strain

STEP 27 TIME = 1.3499969E-002
Z COORDINATE DISPLACEMENT

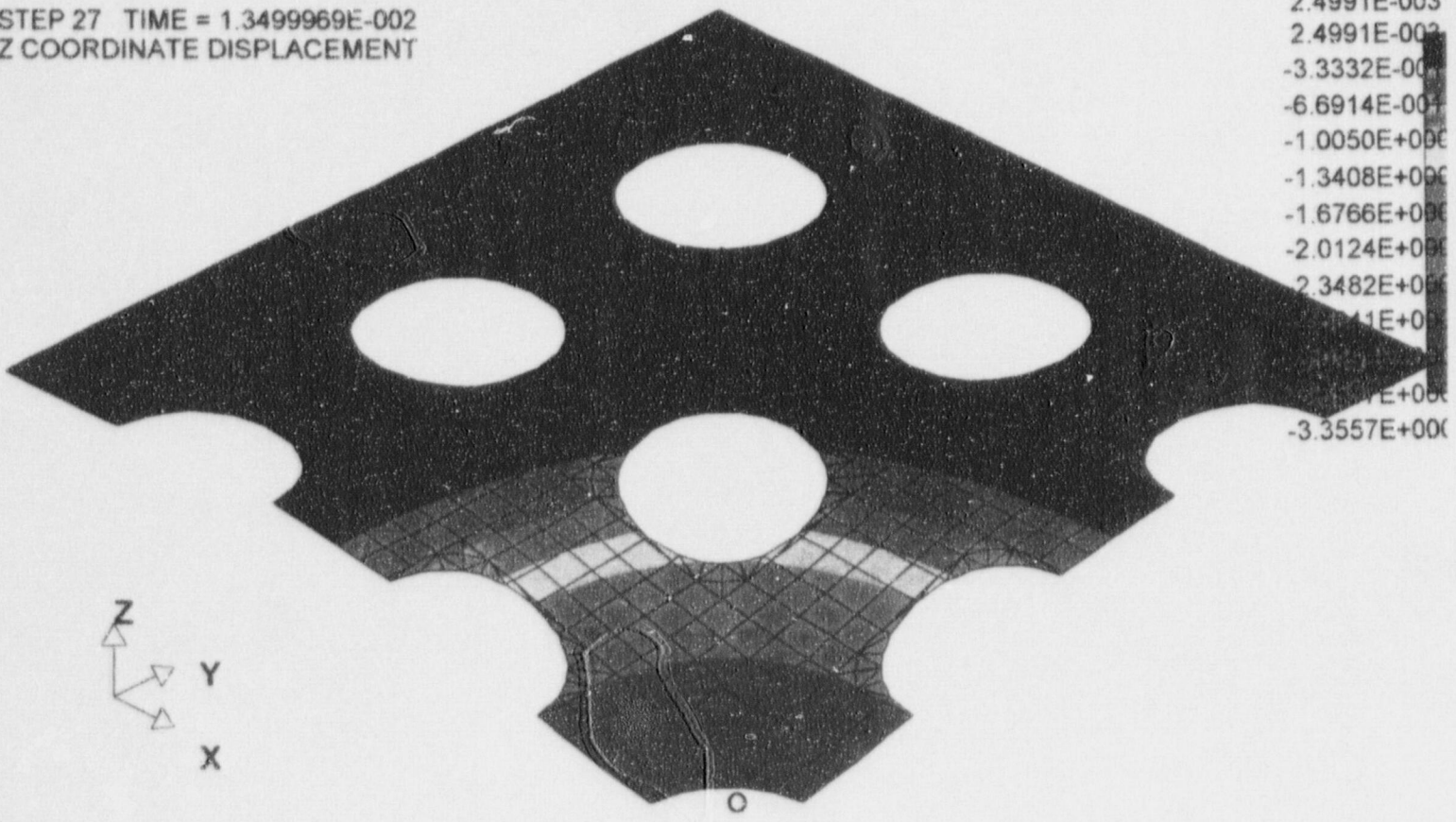
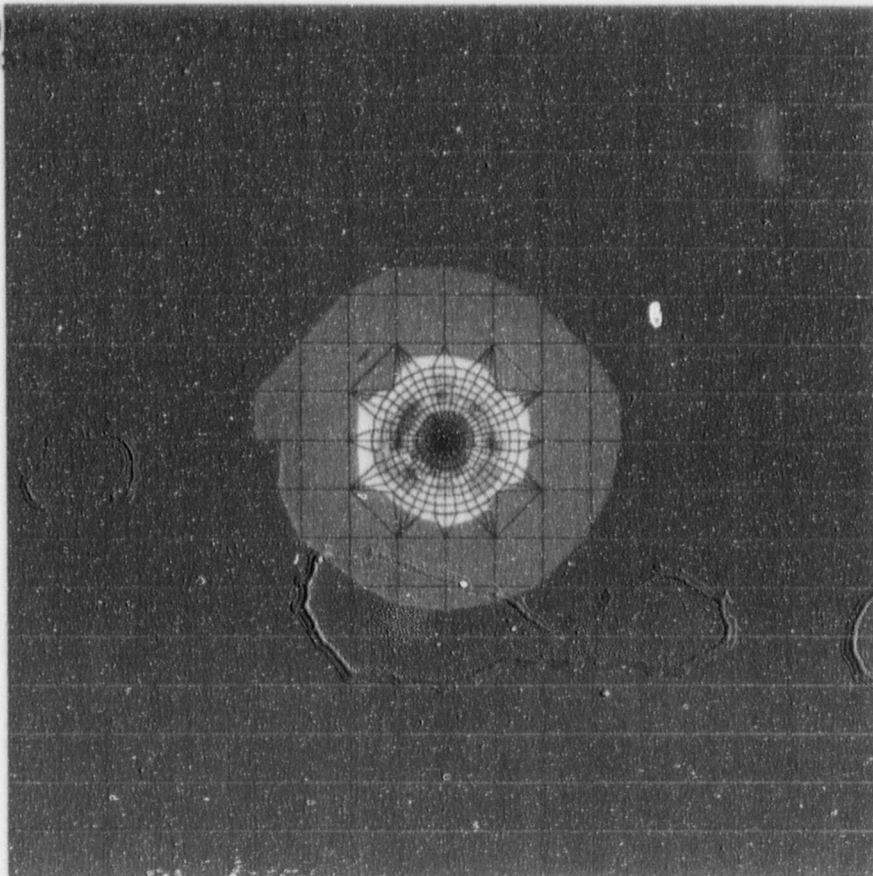


Figure 7.4.12:

RACK I
STEP 17 TIME = 3.3999
MAX_VONMISES



4.5153E+004
4.5153E+004
4.0845E+004
3.6537E+004
3.2230E+004
2.7922E+004
2.3615E+004
1.9307E+004
1.4999E+004
1.0692E+004
6.3839E+003
2.0763E+003
2.0763E+003

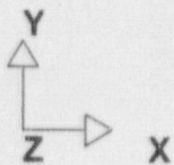


Figure 7.4.13;

“Heaviest Rack” Drop: Maximum Von Mises Stress – Liner

RACK IMPACT ON POOL FLOOR
STEP 16 TIME = 3.1999566E-003
SIGZZ(MID)

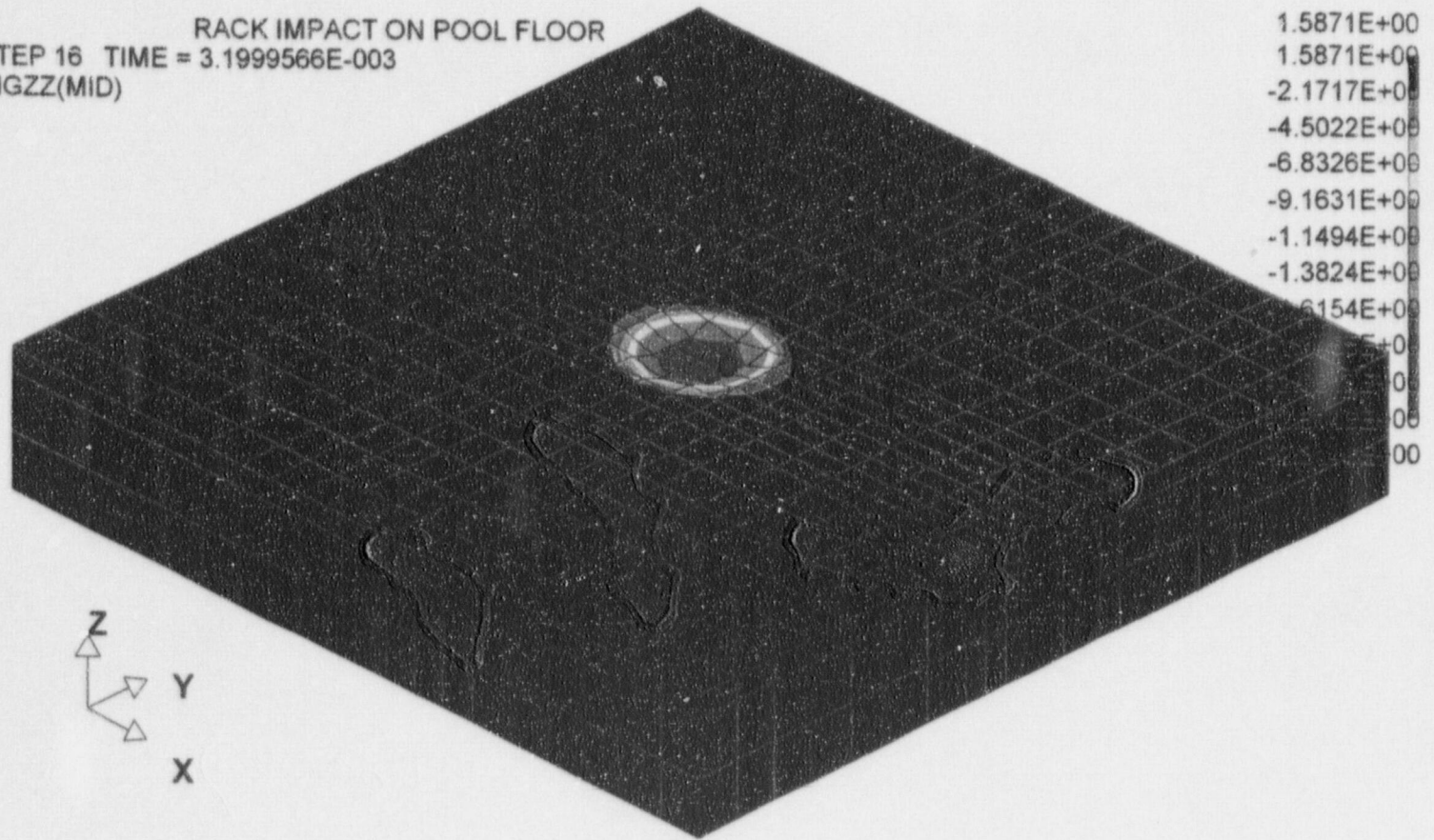


Figure 7.4.i4;

"Heaviest Rack" Drop: Maximum Vertical Stress - Concrete

8.0 CASK PIT STRUCTURE INTEGRITY CONSIDERATIONS

8.1 Introduction

The DBNPS Cask Pit represents a small portion of the Auxiliary Building, which is a safety related, seismic category I, reinforced concrete structure. Spent fuel is to be placed within the new storage racks located in the Cask Pit. This section discusses the analysis to demonstrate structural adequacy of the Cask Pit, herein also referred to as the pool structure. The analysis is performed in accordance with Section IV of the USNRC OT Position Paper [8.1.1].

The numerical investigation is conducted considering the walls as plan plates and using "closed form" solutions available in the technical literature. Results for individual load components are combined using the factored load combinations mandated by SRP 3.8.4 [8.1.2], which are based on the "ultimate strength" design method. It is demonstrated that structural integrity is maintained for the critical factored load combinations. These evaluations were performed for the bounding case when the pools are fully loaded with spent fuel racks, as shown in Figure 1.3 with all storage locations occupied by fuel assemblies.

Both moment and shear capabilities are checked for concrete structural integrity. Bearing integrity of the slab in the vicinity of a rack module support pedestal pad was also evaluated. All structural capacity calculations are made using design formulas meeting the requirements of the American Concrete Institute (ACI).

8.2 Description of Cask Pit Structures

The analyzed reinforced concrete structure, which is comprised of the four perimeter walls of the Cask Pit, is isolated from the remainder of the Auxiliary Building and the Spent Fuel Pool and conservatively considered as an independent structure. The structural evaluation focused on the four reinforced concrete walls surrounding the Cask Pit. These four 46'-2" high reinforced concrete walls are supported at elevation 557'-0" by a massive (15'-0" thick) reinforced concrete

mat, which extends down to bedrock. Figure 8.1.1 shows the area of interest and the major structural dimensions of the pool. The floor liner plate of the Cask Pit is located at elevation 557'. The operating floor is at elevation 603'-0".

The Cask Pit investigation concentrated on a portion of the monolithically constructed reinforced concrete Auxiliary Building structure. The pertinent portion is the area located in the vicinity of the Cask Pit where the storage capacity is proposed to be increased. The thickness of the walls surrounding the Cask Pit are 3'-0" at North and East, and 5'-6" at South and West. The continuity of the Cask Pit East wall is interrupted by the existence of the fuel gate opening.

8.3 Definition of Loads

Pool structural loading involves the following discrete components:

8.3.1 Static Loading (Dead Loads and Live Loads)

- 1) Dead weight of pool structure includes the weight of the Auxiliary Building concrete upper structure.
- 2) Maximum dead weight of rack modules and fuel assemblies stored in the modules based on 289 storage locations, as shown in Figure 1.3.
- 3) The Spent Fuel Cask Crane and Fuel Storage Handling Bridge (Refueling Platform) - The dead weight and the rated lift weight of these cranes are considered as dead load and live load, respectively.
- 4) The hydrostatic water pressure.

8.3.2 Seismic Induced Loads

- 1) Vertical loads transmitted by the rack support pedestals to the slab during a SSE or OBE seismic event.
- 2) Hydrodynamic inertia loads due to the contained water mass and sloshing loads (considered in accordance with [8.3.1]) which arise during a seismic event.
- 3) Hydrodynamic pressures between racks and pool walls caused by rack motion in the pool during a seismic event.
- 4) Seismic inertia force of the walls

8.3.3 Thermal Loading

The temperatures at the faces of the pool concrete walls and slabs define the thermal loading. Two thermal loading conditions are evaluated and are defined by the bulk pool temperatures determined in the thermal-hydraulic evaluations, as described in Table 5.8.1. The normal operating condition considers the bulk pool temperature T_o to be 150°F. The accident condition conservatively considers the bulk pool temperature T_a to be 180°F. The ambient temperature outside of the structure is considered to be -10°F. The temperature in the rooms of the Auxiliary Building and the Transfer Canal is considered to be 50°F. The concrete surface temperature on the side exposed to air is elevated from the air temperatures to account for surface film behavior. The concrete surface temperature on the water side is not adjusted.

The actual bulk pool water temperature under the limiting conditions considered for normal operating conditions exceeds the 150°F concrete temperature limit imposed by the ACI code. However, the use of 150°F for the normal condition in this calculation is acceptable because:

- a. The maximum bulk temperature of the Spent Fuel Pool (SFP) water, which enters the Cask Pit through the connecting gate, is determined to be 151.5°F. The maximum peak

local water temperature in the Cask Pit is determined to be 155.5°F, which occurs at the top of the storage rack cells, away from the concrete walls. The bulk water temperature in the Cask Pit will be between these two values, and probably closer to the 155.5°F. However, the concrete wall surface temperature will be slightly lower, due to the insulating barrier provided by the liner and any trapped air beneath the liner, and the film effect of the water at the liner water interface. Therefore, the concrete surface temperature under the limiting normal conditions is expected to be only slightly higher (~4.5°F) than the 150°F ACI limit.

- b. The SFP bulk temperature will be above 150°F only under the worst case transient conditions and the duration of this temperature in excess of 150°F will occur for less than 28 hours. The Cask Pit bulk temperature duration in excess of 150°F will be longer (~100 hours) under the worst case conditions. These durations are not significant when considering the thermal inertia of the concrete walls and slab. In other words, the concrete temperature will lag such that the bulk of the concrete cross-section will remain well below the 150° F range. In fact, a very small depth, if any, of the concrete will experience temperatures in excess of 150° F.
- c. The normal condition evaluation, which includes the 150°F temperature, has large design margins. A comparison with the accident condition evaluations, with a 30°F higher temperature, indicates that a concrete temperature increase of only 4.5°F will not produce a significant effect on the computed results. Therefore, the evaluation of the concrete for a surface temperature of 150°F instead of 154.5°F produces results of sufficient accuracy.
- d. The corresponding limiting conditions are conservative for storage of spent fuel in the Cask Pit, since the evaluation considers stored fuel to completely fill a completely reracked maximum density SFP (to be sought in a future amendment) and a filled Cask Pit. However, the storage of fuel in the Cask Pit is temporary and will not occur along with a filled reracked SFP, as discussed briefly in Section 1.

The concrete temperature in excess of 150°F under the worst case conditions is acceptable, since it will be experienced for a short duration. Thus, there will be no significant deterioration of the concrete material properties. Based on ACI publication SP25 [8.3.2] and numerous other technical papers, concrete compressive strength decreases about 10% at temperature 200°F as compared with the design specified strength of 4,000 psi. However, based on an ASCE paper [8.3.3], the concrete compressive strength even at boiling conditions of 212°F is higher than the 28 day f_c' , if the strength margin from age is considered. At 212°F the concrete residual modulus of elasticity (E_c) is about 96.5% of the E_c ambient temperature value and the rebar modulus of elasticity (E_s) is about 95% of the E_s ambient temperature value according to ACI 216 [8.3.4].

In general, both thermal expansion in the cross-section and the water pressure tend to create moments which cause the tension side of the concrete in the Cask Pit structure to be on the side away from the elevated temperatures. The rebars on the outside face are not affected by temperature increases within the pool. Therefore, the short term elevated temperatures above the 150°F range do not significantly affect the material properties and evaluation of the cross-sections at 150°F for normal conditions is justified.

8.4 Analysis Procedures

The Cask Pit reinforced concrete walls are subjected to various individual load cases covering the service conditions (the structural weight of the concrete structure, the weights of the upper portion of the Auxiliary Building concrete structure, the Spent Fuel Cask Crane, the hydro-static water pressure and the temperature gradients for normal operating and accident conditions) and seismic induced loads (structural seismic loads, hydro-dynamic water loads, and rack-structure interaction dynamic loads) for OBE and SSE conditions. The service condition loads were considered as static acting loads, while the seismic induced loads for both OBE and SSE seismic events are obtained from the simultaneous application of the three-directional acceleration spectra appropriate to elevation 603'-0".

8.4.1 Boundary Conditions

To simplify the analysis and make it possible to use "closed form" solution results existing in the technical literature, the four walls surrounding the Cask Pit are considered as planar plates having three edges fixed at the contact borders with the adjoined walls and supporting mat. The remaining edge at the upper elevation is considered as a free edge.

8.4.2 Material Properties

The behavior of the reinforced concrete existing in the structural walls is considered elastic and isotropic. The elastic characteristics of the concrete are independent of the reinforcement contained in each structural element for the case when the un-cracked cross-section is assumed. This assumption is valid for all load cases with the exception of the thermal loads, where for a more realistic description of the reinforced concrete cross-section behavior the assumption of cracked concrete is used. The elastic characteristics for the concrete and reinforcement used in this calculation are summarized in Table 8.4.1. To simulate the variation and the degree of cracking patterns, the original elastic modulus of the concrete is modified in accordance with the methodology provided by ACI 349 [8.1.3]. Table 8.4.2 contains the elastic isotropic material properties and the reduced elastic modulus (E_{crack}) pertinent to each wall.

8.4.3 Load Combinations

The various individual load cases are provided in Table 8.4.3. These load cases are combined in accordance with the NUREG-0800 Standard Review Plan [8.1.2] requirements with the intent to obtain the most critical stress fields for the investigated reinforced concrete structural elements.

For "Service Load Conditions" the following load combinations are:

- Load Combination No. 1 = $1.4 * D + 1.7 * L$
- Load Combination No. 2 = $1.4 * D + 1.7 * L + 1.9 * E$
- Load Combination No. 3 = $1.4 * D + 1.7 * L - 1.9 * E$
- Load Combination No. 4 = $0.75 * (1.4 * D + 1.7 * L + 1.9 * E + 1.7 * T_o)$
- Load Combination No. 5 = $0.75 * (1.4 * D + 1.7 * L - 1.9 * E + 1.7 * T_o)$
- Load Combination No. 6 = $1.2 * D + 1.9 * E$
- Load Combination No. 7 = $1.2 * D - 1.9 * E$

For "Factored Load Conditions" the following load combinations are:

- Load Combination No. 8 = $D + L + T_o + E'$
- Load Combination No. 9 = $D + L + T_o - E'$
- Load Combination No. 10 = $D + L + T_a + 1.25 * E$
- Load Combination No. 11 = $D + L + T_a - 1.25 * E$
- Load Combination No. 12 = $D + L + T_a + E'$
- Load Combination No. 13 = $D + L + T_a - E'$

where:

- D = dead loads;
- L = live loads;
- T_o = thermal load during normal operation;
- T_a = thermal load under accident condition;
- E = OBE earthquake induced loads;
- E' = SSE earthquake induced loads.

8.5 Results of Reinforced Concrete Analyses

The structural evaluation focused on the four reinforced concrete walls pertaining to the Cask Pit. The axial forces, bending moments and shear forces were computed for each significant cross-section of the structural elements. The reinforced concrete cross-sectional capacities were determined and used to obtain the safety margins of the structural elements. Safety margins are defined as the allowable load divided by the computed load and acceptability is ensured if the safety margin is in excess of 1.0. The calculated safety margins for all four walls are shown in Tables 8.5.1 through 8.5.4. The limiting safety margin is 1.41.

8.6 Pool Liner

The pool liner is subject to in-plate strains due to movement of the rack support feet during the seismic event. Analyses are performed to establish that the liner will not tear or rupture under limiting loading conditions in the pool, and that there is no fatigue problem under the condition of 1 SSE event plus 20 OBE events. These analyses are based on loadings imparted from rack pedestals in the pool assumed to be positioned in the most unfavorable position. Bearing strength requirements are shown to be satisfied by conservatively analyzing the most highly loaded pedestal located in the worst configuration with respect to underlying leak chases.

8.7 Conclusions

Regions affected by loading the Cask Pit completely with high density racks are examined for structural integrity under bending and shearing action. It is determined that adequate safety margins exist when the factored load combinations are checked against the appropriate structural design strengths. It is also shown that local loading on the liner does not compromise liner integrity under a postulated fatigue condition and that concrete bearing strength limits are not exceeded.

8.8 References

- [8.1.1] USNRC, "OT Position for Review and Acceptance of Spent Fuel Storage and Handling Applications," April 14, 1978, and Addendum dated January 18, 1979
- [8.1.2] NUREC-0800, SRP-3.8.4, Rev. 1., July 1981.
- [8.1.3] ACI 349-85, Code Requirements for Nuclear Safety Related Concrete Structures, American Concrete Institute, Detroit, Michigan.
- [8.3.1] "Nuclear Reactors and Earthquakes, U.S. Department of Commerce, National Bureau of Standards, National Technical Information Service, Springfield, Virginia (TID 7024).
- [8.3.2] ACI Publication SP25, "Temperature and Concrete".
- [8.3.3] ASCE Convention Paper, "Strength Properties of Concrete at Elevated Temperatures," Boston, Mass., April 1979.
- [8.3.4] ACI 216, R-81, "Guidelines for Determining the Fire Endurance of Concrete Elements".

Table No. 8.4.1
Concrete and Rebar Properties

Parameter	Notation	Value
Concrete Compressive Strength (psi)	f_c'	4.000E+03
Un-Cracked Concrete Elastic Modulus (psi)	E_c	3.605E+06
Concrete Poisson's Ratio	ν	0.167
Concrete Weight Density (lb/ft ³)	D_w	150.0
Concrete Thermal Expansion Coefficient	α	5.500E-06
Reinforcement Yield Strength (psi)	F_y	6.000E+04
Reinforcement Elastic Modulus (psi)	E_{rebar}	2.900E+07

Table No. 8.4.2
Material Properties

Structural Element	Thickness (in)	E (psi)	ν	γ_w (lb/ft ³)	α	E_{crack} (psi)
North Wall	36.00	3.605E+06	0.167	150.	5.500E-06	1.250E+06
South Wall	66.00	3.605E+06	0.167	150.	5.500E-06	4.059E+05
West Wall	66.00	3.605E+06	0.167	150.	5.500E-06	4.059E+05
East Wall	36.00	3.605E+06	0.167	150.	5.500E-06	1.250E+06

Table No. 8.4.3
Individual Load Case Description

Load No.	Type	Description
1	D	Structural Concrete Weight
2	D	Water Hydro-Static Pressure
3	L	Auxiliary Building Live Loads
4	E	OBE Rack to Wall Coupling Pressure
5	E'	SSE Rack to Wall Coupling Pressure
6	E	OBE Convective (Sloshing) Pressure
7	E'	SSE Convective (Sloshing) Pressure
8	E	OBE Impulsive Pressure
9	E'	SSE Impulsive Pressure
10	E	OBE Hydro-Dynamic Vertical Pressure
11	E'	SSE Hydro-Dynamic Vertical Pressure
12	E	OBE Structural Inertia Loads
13	E'	SSE Structural Inertia Loads
14	To	Temperature for Operating Condition
15	Ta	Temperature for Accident Condition

Table No. 8.5.1
North Wall Safety Factors

Combination Load Case	Reinforcement Orientation			
	X Direction		Y Direction	
	Axial+Bending	Shear	Axial+Bending	Shear
1	412.59	96.34	93.09	85.82
2	18.69	4.28	21.50	4.63
3	20.08	4.69	39.71	5.19
4	27.43	5.70	28.50	6.18
5	31.74	6.26	52.69	6.92
6	18.81	4.30	22.17	4.67
7	19.94	4.66	37.31	5.15
8	27.43	5.90	30.03	6.61
9	31.25	6.47	55.64	7.43
10	30.98	6.48	31.83	7.01
11	36.61	7.17	62.31	7.93
12	27.94	5.90	30.03	6.61
13	32.35	6.47	55.64	7.43
Min	18.69	4.28	21.50	4.63

Table No. 8.5.2
South Wall Safety Factors

Combination Load Case	Reinforcement Orientation			
	X Direction		Y Direction	
	Axial+Bending	Shear	Axial+Bending	Shear
1	830.97	186.97	206.16	163.13
2	33.17	7.25	46.51	7.74
3	32.35	7.86	77.37	8.55
4	3.51	9.66	58.89	10.32
5	3.77	10.48	98.51	11.40
6	33.35	7.29	43.81	7.79
7	32.16	7.81	67.15	8.49
8	4.31	9.77	59.97	10.75
9	4.74	10.56	98.46	11.87
10	3.81	10.98	64.81	11.72
11	4.08	11.99	114.04	13.06
12	3.79	9.77	59.97	10.75
13	4.08	10.56	98.46	11.87
Min	3.51	7.25	43.81	7.74

Table No. 8.5.3
West Wall Safety Factors

Combination Load Case	Reinforcement Orientation			
	X Direction		Y Direction	
	Axial+Bending	Shear	Axial+Bending	Shear
1	830.97	186.97	194.08	163.13
2	32.73	7.25	40.90	7.74
3	33.50	7.86	68.72	8.55
4	5.78	9.66	53.28	10.32
5	6.78	10.48	89.95	11.40
6	32.92	7.29	41.32	7.79
7	33.30	7.81	64.10	8.49
8	6.93	9.77	54.85	10.75
9	8.52	10.56	91.05	11.87
10	5.68	10.98	59.38	11.72
11	6.51	11.99	105.26	13.06
12	5.62	9.77	54.85	10.75
13	6.54	10.56	91.05	11.87
Min	5.62	7.25	40.90	7.74

Table No. 8.5.4
East Wall Safety Factors

Combination Load Case	Reinforcement Orientation			
	X Direction		Y Direction	
	Axial+Bending	Shear	Axial+Bending	Shear
1	1000	1000	1000	1000
2	7.96	1.41	31.43	4.90
3	7.78	1.41	31.28	4.90
4	12.67	1.87	41.65	6.53
5	12.59	1.87	41.51	6.53
6	7.96	1.41	31.33	4.90
7	7.78	1.41	31.18	4.90
8	11.36	1.73	40.63	7.02
9	11.27	1.73	40.54	7.02
10	14.48	2.14	47.44	7.44
11	14.40	2.14	47.29	7.44
12	11.81	1.73	40.63	7.02
13	11.72	1.73	40.54	7.02
Min	7.78	1.41	31.18	4.90

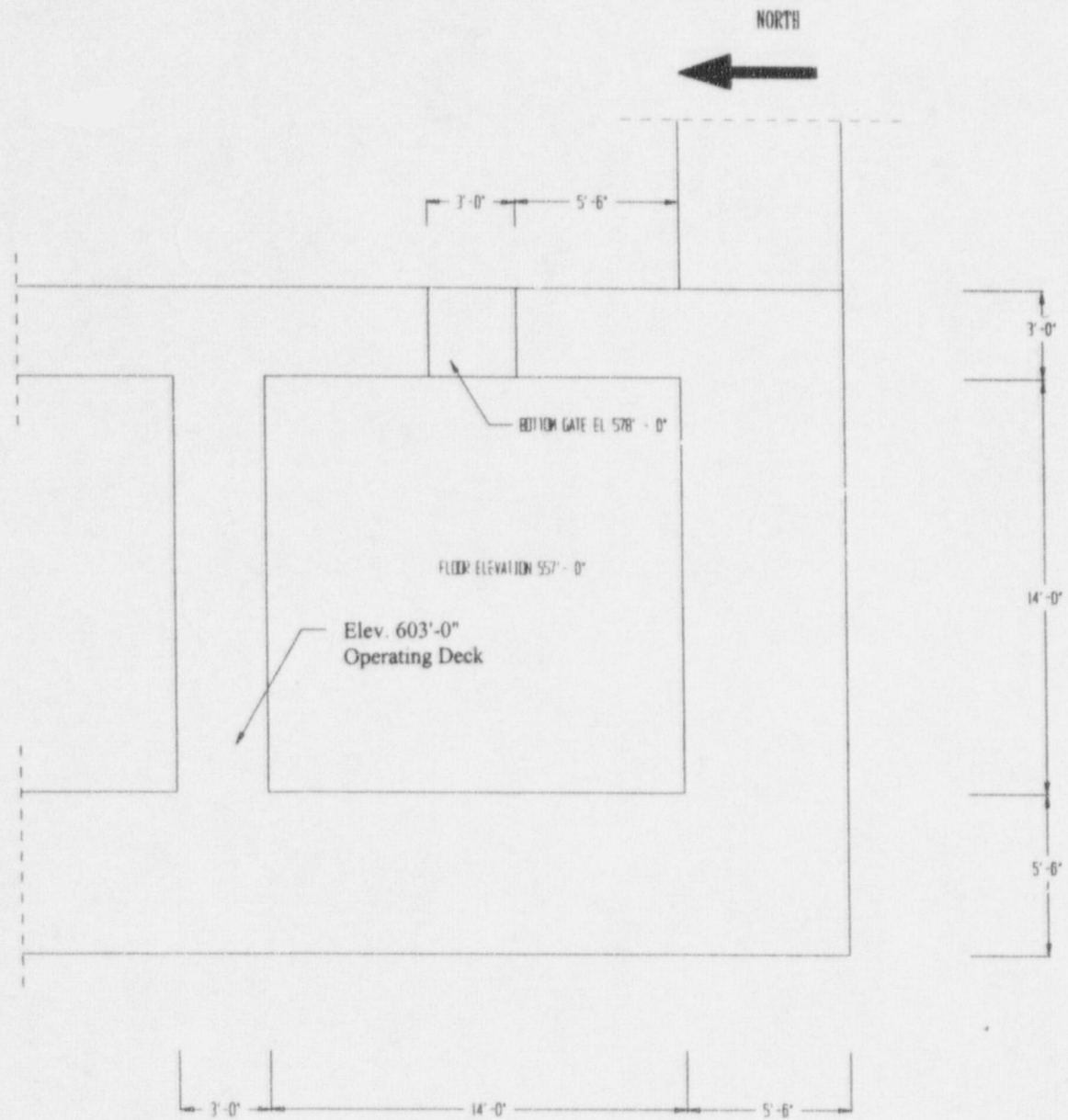


Figure 8.11: Plan View of Cask Pit Area

9.0 RADIOLOGICAL EVALUATION

9.1 Solid Radwaste

The SFP Purification System currently generates approximately 50 cubic feet of solid radioactive waste annually at the DBNPS. No significant increase in the volume of solid radioactive wastes is expected from operating with the expanded storage capacity. The necessity for pool filtration resin replacement is determined primarily by the requirement for water clarity, and the resin is normally changed about once every 18 months. The additional number of fuel assemblies in storage will not significantly affect the frequency of resin replacement.

9.2 Liquid Releases

The number of spent fuel assemblies in storage does not affect the release of radioactive liquids from the plant. The contribution of radioactive materials in the SFP water from the stored assemblies is insignificant relative to other sources of activity, such as the reactor coolant system. The volume of SFP water processed for discharge is independent of the number of fuel assemblies stored.

9.3 Gaseous Releases

Gaseous releases from the fuel storage area are combined with other plant exhausts. Currently there is no detectable contribution from the fuel storage area, and no significant increases are expected as a result of the expanded storage capacity.

Release of radioactive gases by the DBNPS will remain a small fraction of the limits of 10 CFR 20.1301 and the design objectives of Appendix I to 10 CFR 50 following the implementation of the proposed modification to increase spent fuel storage capacity. This conclusion is based on the following supporting statements:

- a) The half-lives of short-lived nuclides such as I-131 are short in comparison to fuel cycle length; therefore, short-lived nuclides are present only in freshly offloaded fuel. The quantity of freshly offloaded fuel placed into the SFP each refueling outage is independent of the number of spent fuel assemblies being stored. Therefore, the inventory of I-131 in the SFP and Cask Pit will not be affected by the increased fuel storage capacity.
- b) Inventories of long-lived fission products (e.g. Kr-85 and ternary tritium) in spent fuel assemblies will decrease slowly within individual fuel assemblies over years in storage. Therefore, an increase in the number of stored spent fuel assemblies would increase the total inventory of these radionuclides. However, these radionuclides are not released in significant amounts from the stored fuel to the SFP water, even for failed fuel, since the fuel pellet temperature of stored fuel is not high enough to create sufficient gas pressure in the gap to overcome the static pressure of the SFP water.
- c) The radioactivity in the SFP water is independent of the number of stored assemblies. The SFP water activity is primarily dependent on the amount of fuel assembly movement within the SFP. The number of fuel assembly movements required for a refueling outage is generally limited to the movements required to complete the outage. The number of plant refueling outages should not change. Typical SFP activities are listed in Table 9.1.1.
- d) The increased number of spent fuel assemblies in storage will raise the heat load on the SFP and could result in an increase in the evaporation rate. Other than a small amount of tritiated water released by evaporation, the radionuclides are non-volatile and consequently are not released from the pool water. The increased evaporation rate of tritiated water would result in an increase in gaseous tritium released in the plant's effluents. However, the discharge of gaseous radioactive effluents will continue to be a small fraction of the limits of 10 CFR 20.1301 and the design objectives of Appendix I to 10 CFR 50.

During normal operations, personnel working in the fuel storage area are exposed to radiation from the SFP. Operating experience has shown that area radiation dose rates originate primarily from radionuclides in the pool water.

During refueling and other fuel-movement operations, pool water concentrations might be expected to increase somewhat due to crud deposits spalling from spent fuel assemblies and due to activities carried into the pool from the primary system. With respect to the rack installation, fuel movements in the SFP may be required in support of this project to reduce the possible dose to personnel during the rack installation. For this reason, although dose rates above and around the Cask Pit perimeter may increase marginally, the dose fields will still approximate conditions seen during normal operating conditions. Routine radiation surveys would identify any change to dose rates, and the appropriate radiological controls would be revised as required.

Radiation dose rates in accessible areas around the spent fuel storage and transfer zones were evaluated based on conservative fuel parameters and were found acceptable. For five year-cooled fuel with design source gammas, the dose rate was determined to be approximately 28 millirems per hour. The DBNPS USAR Chapter 12 describes the current evaluations of personnel dose. USAR Figure 12.1-1 provides the radiation zones for normal operation at elevation 545 feet in the Auxiliary Building. The floor elevation of the Cask Pit is approximately 557 feet elevation. Ground elevation at the DBNPS is approximately 585 feet elevation. The south and west walls of the Cask Pit are underground and present no possibility of exposure. The Auxiliary Building room to the north (Room 106) is designated as Radiation Zone D, with a designated dose rate of ≤ 100 millirems per hour. The Auxiliary Building room to the east (Room 109) is designated as Radiation Zone E1, with a designated dose rate of ≤ 1000 millirems per hour. The dose rate contribution from 3 year cooled fuel, at elevation 558 feet 6 inches, near the ceiling of rooms 106 and 109, was determined by the DBNPS to be approximately 70 millirems per hour.

The Cask Wash Pit floor elevation, to the west of the Cask Pit, is 585 feet. Dose rates at this elevation are not expected to increase. This area is designated as a Radiation Zone D, which should not be affected by storage of spent fuel in the Cask Pit.

As a result, no changes are expected to the Radiation Zone designations evaluated in the DBNPS USAR. Routine radiation surveys will be conducted to confirm the actual dose rates in rooms 106 and 109 when fuel is transferred to the racks in the Cask Pit.

Operating experience at the DBNPS has also shown that there are no detectable concentrations of airborne radioactivity in the SFP area except tritium, at approximately $3E-3$ Derived Air Concentration (DAC). No increase in airborne radioactivity is expected as a result of the expanded storage capacity.

9.5 Anticipated Dose During Rack Installation

All of the operations involved in the rack installation will utilize detailed procedures prepared with full consideration of ALARA principles. Similar operations have been performed in a number of facilities in the past, and there is every reason to believe that re-racking can be safely and efficiently accomplished at the DBNPS, with low radiation exposure to personnel.

Total dose for the re-racking operation is estimated to be between 1.85 and 4.0 person-rem, as indicated in Table 9.5.1. While individual task efforts and doses may differ from those in Table 9.5.1, the total is believed to be a reasonable estimate for planning purposes. Though divers will be used only as necessary, the estimated person-rem burden for rack installation takes into consideration their possible dose. Radiation surveys will be conducted in the Cask Pit to confirm dose rates prior to diving activities. Cleanup of source material, which would contribute to an excessive dose for the divers will be performed, as necessary, in accordance with good practices to limit dose ALARA.

The existing radiation protection program at the DBNPS is adequate for the rack installation operations. Where there is a potential for significant airborne activity, continuous air monitors will be in operation. Personnel will wear protective clothing as required and, if necessary, respiratory protective equipment. Activities will be governed by a Radiation Work Permit, and personnel monitoring equipment will be issued to each individual. Divers will be equipped with the appropriate personal dosimetry. As a minimum, this will include thermoluminescent dosimeters (TLDs) and self-reading dosimeters. Additional personnel monitoring equipment (i.e., extremity TLDs or multiple TLDs) may be utilized as required.

Work, personnel traffic, and the movement of equipment will be monitored and controlled to minimize contamination and to assure that dose is maintained ALARA.

After the rack installations, the lifting device will be washed with demineralized water and wrapped for contamination controls. The lift rig will be stored at the DBNPS site for future planned reracking of the SFP.

Table 9.3.1

AVERAGE ACTIVITY OF WEEKLY SFP SAMPLES

(From February, 1999)

<u>Nuclide</u>	<u>Average Microcuries / cc</u>
Co-57	4.40 E-07
Co-58	1.57E-05
Co-60	8.65E-06
Ag-110M	3.66E-06
Sb-125	2.66E-05
Cs-134	9.88E-06
Cs-137	4.71E-05
Total	1.12E-04

Table 9.5.1

PRELIMINARY ESTIMATE OF PERSON-REM DOSE DURING
CASK PIT RACK INSTALLATION

Step	Number of Personnel	Hours	Estimated Person-Rem Dose
Installation of new rack module - Phase 1	5	20	0.25 to 0.5
Installation of new rack module - Phase 2	5	20	0.8 to 1.5
Install remaining new rack modules - Phase 3	5	35	0.8 to 2.0
Total Dose, person-rem			1.85 to 4.0

10.0 INSTALLATION

10.1 Introduction

The installation phase of the DBNPS Unit 1 Cask Pit rack project is executed by Holtec International's Field Services Division. Holtec, serving as the installer, is responsible for performance of specialized services, such as underwater diving and welding operations, as necessary. All installation work at the DBNPS is performed in compliance with NUREG-0612 (refer to Section 3.0), Holtec Quality Assurance Procedure 19.2, DBNPS project specific procedures, and applicable DBNPS procedures.

Crane operators are trained in the operation of overhead cranes per the requirements of ANSI/ASME B30.2, and the plant's specific training program. Consistent with the installer's past practices, a videotape aided training session is presented to the installation team, all of whom are required to successfully complete a written examination prior to the commencement of work. Fuel handling bridge operations are performed by the DBNPS personnel, who are trained in accordance with DBNPS procedures.

The lifting device designed for handling and installation of the new racks at the DBNPS is engaged and disengaged on lift points at the bottom of the rack. The lifting device complies with the provisions of ANSI N14.6-1978 and NUREG-0612, including compliance with the design stress criteria, load testing at a multiplier of maximum working load, and nondestructive examination of critical welds.

A surveillance and inspection program shall be maintained as part of the installation of the racks. A set of inspection points, which have been proven to eliminate any incidence of rework or erroneous installation in previous rack projects, is implemented by the installer.

Underwater diving operations are required to remove underwater obstructions, to aid in the rack installation by assisting in the positioning of new rack modules, and to verify installation per

design. The DBNPS procedures for control of diving and radiological controls for diving operations are utilized. The DBNPS procedures are supplemented by the safe-practices guidance provided by the diving company. These documents describe the precautions and controls for dive operations and were developed utilizing OSHA Standard 29CFR-1910, Subpart T.

Holtec International developed procedures, to be used in conjunction with the DBNPS procedures, which cover the scope of activities for the rack installation effort. Similar procedures have been utilized and successfully implemented by Holtec on previous rack installation projects. These procedures are written to include ALARA practices and provide requirements to assure equipment, personnel, and plant safety. These procedures are reviewed and approved in accordance with DBNPS administrative procedures prior to use on site. The following is a list of the Holtec procedures, used in addition to the DBNPS procedures to implement the installation phase of the project.

A. Installation/Handling Procedure:

This procedure provides overall direction for the handling and installation of the new maximum density fuel storage rack modules in the Cask Pit. This procedure delineates the steps necessary to receive the new maximum density racks on site, the proper method for unloading and uprighting the racks, staging the racks prior to installation, and installation of the racks. The procedure also provides for the installation of rack bearing pads, adjustment of the rack pedestals and verification of the as-built field configuration to ensure compliance with design documents.

B. Receipt Inspection Procedure:

This procedure delineates the steps necessary to perform a thorough receipt inspection of a new rack module after its arrival on site. The receipt inspection includes dimensional measurements, cleanliness inspection, visual weld examination, and verticality measurements.

C. Cleaning Procedure:

This procedure provides for the cleaning of a new rack module, if required. The modules are to meet the requirements of ANSI N45.2.1, Level B, prior to placement in the Cask Pit. Methods and limitations on materials to be utilized are provided.

D. Pre- and Post-Installation Drag Test Procedure:

These two procedures stipulate the requirements for performing a functional test on a new rack module prior to and following installation into the Cask Pit. The procedures provide direction for inserting and withdrawing an insertion gage into designated cell locations, and establishes an acceptance criteria in terms of maximum drag force.

E. ALARA Procedure:

Consistent with Holtec International's ALARA Program, this procedure provides guidance to minimize the total man-rem received during the rack installation project, by accounting for time, distance, and shielding

F. Liner Inspection Procedure:

In the event that a visual inspection of any submerged portion of the Cask Pit liner is deemed necessary, this procedure describes the method to perform such an inspection using an underwater camera and describes the requirements for documenting any observations.

G. Leak Detection Procedure:

This procedure describes the method to test the Cask Pit liner for potential leakage using a vacuum box. This procedure may be applied to any suspect area of the Cask Pit liner.

H. Liner Repair and Underwater Welding Procedure:

In the event of a positive leak test result, underwater welding procedures may be implemented which provide for a weld repair, or placement of a stainless steel repair patch, over the area in question. The procedures contain appropriate qualification records documenting relevant variables, parameters, and limiting conditions. The weld procedure is qualified in accordance with AWS D3.6-93, Specification for Underwater Welding or may be qualified to an alternate code accepted by the DBNPS and Holtec International.

10.2 Rack Arrangement

The final rack arrangement allows for a total of four freestanding Holtec racks in the Cask Pit, which provides a total of 289 storage locations. Two new fuel storage racks were installed in the Cask Pit to add 153 fuel storage cells, in April 1999. These two rack modules were installed as a plant modification after evaluation in accordance with 10CFR50.59 demonstrated that installation of the empty racks did not involve an unreviewed safety question. The installed racks will remain unused until a license amendment application is approved by the NRC. The two racks were placed in the Cask Pit for the remaining duration of the DBNPS Fuel Cycle 12, which is scheduled to be completed in April 2000. One of these racks provides sufficient storage capacity for full core offload capability for the remainder of Fuel Cycle 12 and the ten year in service inspection (ISI) of the reactor vessel. The ten year ISI is required to be completed during the Cycle 12 Refueling Outage. The two installed racks also provide full core offload capability during Fuel Cycle 13, which is scheduled to occur between May, 2000 and April, 2002. The remaining two racks, consisting of 136 cells, will be installed into the Cask Pit in a future campaign, during Fuel Cycle 13, to support fuel movements required for a full re-racking of the SFP. The SFP re-racking is expected to take place during Fuel Cycle 13. A schematic plan view depicting the Cask Pit with the two newly installed maximum density racks can be seen in Figures 1.2. Figure 1.3 depicts the Cask Pit layout with all four maximum density fuel storage racks installed.

10.3 Cask Pit Survey and Inspection

A Cask Pit survey was performed to determine if any items attached to the liner wall or floor of the Cask Pit would interfere with the placement of the new racks or prevent usage of any cell locations subsequent to installation. This survey determined that an unused light pole support bracket on the south wall of the Cask Pit must be removed. This bracket was originally mounted on a one-half inch mounting plate attached to the Cask Pit liner. The bracket was removed from the mounting plate for installation of the first two racks, leaving the mounting plate intact, without affecting the liner. On the north wall of the Cask Pit is another light pole mounting bracket that will be similarly removed from its mounting plate before installation of racks N3 and N4. Also on the north Cask Pit wall is a fuel handling bridge load test fixture that will be removed and relocated. Finally, the northwest corner of the Cask Pit floor has a sump for draining the Cask Pit. The drain piping enters the pit through the west wall of the pit, takes a 90 degree bend downward, and extends into this sump. To install the N4 rack, this drain line protrusion into the pit and associated supports will have to be removed. The pipe will be cut off parallel to the west wall such that a flange can be welded to the pipe as it enters the pit. The piping will be flanged so that the drain pipe extension can be temporarily removed to accommodate rack N4 and reinstalled in the future after removal of the N4 rack. All four rack modules will be eventually relocated into the SFP during the re-racking on the entire SFP. A stack of solid, stainless steel plates will be placed in the sump on which one leg of the N4 rack will rest. The removal of these interferences will involve underwater diving and mechanical cutting operations.

10.4 Cask Pit Cooling and Purification

10.4.1 Cask Pit Cooling

There is no forced cooling in the Cask Pit. When fuel is transferred into the Cask Pit, the water in the pit will be cooled by natural circulation mixing with the SFP water through the open gate. The SFP water temperature is maintained by forced circulation cooling. During any installation

of racks in the Cask Pit, there will be no fuel in the Cask Pit, and the gate between the SFP and Cask Pit will be installed to prevent the diver from entering the SFP. Since there is no forced cooling in the Cask Pit and the pit will contain no fuel, it is not anticipated that any rack installation activities will require the temporary shutdown of the SFP cooling system.

10.4.2 Purification

A portable vacuum system may be employed to remove extraneous debris, reduce general contamination levels prior to diving operations, and to assist in the restoration of Cask Pit clarity following any installation processes.

10.5 Fuel Movement

Necessary fuel movements are performed prior to Cask Pit rack installation activities. Fuel movement operations are conducted in accordance with DBNPS procedures. Any fuel stored in the Cask Pit racks for the Cycle 12 refueling outage will be returned to the SFP prior to installation of rack modules N3 and N4.

10.6 Installation of New Racks

Installation of the new high density racks, supplied by Holtec International, involves the following activities. The racks are delivered in the horizontal position. A new rack module is removed from the shipping trailer using a suitably rated crane, while maintaining the horizontal configuration. The rack is placed on the up-ender and secured. Using two independent overhead hooks, or a single overhead hook and a spreader beam, the module is up-righted into a vertical position.

The new rack lifting device is engaged in the lift points at the bottom of the rack. The rack is then transported to a pre-leveled surface where, after leveling the rack, the appropriate quality control receipt inspection is performed.

To address ALARA considerations, fuel in the adjacent SFP may be moved away from the gate area in preparation for rack installation. Additionally, the Cask Pit floor is inspected and any debris, which may inhibit the installation of bearing pads, is removed.

After Cask Pit floor preparation, new rack bearing pads are positioned on the pit floor before the module is lowered into the pit. The new rack module is lifted with the Spent Fuel Cask Crane (SFCC) and transported along the pre-established safe load path. The rack module is cautiously lowered into the Cask Pit unto the bearing pads using the SFCC. A temporary hoist, with an appropriate capacity, is attached to the SFCC for installation in order to eliminate contamination of the main hook during lifting operations in the Cask Pit.

Elevation readings are taken to confirm that the module is level. In addition, rack-to-rack and rack-to-wall off-set distances are also measured. Adjustments are made as necessary to ensure compliance with design documents. The lifting device is then disengaged and removed from the Cask Pit under Health Physics direction. Post-installation free path verification is performed using an inspection gage in order to ensure that no cell location poses excessive resistance to the insertion or withdrawal of a fuel assembly. This test confirms final acceptability of the installed rack module.

10.7 Safety, Health Physics, and ALARA Methods

10.7.1 Safety

During the installation phase of the Cask Pit rack project, personnel safety is of paramount importance, outweighing all other concerns. All work shall be carried out in compliance with applicable approved procedures.

10.7.2 Health Physics

Health Physics is carried out per the requirements of the DBNPS Radiation Protection Program.

10.7.3 ALARA

The key factors in maintaining project dose As Low As Reasonably Achievable (ALARA) are time, distance, and shielding. These factors are addressed by utilizing many mechanisms with respect to project planning and execution.

Time

Each member of the project team is trained and provided appropriate education and understanding of critical evolutions. Additionally, daily pre-job briefings are employed to acquaint each team member with the scope of work to be performed and the proper means of executing such tasks. Such pre-planning devices reduce worker time within the radiologically controlled area and, therefore, project dose.

Distance

Remote tooling such as lift fixtures, pneumatic grippers, a support leveling device and a lift rod disengagement device have been developed to execute numerous activities from the Cask Pit surface, where dose rates are relatively low. For those evolutions requiring diving operations, diver movements shall be restricted to the empty Cask Pit by installation of the gate between the SFP and the Cask Pit. If necessary, additional fuel in the adjacent SFP may be moved to satisfy ALARA principles.

Shielding

During the course of the rack installation, the concrete wall between the SFP and the Cask Pit, and the water in the Cask Pit provides shielding. If necessary, additional shielding may be utilized to meet ALARA principles.

10.8 Radwaste Material Control

Radioactive waste generated from the rack installation will be controlled in accordance with established DBNPS procedures.

11.0 ENVIRONMENTAL COST / BENEFIT ASSESSMENT

11.1 Introduction

Article V of the USNRC CYT Position Paper [11.1] requires the submittal of a cost/benefit analysis for a fuel storage capacity enhancement. This section provides justification for selecting installation of racks in the Cask Pit as the most viable alternative.

11.2 Imperative for Rack Installation

The DBNPS lost full core offload capability (FCOC) in April 1998, during the refueling outage conducted after Fuel Cycle 11. Although FCOC is neither a license condition nor commitment for the DBNPS, it is considered a prudent operating practice. In January of 1996, the DBNPS completed storage of 72 spent fuel assemblies in the certified NUHOMS® dry spent fuel storage system in accordance with the requirements of 10CFR72 Subpart K. After the vendor for the NUHOMS® system temporarily stopped production, a decision had to be made to implement another spent fuel storage plan.

At the present time, the SFP has 114 open storage cells. The DBNPS reactor core contains 177 fuel assemblies, and is currently operating without FCOC. The present fuel storage rack arrangement contains 735 storage cells and there is no available area for installation of additional racks in the SFP. The SFP currently contains 601 irradiated fuel assemblies, one dummy fuel assembly, and 2 inaccessible storage cells. An additional 17 storage cell locations are used or reserved for failed fuel assemblies, surveillance specimen storage, control component handling containers, abandoned fuel assembly cages from fuel assembly reconstitution campaigns, and radioactive trash containers. Control components are generally stored within irradiated fuel assemblies.

Placing two fuel rack modules in the Cask Pit adds 153 fuel assembly storage locations. This addition will serve to regain FCOC during Fuel Cycle 12. Cycle 12 started in May of 1998, and

is scheduled to be complete in April of the year 2000. FCOC at the end of Fuel Cycle 12 is required to allow completion of the 10-year reactor vessel in-service inspection (ISI). As the 10-year ISI is a regulatory requirement for operation, without additional storage capacity, operation of the DBNPS can not continue. Approximately 72 fuel storage locations will be used for the next refueling. As a result, 195 storage cells should be available to maintain FCOC during Fuel Cycle 13 which is scheduled to begin in May, 2000 and end for the thirteenth refueling outage in April of the year 2002.

The remaining two rack modules (total of four) addressed by this license amendment request are required to provide fuel storage during a future re-racking of the entire SFP, which is scheduled to take place during Fuel Cycle 13. As part of the SFP re-racking, the four Cask Pit rack modules will be placed in the SFP near the end of the re-racking sequence.

11.3 Appraisal of Alternative Options

Adding fuel storage space to the DBNPS Cask Pit is the most viable option for temporarily increasing spent fuel storage capacity.

The key considerations in evaluating the alternative options included:

- Safety: Minimize the risk to the public
- Economy: Minimize capital and O&M expenditures
- Security: Protection from potential saboteurs, natural phenomena
- Non-intrusiveness: Minimize required modifications to existing plant systems
- Maturity: Extent of industry experience with the technology
- ALARA: Minimize cumulative dose
- Schedule: Minimize time to regain full-core offload capability
- Risk Management: Maximize probability of completing the expansion to support fuel storage needs

Rod Consolidation

Rod consolidation involves disassembly of spent fuel, followed by the storage of the fuel rods from two assemblies into the volume of one, and the disposal of the fuel assembly skeleton outside of the pool (this is considered a 2:1 compaction ratio). The rods are stored in a stainless steel can that has the outer dimensions of a fuel assembly. The can is stored in the spent fuel racks. This technology is still in its developmental infancy and thus, based on the aforementioned DBNPS schedule, is not a viable option based on the time frame.

On-Site Dry Cask Storage

Dry cask storage is a method of storing spent nuclear fuel in a high capacity container. The cask provides radiation shielding and passive heat dissipation. Typical storage system capacities for PWR fuel range from 21 to 37 assemblies that have been removed from the reactor for at least five years.

In the early 1990s, Toledo Edison made the decision to reclaim some of the DBNPS SFP storage using a dry fuel storage system. In January 1996, seventy-two spent fuel assemblies were loaded into three Dry Shielded Canisters and were placed in dry fuel storage utilizing the certified NUHOMS[®] system, in accordance with 10CFR72.214, Certificate Number 1004. Changes within the dry spent fuel storage industry have caused cost increases. The contracted supplier of the NUHOMS system voluntarily stopped fabrication activities and was unable to provide additional storage systems within an acceptable schedule. Further use of this technology was re-evaluated and determined not to be the best choice for future storage expansion at the DBNPS. This decision was based on economics, schedule, and risk management.

Other Storage Options

Other options such as Modular Vault Dry Storage, Horizontal Silo Storage, and a new Fuel Storage Pool are overly expensive as compared to placing racks in the Cask Pit. Due to the complexity of implementation, these options could not meet the required schedule for regaining and maintaining full-core offload capability.

11.3.1 Alternative Option Summary

An estimate of relative costs in 1998 dollars for the aforementioned options is provided in the following:

Cask Pit Rack Expansion:	\$1-3 million
Horizontal Silo:	\$35-45 million
Rod consolidation:	\$25 million
Metal cask (MPC):	\$68-100 million
Modular vault:	\$56 million
New fuel pool:	\$150 million

The above estimates are consistent with estimates by EPRI and others [11.2, 11.3].

To summarize, based on the required short time schedule, the status of the dry spent fuel storage industry, and the storage expansion costs, the most acceptable alternative for increasing the on-site spent fuel storage capacity at the DBNPS is expansion of the wet storage capacity. First, there are no commercial independent spent fuel storage facilities operating in the United States. Second, the adoption of the Nuclear Waste Policy Act (NWPA) created a de facto throw-away nuclear fuel cycle. Since the cost of spent fuel reprocessing is not offset by the salvage value of the residual uranium, reprocessing represents an added cost for the nuclear fuel cycle which already includes the NWPA Nuclear Waste Fund fees. In any event, there are no domestic

reprocessing facilities. Third, at over \$½ million per day replacement power cost, shutting down the DBNPS is many times more expensive than addition of high density racks to the existing SFP Cask Pit and the future re-racking of the SFP.

11.4 Cost Estimate

The plant modification proposed for the DBNPS fuel storage expansion utilizes freestanding, high density, poisoned spent fuel racks in the Cask Pit. The engineering and design is completed for full racking of the Cask Pit. As stated in section 11.2, the first two racks placed in the Cask Pit will provide full-core offload capability through Fuel Cycle 13. This will allow time for the complete re-racking of the SFP during Cycle 13.

The total capital cost is estimated to be approximately \$1.5 million as detailed below.

Engineering, design, project management:	\$1/2 million
Rack fabrication:	\$1/2 million
Rack installation:	\$1/2 million

As described in the preceding section, other fuel storage expansion technologies were evaluated prior to deciding on the use of Cask Pit racks. Storage rack capacity expansion provides a cost advantage over other technologies.

11.5 Resource Commitment

The expansion of the DBNPS Spent Fuel Pool capacity via the Cask Pit is expected to require the following primary resources:

Stainless steel:	18 tons
Boral neutron absorber:	2 tons, of which 1.5 tons is Boron Carbide powder and 0.5 tons are aluminum.

The requirements for stainless steel and aluminum represent a small fraction of total world output of these metals (less than 0.001%). Although the fraction of world production of Boron Carbide required for the fabrication is somewhat higher than that of stainless steel or aluminum, it is unlikely that the commitment of Boron Carbide to this project will affect other alternatives. Experience has shown that the production of Boron Carbide is highly variable, depends upon need, and can easily be expanded to accommodate worldwide needs.

11.6 Environmental Considerations

Due to the additional heat-load arising from increased Spent Fuel Pool inventory, the anticipated maximum bulk pool temperature will increase by about 4°F. † at the time when the pool's capacity is exhausted. The increased bulk pool temperature will result in an increase in the pool water evaporation rate. This increase has been determined to increase the relative humidity of the Fuel Building atmosphere by less than 25 percent relative humidity †. This increase is within the capacity of both normal and the ESF Ventilation System. The net result of the increased heat loss and water vapor emission to the environment is negligible.

† These numbers are based on more than doubling the amount of fuel in the Spent Fuel Pool by re-racking the entire pool. This will be very conservative for the heat load added by placing fuel in Cask Pit racks

References

- [11.1] OT Position Paper for Review and Acceptance of Spent Fuel Storage and Handling Applications, USNRC (April 1978).
- [11.2] Electric Power Research Institute, Report No. NF-3580, May 1984.
- [11.3] "Spent Fuel Storage Options: A Critical Appraisal", Power Generation Technology, Sterling Publishers, pp. 137-140, U.K. (November 1990).